ACADEMIC REPORT
2022-2023

शैक्षणिक प्रतिवेदन
2022-23

होमी भाभा राष्ट्रीय संस्थान
HOMI BHABHA NATIONAL INSTITUTE
परमाणु ऊर्जा विभाग की सहायता प्राप्त संस्था
और यूजीसी अधिनियम 1956 की धारा 3 के तहत विश्वविद्यालय माना जाता है
(A Deemed to be University u/s 3 of UGC Act 1956 and a Grant-in-Aid
Institute of the Department of Atomic Energy, Govt. of India)

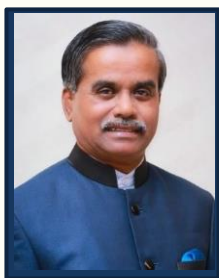# Location of HBNI Central Office, Constituent Institutions & Off Campus Centre

HRI, Allahabad

IPR, Gandhinagar

RRCAT, Indore

BARC, Mumbai

TMC, Mumbai

HBNI Central Office

INDIA

VECC, Kolkata

SINP, Kolkata

IoP, Bhubaneswar

NISER Bhubaneswar

IMSc, Chennai

IGCAR, Kalpakkam

Academic Report
2022-23

<u>Contents</u>

From the Vice Chancellor's Desk

It is with great pleasure that I present the academic report of HBNI for the year 2022-23. In the eighteen years of its existence, HBNI has emerged as one of the best research universities offering challenging research opportunities in frontier areas of science, engineering, technology and mathematics. HBNI also offers academic programs that contribute to skill development of its students. The courses in Oncology, clinical research and nursing are making effective contributions to the country's human resource base in these important areas. During the academic year (August 1, 2022-July 31, 2023) HBNI offered 43 academic programmes and awarded 218 PhD degrees, 84 M. Tech., 183 M.Sc./Integrated M.Sc. in various science disciplines, and 109 post graduate & super specialty medical degrees. Till July 31, 2023, total degrees awarded include 2351 PhD, 728 MD, 195 DM, 228 MCh, 1344 MSc. degrees.

In the MoE's National Institute Ranking Framework exercise for the academic year 2022-23, HBNI received 15th rank in Research Institution category, 17th rank in university category and 30th rank in the Overall category. The analysis of the score obtained by HBNI reveals that it is possible for HBNI to improve its ranking substantially in coming years. Based on high-quality publications in high impact selected journals, the Nature Index 2023 has placed HBNI in the third position, among all institutions in India and in first position among all institutions regarding publications in the discipline of physical sciences during the academic year. These results are due to the remarkable efforts of our faculty members and students. During the academic year 2022-23, HBNI has implemented a few of the guidelines for HEIs as per NEP-2020, viz., industry linkage centre, academic break, credit system, and student transfer. The remaining guidelines will also be implemented in a phased manner in the ensuing academic year.

The high quality of the research being carried out at different CIs/OCC of HBNI is evident through the perusal of the highlights of the theses included in this report. The research output presented in the report clearly shows that the efforts of HBNI to foster multidisciplinary and interdisciplinary research are bearing fruits. It gives me immense pleasure to note that our faculty members and students have been recognized for their research efforts and received several awards, academic honors, and fellowship during the academic year.

I take this opportunity to extend my gratitude to Shri K. N. Vyas, Former Chairman, Council of Management (CoM), HBNI and Prof. A. K. Mohanty, Chairman, CoM, HBNI for their guidance and support in all ventures of HBNI. I express my sincere thanks to Prof. R. B. Grover, Emeritus Professor, HBNI for providing guidance in several matters of HBNI. I also thank all the members of CoM, HBNI, academic Council, HBNI and Planning and Monitoring Board, HBNI. Thanks are due to Board of Study members, Deans (Academic), Deans (Student Affairs), nodal officers at our CIs/OCC and HBNI colleagues and staff for their devoted efforts towards making HBNI a renowned centre of academic excellence and a leader in research nationally and internationally

(U. Kamachi Mudali)

Section I
(OVERVIEW)

Academic Programmes of the Institute

The Homi Bhabha National Institute (HBNI) brings together the academic and research programmes conducted by the following eleven premier institutions of DAE, as its Constituent Institutions (CIs)/ Off Campus Centre (OCC):

1. Bhabha Atomic Research Centre (BARC), Mumbai
2. Indira Gandhi Centre for Atomic Research (IGCAR), Kalpakkam
3. Raja Ramanna Centre for Advanced Technology (RRCAT), Indore
4. Variable Energy Cyclotron Centre (VECC), Kolkata
5. Saha Institute of Nuclear Physics (SINP), Kolkata
6. Institute for Plasma Research (IPR), Gandhinagar
7. Institute of Physics (IoP), Bhubaneswar
8. Harish-Chandra Research Institute (HRI), Allahabad
9. Institute of Mathematical Sciences (IMSc), Chennai
10. Tata Memorial Centre (TMC), Mumbai
11. National Institute of Science Education and Research (NISER), Bhubaneswar

The HBNI offers a range of academic programmes in Chemical Sciences, Engineering Sciences, Medical & Health sciences, Life Sciences, Mathematical Sciences and Physical Sciences. It also has a program in Applied Systems Analysis. All institutions, except NISER, conduct programmes at post-graduate level. NISER admits Higher Secondary passed students for its five years Integrated M.Sc. program.

❖ **Disciplines in which HBNI Offers Ph.D.**
- ✓ Applied System Analysis
- ✓ Chemical Sciences
- ✓ Computer Science
- ✓ Computational Biology
- ✓ Earth & Planetary Science
- ✓ Engineering Sciences
- ✓ Humanities & Social Sciences
- ✓ Life Sciences
- ✓ Mathematical Sciences
- ✓ Medical & Health Sciences
- ✓ Physical Sciences
- ✓ Theoretical Computer Science

Most of the Ph.D. programmes are multi-disciplinary in nature having guides and co-guides from different branches of science and engineering.

❖ **Disciplines in which HBNI Offers Integrated Ph.D.**

✓ Applied System Analysis
✓ Computational Biology
✓ Engineering Sciences

❖ **M.Tech.** in Engineering Sciences consists of one year of course work and one year of project work. The course work is offered at all the campuses of BARC Training School and IPR Training School. Project work is offered at BARC, IGCAR, RRCAT, VECC, IPR and units of DAE. Those who are not able to pursue or are not interested in pursuing a project/research work have the option to get a post graduate diploma in lieu of M.Tech.. BARC training school also offers post graduate diploma in Life Sciences after one year of course work.

❖ **M.Sc. (Engg)** program emphasizes on research project work extending upto one and a half years after one year of course work. This program is offered at BARC, IGCAR, VECC, RRCAT and IPR.

❖ **Integrated M.Sc.** of five-year duration in Physical Sciences, Chemical Sciences, Mathematics and Life Sciences is offered at NISER. M.Sc. in Physical Sciences of two-year duration is offered at HRI. M.Sc. in Medical & Radiological Physics of two-year duration is offered at NISER.

Super Specialty Courses in Medical & Health Sciences offered at TMC are listed below:

❖ **Doctor of Medicine (D.M.)** in Medical Oncology, Pediatric Oncology, Gastroenterology, Critical Care, Oncopathology and Interventional Radiology

❖ **Master of Chirurgiae (M.Ch)** in Surgical Oncology, Gynecological Oncology, Plastic Surgery & Reconstructive Surgery, Head & Neck Oncology

Two years Certified Fellowship Programmes in Medical & Health Sciences offered at TMC are listed below:

Post-MD fellowship program is offered with specialization in Orthopedic Oncology, Breast Oncology, Thoracic Oncology, Uro Oncology, Interventional Oncology, Surgical Pathology, Haemato Pathology, Dental & Prosthetic Surgery, Preventive Oncology, Infectious Diseases & HIV Medicine, Gastrointestinal Oncology, Pulmonary Oncology, Molecular Haemato Oncology, Oral Oncology with Reconstructive Surgery

Post Graduate Courses in Medical & Health Sciences at TMC include:

❖ **MD** (Pathology, Anaesthesia, Radio-diagnosis, Radiation Oncology, Microbiology, Nuclear Medicine, Palliative Medicine, Immuno-Hematology & Transfusion Medicine and in Nuclear Medicine).

❖ **M.Sc. (**Nursing**), M.Sc. (**Clinical research), **M.Sc**. (Public Health in Epidemiology) and **M.Sc**. (Occupational Therapy in Oncology) programmes are offered at TMC.

❖ **M.Sc. (Nuclear Medicine and Molecular Imaging Technology)** is offered at TMC & Radiation Medicine Centre of BARC.

❖ **M.Sc. (Hospital Radiophamacy**) is offered at Radiation Medicine Centre of BARC.

Post Graduate Courses in Medical & Health Sciences offered at RMC-BARC:

❖ **M.D. (Nuclear Medicine)**

❖ **M.Sc. (Nuclear Medicine and Molecular Imaging Technology)**

PG Diploma offered at TMC:

❖ **Fusion Imaging Technology (PGDFIT)**

PG Diploma Courses offered at BARC:

❖ **Diploma in Radiological Physics (DipRP)**

❖ **Diploma in Medical Radio Isotope Techniques (DMRIT)**

❖ **Diploma in Nuclear Science and Engineering (DipNSE)**

Management of HBNI

The **Council of Management** chaired by Secretary, DAE is the apex body for the management of HBNI. **Academic Council** chaired by Vice Chancellor, HBNI manages the academic issues and functions of the institute on the advice of the **Board of Studies** which has been constituted for each major discipline and has representatives from all CIs and OCC as well as experts from other reputed Indian institutes.To manage the affairs of the HBNI, each CI has one or more **Deans (Academic) Standing Committee of Deans chaired by VC, HBNI** and comprising of Dean, HBNI, Associate Deans at HBNI, Deans (Academic) from all the institutions, ensures harmony in the processes. CIs have also established a robust framework of admission to different academic programmes by **Standing Academic Committee**.

The Council of Management is the prime body for the management of the Institute.

<div style="border:1px solid black">

Council of Management (CoM)
(As on July 31, 2023)

Prof. A. K. Mohanty, Secretary DAE & Chairman, AEC	**Chairman**
Prof. U. Kamachi Mudali, Vice Chancellor	Member
Shri Talleen Kumar, Member (Finance), AEC	Member
Prof. A. K. Mohanty, Director, BARC	Member
Prof. B. Venkatraman, Director, IGCAR	Member
Prof. R. A. Badwe, Director, TMC	Member
Prof. Sudhakar Panda, Director, NISER	Member
Prof. Surendra Prasad, Former Chairman NBA & Former Director, IIT Delhi	Member
Prof. Mustansir Barma, Professor Emeritus, TIFR Centre for Inter-Disciplinary Sciences, Hyderabad	Member
Shri S. S. Sandhu, IAS, Additional Secretary, Department of Higher Education, MHRD, New Delhi	Member
Prof. P. D. Naik, Dean, HBNI	Member
Prof. P. C. Selvin, Registrar, HBNI	Secretary

</div>

Academic Council
(As on July 31, 2023)

Prof. U. Kamachi Mudali, Vice Chancellor	**Chairperson**
Prof. A. K. Mohanty, Director, BARC	Member
Prof. B. Venkatraman, Director, IGCAR	Member
Prof. R. A. Badwe, Director, TMC	Member
Prof. Sudhakar Panda, Director, NISER	Member
Prof. S. M. Yusuf, Director, IoP	Member
Shri S. V. Nakhe, Director, RRCAT	Member
Dr. Sumit Som, Director, VECC	Member
Prof. Shashank Chaturvedi, Director, IPR	Member
Prof. Gautam Bhattacharyya, Director, SINP	Member
Prof. Pinaki Majumdar, Director, HRI	Member
Prof. V. Arvind/Prof. V. Ravindran, Director, IMSc	Member
Prof. Indranil Manna, IIT Kharagpur	Member
Prof. Kannan N. Iyer, IIT Bombay	Member
Prof. E. D. Jemmis, IISc, Bangalore	Member
Prof. Shishir Deshpande, Director, ITER-IPR	Member
Prof. P. K. Pujari/Prof. Vivekanand Kain, BARC	Member
Prof. P. D. Naik, Dean, HBNI	Member
Prof. R. B. Grover, Convenor, BoS (Applied Systems Analysis)	Member
Prof. S. M. Yusuf, Convenor, BoS (Physical Sciences)	Member
Prof. A. P. Tiwari, Convenor, BoS (Engineering Sciences)	Member
Prof. Prasanna Venkatraman, Convenor, BoS (Life Sciences)	Member
Prof. Meena Mahajan, Convenor, BoS (Mathematical Sciences)	Member
Prof. S. D. Banavali, Convenor, BoS (Medical & Health Sciences)	Member
Prof. S. Kannan, Convenor, BoS (Chemical Sciences)	Member
Prof. Bedangadas Mohanty, Convenor, BoS (Integrated Masters Programme)	Member
Prof. P. C. Selvin, Registrar, HBNI	Secretary

Advisory Committee

Secretary, DAE and Chairman, AEC	**Chairman**
Vice Chancellor, HBNI	Member
Director, BARC	Member
Director, IGCAR	Member
Director, RRCAT	Member
Director, VECC	Member
Director, IPR	Member
Director, SINP	Member
Director, TMC	Member
Director, IMSc	Member
Director, TIFR	Member
Director, NISER	Member
Director, HRI	Member
Director, IOP	Member
Dean, HBNI	Member-Secretary

Officers of the Institute
(As on July 31, 2023)

Academic		Administrative	
Prof. U. Kamachi Mudali	Vice Chancellor	Prof. P. C. Selvin	Registrar
Prof. P. D. Naik	Dean	Smt. Bharati Suwarna	Administrative Officer-III
Prof. D. K. Maity	Associate Dean	Smt. Neeta Rathod	Assistant Registrar
Prof. D. Dutta	Associate Dean	Shri S. Jakhotia	Finance Officer
Prof. Naveen Kumar	Associate Dean		
Prof. B. K. Nayak	Associate Dean		
Prof. H. Pal	Associate Dean		
Prof. Sunil Ghosh	Associate Dean		

Board of Studies of HBNI
(As on July 31, 2023)

❖ **BoS (Chemical Sciences)**
1. Prof. P. K. Mohapatra, BARC - Convener
2. Prof. V. Sudarsan, BARC - Co-Convener
3. Prof. A. Dutta, IIT, Bombay
4. Prof. A. Srinivasan, NISER
5. Prof. D. K. Maity, HBNI
6. Prof. K. A. Venkatesan, IGCAR
7. Prof. Tapas Das, BARC
8. Prof. H. S. Biswal, NISER
9. Prof. Deepa Khushalani, TIFR
10. Prof. Avinash Kumbhar, SPPU

Balancing Members:
1. Prof. B. S. Patro, BARC

❖ **BoS (Engineering Sciences)**
1. Prof. R. Tewari, BARC-Convener
2. Prof. J. Chattopadhyay, BARC
   Co-Convener
3. Prof. S. Dikshit, BARC
4. Prof. V. G. Gaikar, ICT
5. Prof. C. P. Paul, RRCAT
6. Prof. P. Y. Nabhiraj, VECC
7. Prof. S. K. Pathak, IPR
8. Prof. Anish Kumar, IGCAR

Balancing Members:
1. Prof. Gopika Vinod, VECC
2. Prof. A. K. Dureja, BARC

❖ **BoS (Medical & Health Sciences)**
1. Prof. S. D. Banavali, TMC – Convener
2. Prof. Sandeep Basu, RMC-Co-Convener
3. Prof. Sudeep Gupta, Director ACTREC, TMC
4. Dr. Nithya Gogtay, KEM Hospital, Mumbai
5. Dr. Ashutoshnath Agarwal, PGIMER, Chandigarh
6. Dr. Manisha Pawar, TMH
7. Prof. Siddhartha Laskar, TMC
8. Dr. Ajay Puri, TMC
9. Dr. J. P. Agarwal, TMC

10. Dr. Suyash Kulkarni, TMC

Balancing Members:
1. Dr. Rajesh Kinhikar, TMC
2. Prof. D. K. Maity, HBNI

❖ **BoS (Life Sciences)**
1. Prof. Partha Saha, SINP - Convener
2. Prof. S. Gautam, BARC - Co-Convener
3. Prof. Praful Singru, SBS, NISER
4. Prof. Rahul Siddharthan, IMSc
5. Prof. Sorab Dalal, ACTREC
6. Prof. Harapriya Mohaptra, NISER
7. Prof. B. S. Patro, BARC
8. Prof. B. N. Pandey, BARC
9. Prof. Y. V. Nancharaiah, IGCAR
10. Prof. Sharmila Bapat, NCCS, Pune

Balancing Members:
1. Prof. Shovan Majumder, RRCAT
2. Prof. Sunil K. Ghosh, HBNI
3. Prof. D. K. Maity, HBNI

❖ **BoS (Mathematical Sciences)**
1. Prof. Meena Mahajan, IMSc - Convener
2. Prof. D. Surya Ramana, HRI
   Co-Convener
3. Prof. Anish Ghosh, TIFR, Mumbai
4. Prof. K. Sandeep, TIFR, Bengaluru
5. Prof. Jugal K. Verma, IIT Bombay
6. Prof. B. Sury, ISI, Bengaluru
7. Prof. K. N. Raghavan, IMSc
8. Prof. K. V. Subrahmanyam, CMI-Chennai
9. Prof. Brundaban Sahu, NISER

Balancing Members:
1. Prof. B. K. Nayak, HBNI
2. Prof. D. Dutta, HBNI

❖ **BoS (Physical Sciences)**
1. Prof. B. Mohanty, NISER -Convener
2. Prof. V. K. Aswal, BARC -Co-Convener
3. Prof. Anushuman Maharana, HRI
4. Prof. Awadesh Mani, IGCAR

5. Prof. D. Indumathi, IMSc
6. Prof. Biju Raja Sekhar, IoP
7. Prof. Sudip Sengupta, IPR
8. Prof. Shovan Majumder, RRCAT
9. Prof. Gopal Mukherjee, VECC
10. Prof. Kumar Sankar Gupta, SINP

Balancing Members:

1. Prof. B. K. Nayak, HBNI
2. Prof. D. Dutta, HBNI

❖ **BoS (Applied Systems Analysis)**

1. Prof. R. B. Grover, HBNI-Convener
2. Prof. Pranay Swain, NISER
   Co-Convener
3. Prof. Karuna Jain, IIT Bombay
4. Prof. A. K. Dureja, BARC
5. Prof. Surinder Jaswal, TISS
6. Prof. Amit Garg, IIM Ahmedabad
7. Prof. P. K. Mohapatra, BARC
8. Prof. A. K. Nayak, NCPW
9. Prof. Garima Sharma, NCPW

❖ **BoS (Integrated Masters Programme)**

1. Prof. C. Gunanathan, NISER - Convener
2. Prof. Pranay Swain, NISER
   Co-Convener
3. Chair, School of Life Sciences, NISER (Ex-Officio)
4. Chair, School of Chemical Sciences, NISER (Ex-Officio)
5. Chair, School of Mathematics, NISER (Ex-Officio)
6. Chair, School of Physical Sciences, NISER (Ex-Officio)
7. Chair, School of Undergraduate Studies Committee, NISER (Ex-Officio)
8. Prof. Anirban Basu, HRI
9. Prof. B. R. Sekhar, IoP
10. Prof. Sujit Roy, IIT Bhubaneswar

Balancing Members:

1. Prof. D. Dutta, HBNI
2. Prof. Meena Mahajan, IMSc
3. Prof. Partha Saha, SINP

Deans (Academic) at Constituent Institutions (CIs)/Off-Campus Centre (OCC)
(As on July 31, 2023)

S. No.	Name of the CI/Off-campus centre	Discipline	Name of the Dean Academic
1.	Bhabha Atomic Research Centre	Life Sciences	Prof. B. S. Patro
		Chemical Sciences	Prof. C. N. Patra
		Physical & Mathematical Sciences	Prof. Dinesh Udupa
		Engineering Sciences Stream-I	Prof. Sulekha Mukhopadhyay
		Engineering Sciences Stream-II	Prof. Gopika Vinod
		Medical & Health Sciences	Prof. Sandip Basu
2.	Indira Gandhi Centre for Atomic Research	Chemical Sciences	Prof. C. V. S. B. Rao
		Physical Sciences	Prof. Awadesh Mani
		Engineering Sciences	Prof. Anish Kumar
3.	Raja Ramanna Centre for Advanced Technology	All Disciplines	Prof. S. R. Mishra
4.	Variable Energy Cyclotron Centre	Physical Sciences	Prof. Parnika Das
		Engineering Sciences	Prof. P. Y. Nabhiraj
5.	Saha Institute of Nuclear Physics	Chemical & Life Sciences	Prof. Partha Saha
		Physical Sciences	Prof. Harvendra Singh
6.	Institute for Plasma Research	All Disciplines	Prof. Mainak Bandopadhyay
7.	Institute of Physics	Physical Sciences	Prof. Arijit Saha
8.	Institute of Mathematical Sciences	Mathematical Sciences	Prof. K. Srinivas
		Physical Sciences	Prof. P. Rajesh
		Life Sciences	Prof. Sitabhra Sinha
9.	Harish-Chandra Research Institute	All Disciplines	Prof. Manoj Kumar
10.	Tata Memorial Centre	All Disciplines	Prof. Shripad Banavali
11.	National Institute of Science Education and Research	All Disciplines	Prof. Pranay Swain

HBNI

1.	Prof. U. Kamachi Mudali
2.	Prof. Prakash Dattatray Naik
3.	Prof. Ravi Bhushan Grover
4.	Prof. Jyeshtharaj Bhalchandra Joshi
5.	Prof. Dilip K. Maity
6.	Prof. Haridas Pal
7.	Prof. Sunil Kumar Ghosh
8.	Prof. B. K. Nayak
9.	Prof. Dilip K. Maity
10.	Prof. D. Dutta
11.	Prof. Naveen Kumar

BARC

❖ Chemical Sciences

12.	Prof. A. C. Bhasikuttan
13.	Prof. A. K. Tyagi
14.	Prof. Arya Ashok Kumar
15.	Prof. Awadhesh Kumar
16.	Prof. Prasanta Kumar Mohapatra
17.	Prof. S. Kannan
18.	Prof. Sharmila Banerjee
19.	Prof. Tapan Kumar Ghanty
20.	Prof. A. K. Tripathi
21.	Prof. A. L. Rufus
22.	Prof. A. C. Bhasikuttan
23.	Prof. A. C. Sahayam
24.	Prof. Chiranjib Majumder
25.	Prof. Hari Prasad Upadhyaya
26.	Prof. P. A. Hassan
27.	Prof. Hirendra Nath Ghosh
28.	Prof. Jyotirmayee Mohanty
29.	Prof. K. Dash
30.	Prof. Niharendu Choudhury
31.	Prof. M. C. Rath
32.	Prof. Patra Chandra Nath
33.	Prof. R. Mishra
34.	Prof. Raghunath Acharya
35.	Prof. Rajesh V. Pai
36.	Prof. Rakesh Kumar Singhal

37.	Prof. S. K. Jha
38.	Prof. S. N. Achary
39.	Prof. Salil Verma
40.	Prof. Sangita D Kumar
41.	Prof. Soumyakanti Adhikari
42.	Prof. Sreenivas T.
43.	Prof. Subir Kumar Ghosh
44.	Prof. Sudarsan V.
45.	Prof. Sukhendu Nath
46.	Prof. Suresh C. Parida
47.	Prof. Tapas Das
48.	Prof. Tusar Bandyopadhyay
49.	Prof. Y. K. Bhardwaj
50.	Dr. A Jahur Mondal
51.	Dr. Adya Prasad Mishra
52.	Dr. Ajay K. Singh
53.	Dr. Amit Kunwar
54.	Dr. Anshu Singhal
55.	Dr. Anupkumar B.
56.	Dr. Aparna Banerjee
57.	Dr. Aruna Korde
58.	Dr. Arunasis Bhattacharyya
59.	Dr. Arup Kumar Pathak
60.	Dr. Ashis Kumar Satpati
61.	Dr. Asim Kumar Ghosh
62.	Dr. Atanu BArik
63.	Dr. Dayamoy Banerjee
64.	Dr. Dhandeep Dutta
65.	Dr. Dhurva Kumar Singh
66.	Dr. Dimple Dutta
67.	Dr. Drishty Satpati
68.	Dr. Gunjan Verma
69.	Dr. Hemant Shivram Sodaye
70.	Dr. Jayshree Ramkumar
71.	Dr. Jyotirmayee Mohanty
72.	Dr. Kallola Kumar Swain
73.	Dr. Kedarnath G.
74.	Dr. Kumar Abhinav Dubey
75.	Dr. Madhava B Mallia
76.	Dr. Madhumita Goswami

77.	Dr. Mainak Roy		120.	Dr. Arnab Sarkar
78.	Dr. Manidipa Basu		121.	Dr. Atindra Banerjee
79.	Dr. Manoj Kumbhakar		122.	Dr. Balaji Prasad Mandal
80.	Dr. Manoj Mohapatra		123.	Dr. Beena G. Singh
81.	Dr. Mrinal R. Pai		124.	Dr. Biswajit Sadhu
82.	Dr. Musharaf Ali S. K.		125.	Dr. Brindaban Modak
83.	Dr. N. N. Meeravli		126.	Dr. Chhavi Agarwal
84.	Dr. Naina Raje		127.	Dr. Debasis Banerjee
85.	Dr. Nandita Maiti		128.	Dr. Dibakar Goswami
86.	Dr. Neetika Rawat		129.	Dr. Hirakendu Basu
87.	Dr. P. S. Ramanjaneyulu		130.	Dr. J. Selvakumar
88.	Dr. P. Mathi		131.	Dr. Jayashree Biswal
89.	Dr. Prabhat Kumar Singh		132.	Dr. Jyoti Prakash
90.	Dr. Pradeep Kumar		133.	Dr. K. C. Barick
91.	Dr. Pramod Sharma		134.	Dr. K. R. S. Chandrakumar
92.	Dr. R. Ganguly		135.	Dr. Mahesh Sundararajan
93.	Dr. Rahul Tripathi		136.	Dr. Mahesh Tiwari
94.	Dr. Ritu M Srivastava		137.	Dr. Malaya Kumar Nayak
95.	Dr. Rubel Chakravarty		138.	Dr. Manjulata Saha
96.	Dr. S. Jayakumar		139.	Dr. Manoj Kumar Sharma
97.	Dr. Sandeep Nigam		140.	Dr. Mhejabeen Sayed
98.	Dr. Sandip Dey		141.	Dr. Mohini Guleria
99.	Dr. Sanjukta A Kumar		142.	Dr. Nilanjal Misra
100.	Dr. Sharmishtha Dutta Choudhury		143.	Dr. Nilotoal Barooah
101.	Dr. Shilpa N Sawant		144.	Dr. N. R. Singh
102.	Dr. Sipra Choudhury		145.	Dr. P. Chandramohan
103.	Dr. Soumyaditya Mula		146.	Dr. Pankaj Kumar Patro
104.	Dr. Suchandra Chatterjee		147.	Dr. Prasad Padmakar Phadnis
105.	Dr. Suchismita Mishra		148.	Dr. Priya Maheshwari
106.	Dr. Sudarshan Kathi		149.	Dr. Raghunath Chowdhury
107.	Dr. Sumit Kumar		150.	Dr. Rajib Ghosh
108.	Dr. Suparna Sodaye		151.	Dr. Ritesh Ruhela
109.	Dr. Tirumalesh Keesari		152.	Dr. Ruma Gupta
110.	Dr. Usha Pandey		153.	Dr. Sabyasachhi Rout
111.	Dr. Vandana Pulhani		154.	Dr. Sajeev Y.
112.	Dr. Veena Subramanian		155.	Dr. Sandeep Kumar Sharma
113.	Dr. Vinita Grover Gupta		156.	Dr. Sangita D. Lenka
114.	Dr. Virendra Kumar		157.	Dr. Sanhita Chaudhury
115.	Dr. Aishwarya Soumitra Kar		158.	Dr. Sanjay Kumar
116.	Dr. Ajish Kumar K. S.		159.	Dr. Santosh Kumar Gupta
117.	Dr. Ankita Rao		160.	Dr. Saurav Kumar Guin
118.	Dr. Apurav Guleria		161.	Dr. Seemita Banerjee
119.	Dr. Arijit Sengupta		162.	Dr. Seraj Ahmad Ansari

163.	Dr. Srinivasu Kancharlapalli
164.	Dr. Soumyaditya Mula
165.	Dr. Sumana Sengupta
166.	Dr. Surajit Panja
167.	Dr. Tijo Joseph V.

❖ Engineering Sciences

168.	Prof. Akhilanand Pati Tiwari
169.	Prof. Archana Sharma
170.	Prof. Arun Kumar Nayak
171.	Prof. Deb Mukhopadhyay
172.	Prof. Gopal Joshi
173.	Prof. Gopalakrishnan Sugilal
174.	Prof. Jayanta Chattaopadhyay
175.	Prof. N. K. Maheshwari
176.	Prof. Prabhakar V. Varde
177.	Prof. Raghvendra Tewari
178.	Prof. Ram Nivas Singh
179.	Prof. Siddaratha Mukhopadhyay
180.	Prof. Soumitra Kar
181.	Prof. Vivekanand Kain
182.	Prof. A. Vinod Kumar
183.	Prof. A. K. Dureja
184.	Prof. Alok Awasthi
185.	Prof. Amit Sinha
186.	Prof. Aniruddha Biswas
187.	Prof. Anita Vinay Topkar
188.	Prof. Betty C. A.
189.	Prof. Biswaranjan Dikshit
190.	Prof. D. Mandal
191.	Prof. D. C. Kar
192.	Prof. Deep Prakash
193.	Prof. Dinesh Kumar Chandraker
194.	Prof. Gopika Vinod
195.	Prof. Joydipta Banerjee
196.	Prof. Jung Bahadur Singh
197.	Prof. Kapilesh Bhargava
198.	Prof. Kulwant Singh
199.	Porf. M. K. Samal
200.	Prof. Namita Maiti
201.	Prof. Paritosh Prabhakar Nanekar.
202.	Prof. R. K. Bajpai
203.	Prof. Rajeev Kapoor
204.	Prof. S. K. Satpati

205.	Prof. S. R. Shimijith
206.	Prof. Samiran Sengupta
207.	Prof. Sudipta Chakraborty
208.	Prof. Sulekha Mukhopadhyay
209.	Prof. Suneel Kumar Gupta
210.	Prof. Supratik Roychowdhury
211.	Prof. Tarasankar Mahata
212.	Prof. Tessy Vincent
213.	Prof. V. H. Patankar
214.	Prof. Yogita Parulekar
215.	Dr. Abhijeet Mohan Vaidya
216.	Dr. Anil Kumar Tiwari
217.	Dr. Anindya Chakravarty
218.	Dr. Arijit Laik
219.	Dr. Chiradeep C Gupta
220.	Dr. Debanik Roy
221.	Dr. Gaurav Bhutani
222.	Dr. Imran Ali Khan
223.	Dr. K. K. Singh
224.	Dr. Kamal Sharma
225.	Dr. Kamlesh Chandra
226.	Dr. Kinshuk Dasgupta
227.	Dr. Maha Nand Jha
228.	Dr. Noble Jacob
229.	Dr. Pranesh Sengupta
230.	Dr. Praveen Kumar
231.	Dr. R Karthikeyan
232.	Dr. Ranjan Kumar
233.	Dr. Rishi Verma
234.	Dr. Sanjib Majumdar
235.	Dr. Soumitra Kar
236.	Dr. Suman Neogy
237.	Dr. Surender Kumar Sharma
238.	Dr. T. Sree Rama Chandra Murthy
239.	Dr. Abhijit Raha
240.	Dr. Bhaskar Paul
241.	Dr. Nirvik Sen
242.	Dr. Onkar Suresh Gokhale
243.	Dr. Sabyasachi Mitra
244.	Dr. Sangeeta Pal
245.	Dr. Vishwanadh Bathula

❖ Life Sciences

246.	Prof. Anand Ballal

247.	Prof. B. N. Pandey		290.	Dr. Suvendu Mondal
248.	Prof. Bhavani S. Shankar		291.	Dr. Sweetie R. Kanatt
249.	Prof. Birajalaxmi Das		292.	Dr. Vishal Prashar
250.	Prof. Briija Sankar Patro		293.	Dr. Vishwas M Kulkarni
251.	Prof. Hema Rajaram		294.	Dr. Yogendra Singh Rajpurohit
252.	Prof. Joy G. Manjeya		295.	Dr. Amit Kumar
253.	Prof. Mahesh Subramanian		296.	Dr. Archana N. Rai
254.	Prof. Prasun Kumar Mukherjee		297.	Dr. Avik Chakraborty
255.	Prof. Ravindra D. Makde		298.	Dr. Celin Acharya
256.	Prof. Sandur Santosh Kumar		299.	Dr. Dharmendra Kumar Maurya
257.	Prof. Satyendra Gautam		300.	Dr. Hiren Joshi
258.	Prof. Savita Kulkarni		301.	Dr. Jayakumar Sundarraj
259.	Prof. Toleti Subba Rao		302.	Dr. Jyoti Tripathi
260.	Prof. Y. V. Nancharaiah		303.	Dr. Manisha Banerjee
261.	Dr. Ajay Saini		304.	Dr. Murali M S Balla
262.	Dr. Amit Das		305.	Dr. P Sriyutha Murthy
263.	Dr. Anand M Badigannavar		306.	Dr. Promod umar Gupta
264.	Dr. Anu Ghosh		307.	Dr. Rachna Agarwal
265.	Dr. Archana Joshi Saha		308.	Dr. Rahul Checkar
266.	Dr. Archana Mukherjee		309.	Dr. S. T. Mehetre
267.	Dr. Aruna Jyothi Kora		310.	Dr. Sachin Nandkumar Hajare
268.	Dr. Ashish Kumar Srivastava		311.	Dr. Shraddha Singh
269.	Dr. B. K. Das		312.	Dr. Sonia Chadha
270.	Dr. Bhakti Basu		313.	Dr. Sudhir Kumar Gupta
271.	Dr. Bhaskar Sanyal		314.	Dr. Sudhir Kumar Shukla
272.	Dr. B. B. Mishra		315.	Dr. Sumit Gupta
273.	Dr. Deepak Sharma		316.	Dr. Swathi Kota
274.	Dr. Gagan Deep Gupta		317.	Dr. Vandan Nagar
275.	Dr. Himanshi N. Mishra		318.	Dr. Vinay Jain
276.	Dr. J. Souframanien		❖ **Medical & Health Sciences**	
277.	Dr. Jitendra Kumar		319.	Prof. A. J. Khandekar
278.	Dr. Nagesh Bhat		320.	Prof. Anita Gadgil
279.	Dr. R. Shashidhar		321.	Prof. Gaurav Malhotra
280.	Dr. Rajani Kant Chittela		322.	Prof. R. V. Jadhav
281.	Dr. Rajesh Kumar		323.	Dr. Rahul Vithalrao Parghane
282.	Dr. Ramesh Hire		324.	Prof. Sandip Basu
283.	Dr. Rath Devashish		325.	Dr. Ashwini Kalshetty
284.	Dr. S. N. Jamdar		326.	Dr. J. G. Kalbhande
285.	Dr. S. P. Chawla		327.	Dr. Priyanka Verma
286.	Dr. S. N. Hajare		328.	Dr. Satish C. Mishra
287.	Dr. Sheetal Uppal		329.	Dr. Sunil Dutta Sharma
288.	Dr. S. C. Bihani		330.	Dr. Sunita Nitin Sonavane
289.	Dr. Sudhir Singh		331.	Dr. Sushmita Rath

332. Dr. Yogesh K. Shejul	374. Prof. Srikumar Ghorui
333. Dr. Basant L. Malpani	375. Prof. Subhankur Mitra
❖ **Physical Sciences**	376. Prof. Sudhir Ranjan Jain
334. Prof. Dinesh Kumar Aswal	377. Prof. T Palani Selvam
335. Prof. Kannan Umasankari	378. Prof. Tej Singh
336. Prof. S. M. Yusuf	379. Prof. V. Jha
337. Prof. Srinivas Krishnagopal	380. Dr. A. K. Rajarajan
338. Prof. V. K. Aswal	381. Dr. Ajay Kumar Mishra
339. Prof. Vinay Bhaskar Chandratre	382. Dr. Ajay Singh
340. Prof. A. K. Debnath	383. Dr. Amit Kumar
341. Prof. A. K. Gupta	384. Dr. Amitava Roy
342. Prof. Abhas Kumar Mitra	385. Dr. Aparna Shastri
343. Prof. Aditi Ray	386. Dr. Arup Biswas
344. Prof. Alka B. Garg	387. Dr. Asavari Santosh Dhavale
345. Prof. Amitabh Das	388. Dr. Asawari D Rath
346. Prof. Anil Kumar Chauhan	389. Dr. Ashok Kumar Bakshi
347. Prof. Aniruddha Kumar	390. Dr. Ashok Kumar Verma
348. Prof. Anurag Gupta	391. Dr. Bhushan Dhabekar
349. Prof. Aradhana Shrivastava	392. Dr. Biplab Ghosh
350. Prof. B. K. Sapra	393. Dr. Brahmananda Chakraborty
351. Prof. B. N. Rajasekhar	394. Dr. C. D. Sijoy
352. Prof. Debabrata Biswas	395. Dr. Chitra Murli
353. Prof. Debasis Sen	396. Dr. D. R. Mishra
354. Prof. Dibyendu Bhattacharyya	397. Dr. Debarati Bhattacharya
355. Prof. Dinesh Venkatesh Udupa	398. Dr. G. Sridhar
356. Prof. Divakar K Rao	399. Dr. Himanshu Kumar Poswal
357. Prof. J. Padma Nilaya	400. Dr. Jayanta Mondal
358. Prof. K. K. Yadav	401. Dr. Keka R. Chakraborty
359. Prof. Keshaw D. Joshi	402. Dr. Krishan Kumar Pandey
360. Prof. Kripamay Mahata	403. Dr. Manoj Kumar Warrier
361. Prof. Lalit Mohan Pant	404. Dr. Mayank Shukla
362. Prof. M. V. Suryanarayana	405. Dr. Munish Kumar
363. Prof. Mala N Rao	406. Dr. Paritosh Modak
364. Prof. Mukesh Kumar	407. Dr. Partha Sarathi Sarkar
365. Prof. Mukund Shrinivas Kulkarni	408. Dr. Prakash Chandra Rout
366. Prof. N. Padma	409. Dr. Pratap Baburao Wagh
367. Prof. Nandini Garg	410. Dr. Priyamvada M. Dighe
368. Prof. P U Sastry	411. Dr. Raghwendra Kumar
369. Prof. Prashant Shukla	412. Dr. Rajeev Kumar
370. Prof. Ranjan Mittal	413. Dr. Rajul Ranjan Choudhury
371. Prof. Rekha Rao	414. Dr. Ramesh Chandra Das
372. Prof. Satyaranjan Santra	415. Dr. Renju George Thomas
373. Prof. Shambhu Nath Jha	416. Dr. Rohit Shukla

417.	Dr. S. Anand	460.	Dr. R. B. Tokas
418.	Dr. Sanjay Kumar Sahu	461.	Dr. Rajib Kar
419.	Dr. Sanjay V. Thakare	462.	Dr. Ranita Basu
420.	Dr. Santanu Bera	463.	Dr. Rosaline Mishra
421.	Dr. Shashwati Sen Yeram	464.	Dr. S. P. Tripathy
422.	Dr. Soumen Bhattacharyya	465.	Dr. Sanjay Kumar Mishra
423.	Dr. Subir Bhattacharyya	466.	Dr. Shankar Prasad Koiry
424.	Dr. Sukanta Karmakar	467.	Dr. Shiv Govind Singh
425.	Dr. Surendra Singh	468.	Dr. Shivanand Chaurasia
426.	Dr. Swapan Das	469.	Dr. Shovit Bhattacharya
427.	Dr. Swarupananda Pradhan	470.	Dr. Somsundar Mukhopadhyay
428.	Dr. T. Jayasekharan	471.	Dr. Sugam Kumar
429.	Dr. Venkata Ramana Ikkurthi	472.	Dr. Sunit Kedia
430.	Dr. Vinod Singh Rawat	473.	Dr. V. V. Parkar
431.	Dr. Vir Krishen Dhar	474.	Dr. Veerendra Kumar Sharma
432.	Dr. Yogesh K. Gupta	475.	Dr. Vibha Saxena
433.	Dr. Yogesh Kashyap	476.	Dr. Vinayak Mishra
434.	Dr. Amit P Srivastava	477.	Dr. Yogesh K Gupta
435.	Dr. Amit Verma	**IGCAR**	
436.	Dr. Anil Jain	❖ **Chemical Sciences**	
437.	Dr. Anup Kumar Bera	478.	Prof. A. Suresh
438.	Dr. Apu Sarkar	479.	Dr. C. V. S. Brahmmananda Rao
439.	Dr. Ashish Kumar Agrawal	480.	Prof. K. A. Venkatesan
440.	Dr. B. Sunder Sahayanathan	481.	Prof. K. Ananthasivan
441.	Dr. Babita Tiwari	482.	Prof. N. Sivaraman
442.	Dr. Debjani Karmakar	483.	Prof. R. V. Subbarao
443.	Dr. Giri Dhari Patra	484.	Prof. R. Kumar
444.	Dr. Goutam Dev Mukherjee	485.	Prof. Rajesh Ganesan
445.	Dr. H. Kumawat	486.	Prof. V. Jayaraman
446.	Dr. Himal Bhatt	487.	Dr. Durairaj Onraju
447.	Dr. Jitendra Bahadur	488.	Dr. K. I. Gnanasekar
448.	Dr. Kiran R. M.	489.	Dr. K. Sundararajan
449.	Dr. Krishna Kumar Singh	490.	Dr. N. Ramanathan
450.	Dr. Manmeet Kaur	491.	Dr. Puspalata Rajesh
451.	Dr. Mayanak Kumar Gupta	492.	Dr. Sublime Ningshen
452.	Dr. Mohit Tyagi	493.	Dr. A. Sree Rama Murthy
453.	Dr. Niranjan Suryakant Ramgir	494.	Dr. Arindam Das
454.	Dr. Nishant Chaudhary	495.	Dr. Ashish Jain
455.	Dr. Param Jeet Singh	496.	Dr. B. Anandkumar
456.	Dr. Parasmani Rajput	497.	Dr. B. Sreenivasulu
457.	Dr. Parth Sarathi Ghosh	498.	Dr. Chowdari Jagadeeswara Rao
458.	Dr. Pramod Bhatt	499.	Dr. G. Gopakumar
459.	Dr. Purushottam Jha	500.	Dr. Hrudananda Jena

501.	Dr. Pavan Kumar Narayanam
502.	Dr. R. Kumaresan
503.	Dr R Venkata Krishnan
504.	Dr. Satendra Kumar

❖ **Engineering Sciences**

505.	Prof. B. P. C. Rao
506.	Prof. A. John Arul
507.	Prof. Aniruddha Moitra
508.	Prof. Anish Kumar
509.	Prof. M. Vasudevan
510.	Prof. V. Karthik
511.	Dr. A. Nagesha
512.	Dr. A. Jasmin Sudha
513.	Dr. C. Sudha
514.	Dr. Chitta Ranjan Das
515.	Dr. Mahadevan S.
516.	Dr. P Mangarjuna Rao
517.	Dr. R. Mythili
518.	Dr. V. S Srinivasan
519.	Dr. Vani Shankar
520.	Dr. A. Ravi Shankar
521.	Dr. B. Arivazhagan
522.	Dr. David Vijayanand V
523.	Dr. Diptimayee Samantaray
524.	Dr. G. V. Prasad Reddy

❖ **Physical Sciences**

525.	Prof. B. Venkataman
526.	Prof. G. Amarendra
527.	Prof. Ramachandran Divakar
528.	Prof. Arup Dasgupta
529.	Prof. Awadhesh Mani
530.	Prof. C. Venkata Srinivas
531.	Prof. Christopher David
532.	Prof. John Philip
533.	Prof. K. Devan
534.	Prof. N. Subramanian
535.	Prof. N. V. Chandra Shekar
536.	Prof. R. Govindaraj
537.	Prof. R. Rajaraman
538.	Prof. Sandip Kumar Dhara
539.	Prof. T. R. Ravindran
540.	Dr. B. Sundaravel
541.	Dr. Nithya Ravindran

542.	Dr. Parthasarathi Gangopadhyay
543.	Dr. R. Ramaseshan
544.	Dr. S. Amirthapandian
545.	Dr. S. Tripura Sundari
546.	Dr. S. Ganesamoorthy
547.	Dr. Sharat Chandra
548.	Dr. V. Sivasubramanian
549.	Dr. V. Subramanian
550.	Dr. Amit Kumar
551.	Dr. Anees P.
552.	Dr. Arun K. Prasad
553.	Dr. Barid Baran Lahiri
554.	Dr. Chanchal Ghosh
556.	Dr. Dipak Kumar Baisnab
557.	Dr. Edward Prabu Amaladass
558.	Dr. Haraprasanna Tripathy
559.	Dr. K. Ganesan
560.	Dr. K. Prabhakar
561.	Dr. N. R. Sanjay Kumar
562.	Dr. O. Annalakshmi
563.	Dr. Rajendra Ganpat Joshi
564.	Dr. Ramanathaswamy Pandian
565.	Dr. Ravi Chinnappan
566.	Dr. S. Abhaya
567.	Dr. S. C. Vanithakumari
568.	Dr. Sainath G.
569.	Dr. Syamalarao Polaki
570.	Dr. T. Sathyanarayana Annam
571.	Dr. Vinod K.

RRCAT

❖ **Chemical Sciences**

572.	Dr. Dipankar Nanda

❖ **Engineering Sciences**

573.	Prof. Christ Prakash Paul
574.	Prof. Mangesh Balkrishna Borage
575.	Prof. Ajit Upadhyay
576.	Dr. Prabhat Kumar Gupta
577.	Dr. Vikas Kumar Jain
578.	Dr. Rahul Shukla

❖**Life Sciences**

579.	Prof. Alok Dube
580.	Dr.Khageshwar Sahu. Alok Dube
581.	Dr. Rashni Shrivastava

❖ Physical Sciences

582.	Prof. Kushvinder Singh Bindra
583.	Prof. Anand Moorti
584.	Prof. Aparna Chakrabarti
585.	Prof. Arup Banerjee
586.	Dr. Gurvinderjit Singh
587.	Dr. Indranil Bhaumik
588.	Prof. J. A. Chakera
589.	Prof. M. K. Chattopadhyay
590.	Prof. Mohammed Hussein Modi
591.	Prof. Mukesh Joshi
592.	Prof. Om Prakash
593.	Prof. Sanjay Kumar Rai
594.	Prof. Satya Ram Mishra
595.	Prof. Shovan K Majumder
596.	Prof. Sudhir Kumar Dixit
597.	Prof. Suni Verma
598.	Prof. Tapas Ganguli
599.	Prof. Tarun Kumar Sharma
600.	Prof. Vibhuti Bhushan Tiwari
601.	Prof. Vinit Kumar
602.	Dr. Arvind Kumar Srivastava
603.	Dr. Avnish K Sharma
604.	Dr. Brahma Nand Upadhyaya
605.	Dr. Chandrachur Mukherjee
606.	Dr. Haranath Ghosh
607.	Dr. J. Jayabalan
608.	Dr. Maheswar Nayak
609.	Dr. Manoj Kumar Tiwari
610.	Dr. Manoranjan Prasad Singh
611.	Dr. P K Mukhopadhyay
612.	Dr. Pankaj Misra
613.	Dr. Rajeev Bhatt
614.	Dr. Raktim Dasgupta
615.	Dr. Ramakanta Biswal
616.	Dr. Shreyashkar Dev Singh
617.	Dr. Srinibas Satapathy
618.	Dr. Surya Mohan Gupta
619.	Dr. Vijay Kumar Dixit
620.	Dr. Yogesh Verma
621.	Dr. Archana Sagdeo
622.	Dr. Arun Kumar Rai
623.	Dr. C. Kamal

624.	Dr. Chandra Pal Singh
625.	Dr. Himanshu Singhal
626.	Dr. Himanshu Srivastava
627.	Dr. L S Sharath Chandra
628.	Dr. Manoj Kumar Singh
629.	Dr. Pooja Gupta
630.	Dr. Pragya Tiwari
631.	Dr. Ravindra Jangir
632.	Dr. Sachin Kumar Srivastava
633.	Dr. Salahuddin Khan
634.	Dr. Sanyasi Rao Bobbili
635.	Dr. Shailesh Kumar Khamari
636.	Dr. Shankar Lal
637.	Dr. Soma Banik
638.	Dr. Suparna Pal
639.	Dr. Uday Chakravarty
640.	Dr. Vishnu Kumar Sharma

VECC

❖ Engineering Sciences

641.	Prof. P. Y. Nabhiraj
642.	Prof. Paramita Mukherjee
643.	Prof. Sandip Pal
644.	Prof. Sarbajit Pal
645.	Dr. Hemendra Kumar Pandey
646.	Dr. Tapatee Kundu Roy

❖ Physical Sciences

647.	Prof. Jedidiah Pradhan
648.	Prof. Jane Alam
649.	Prof. Arup Bandyopadhyay
650.	Prof. Parnika Das
651.	Prof. Sourav Sarkar
652.	Prof. Subhasis Chattopadhyay
653.	Dr. Gargi Chaudhri
654.	Dr. Gayathri N. Banerjee
655.	Dr. Gopal Mukherjee
656.	Dr. Kaushik Banerjee
657.	Dr. Nisith Kumar Das
658.	Dr. Sanyal Dirtha
659.	Dr. Sarmishtha Bhattacharyya
660.	Dr. Siddhartha Dechoudhury
661.	Dr. Tumpa Bhattacharjee
662.	Dr. Vaishali Naik
663.	Dr. Ajay Kumar Himanshu

664.	Dr. Anand Kumar Dubey
665.	Dr. Animesh Goswami
666.	Dr. Arindam Kumar Sikdar
667.	Dr. Ayan Ray
668.	Dr. Debasis Bhowmick
669.	Dr. Deepak Pandit
670.	Dr. Partha Pratim Bhaduri
671.	Dr. Prasanta Karmakar
672.	Dr. Pratap Roy
673.	Dr. Rupa Chatterjee
674.	Dr. Sadhukhan Jhilam
675.	Dr. Samir Kundu
676.	Dr. Shashi C Srivastava
677.	Dr. Supriya Mukhopadhyay
678.	Dr. Swagata Mallik
679.	Dr. Tapan Kumar Rana
680.	Dr. Tilak Kumar Ghosh
681.	Dr. Uttam Bhunia
682.	Dr. Zubayer Ahammed

HRI

❖ **Mathematical Sciences**

683.	Prof. Kalyan Chakraborty
684.	Prof. Manoj kumar
685.	Prof. P. K. Ratnakumar
686.	Prof. Punita Batra
687.	Prof. R. Thangadurai
688.	Prof. Surya D. Ramana
689.	Dr. N. Raghavendra
690.	Dr. Amrita Ghosh
691.	Dr. Aprameyo Pal
692.	Dr. N. Raghavendra
693.	Dr. Bhamidi Sai Somanjana Sreedhar
694.	Dr. Gyan Prakash
695.	Dr. Hemangi Madhusudan Shah
696.	Dr. Jishnu Ray
697.	Dr. Tuhin Ghosh
698.	Dr. Umeshkumar V. Dubey

❖ **Physical Sciences**

699.	Prof. Pinaki Majumdar
700.	Prof. Aditi Sen De
701.	Prof. Asesh Krishna Datta
702.	Prof. Dileep Prabhakar Jatkar
703.	Prof. Prasenjit Sen

704.	Prof. Ujiwal Sen
705.	Dr. Anirban Basu
706.	Dr. Anshuman Maharana
707.	Dr. Santosh Kumar Rai
708.	Dr. T. P. Pareek
709.	Dr. Tapas Kumar Das
710.	Dr. Debraj Rakshit
711.	Dr. Sayan Choudhury
712.	Dr. Sudip Chakraborty
713.	Dr. Tathagata Ghosh

IMSc

❖ **Life Sciences**

714.	Prof. Gautam I. Menon
715.	Dr. Areejit Samal
716.	Dr. Rahul Siddharthan
717.	Dr. Sandeep Choubey

❖ **Mathematical Sciences**

718.	Prof. Amritanshu Prasad
719.	Prof. C. R. Subramanian
720.	Prof. Jaya N. Iyer
721.	Prof. Meena Bhaskar Mahajan
722.	Prof. Saket Saurabh
723.	Prof. Sankaran Viswanath
724.	Prof. Sanoli Gun
725.	Prof. Srinivas Kotyada
726.	Prof. Vijay Kodiyalam
727.	Dr. Anilesh Mohari
728.	Dr. Anirban Mukhopadhyay
729.	Dr. Dishant Mayurbhai Pancholi
730.	Dr. Pralay Chatterjee
731.	Dr. Vikram Sharma
732.	Dr. Anup Biswanath Dixit
733.	Dr. C. Ramya
734.	Dr. Indrava Roy
735.	Dr. Prakash Saivsan
736.	Dr. S. Sundar
737.	Dr. Sushmita Gupta
738.	Dr. Sushmita Venugopal

❖ **Physical Sciences**

739.	Prof. V. Ravindran

740.	Prof. Indumathi D.		775.	Dr. Debottam Das
741.	Prof. Raghib Hassan Syed		776.	Dr. Dinesh Topwal
742.	Prof. Rajesh R.		777.	Dr. Goutam Tripathy
743.	Prof. Satyavani Vemparala		778.	Dr. Kirtiman Ghosh
744.	Prof. Sibasish Ghosh		779.	Dr. Manimala Mitra
745.	Prof. Sitabhra Sinha		780.	Dr. Samal Debakanta
746.	Dr. Gopalakrishna Sharihari		781.	Dr. Sanjib Kumar Agarwalla
747.	Dr. Manjari Bagchi		782.	Dr. Saptarshi Mandal
748.	Dr. Mukul S. Laad		783.	Dr. Satyaprakash Sahoo
749.	Dr. Partha Mukhopadhyay		784.	Dr. Shamik Banerjee
750.	Dr. Pinaki Chaudhuri		**IPR**	
751.	Dr. Ronojoy Adhikari		❖ **Chemical Sciences**	
752.	Dr. Sanatan Digal		785.	Prof. Sudhir Kumar Nema
753.	Dr. Sujay K. Ashok		❖**Engineering Sciences**	
754.	Dr. V. S. Nemani		786.	Prof. Shashank Chaturvedi
755.	Dr. Ajit Coimbatore Balram		787.	Prof. Surya Kumar Pathak
756.	Dr. Arnab Pal		788.	Prof. Paritosh Chaudhuri
757.	Dr. Chandrashekar C. M.		789.	Prof. Vipulkumar L. Tanna
758.	Dr. Dhiraj Kumar Hazra		790.	Dr. Alphonsa Joseph
759.	Dr. Ganesh Ramchadran		791.	Dr. Manoj Kumar Gupta
760.	Dr. Padmanath Madanagopalan		792.	Dr. Nirav I. Jamnapara
761.	Dr. Roji Pius		793.	Dr. Rajesh Kumar
762.	Dr. Sayantan Sharma		794.	Dr. Suryakant B. Gutpa
IOP			795.	Dr. Rana Pratap Yadav
❖ **Physical Sciences**			❖ **Physical Sciences**	
763.	Prof. Karuna Kar Nanda		796.	Prof. Mahendrajit Singh
764.	Prof. B K Panigrahi		797.	Prof. Mainak Bandopadhyay
765.	Prof. Biju Raja Sekhar		798.	Prof. Prabal Kumar Chattopadhyay
766.	Prof. Pankaj Agrawal		799.	Prof. Pramod Kumar Sharma
767.	Prof. Pradip Kumar Sahu		800.	Prof. Subrata Pradhan
768.	Prof. Shikha Varma		801.	Prof. Subroto Mukherjee
769.	Prof. Som Tapobrata		802.	Prof. Sudip Sengupta
770.	Prof. Sudipta Mukherji		803.	Dr. Abhijit Sen
771.	Prof. Suresh Kumar Patra		804.	Dr. Anitha V. P.
772.	Dr. Arijit Saha		805.	Dr. Asim Kumar Chattopadhyay
773.	Dr. Aruna Kumar Nayak		806.	Dr. Debasis Chandra
774.	Dr. Debasish Chaudhuri		807.	Dr. Ganesh Rajaraman

808.	Dr. Hiteshkumar B Pandya	843.	Dr. Amarjeet Nayak
809.	Dr. Indranil Bandyopadhyay	844.	Dr. Debashis Pattanaik
810.	Dr. Jana Mukti Ranjan	845.	Dr. Joe Varghese Yeldho
811.	Dr. Joydeep Ghosh	846.	Dr. Pranaya Kumar Swain
812.	Dr. Lalit Mohan Awasthi	847.	Dr. Rooplekha Khuntia
813.	Dr. Mrityunjay Kundu	❖ **Chemical Sciences**	
814.	Dr. Mukesh Ranjan	848.	Prof. Alagar Srinivasan
815.	Dr. Nirmal Kumar Bisai	849.	Dr. Bhargava B. L.
816.	Dr. Rajendraprasad Bhattacharyay	850.	Dr. Chandra Shekhar Purohit
817.	Dr. Raju Daniel	851.	Dr. Chidambaram Gunanathan
818.	Dr. Saikia Bipul	852.	Dr. Himansu Sekhar Biswal
819.	Dr. Samir Khirwadkar	853.	Dr. Jogendra Nath Behera
820.	Dr. Sanjeev Kumar Sharma	854.	Dr. Moloy Sarkar
821.	Dr. Sanjeev Kumar Varshney	855.	Dr. Nagendra Kumar Sharma
822.	Dr. Shantanu Kumar Karkari	856.	Dr. Nembenna Sharanappa
823.	Dr. Ziauddh Khan	857.	Dr. P. C. Ravikumar
824.	Dr. Amreen Ara Hussain	858.	Dr. Prasenjit Mal
825.	Dr. C. Balasubramanian	859.	Dr. Sanjib Kar
826.	Dr. Devendra Sharma	860.	Dr. Saravanan Peruncheralathan
827.	Dr. Gourab Bansal	861.	Dr. Subhadip Ghosh
828.	Dr. Harshita Raj	862.	Dr. Sudip Barman
829.	Dr. Jinto Thomas	863.	Dr. Upakarasamy Lourderaj
830.	Dr. Jyoti Shankar Mishra	864.	Dr. Venkatasubbaiah Krishnan
831.	Dr. Kishore Kanti Mishra	865.	Dr. Arindam Ghosh
832.	Dr. N Ramasubramanian	866.	Dr. Bidraha Bagh
833.	Dr. Pintu Bandyopadhyay	867.	Dr. Bishnu Prasad Biswal
834.	Dr. Ramkrishna Rane	868.	Dr. Dipak Samanta
835.	Dr. Ravi G.	❖ **Engineering Sciences**	
836.	Dr. Sarveshwar Sharma	869.	Dr. Anup Kumar Bhattacharya
837.	Dr. Sejal Shah	870.	Dr. Sabyasachi Karati
838.	Dr. Shekar Goud Thatipamula	❖ **Life Sciences**	
839.	Dr. Shishir Purohit	871.	Dr. Chandan Goswami
840.	Dr. Smruti R. Mohanty	872.	Dr. Debasmita Pankaj Alone
841.	Dr. Subhash P. V.	873.	Dr. Harapriya Mohapatra
NISER		874.	Dr. K. Chandrasekhar Panigrahi
❖ **Applied Systems Analysis**		875.	Dr. Manjusha Dixit
842.	Dr. Amarendra Das	876.	Dr. Palok Aich

877. Dr. Pankaj Vidyadhar Alone	914. Dr. Sumana Hatui
878. Dr. Praful S. Singru	915. Dr. Tushar Kanta Naik
879. Dr. Subhasis Chattopadhyay	❖ **Physical Sciences**
880. Dr. Anirudhha Datta Roy	916. Prof. Sudhakar Panda
881. Dr. Himabindu Vasuki Kilambi	917. Prof. Bedangadas Mohanty
882. Dr. K. Venkatsai Badireenath	918. Dr. Ashok Kumar Mohapatra
883. Dr. Mohammed Saleem	919. Dr. Colin Benjamin
884. Dr. Renjith Mathew	920. Dr. Prasanjit Samal
885. Dr. Rudresh Acharya	921. Dr. Pratap Kumar Sahoo
886. Dr. Srinivasan Ramanujam	922. Dr. Ritwik Das
887. Dr. Swagata Ghatak	923. Dr. Sanjay Kumar Swain
888. Dr. Tirumala Kumar Chowdary	924. Dr. Subhankar Bedanta
❖ **Mathematical Sciences**	925. Dr. A.V. Anil Kumar
889. Dr. Anil Kumar Karn	926. Dr. Abdur Rahman
890. Dr. Binod kumar Sahoo	927. Dr. Ajaya Kumar Nayak
891. Dr. Brundaban Sahu	928. Dr. Amaresh Kumar Jaiswal
892. Dr. Anisur Rahaman Molla	929. Dr. Anamitra Mukherjee
893. Dr. Anupam Pal Chowdhary	930. Dr. Ashis Kumar Nady
894. Dr. Arita Banik	931. Dr. Chethan N. Gowdigere
895. Dr. Chitrabhanu Chaudhury	932. Dr. Guneshwar Thangjam
896. Dr. Deepak Kumar Dalai	933. Dr. Jaya Khanna
897. Dr. Dinesh Kumar Keshari	934. Dr. Jayesh M Goyal
898. Dr. Kamal Lochan Patra	935. Dr. Joydeep Bhattacharjee
899. Dr. Kaushik Majumder	936. Dr. Kartikeswar Senapati
900. Dr. Krishanu Dan	937. Dr. Kush Saha
901. Dr. Manas Ranjan Sahoo	938. Dr. Liton Majumdar
902. Dr. Manoj Mishra	939. Dr. Najmal Haque
903. Dr. Meher Jaban	940. Dr. Nishikanta Khandai
904. Dr. Nabin Kumar Jana	941. Dr. Pathikrit Bhattacharya
905. Dr. Panchugopal Bikram	942. Dr. Prolay Kumar Mal
906. Dr. Ramesh Manna	943. Dr. Sayantani Bhattacharyya
907. Dr. Rishiraj Bhattacharyya	944. Dr. Subhasish Basak
908. Dr. Ritwik Mukherjee	945. Dr. Sumedha
909. Dr. Roy Sutanu	946. Dr. Surya Snata Rout
910. Dr. Sanjay Parui	947. Dr. Tapan Mishra
911. Dr. Senthil Kumar K.	948. Dr. Tuhin Ghosh
912. Dr. Subhankar Mishra	949. Dr. V. Ravi Chandra
913. Dr. Sudhir Kumar Pujahari	

950.	Dr. Victor Roy
951.	Dr. Yogesh Kumar Srivastava

SINP

❖ **Chemical Sciences**

952.	Dr. Dulal Senapati
953.	Dr. Montu K. Hazra
954.	Dr. Padmaja Prasad Mishra

❖ **Life Sciences**

955.	Dr. Partha Saha
956.	Dr. Rahul Banerjee
957.	Dr. Sampa Biswas
958.	Dr. Udayaditya Sen
959.	Dr. Chandrima Das
960.	Dr. Debashis Mukhopadhyay
961.	Dr. Gautam Garai
962.	Dr. H. Raghuraman
963.	Dr. Kaushik Sengupta
964.	Dr. Oishee Chakrabarti
965.	Dr. Sangram Bagh
966.	Dr. Soumen Kanti Manna
967.	Dr. Subhabrata Majumder
968.	Dr. Subhendu Roy
969.	Dr. Tofayel Ahmed

❖ **Physical Sciences**

970.	Prof. Gautam Bhattacharyya
971.	Prof. Abhik Basu
972.	Prof. Ambar Ghosal
973.	Prof. Bijay Kumar Agrawal
974.	Prof. Bireswar Basu Mallick
975.	Prof. Chandan Mazumder
976.	Prof. Debasish Majumdar
977.	Prof. Harvendra Singh
978.	Prof. Indranil Das
979.	Prof. Kumar Sankar Gupta
980.	Prof. Mustafa Munshi Golam
981.	Prof. P. M. G. Namissan
982.	Prof. Pradip Kumar Roy
983.	Prof. Prakash Mathews
984.	Prof. Satyajit Hazra
985.	Prof. Sukalyan Chattaopadhyay
986.	Prof. Supratik Mukhopadhyay
987.	Prof. Ushasi Datta
988.	Dr. Amit Ghosh

989.	Dr. Anjali Mukherjee
990.	Dr. Arunava Mukherjee
991.	Dr. Chinmay Basu
992.	Dr. Krishnakumar S. R. Menon
993.	Dr. Maitreyee Nandy
994.	Dr. Manoj K. Sharan
995.	Dr. Nayana Majumdar
996.	Dr. Satyaban Bhunia
997.	Dr. Satyaki Bhattacharya
998.	Dr. Subir Sarkar
999.	Dr. Suchandra Dutta
1000.	Dr. Supratic Chakraborty
1001.	Dr. Akashrup Banerjee
1002.	Dr. Arnab Kundu
1003.	Dr. Arti Garg
1004.	Dr. Augustine Kshetrimayum
1005.	Dr. Biswajit Karmakar
1006.	Dr. Biswarup Satpati
1007.	Dr. Debasish Banerjee
1008.	Dr. Debasish Das
1009.	Dr. Kalpataru Pradhan
1010.	Dr. Krishanu Roychowdhury
1011.	Dr. Mala Das
1012.	Dr. M. K. Mukhopadhyay
1013.	Dr. Pratik Majumdar
1014.	Dr. Samik Duttagupta
1015.	Dr. Sankar De
1016.	Dr. Sudipto Chakrabarti

TMC

❖ **Life Sciences**

1017.	Prof. Arvind D Ingle
1018.	Prof. Sorab Nariman Dalal
1019.	Dr. Abhijt De
1020.	Dr. Amit Dutt
1021.	Dr. Ashok Varma
1022.	Dr. Chilakapati Murali Krishna
1023.	Dr. Joyti Anand Kode
1024.	Dr. Kakoli Bose
1025.	Dr. Manoj Balkrishna Mahimkar
1026.	Dr. Pritha Ray
1027.	Dr. Rukmini Balkrishna Govekar
1028.	Dr. Sanjay Gupta
1029.	Dr. Venkatraman Prasanna

1030. Dr. Vikram Suryaprakash Gota	1072. Prof. Hasmukh Kantilal Jain
1031. Dr. Dibyendu Bhattacharyya	1073. Prof. Jai Prakash Agarwal
1032. Dr. Khizer Hasan Syed	1074. Dr. Jaya Ghosh
1033. Dr. Nandini Verma	1075. Dr. Jayita Kedar Deodhar
1034. Dr. Rohan Jayant Khadilkar	1076. Dr. Jeson Rajan Doctor
1035. Dr. Sanjeev Waghmare	1077. Prof. Jyoti Bajpai
1036. Dr. Sejal Patwardhan	1078. Prof. Kedar Kamalakar Deodhar
1037. Dr. Sharath Chandra Arandkar	1079. Prof. Madhavi G. Shetmahajan
1038. Dr. Shilpee Dutt	1080. Prof. Mahendra Pal
1039. Dr. Sonam Mehrotra	1081. Prof. Mahesh Goel
1040. Dr. Subir Biswas	1082. Prof. Malini Premkumar Joshi
1041. Dr. Sunil S. Kumar Sheety	1083. Prof. Manish Suresh Bhandare
❖ **Medical & Health Sciences**	1084. Prof. Manisha Nandkumar Pawar
1042. Prof. Rajendra Achyut Badwe	1085. Prof. Manju Sengar
1043. Prof. Ajay Puri	1086. Prof. Maya Prasad
1044. Prof. Aliasgar V Moiyadi	1087. Prof. Mukta Ravindra Ramdwar
1045. Prof. Amit Prakashchandra Joshi	1088. Prof. Munita Meenu Bal
1046. Prof. Amita Maheswari	1089. Prof. Murthy Vedang
1047. Prof. Amol Trymbakrao Kothekar	1090. Prof. Navin Khattry
1048. Prof. Anant Gokarn	1091. Prof. Nayana Shekar Amin
1049. Prof. Anant Ramaswamy	1092. Prof. Neha Mittal
1050. Prof. Anuja Dhananjay Deshmukh	1093. Prof. Nehal Rishi Khanna
1051. Prof. Aparna Sanjay Chatterjee	1094. Prof. Nikhil Vijay Patkar
1052. Prof. Archi Ramesh Agrawal	1095. Prof. Nilendu C. Purandare
1053. Prof. Ashwin Luis Desouza	1096. Prof. Nilesh Pandurang Sable
1054. Prof. Ashwini Narsingrao Budrukkar	1097. Prof. Nitin Sudhakar Shetty
1055. Prof. Atul M. Budukh	1098. Prof. Pankaj Chaturvedi
1056. Prof. Atul Prabhakar Kulkarni	1099. Prof. Papagudi G. Subramanian
1057. Prof. Avanish Parmesh Saklani	1100. Prof. Poonam K. Panjwani
1058. Prof. Ayushi Sahay	1101. Prof. Prabhash Kumar
1059. Prof. Bharat Rekhi	1102. Prof. Prachi Sunil Patil
1060. Prof. Bhausaheb Pandurang Bagal	1103. Prof. Prakash Shetty
1061. Prof. Conjeevaram S. Parmesh	1104. Prof. Prashant Ramesh Tembhare
1062. Prof. Deepa Ravindranathan Nair	1105. Prof. Prathamesh Pai Srinivas
1063. Prof. Devendra Arvind Chaukar	1106. Prof. Priti Dhansukhbhai Desai
1064. Prof. Dushyant Jaiswal	1107. Prof. Priya Ranganathan
1065. Prof. Gagan Prakash	1108. Prof. Raghu Sudarshan Thota
1066. Prof. Gaurav Narula	1109. Prof. Rajesh Ashok Kinhikar
1067. Prof. Gauravi Ashish Mishra	1110. Prof. Rajesh Prabhakar Dikshit
1068. Prof. Girish Chinnaswamy	1111. Prof. Rajiv Kumar
1069. Prof. Goda Jayant Sastri	1112. Prof. Reena Zarir Engineer
1070. Prof. Gouri Himalaya Pantvaidya	1113. Prof. Reshma Ambulkar
1071. Prof. Gulia Seema	1114. Prof. Sabita Shambhulal Jiwnani

1115.	Prof. Sachin Punatar
1116.	Prof. Sajid Shafique Quresh
1117.	Prof. Sandeep Vivek Gurav
1118.	Prof. Sangeeta Bhikaji Desai
1119.	Prof. Sanjay Biswas
1120.	Prof. Santosh Menon
1121.	Prof. Sarbani Ghosh Laskar
1122.	Prof. Shaesta Abdulaziz Mehta
1123.	Prof. Shailesh Vinayak Shrikhande
1124.	Prof. Shalaka Prakash Joshi
1125.	Prof. Sharmila Anil Pimple
1126.	Prof. Shashank Ojha
1127.	Prof. Sheela Prashant Sawant
1128.	Prof. Sheila Nainan Myatra
1129.	Prof. Shilpushp Jagannath Bhosale
1130.	Prof. Shraddha Patkar
1131.	Prof. Shripad Dinanath Banavali
1132.	Prof. Siddhartha Sankar Laskar
1133.	Prof. Sneha Shah
1134.	Prof. Sohan Lal Solanki
1135.	Prof. Sridhar Epari
1136.	Prof. Subhash Chotelal Yadav
1137.	Prof. Sudeep Gupta
1138.	Prof. Sudhir Vasudevan Nair R.
1139.	Prof. Sumeet Gujral
1140.	Prof. Sumitra Ganesh Bakshi
1141.	Prof. Supriya Jayant Sastri
1142.	Prof. Swapnil Yeshwant Parab
1143.	Prof. Tabassum Abdulwahid Wadasadawala
1144.	Prof. Tanuja Manjanath Shet
1145.	Prof. Tejpal Gupta
1146.	Prof. Vandana Agarwal
1147.	Prof. Vanita Maria Noronha
1148.	Prof. Venkatesh Rangarajan
1149.	Prof. Vijay Maruti Patil
1150.	Prof. Vijaya Prakash Patil
1151.	Prof. Vikas Sureshchand Ostwal
1152.	Prof. Vikram Anil Chaudhari
1153.	Prof. Vinay Kant Shankhdhar
1154.	Prof. Vivek Gajanan Bhat
1155.	Prof. Jagmohan Lal Meena
1156.	Prof. Manjusha Vagal

1157.	Prof. Anita D'Souza
1158.	Prof. Ashish Kumar Jha
1159.	Prof. Bhakti Sachin Shetye
1160.	Prof. Bhavesh Arun Popat
1161.	Prof. Meera Sharad Achrekar
1162.	Prof. Prakash R. Nayak
1163.	Prof. Rituraj Upreti
1164.	Prof. Shweta Janardan Ghag
1165.	Prof. Sindhu Shibu Nair
1166.	Prof. Sneha Mithun
1167.	Dr. Abhishek Chatterjee
1168.	Dr. Aekta Shah
1169.	Prof. Akshay Dwarkadas Baheti
1170.	Prof. Ameya Dattatraya Puranik
1171.	Dr. Amrita Guha
1172.	Dr. Anjana S Wajekar
1173.	Dr. Anuja Dhananjay Deshmukh
1174.	Dr. Arpita Sahu
1175.	Dr. Asawari Jingonda Patil
1176.	Dr. Bhakti Dushyant Trivedi
1177.	Dr. Bindiya Gaurav Salunke
1178.	Dr. Chetan Anil Dhamne
1179.	Dr. Janu Amit Kumar
1180.	Dr. Kinjalka Ghosh
1181.	Dr. Kunal B Gala
1182.	Dr. Lingaraj Nayak
1183.	Dr. Madhavi Dattatraya Desai
1184.	Dr. Manish Pruthi
1185.	Dr.Nandini Sharrel Menon
1186.	Dr. Naveen Mummudi
1187.	Dr. Palak Bhavesh Popat
1188.	Dr. Poonam Joshi
1189.	Dr. Prabhat Bhargava
1190.	Dr. Pradip Ramdas Chaudhari
1191.	Dr. Rahul Krishnatry
1192.	Dr. Richa Vaish
1193.	Dr. Sheetal Vidyadhar Gaikwad
1194.	Dr. Shiva Kumar Thiagarajan
1195.	Dr. Sukhada D. Savarkar
1196.	Dr. Sumathi S Hiregoudar
1197.	Dr. Sushmita Rath
1198.	Dr. Swapnil Rane
1199.	Dr. Trupti Pal

1200.	Dr. Uma M. Sakhadeo	1220.	Dr. Kajari Bhattacharya
1201.	Dr. Vasundhara Patil	1221.	Dr. Katha Nikhil Rabade
1202.	Dr. Vidisha Vipin Tuljapurkar	1222.	Dr. Meenakshi Singh
1203.	Dr. Vikas Singh	1223.	Dr. Nivedita Chakrabarty
1204.	Dr. Akanksha Chichra	1224.	Dr. Omshree Shetty
1205.	Dr. Ameya Rajan Bindu	1225.	Dr. Parthiban K Velayutham
1206.	Dr. Amit Kumar Jayant Choudhari	1226.	Dr. Prachi Mittal
1207.	Dr. Anisha A Navkudkar	1227.	Dr. Pratik Chandrani
1208.	Dr. Anuprita Dilip Daddi	1228.	Dr. Sangeeta Kakoti
1209.	Dr. Aparna Katdare	1229.	Dr. Shivkumar Gudi
1210.	Dr. Archya Dasgupta	1230.	Dr. Shrikant C Raut
1211.	Dr. Ashwini D Rane	1231.	Dr. Shruti Gairola
1212.	Dr. Atanu Bhattacharjee	1232.	Dr. Shwetabh Sinha
1213.	Dr. Avinash Rameshrao Pagdhune	1233.	Dr. Shyam Srinivasan
1214.	Dr. Badira Cheriyalinkal Parambil	1234.	Dr. Sudivya Prashast Sharma
1215.	Dr. Dhanlaxmi L. Shetty	1235.	Dr. Sujata Lall
1216.	Dr. Gaurav Vijay Salunke	1236.	Dr. Sumeet Prakash Mirgh
1217.	Dr. Gauri Raman Gangakhedkar	1237.	Dr. Suryatapa Saha
1218.	Dr. Gauri Rohan Deshpande	1238.	Dr. Vineet Kumar
1219.	Dr. Jifmi Jose Manjali		

HBNI at a Glance

During the last academic year (August 1, 2022-July 31, 2023) HBNI has awarded 218 Ph.D. degrees. The total number of Ph.D. degrees awarded by HBNI till July 31, 2023 stands at 2351. HBNI also awarded 84 M. Tech., 183 M.Sc./Integrated M.Sc. in various science disciplines, 109 post graduate & super specialty medical degrees, and 25 diplomas in Radiological Physics (DipRP) during this period. 856 students have been admitted to different academic programmes during 2022-23, out of which 336 students are for Ph.D. program.

Year wise Ph.D results declared *
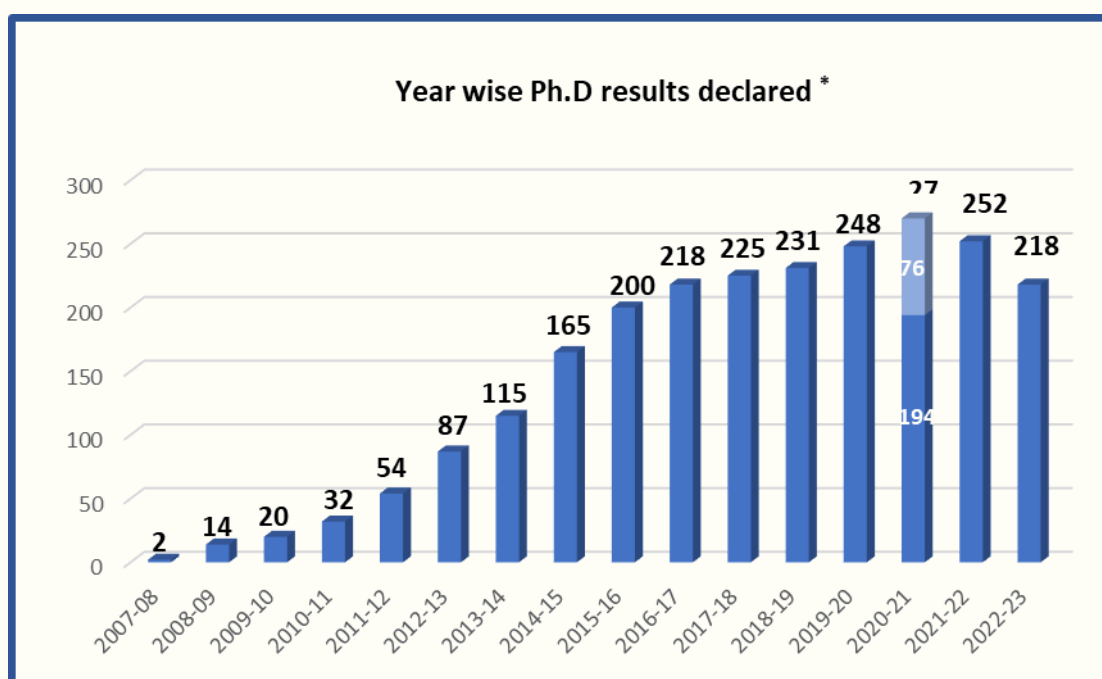
*The data from 2007-08 to 2019-20 is for the period April 1 of preceding year to March 31 of the ending year. The data for 2020-21 is for the period April 1, 2020 to July 31, 2021. Dark blue area (194) gives the data from April 1, 2020 to March 31, 2021, light blue area (76) gives the data from April 1, 2021 to July 31, 2021. The data for 2021-22 and 2022-23 is for the period August 1 of the preceding year to July 31 of the ending year.

Discipline wise distribution of Total (2351) Ph.D. results declared

Legend:
- Applied Systems Analysis
- Chemical Sciences
- Engineering Sciences
- Life Sciences
- Mathematical Sciences
- Medical and Health Sciences
- Physical Sciences

Year wise M.Tech results declared *
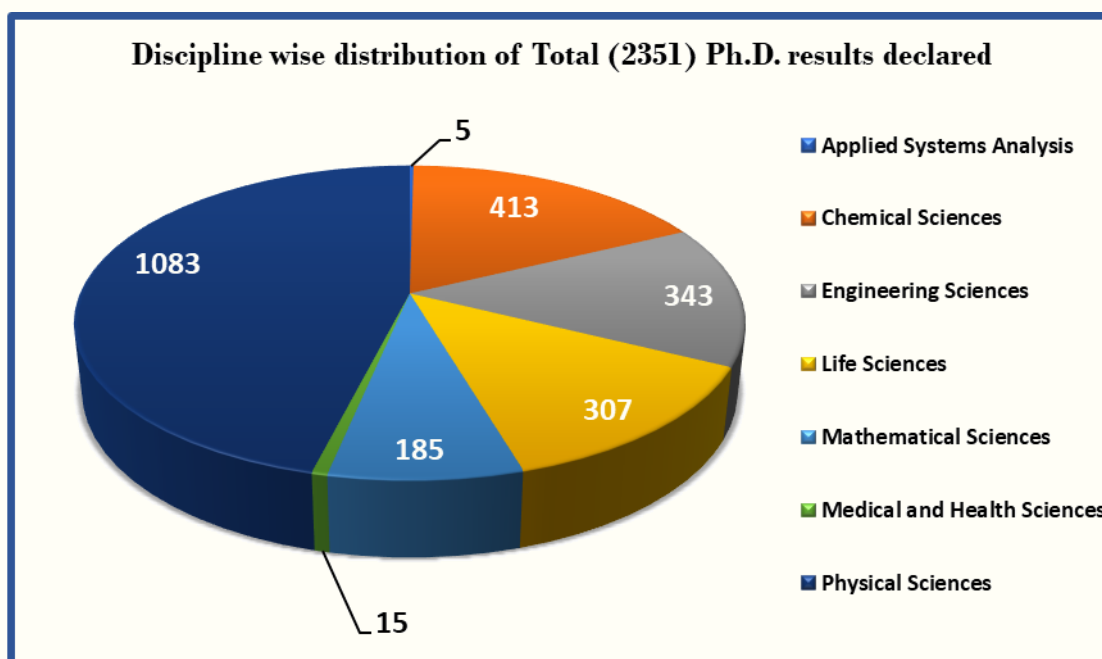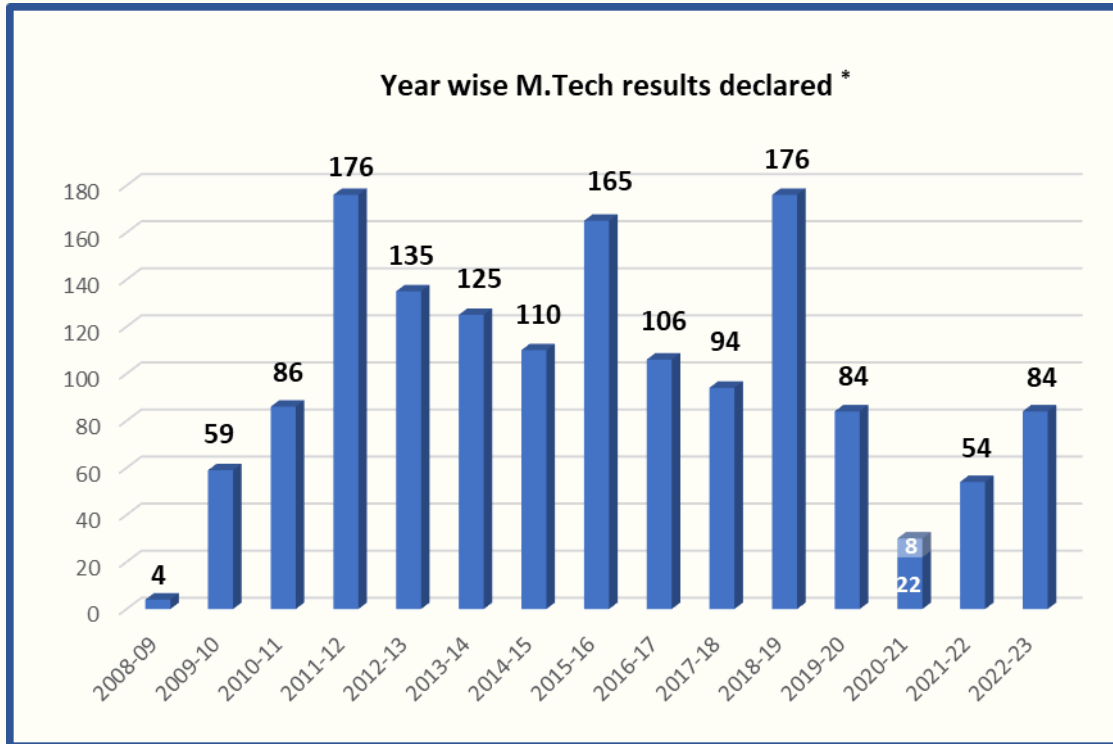
*The data from 2008-09 to 2019-20 is for the period April 1 of the preceding year to March 31 of the ending year. The data for 2020-21 is for the period April 1, 2020 to July 31, 2021. Dark blue area (22) gives the data from April 1, 2020 to March 31, 2021, light blue area (8) gives the data from April 1, 2021 to July 31, 2021. The data for 2021-22 and 2022-23 is for the period August 1 of the preceding year to July 31 of the ending year.

Year wise MD/DM/MCh results declared*
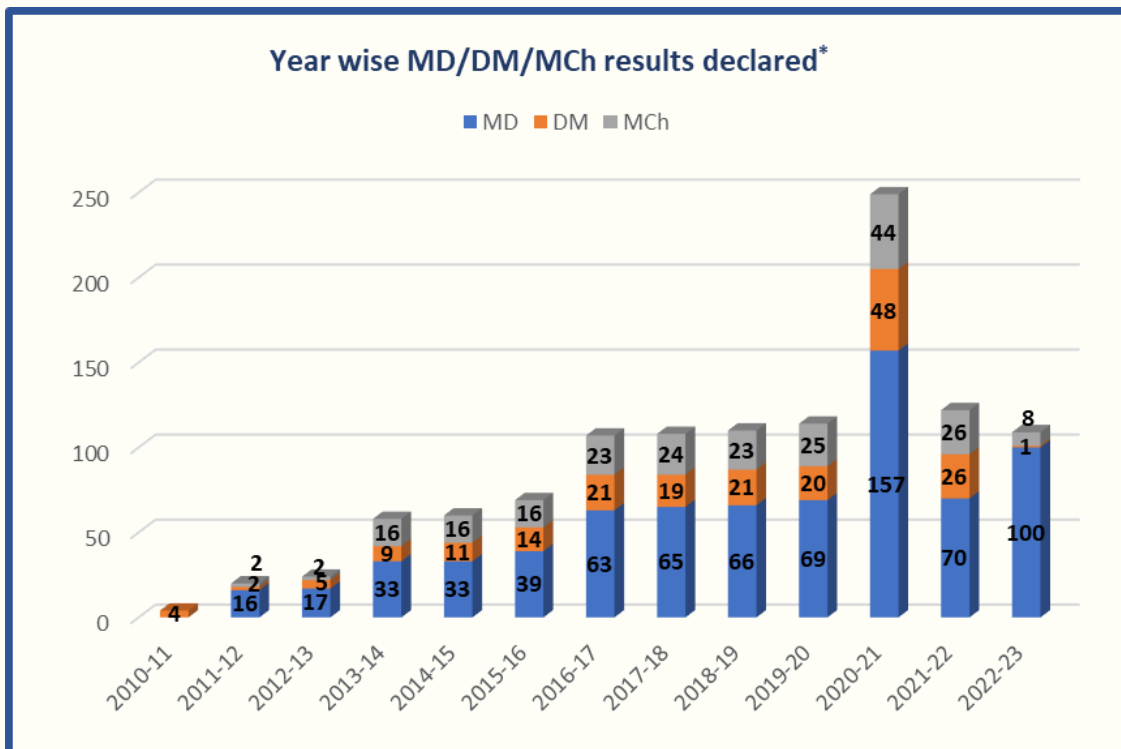
*The data from 2010-11 to 2019-20 is for the period April 1 of preceding year to March 31 of the ending year. The data for 2020-21 is for the period April 1, 2020 to July 31, 2021. The data for 2021-22 and 2022-23 is for the period August 1 of the preceding year to July 31 of the ending year.

Programme wise Admission Details during 2022-23 (Total = 856)
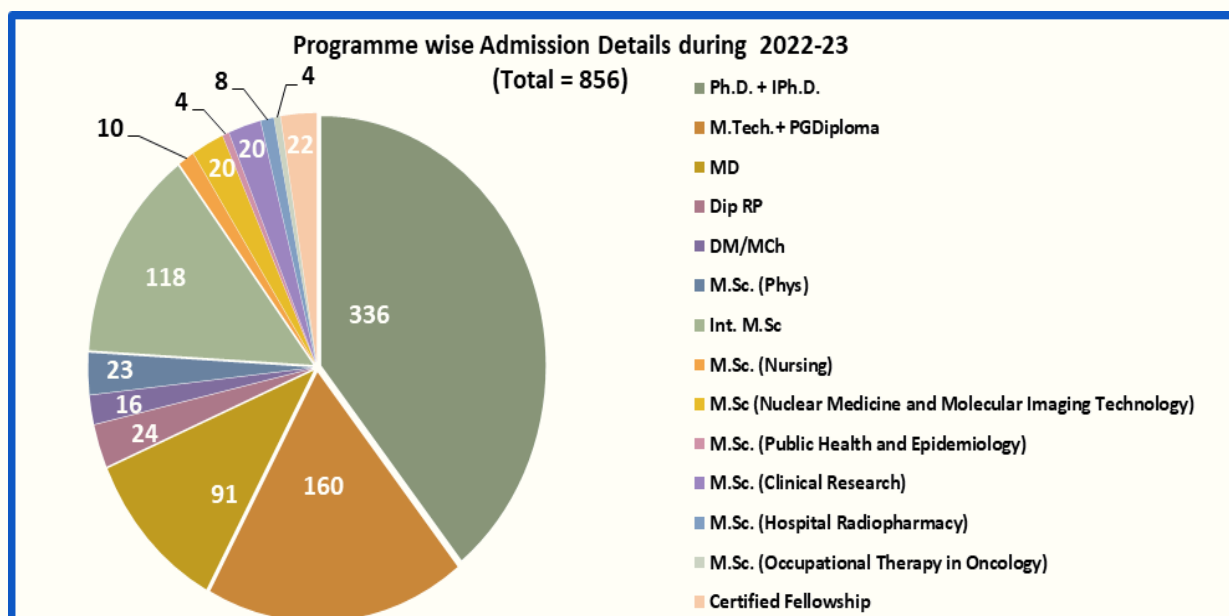
Number of students admitted to the different academic programmes of CIs/OCC during August 1, 2022 –July 31, 2023

Academic Programme	BARC	IGCAR	RRCAT	VECC	SINP	IPR	TMC	IoP	IMSc	HRI	NISER	Total
Ph.D. + Integrated Ph.D	36	44	16	6	30		25	61	19	12	87	**336**
M.Tech + PG Diploma	115	29	7	….	….	9	….	….	….	….	….	**160**
M.D.	….	….	….	….	….	….	91	….	….	….	….	**91**
Dip RP	24	….	….	….	….	….	….	….	….	….	….	**24**
D.M./M.Ch.	….	….	….	….	….	….	16	….	….	….	….	**16**
M.Sc. (Physics)	….	….	….	….	….	….	….	….	….	14	9	**23**
Integrated M.Sc.											118	**118**
M.Sc. (Nursing)	….	….	….	….	….	….	10	….	….	….	….	**10**
M.Sc (Nuclear Medicine and Molecular Imaging Technology)	10	….	….	….	….	….	10	….	….	….	….	**20**
M.Sc. (Public Health and Epidemiology)	….	….	….	….	….	….	4	….	….	….	….	**4**
M.Sc. Clinical Research							20					**20**
M.Sc. (Hospital Radiopharmacy)	8	….	….	….	….	….	….	….	….	….	….	**8**
M.Sc. (Occupational Therapy in Oncology)	….	….	….	….	….	….	4	….	….	….	….	**4**
Certified fellowship	….	….	….	….	….	….	22	….	….	….	….	**22**
Total	**193**	**73**	**23**	**6**	**30**	**9**	**202**	**61**	**19**	**26**	**214**	**856**

Section II
(Theses at a Glance)

1. Applied System Analysis

During the period of the report, one doctoral student received Ph.D. degree in Applied System Analysis in the subject Humanities and Social Sciences from Homi Bhabha National Institute. The thesis highlight is given below.

1.1 National Institute of Science Education and Research

1.1.1 Disrupted Lives: A Qualitative Study of the Experiences of Living with Cancer among Cancer Patients and their Family Caregivers

The present thesis intends to provide a detailed, empirically grounded understanding of what it is like to live with cancer and caring for those with cancer within the family. This was achieved by exploring the experience of both the individual with cancer and that of their family caregiver through an analysis of their narratives. An ethnographic approach was used, involving observations and a series of in-depth interviews of eight dyads of cancer patients and their family caregivers. Thematic analysis was undertaken to identify relevant themes within the narratives.

This research shows that the experience of living with cancer was a complex, difficult, and arduous struggle. Participants said that 'living with cancer is difficult', as the effects of cancer has pervaded every aspect of their lives. Experience of cancer consisted several facets such as the difficult nature of cancer, the work of cancer, sufferings due to cancer and its care, and the coping strategies. Analysis revealed that participants faced disruption in their day-to-day normalcy since the moment of diagnosis. Disruptions were observed in their perception of their self and others, and during the performances of their routine activities including the maintenance or continuance of their roles and in their social relations which led to profound suffering that induced alienation, uncertainty, and emotional struggles. Living with cancer required participants to adjust at first, and over time and with experience, they learned to 'negotiate' or 'get on with it'.

The findings of this study suggest more emphasis on the individual supportive care based on the patients' and their family caregivers' perceived necessities and their crises. It is suggested that an increased awareness of the psycho-social difficulties of people living with cancer can contribute to an enhanced understanding of what and how people with cancer manage these in their everyday lives. Moreover, the doctoral work emphasizes that more precedence is required not only to policy, education, and research that stresses on patient's existential wellbeing but also to the wellbeing of the caregivers living with tensions of caring and comforting.

2.   Chemical Sciences

During the period of the present report, 45 research fellows have received their Ph.D. degrees in Chemical Sciences from Homi Bhabha National Institute. As in the earlier years, quite diverse areas of research have been covered in these theses work. Following are the highlights of some selected theses in Chemical Sciences.

2.1   Bhabha Atomic Research Centre

2.1.1   Investigation of the Molecular Packing in Polymer Nanocomposites and its Role on the Bulk Physical Properties

Polymer nanocomposites (PNCs) are complex multiphasic systems having multitude of enthalpic and entropic interactions among various constituents which govern their thermo-mechanical and electrical properties. Molecular packing and free volume (FV) structure of polymer in PNCs play governing role in the evolution of bulk physical properties. Investigating the changes in microstructure/FV characteristics of polymer phase using suitable experimental techniques provide deeper insights in the understanding of structure-property correlations. In the present thesis, Polyethylene oxide (PEO) based PNCs were investigated aiming their applications as solid polymer electrolytes (SPEs) in energy storage devices, e.g. Li-ion battery. SPEs are one of the best substitutes to current state-of-the-art Li-ion battery electrolytes (e.g. carbonate based volatile organic liquids) suffering from major safety issues in terms of leakage, fire and/or explosion. With SPEs, the issue of their low ionic conduction (IC) at room temperature is a major obstacle for practical applications. To circumvent this, it is important to understand the role of their FV and relaxation dynamics (RD) on their ionic conductivity, which was the main motivation of the present thesis. In the present investigation, PEO based SPEs filled with lithium bis(trifluoromethanesulfonyl) imide (LiTFSI) salt was chosen as the suitable matrices for their application in Li-ion battery. FFV and RD of the studied matrices were comprehensively investigated using positron annihilation spectroscopy (PAS) and broadband dielectric spectroscopy (BDS) techniques. Many other complementary techniques such as XRD, XPS, FTIR, Raman spectroscopy, SEM, TEM, SAXS, DSC, TGA, tensile testing, and electrochemical impedance spectroscopy were also used to derive structure-property correlation. Nanofillers like SiO_2, Al_2O_3 increased amorphous fraction and FV of the polymer. Anisotropic nanofillers (Al_2O_3 nanorods) were more pronounced in enhancing FV and IC as compared to spherical Al_2O_3 nanoparticles, confirming the role of interphase assisted IC with orderly oriented nanofillers. Crystalline porous Zeolitic imidazolate framework-8 (ZIF-8) with long range (µm scale) pore interconnectivity was found to provide fast IC channels for Li^+ transport. PEO-ZIF-8 based quasi-solid-state electrolyte helped in realizing very high IC ($\sim 6 \times 10^{-4}$ S.cm^{-1}) and excellent compatibility with Li-metal anode and high voltage $LiNi_{0.6}Mn_{0.2}Co_{0.2}O_2$ (NMC622) intercalation cathode in Li coin cell. Results in the present thesis suggest the PEO-ZIF-8 based solid/quasi-solid-state electrolytes as very promising substitutes to the state-of-the-art liquid electrolytes as a much safer alternative in the next generation energy storage devices.
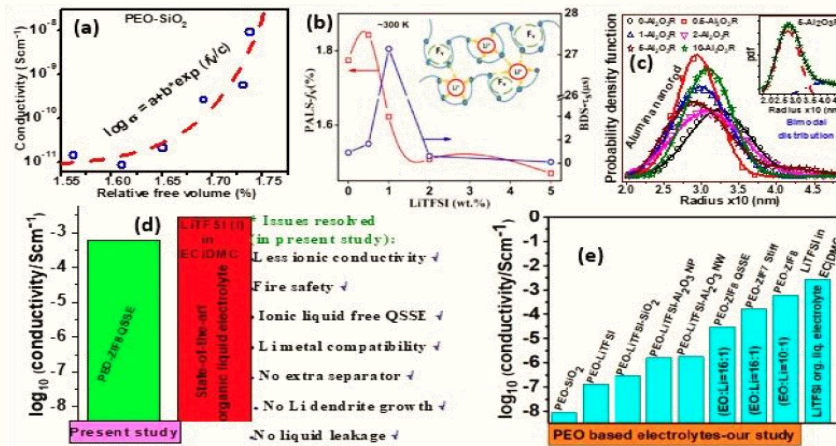
(a) Conductivity dependence on free volume; (b) correlation of free volume and segmental dynamics at different salt loading; (c) bimodal distribution of free volume nanoholes in anisotropic nanofiller; (d) & (e) comparison of polymer electrolytes with state-of-the-art liquid electrolyte in Li-ion battery.

2.1.2 Synthesis and Characterization of Inorganic Materials for Potential Applications in Neutron Dosimetry

Neutron dosimetry is of utmost importance due to the high relative biological effectiveness (RBE) of neutrons as compared to other ionizing radiations such as β or γ radiations. It is in general subdivided into two broad categories, viz. personnel and clinical. Thermoluminescence (TL) is one of the most widely used techniques where till date $^{6/7}$LiF:Mg,Ti material is used both for personnel and clinical (such as boron neutron capture therapy, BNCT) neutron dosimetry applications. However, literature study reflects that there are several shortcomings of LiF based host materials. Moreover, the number of articles reporting systematic approach towards development of new and better materials for neutron dosimetry is very low as compared to that of gamma radiation. In view of the above, the present dissertation aimed to develop new TL materials for applications in personnel dosimetry and neutron dosimetry involving high intensity thermal neutron beams used in clinical field. For the dosimetry of high intensity thermal neutron beams, four systems viz. $Al_5{}^{10}BO_9$:Mn,Li, $Al_5{}^{10}BO_9$:Ce^{3+}, $Al_5{}^{10}BO_9$:Eu^{3+} and $Al_5{}^{10/11}BO_9$:Tb^{3+} were synthesized, structurally characterized and studied their TL based dosimetry applications up to 1.2×10^{11} n/cm^2 of thermal neutron beams. Among these $Al_5{}^{10/11}BO_9$:Tb^{3+} showed the best potential for the desired applications. Similarly, for personnel neutron dosimetry application, LiMgBO$_3$:Tb^{3+} phosphor was developed that demonstrated 2.2 times more neutron induced TL sensitivity with relatively simple TL glow curve (dosimetry peak at 475 K) as compared to the existing LiF:Mg,Ti dosimeter. Also, the ratio of TL response per unit dose of neutron to per unit dose of gamma radiation for LiMgBO$_3$:Tb^{3+} and standard LiF:Mg,Ti was found to be about 54 and 12, respectively. This is highly advantageous for dosimetry in mixed neutron field. Moreover, LiMgBO$_3$:Tb^{3+} showed excellent neutron dose linearity up to about 100 mSv and the fading of TL signal even up to storage of 90 days was found to be less than 10%. In addition, based on the detailed Photoluminescence (PL) and Electron Paramagnetic resonance (EPR) studies the underlying TL mechanism was delineated through identifying different neutron induced defect centers. The results suggest that the presently developed LiMgBO$_3$:Tb^{3+} has a potential for its uses as an alternative to the existing LiF based material for the TL based personnel neutron dosimetry applications.
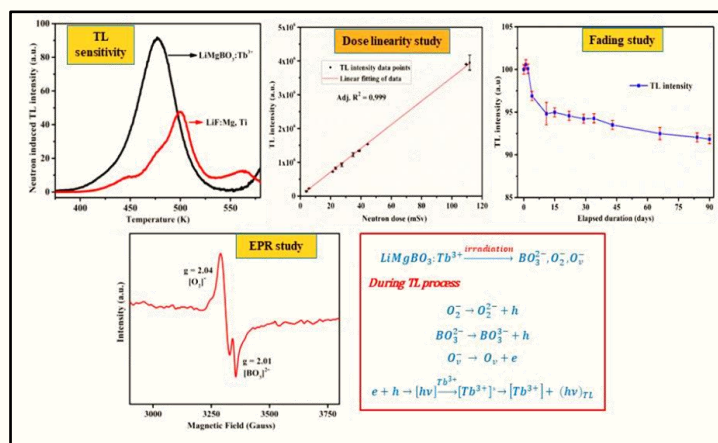
Comparison of neutron induced TL sensitivity of developed LiMgBO$_3$:Tb^{3+} with commercial LiF:Mg,Ti phosphor along with personnel neutron dosimetry studies and probable TL mechanism

2.1.3 Synthesis, Characterization and Cancer Therapy Evaluation of Fe$_3$O$_4$ and Up-conversion Based Nanostructured Materials

Up-conversion nanoparticles (UCNPs), particularly lanthanide-doped nanocrystals, which emit high energy photons under excitation using near-infrared (NIR) light, have found potential applications in many different fields, including biomedicines. Compared with traditional down-conversion fluorescence imaging, the NIR light excited up-conversion luminescence (UCL) imaging relying on UCNPs exhibits improved tissue penetration depth, higher photochemical stability, and free of auto-fluorescence background, promises superior biomedical imaging with high sensitivity. On the other hand, the unique up-conversion process of UCNPs may be utilized to activate photosensitive therapeutic agents for applications in cancer treatment. Moreover, the integration of UCNPs with other functional nanostructures could result in the obtained nanocomposites having highly enriched functionalities, useful in imaging-guided cancer therapies. In the present thesis synthesis, characterization, and cancer therapy evaluation of Fe$_3$O$_4$ and different up-conversion based nanostructured materials like NaGdF$_4$/Ho–Yb@m-SiO$_2$, NaErF$_4$:0.5%Tm@NaYF$_4$:20%Yb, etc. were investigated aiming their possible cancer therapeutic applications.
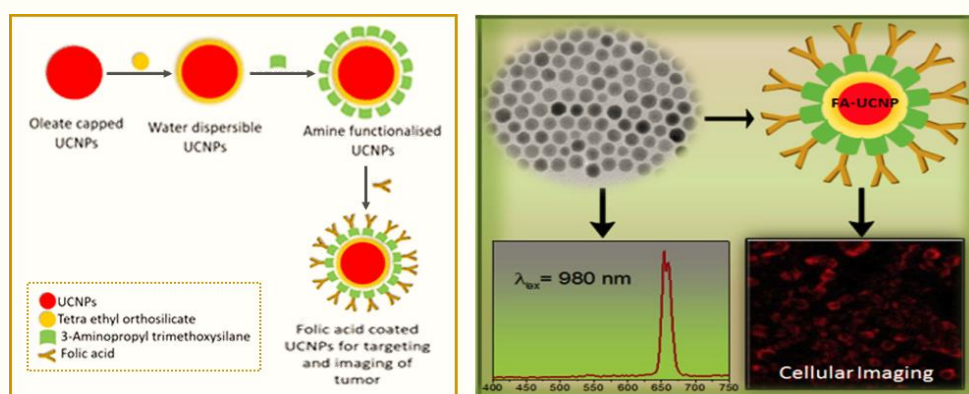
Functionalization of UCNPs and their conjugation with targeting moiety (left). Emission of UCNP system used in the imaging after conjugation with targeting moieties (right)

2.2   Indira Gandhi Centre for Atomic Research

2.2.1   Synthesis and Characterization of Nano-Crystalline Zeolites Using Kaolin and Fly Ash for Nuclear Waste Immobilization

Waste management of spent nuclear fuel is essential for sustained growth of nuclear power program. Zeolites have attracted immense attention for possible applications in nuclear fuel reprocessing and waste managements. Conventional synthetic zeolites like zeolite-A and zeolite-X have been extensively studied for ion exchange and immobilization of heat-generating radio nuclides like ^{137}Cs and ^{90}Sr from aqueous solution. Though borosilicate glasses are being used for the vitrification of high-level waste (HLW) worldwide, they have their limitations in immobilizing HLW when it contains chloride or fluoride ions. Considering various waste compositions produced from reprocessing of spent fuels from thermal and fast reactors, appropriate ceramic and glass-bonded ceramic materials and matrices are required for the safe immobilization of these radio-nuclides. Various zeolites have been investigated in this regard to investigate their usefulness in the immobilization of the radio-nuclides. With the same perspective, in the present thesis, zeolites were synthesized using kaolin and fly ash employing alkali fusion method followed by hydrothermal technique and their effectiveness in the nuclear waste immobilization were investigated systematically. Accordingly, number of zeolites were synthesized and their efficacy was explored for their ion exchange efficiencies for fission products like ^{137}Cs and ^{90}Sr from aqueous solutions. Studies were carried out to understand the insights of the ion-exchange processes, solid-state loading capacities of chloride salts, and the glass bonding abilities of zeolites with borosilicate and iron phosphate glasses. The results are having relevance towards nuclear fuel reprocessing and waste management strategies.
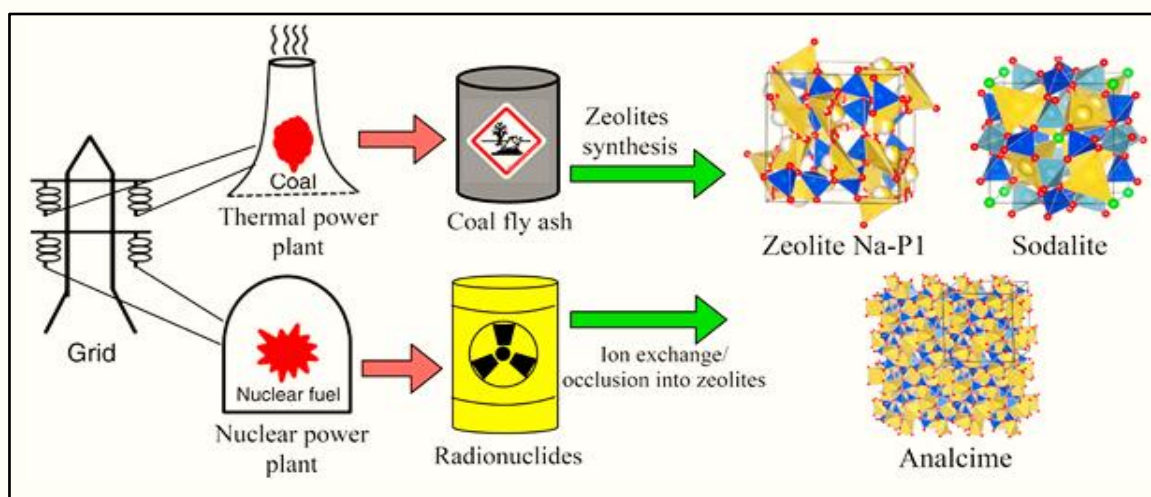
Schematics of the zeolite synthesis from fly ash and its utilization in nuclear waste immobilization.

2.2.2   Synthesis and Evaluation of Hexaalkyl Phosphoramides as Extractants for Actinide Extraction and Applications

Number of new hexaalkyl phosphoramides (HAPAs) based on functionalities and designated as HPPA, HiPPA, HBPA, HiBPA and HHPA, respectively, were synthesized by condensation reaction of

corresponding dialkyl amines with POCl₃ and the compounds were purified by column chromatography and characterized by NMR (C13, H1& P31), IR and CHNS analysis. The physicochemical properties and radiation degradation behavior of the HAPA in n-Dodecane (n-DD) and Xylene (Xy) were investigated along with their extraction behaviors towards actinides and fission products and the results were compared with those of the TBP/n-DD system.
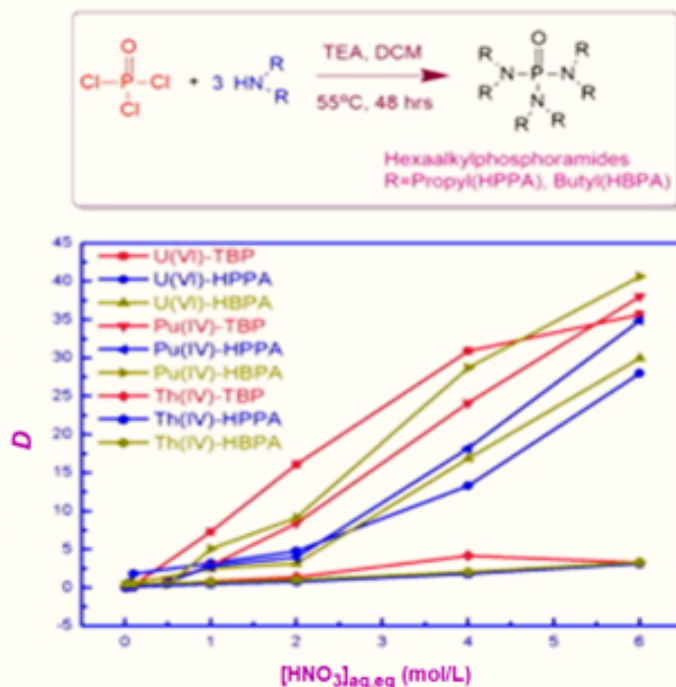
Hexaalkyl phosphoramides used as the extractants for actinides and fission products.

It is found that the physicochemical properties (e.g., density, viscosity, aqueous solubility, etc.), extractability, as well as the third-phase formation behavior depend largely on the alkyl chain length and the structure of the studied extractant materials. There were no significant changes observed when n-DD or Xy were used as the diluents in the extraction process. Further, there was no third phase formation was observed duing extraction of Pu(IV) and Th(IV), and theoretical loading in these cases were 120 g/L for Pu(IV) and 70 g/L for Th(IV)], which are significantly higher than the values for 1.1 M TBP/n-DD system under identical conditions. Among all the investigated observed HAPA systems, the HBPA was found to be display relatively more attractive results over TBP and other phosphoramides used as the extractants for extraction of actinides and fission products.

2.2.3 Synthesis, Characterisation and Evaluation of Crosslinked Poly(ionic liquid)s as Sorbents for Antimony, Chromium and Iodine

In recent years there is resurgence in the field of ionic liquids (ILs) in exploring them for new applications. Preparation of charged polymers using IL monomers is one such recently emerging research area. The most easily accessible IL monomers are the ones having vinyl substituted imidazolium cationic moiety, which on polymerization yields cationic binding sites. Present thesis deals with the development of IL based polymeric receptors containing cationic binding sites for effective removal of antimony, chromium and iodine, relevant to nuclear decontamination process

and reprocessing of nuclear effluents. A robust cationic IL polymer, namely, crosslinked poly(1-butyl-3-vinyl imidazolium)bromide, C-P(BVIm-Br), was synthesized in the present study using 1-butyl-3-vinyl imidazolium bromide as the IL monomer and N,N'-methylenebisacrylamide as the crosslinker. Sorption properties and binding mechanism of C-P(BVIm-Br) for both Sb(III) and Sb(V) containing anionic species (e.g. potassium antimony titrates) were investigated along with a comparative study involving crosslinked poly(vinylimidazolium) IL, namely, P(VIm-Br), whereby C-P(BVIm-Br) displayed better selectivity towards Sb sorption. The C-P(BVIm-Br) also showed pH dependent variation in Sb uptake in the presence of typically complexing agents used in nuclear decontamination process. Interestingly, C-P(BVIm-Br) showed preferential binding of Sb(III) over Sb(V) in the presence of NTA (or EDTA) and citric acid at pH 4.0 and 2.0 respectively. It was shown that by tuning the solution condition the selectivity of C-P(BVIm-Br) towards Sb(V) and Sb(III) can be controlled usefully, making the polymer as an excellent solid phase extractant for Sb(III)/Sb(V) separation. Very recent reports have shown strong binding between iodine and ILs. Based on a recent report that suggest strong binding interaction of iodine with ILs, the efficacy of C-P(BVIm-Br) for iodine binding was also evaluated in this study. Due to the unique nature of the binding site, the polymer showed excellent sorption behavior for both molecular and ionic forms of iodine, involving either halogen bonding or anion exchange mechanism, respectively. Compared to C-P(BVIm-Br), the P(VIm-Br), however, could display reasonable sorption for molecular iodine only. The suitability of C-P(BVIm-Br) was also evaluated for effective removal of Cr(VI) containing anions from low level of chromium contaminated water sources and high level of chromium containing tannery effluents. Further, a series of crosslinked poly(IL) systems having cations containing varying alkyl groups of different chain length and possessing different counter ions (Cl-, Br-, I-, BF4-, PF6-, TFSI-) were synthesized and the effect of structural variations of these polymers on physical and sorption properties were delineated in the present study. The thesis has thus brought out the high potential of crosslinked poly(IL) systems for use as the sorbent materials for the removal of antimony, chromium and iodine, especially
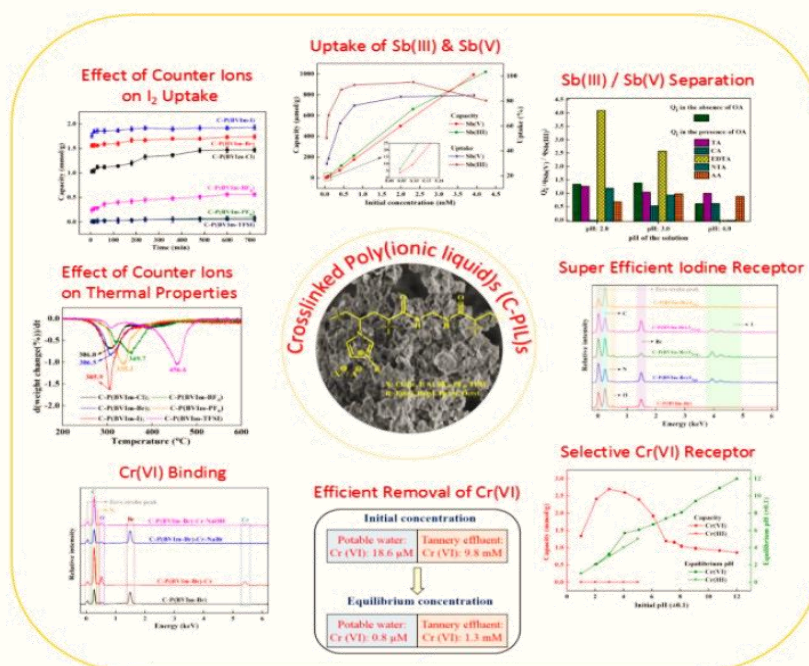
Crosslinked poly(ionic liquid)s for the removal of antimony, iodine and chromium.

2.3   National Institute of Science Education and Research

2.3.1   Sustainable Approaches Towards C-X (-N, -C, -O) Bond Formation Reactions in Organic Synthesis

Finding sustainable and step-economic strategies for the synthesis and functionalization of organic compounds has recently become an important topic of research. The major focus of this thesis is to introduce mild and sustainable protocols for C-X (-N, -C, -O) bond formation reactions for the synthesis and functionalization of heterocycles. Various strategies like utilization of the multitasking reagent, *tert*-Butyl Nitrite (TBN), and implementation of visible-light photocatalysis, were adopted in this research. Regioselective C_5- or C_7- mono-nitration of indolines was achieved by implementing *tert*-butyl nitrite (TBN) as the nitrating agent without using any additive. Mild and convenient approach toward the synthesis of 3-nitro coumarins was explored using TBN through nitrative cyclization of aryl alkynoates. A protocol for C-H hydroxylation of quinoxalin-2(1*H*)-ones using TBN through *ipso*-substitution strategy was also explored. In addition, visible-light mediated regioselective oxygenation of quinoxalin-2(1*H*)-one was achieved by employing 9-mesityl-10-methylacridinium perchlorate as visible-light photocatalyst and O_2 as a green oxidant. Overall, a couple of mild and sustainable protocols were developed in this thesis for C-X (-N, -C, -O) bond formation reactions with high regioselectivity and good functional group tolerance, which will contribute significantly to the research areas like metal-free nitration of heterocycles, nitrative cyclization reactions, cascade cyclization reactions, metal-free hydroxylation of heterocycles, visible-light photocatalysis, and oxygenation of heterocycles.
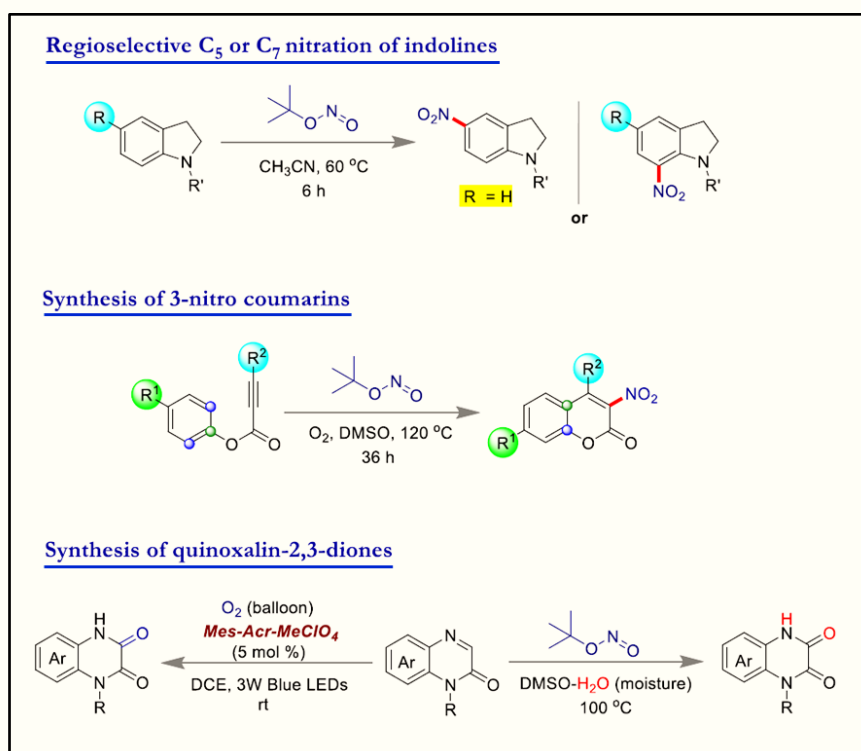
Schematics of the different synthesis protocols explored in the doctoral work

2.3.2 Synthesis of Hexahydrobenzo[c]phenanthridine and β-Carboline-1-one Derivatives via Transition Metal Catalyzed C-H Bond Activation

The transition metal catalyzed C-H activation process has become an increasingly potent platform in organic syntheses, which streamlines the synthesis of drug molecules and several natural products. Many bioactive compounds have been identified to have the skeletons of β-carboline-1-one and hexahydrobenzo[c]phenanthridine alkaloids as core skeletons. Therefore, synthesis of such heterocyclic compounds has immense importance in organic synthesis. Among various C-C bond forming processes, annulation reactions of cyclic alkenes with amides are less frequently used to synthesize bioactive compounds. In this context, present thesis reports various methodologies for efficient annulation reactions of cyclic alkenes with amides, demonstrating the annulation reactions of three different types of cyclic alkenes with several amides as achieved through transition metal catalyzed C-H bond activations. It is revealed that Rh(III)-catalyzed C-H bond activation provides an effective access to the core skeletons of hexahydrobenzo[c]phenanthridine for its annulation reaction with benzamides. Similarly, it is also established that the Co(II)-catalyzed C-H bond activations provide very effective annulation reactions of (i) β-Carboline-1-one derivatives with indole-2, (ii) cyclic alkenes with benzamides, and (iii) bicycloalkenes with indole-2-carboxamides, where annulation reactions occur under quite mild reaction conditions.
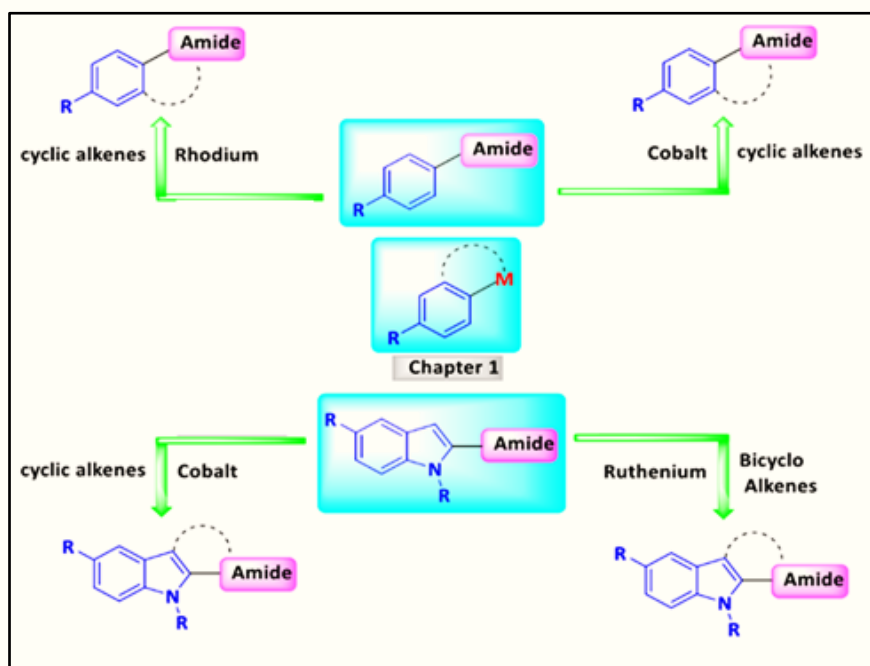
Transition metal catalyzed annulation reactions of various cyclic alkenes with amides.

2.3.3 Activation of Methanol as a C1 Source Using Pd, Ru and Co-compounds to Make New C-C Bonds

Over the last few decades, significant efforts have been made to develop environmentally benign borrowing hydrogen (BH) and interrupted-borrowing hydrogen (I-BH) approaches for indirect functionalization of methanol as methylating agent. These approaches provide a greener alternative to regular H_3C-C and C-CH_2-C bond forming reactions, as they generate only H_2O and/or H_2 as the by-

products. Importantly methyl group is one of the most valuable substituents present in many drugs, biomolecules, and natural products. This thesis reports a unique approach for the activation of methanol in the synthesis of 1,5-diketones using a simple Co(II)-porphyrin as a catalyst. The developed approach is based on the activation and utilization of methanol as a C1 source using an I-BH method. Present protocol was successfully utilized for the synthesis of many substituted pyridines via sequential additions. A unique ligand selective protocol for the synthesis of α-methylated ketones and 1,5-diketones, utilizing N,C–Ru and N,N–Ru catalysts, respectively. These reactions proceeded through ligand selective BH and I-BH methods for the activation of methanol. A methylated product is obtained using N,C–Ru catalyst through BH method, and a 1,5-diketone product is obtained through I-BH method using N,N–Ru catalyst. The thesis provides a brief discussion on one-pot isomerization and methylation of allyl alcohol to synthesize α-methylated ketones, catalyzed by commercially available Pd(OAc)$_2$ catalyst. This protocol is based on the tandem isomerization and methylation of allyl alcohol utilizing methanol as C1 source through BH method. One-pot isomerization and methylenation of allyl alcohol, followed by a sequential addition protocol to synthesize symmetrical pyridines have also been demonstrated. This protocol was catalyzed by N,N-Ru catalyst for the isomerization-methylenation of allyl alcohol utilizing MeOH as a C1 source through I-BH strategy.
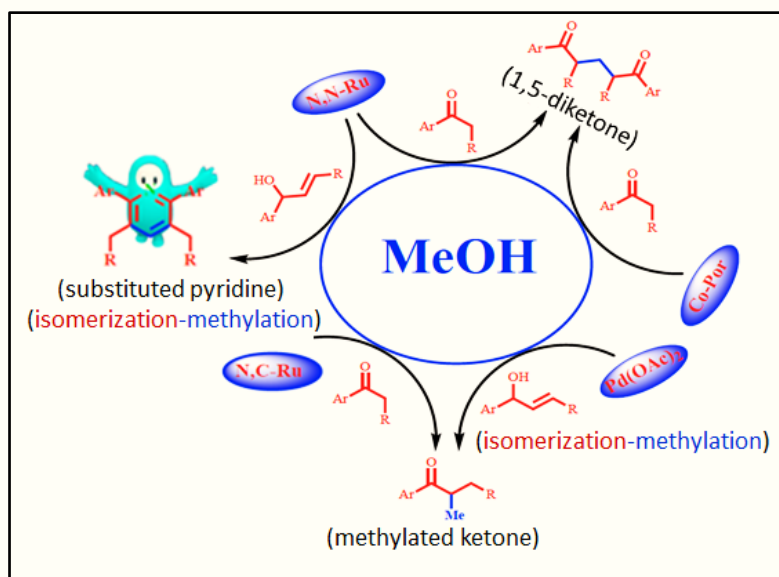
Schematics of the strategies adopted for new C-C bond formations through BH and I-BH approaches.

2.3.4 Synthesis and Spectroscopic Characterization of Metallocorroles and Porphyrins and their Applications

In nature, porphyrins are abundant and they play pivotal roles in various biological systems. Porphyrinoids and metallated porphyrinoids are present in various aromatic heterocyclic and macrocyclic derivatives such as heme, chlorophylls, bacteriochlorophylls, etc. Attempts to artificially synthesize porphyrin derivatives have been done since the applications of these macrocycles came into light. This thesis describes some new methodologies investigated for the synthesis of porphyrins. Similar to porphyrins, corroles are another class of tetrapyrrolic macrocyclic systems, which are more compressed than porphyrin and hence their inner π systems are more electron-rich and thus can stabilize higher oxidation states of metals. Along with porphyrins, this thesis also investigates some of

the underexplored areas of metallocorrole chemistry along with their synthesis. A new method for the synthesis of meso-substituted trans-A_2B_2 porphyrins via a two-step methodology has been reported which is different from the previously reported methodologies in many aspects and it can be performed easily in the gram scale synthesis of the desired product. The synthetic protocol of two new corrolato-Sb(III) complexes and two new (corrolato)(oxo)-Sb(V) complexes have also been presented in the thesis. The luminescent properties of these corrolato-Sb(III)/Sb(V)=O complexes have also been reported, which are having prospects in various photocatalytic oxygen atom transfer reactions. A modified methodology for the synthesis of a series of meso−substituted symmetric A_4−porphyrins and trans−A_2B_2-porphyrins in mild conditions has also been demonstrated. An unusual reaction of corrolato-Sb(III) complex with nitrosonium-tetrafluoroborate in the presence of air (O_2) is shown to generate trans-difluorocorrolato-Sb(V) species along with dinitration of the corrole ring. Importantly, the so formed trans-difluoro(3,17-dinitro−corrolato)-Sb(V) species showed oxygenation reaction under photoredox conditions in the presence of air and light at ambient temperature.
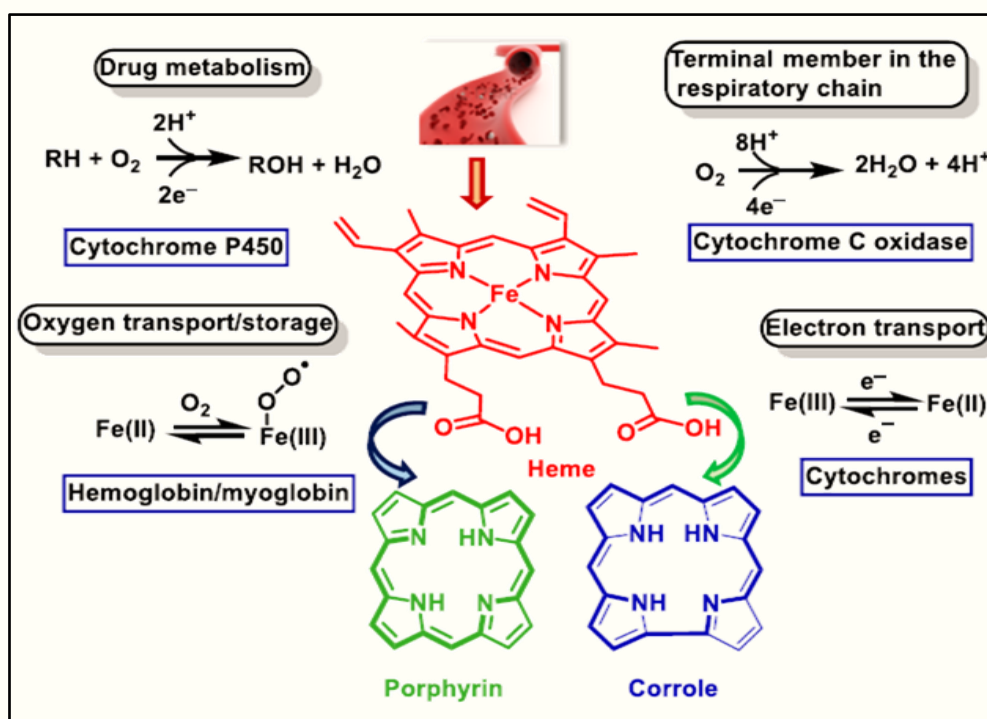
Schematics of the oxygenation and electron transport reactions involving porphyrins and corroles.

2.3.5 Conjugated Bis-Guanidinate (CBG) Stabilized Aluminum Complexes: Synthesis and Their Catalytic Applications

In recent years, the use of main group metal complexes in catalysis has surpassed that of transition elements. As aluminum is the cheapest and abundant element in the periodic table, attention is being drawn for its uses in catalysis. Present thesis is based on a thorough application of aluminum complexes in catalysis research. At first conjugated bis-guanidinate (CBG) stabilized neutral and cationic aluminum hydrides and alkyl complexes were isolated and following that the CBG-aluminum hydride was employed for catalytic hydroboration (B-H addition) of carbonyl compounds and various cross-dehydrocoupling reactions to corresponding hydroborated products using pinacolborane

(HBpin) as the reducer. Additionally, the chemoselective synthesis of amides, aminals, and N-methyl amines from respective heteroallenes such as carbodiimides, isocyanates, isothiocyanates, and isoselenocyanates was demonstrated under solvent-free conditions at low catalyst load. The B-H addition across double (alkene, isonitrile) and triple (alkyne, nitrile) bonds were also investigated producing borylamines and vinyl boronate esters with high-yields. The CBG aluminum methyl cation-based Si-H additions to carbonyls (aldehyde, ketone), alkenes, and phenylacetylene were also investigated using triethylsilicon hydride (HSiEt$_3$) as the reagent. The synthesis methodologies thesis demonstrated in the thesis will provide excellent guidelines for reducing challenging unsaturated functional groups via hydroboration and hydrosilylation methods using CBG-aluminum complexes as the catalysis under mild conditions.
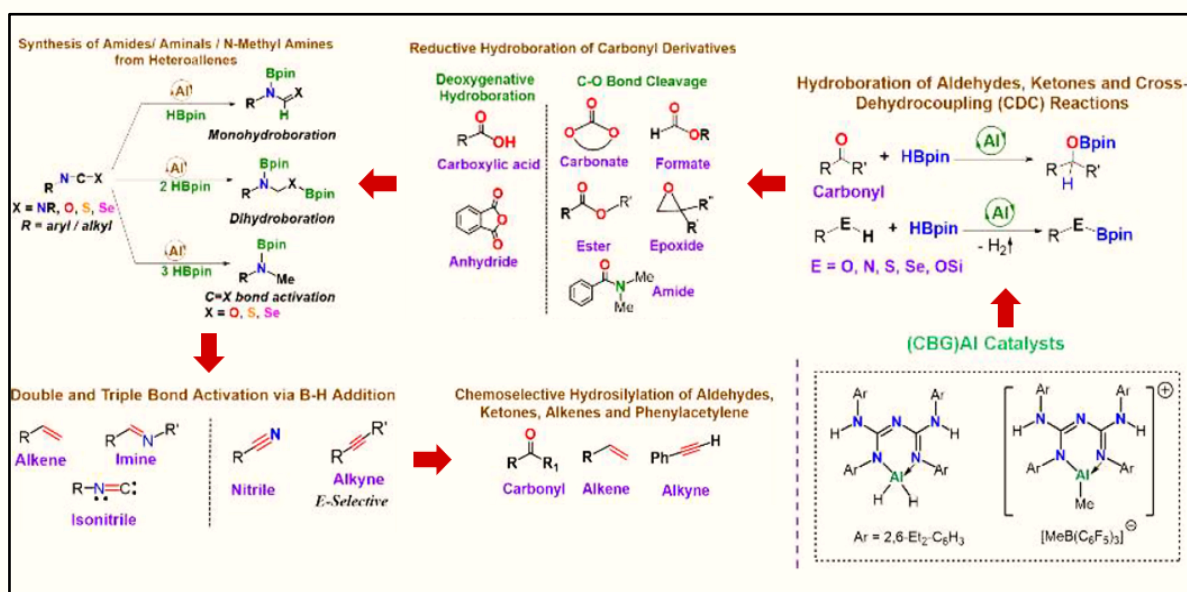
Schematic showing investigated approaches for the reduction of unsaturated organic functionalities

2.3.6 Noncovalent Interactions with Carbon in Small Molecules and Proteins: Theoretical Predictions and Experimental Challenges

In the realm of the noncovalent interactions (NCIs) the hydrogen bond (H-bond) is the most celebrated one. But, in most of the cases, the H-bonds are formed with electron donation from conventional electron donors like oxygen, nitrogen or chalcogen atoms. Very few studies report electron donation from neutral carbon atom. On the other hand, NCIs where carbon can accept electron in the σ*- or π*-orbitals, leading to the formation of carbon bond (C-bond) and n→π* bond interactions, respectively, still need special attention. Present thesis focuses on such type of uncommon NCIs. With the help of IR and NMR spectroscopic methods, aided by MD simulations and high-level DFT calculations, the existence of intermolecular n→π* interactions along with C-bond formation in solution has been explored. These NCIs involve electron donation from a suitable electron donor. Present thesis also provides evidence of NCIs that do not involve lone-pair of electrons or π-electrons. Thus, a new type of NCI, namely the carbo-hydrogen bond, has been identified in this thesis, where back and forth σ→σ* interactions exist. This new NCI has a binding energy between H-bond and C-bond binding energies. Controlling the turn over frequency of an enzymatic catalysis and the

construction of noncovalent organic frameworks are some of the possible implications of this type of newly discovered NCI. Present thesis also explores the carbon-centered H-bonds in proteins first time, where a neutral sp^3-hybridised carbon attached to the metal atom acts as a H-bond acceptor. These H-bonds are important to organic chemists for yielding products selectively in the C-H bond activation process via σ-bond metathesis. The presence of Me...Me interactions within the protein residues have also been confirmed from high-level quantum mechanical calculations, which are found to be important in controlling the folding-unfolding of proteins.
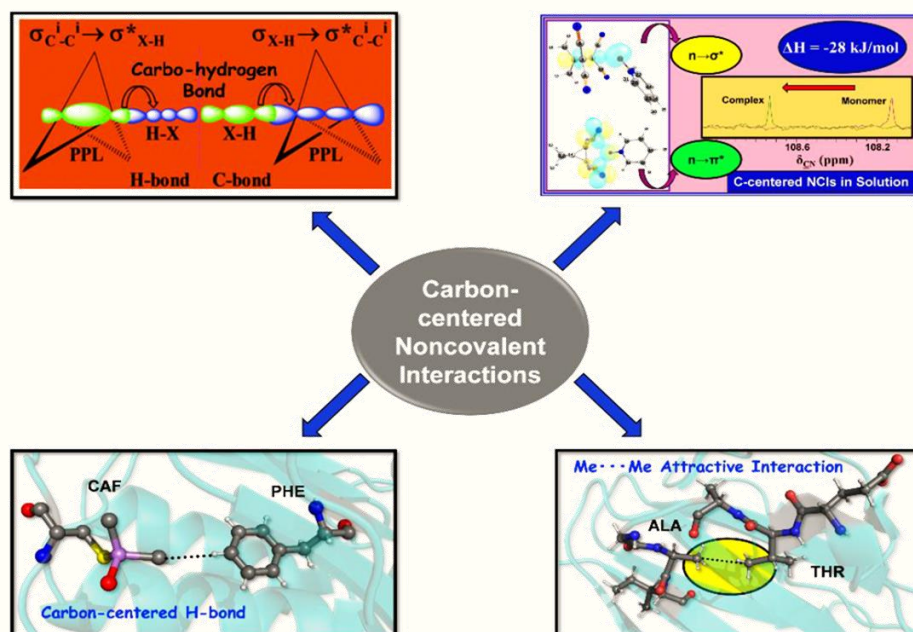
Schematic showing different noncovalent interactions (NCIs) explored in the present thesis

2.3.7 Design of Inorganic-Carbon Composites, Porous Carbons for Sustainable Environmental and Electrochemical Energy Storage/Conversion Applications

It is highly necessary to explore the strategies for the renewable energy conversion and storage to fulfil our future energy needs. In this context, present thesis reports the research work carried out on water electrolyzers (WEs) and the fuel cells (FCs). Different fuel cell processes like hydrogen oxidation reaction (HOR), oxygen reduction reaction (ORR), and hydrogen evolution reaction (HER), oxygen evolution reaction (OER) of the water electrolyzer have been addressed in this thesis. Present thesis also discusses on the reaction stages, mechanisms, as well as the kinetics of these processes. It also discusses the working principle of aqueous supercapacitors and developments of potential electrode materials for both anode and cathode of the water electrolyzer devices. The working principles of secondary lithium and sodium ion batteries and ion-storage mechanisms of anodes are also highlighted followed by a discussion on the design of suitable electrode materials. Synthesis of Rhodium metal–rhodium oxide ($Rh–Rh_2O_3$) nanostructures was carried out with relevance to HER and HOR in acidic and alkaline conditions. It is inferred that a bi-functional mechanism prevails for the alkaline HER/HOR activity of the studied catalyst. Synthesis and application of $Co_3V_2O_8/CN_x$ hybrid nanocomposite for aqueous supercapacitor has also been investigated using this material as positive

electrode and activated carbon (AC) as negative electrode for the asymmetric supercapacitor (ASC). Preparation of activated N-doped and S-doped carbon was also carried out for applications in capacitive energy storage as well as in physisorption of gases like H_2, CO_2, and CH_4. An easy direct synthesis procedure for preparation of N-doped soft carbon and S-doped hard carbon materials from organic precursors have been achieved which are having applications as anodes for Na ion batteries.
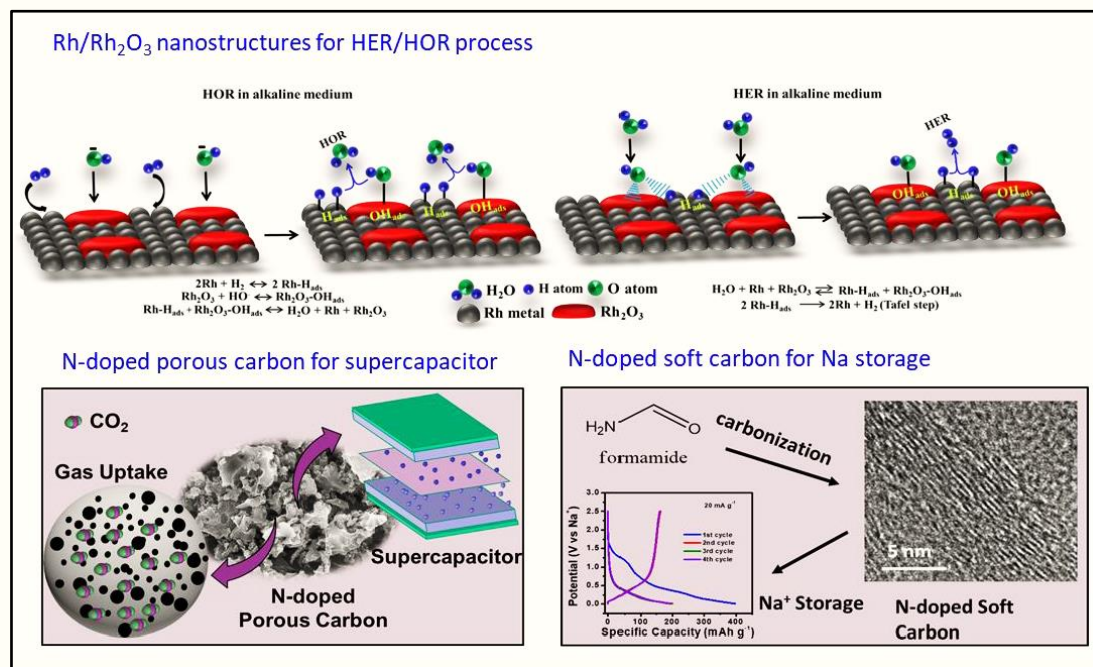
Various sustainable approaches towards energy storage and energy conversion applications

2.3.8 Synthesis, Characterization, and Photophysical Studies on Some Inorganic, Organic, and Inorganic-Organic Hybrid Nanomaterials

Nanomaterials like organic aggregates, quantum dots (QDs), and carbon dots (CDs) have emerged as building blocks in optoelectronic devices like solar cells, light-emitting diodes (LEDs), lasers, photodetectors, etc. The interest in organic–inorganic nanohybrids has been driven by the fact that the optoelectronic properties of these materials are very different from those of their individual components. The phenomena like energy and electron transfer processes in inorganic and organic excitons, how excitons interact with each other in a nanohybrid assemblies, and the mechanism of binding of various analytes to such nano materials have not been understood very well yet. Further, though many studies have been carried out, yet the knowledge about the surface chemistry of most nanomaterials is still not adequate. Additionally, various nanomaterials find their limited application due to their inherent toxic nature and water insolubility. In the present thesis attempts have been made to address these issues through studies on different organic aggregate, QD, and CD materials. Photophysical responses of glutathione-capped zinc-silver-indium-sulfide (ZAIS) QDs has been investigated towards various metal ions, demonstrating especially the selective detection of Cd^{2+} ion. Photophysical studies on ZAIS in the presence of organic analytes demonstrates the role of defect-mediated charge carrier recombination dynamics for the changes in the optical properties of these materials. Highly efficient energy transfer process has been observed between ZAIS QDs and organic

J-aggregates, having relevance to light harvesting and biological applications. Binding interaction and the associated FRET process between ZAIS QD and BSA protein have also been investigated in the present thesis. Complex fluorescence behavior of CDs has also been investigated with the aim to understand the mechanistic details pf their luminescence behavior.
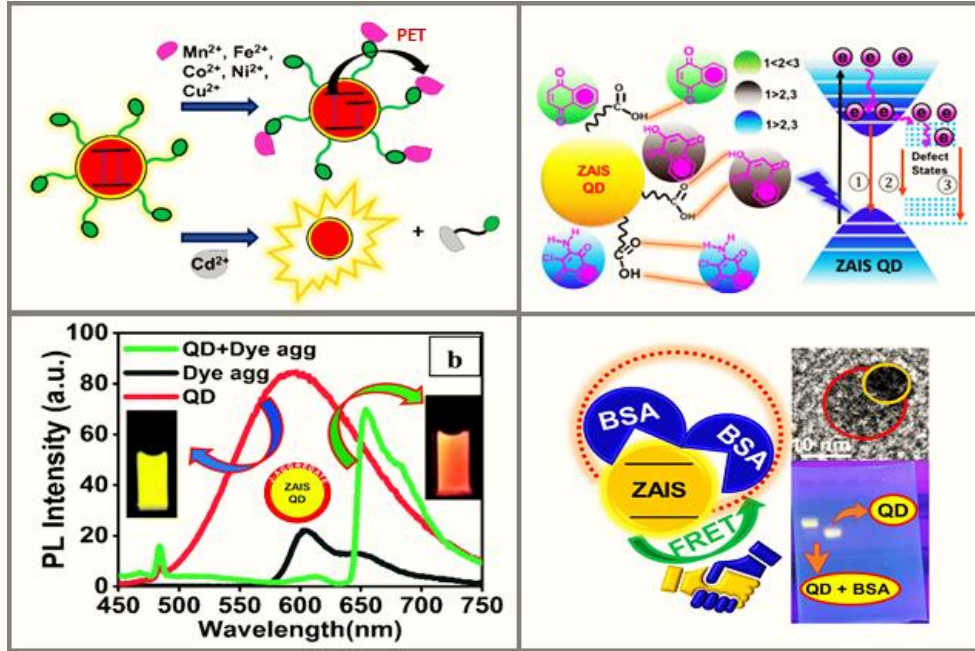
Schematic representation of different studies carried out using ZAIS QD materials
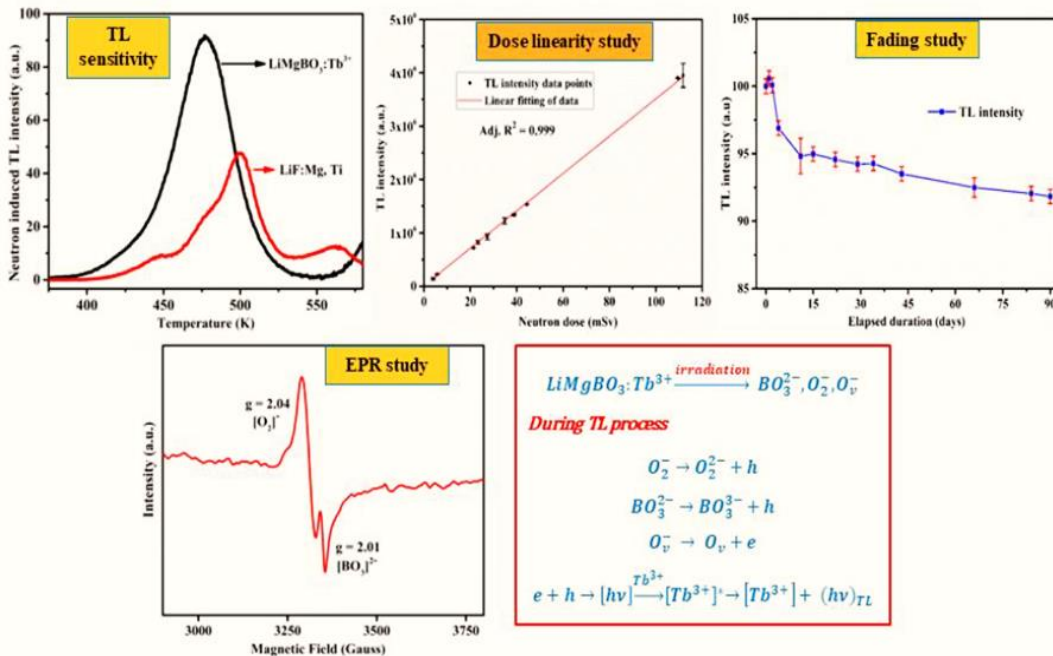
Comparison of neutron induced TL sensitivity of developed LiMgBO₃:Tb³⁺ with commercial LiF:Mg,Ti phosphor along with personnel neutron dosimetry studies and probable TL mechanism

2.3.9 Synthesis of Isocoumarins, 1,6-Diketones, and 1,3-Enynes via Rhodium and Palladium-Catalyzed C–H/C–C Bond Activation

The transition metal-catalyzed inert bond activation has become a very powerful tool in organic synthesis and is the most explored areas in organic synthesis in the last two decades providing the chemists with new retrosynthetic pathways. This strategy provides both step, cost, and atom economy, by avoiding the need for pre-functionalized substrates and thus streamlining organic synthesis. Present thesis explores the concept of directed C–H bond activation/functionalization chemistry in the synthesis of different isocoumarin systems, which are present as the core skeletons in numerous biologically active molecules and natural products. In the present work, isocoumarin synthesis was explored following rhodium-catalyzed redox-neutral protocol. Thus, rhodium-catalyzed redox-neutral synthesis of biologically active alkynylated isocoumarin, bis-isocoumarin, and isocoumarin were realized in this work. The C-C bond activation of cyclopropanol via the β-carbon elimination pathway has been well depicted in this thesis. Present thesis also showcases rhodium-catalyzed synthesis of 1,6-diketones and palladium catalysed synthesis of 1,3-enynes. It is anticipated that the present thesis will contribute significantly to the research areas of C-H and strain driven CC bond activation for the synthesis of diverse heterocycles with various molecular architectures.
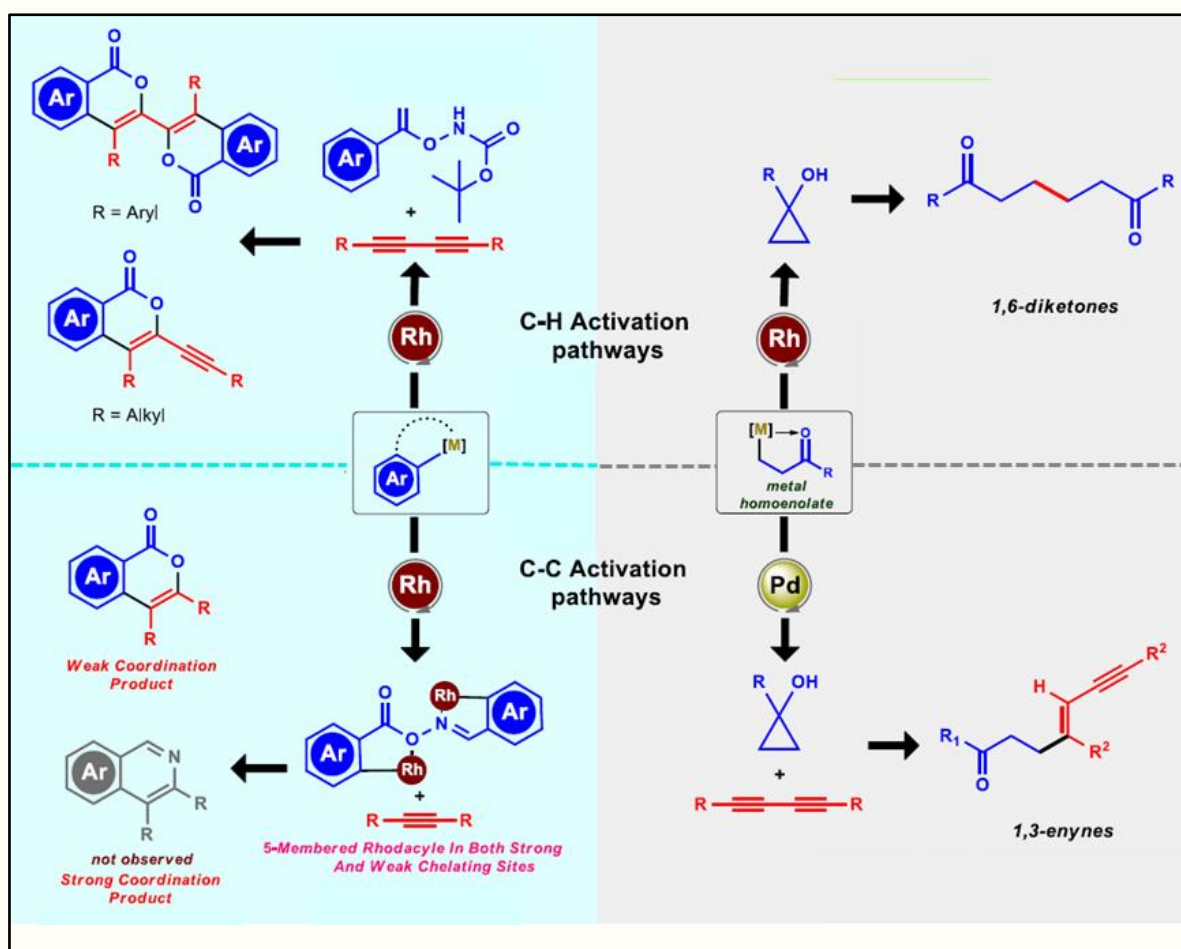
Different transition metal-catalyzed C-H and C-C bond activation strategies explored in the thesis.

3. Engineering Sciences

During the period of the present report, 34 research fellows have received their Ph.D. degrees in Engineering Sciences from Homi Bhabha National Institute. Following are the highlights of some selected theses in Engineering Sciences.

3.1 Bhabha Atomic Research Centre

3.1.1 Microstructural Characterization of Irradiation Induced Defects in Nuclear Structural Materials

In the present study, the investigation of microstructural and mechanical property changes in binary Zr-based alloys induced by heavy ion (Ar9+) irradiation are reported. For this purpose, four Zr-based binary alloys, namely Zr-0.17 wt.% O, Zr-0.33 wt.% Sn, Zr-2.9 wt.% Sn and Zr-2.5 wt.% Nb, with starting microstructures exemplifying annealing, hot-extrusion and cold-pilgering operations, respectively, were selected. The alloys were irradiated at room temperature using 315 keV energy Ar9+ heavy ion irradiation to the fluences ranging from 3.1x1015 to 4.17x1016 Ar9+cm-2. The induced damage was simulated using NRT and arc-dpa models. Considerable differences were observed amongst the damage-depth profiles predicted by these models with former overestimating the dpa value. S-parameter, probed using positron annihilation spectroscopy, showed an increase with fluence. A comparison between the experimentally determined damage-depth profile using positron annihilation Doppler broadening spectroscopy (PADBS) with the simulated profiles indicated an underestimation of damage-depth in simulations. The differences observed between Zr-2.5Nb and Zr-0.33Sn with that of Zr-0.17O in respect of percentage change in S-parameter and its depth-wise variation upon irradiation were rationalized invoking interaction of the alloying elements with irradiation induced point defects.

The microstructural Changes attributes, viz., the coherently scattering domain size, microstrain, dislocation density and residual stress, were ascertained through grazing incidence X-ray diffraction. A decrease in domain size and increase in both microstrain and dislocation density were observed in addition to development of compressive stress in place of tensile after irradiation. The mechanical properties like nanohardness and yield strength (derived from nanohardness) with the varying fluences were also investigated for the selected alloys. The nano-hardness of the irradiated samples was found to be higher in comparison of unirradiated one. Transmission electron microscopy investigation exemplified the formation of <a>- and <c>- type dislocation loops upon irradiation. The above findings have been rationalized based on the defects generated during the Ar9+ heavy ion irradiation.

3.1.2 Studies on Recovery of Metal Ions from Low-level Nuclear Effluent using a Complexation Filtration Extraction Hybrid Technique

Several countries are pursuing an attempt to reduce low and intermediate level effluent generated in nuclear facilities. Effectiveness of any process to achieve this depend largely on the chemical and radio-chemical composition of the liquid waste. In this regard complexation, filtration, solid phase extraction hybrid technique may prove to be worthy. The present study attempts to treat a low level

radioactive waste using the hybrid technique. The method enables reuse of treated water, minimise fresh water consumption, protect ecology and environment, helps in reducing toxicity in the food chain and promotes a sustainable growth. The proposed process is depicted in the following graphical representation. Polymers with O and N donor atoms are able to complex with metal ions in varying degrees which can be arrested by ultrafiltration membrane. The permeate from UF when passed through Polyhydroxamic resin bed will be stripped of all metal ions. A typical radioactive waste generated during the Calciothermic reduction of uranium oxide was treated using the bench scale. setup. The Uranium concentration was around 1000 ppm and total metal concentration was around 1200 ppm. A decontamination factor w.r.t metal ion concentration was found to be around 1200 and the volume reduction factor was around 10. The resin and the membrane can be regenerated with 1 N HCl. Thus, the life cycle of the process is largely enhanced.
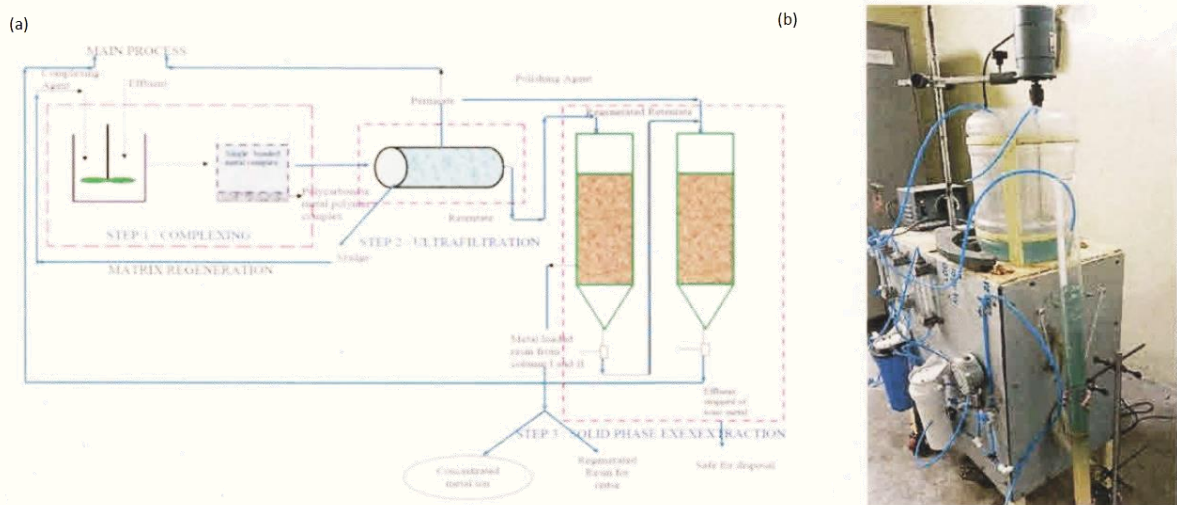
(a) Schematic diagram of the conceptualized hybrid process for waste treatment,
(b) Bench scale set up for radioactive waste treatment.

3.1.3 Deformation and Fracture Behaviour of FCC-based Single Crystals: Experimental and Numerical Studies

As industrial advancement increases, the need for reliable design for single crystal based components simultaneously rises. Understanding the mechanical behaviour of single crystals thus becomes essential to facilitate the development of advanced component design. Plasticity in metallic single crystals, which promotes damage owing to shear localization, precedes fracture. Fracture is also affected by the anisotropy of the material in the localised zone. Crystal plasticity theory, provides a rationale for anisotropic constitutive relations, combining with finite element method has been extensively used to investigate the orientation effect on plastic deformation. On the other hand, crystal plasticity finite element method has been applied to fracture mechanics problems to examine the crack tip plasticity due to localise deformation for various orientations of crack. However, a detail study considering the aspects of both the microstructural effects and damage evolution and hence facilitating simulation to determine fracture properties such as crack tip J-initiation, stress-triaxiality, etc., as a function of crystallographic orientations within the crystal plasticity framework is not properly elucidated. The present work is therefore an effort toward that direction to model the single crystal behaviour within the hierarchical modelling framework.

The schematic shown below presents the methodology adopted to investigate the orientation dependent mechanical behaviour in terms of deformation and fracture of single crystalline materials w.r.t. crystallographic orientations subjected to different loading conditions. At first, a combined experimental-numerical study on the deformation of FCC crystals is performed. To analyze the deformation responses of FCC single crystals, a crystal plasticity finite element model that considers non-Schmid effects is employed. An assessment of the constitutive model by comparison against measurements from experiments is subsequently conducted. The capabilities of the modelling framework to evaluate the fracture initiation of a single crystal edge-crack specimen subjected to tensile load is then discussed. Finally, the constitutive framework is applied to determine fracture behaviour of a cracked intermetallic single crystal turbine blade subjected to tensile load simulating centrifugal force due to rotation. This makes the present methodology as a potential option for design applications to analyse single crystal complex structures with cracks subjected to loading for various crystallographic orientations.
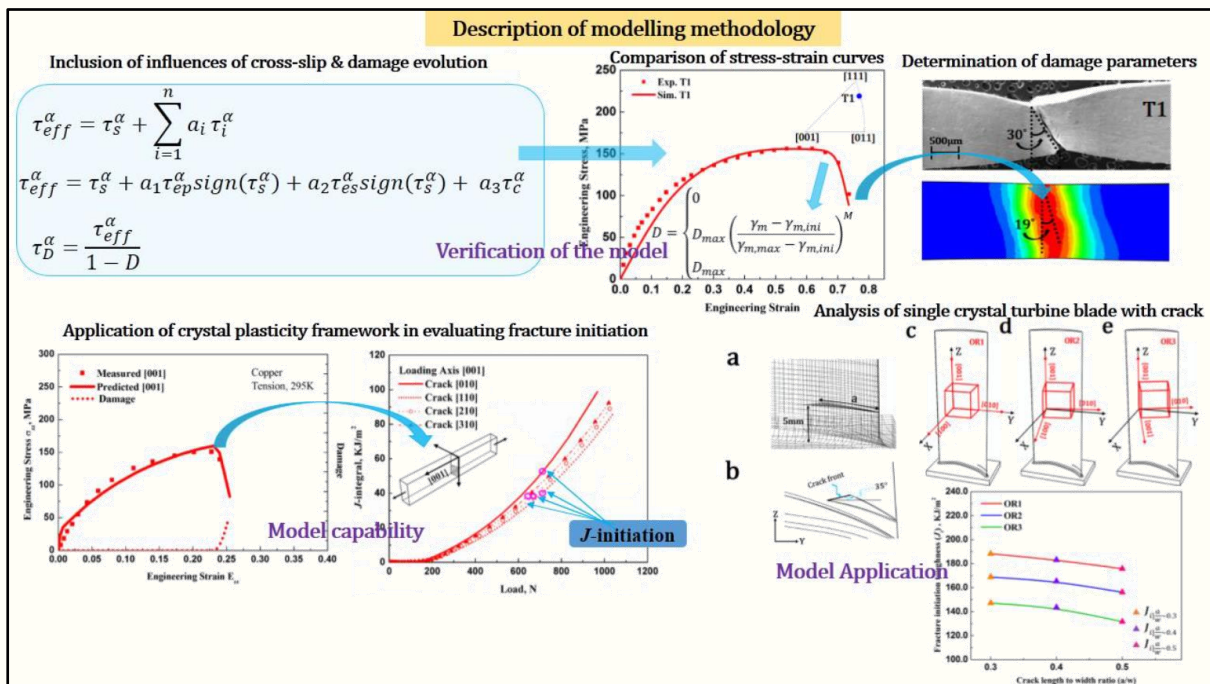
Schematic showing the methodology adopted to investigate the orientation dependent mechanical behaviour in terms of deformation and fracture of single crystalline materials w.r.t. crystallographic orientations subjected to different loading conditions.

3.1.4 Studies on the Recovery and Separation of Hydrogen Isotopes from Inert Gas

The objective of the present study is the evaluation of different processes for the recovery and separation of hydrogen isotopes from inert gas such as helium. The processes such as oxidation, adsorption, permeation, and electrochemical separation were studied in detail. In most of the cases, the experimental data on kinetics using heavier isotopes of hydrogen are very scarce. In catalytic oxidation, multi-step reaction mechanism in presence of platinum catalyst was analyzed and a simple rate expression is proposed and validated. A new mass transfer correlation was proposed to determine the gas film mass transfer coefficient in terms of Sherwood number, Schmidt number, and Reynolds number. The feasibility of recovery of hydrogen from helium by oxidation using metal oxides (viz, CuO) was established in a temperature range from 100oC to 200oC and the system was modeled

using classical shrinking core model. Further, the recovery of hydrogen isotopes from helium using palladium based adsorbent was studied and the rate limiting step is found out to be internal diffusion. A schematic of the process and the results are summarized in Fig.1. A composite tantalum membrane was fabricated in-house using sputter coating technique. An optimum temperature range of operation is determined using tantalum membrane for hydrogen and deuterium. The separation of hydrogen from helium was studied further using an electrochemical reactor. In the electrochemical reactor, a current density of 2000 Am-2 could be achieved at a cell voltage of less than 100 mV and the electrochemical reactor was modeled as a plug flow reactor with side withdrawal. Finally, a comparison of different processes was made based on different criterions such as percentage gas recovery, mode of operation (batch/continuous), energy required, operating temperature and gas purity achieved in different processes. Based on all the above criterions, the electrochemical separation is proposed to be a promising option.
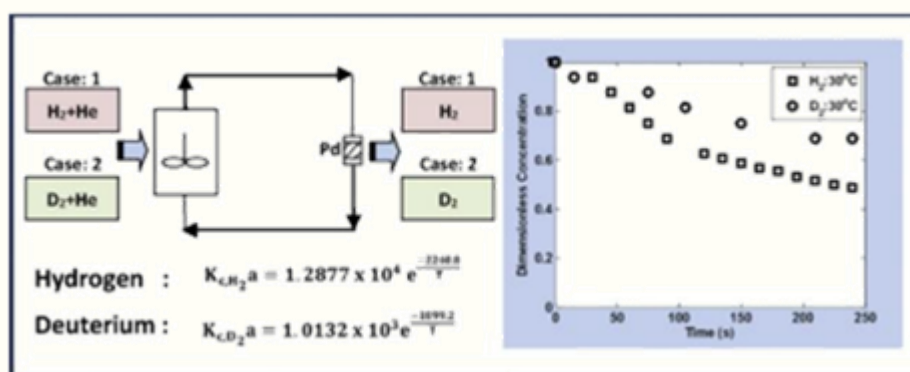
Schematic showing process and dimensionless concentration vs. time for adsorption

3.1.5 A Study on The Effect of Surface Finishing Operations on The Electrochemical Nature of Oxide Film Formed On 304l Ss In Aqueous Environments.

Protectiveness of the oxide formed on austenitic stainless steel (SS) surface determines the component's life during service in primary circuit of light water reactors. The present study used type 304L SS with four different surface states (machined, SiC paper polished (SiC-P), diamond polished (DP) and electropolished (EP)) to understand the effect of surface finishing operations on the protectiveness of oxide formed on type 304L SS in aqueous environments. Machining resulted in a top severely plastically deformed (SPD) layer (having highly strained nano/ultrafine grains (NUGs)) and deformed subsurface layers (unfragmented grains with high density of deformation bands). Using a novel controlled material removal process and electrochemical tests at room temperature, it was shown that both the SPD and subsurface deformed layers adversely affect the protective nature of the oxide, wherein the defect density in the oxide formed over machined surfaces were twice than in that formed over diamond polished surfaces. Detrimental effect of machining was observed so long as substantial strain induced due to machining was present within the matrix. The point defect model was used to explain the role of machining on passive film stability.

High temperature oxidation (at 300 °C) in deaerated demineralised water of specimens having all four surface states resulted in thinner oxide with higher Cr % and lower defect density on machined surfaces, as compared to oxide formed on less strained SiC-P and DP specimens. At high temperature (300 °C), the dislocations and NUG boundaries in the machined SS enhanced the diffusion of Cr.

Thinnest oxides with highest Cr % and least defect density (hence, most protective) formed on EP specimens. However, the mechanism of Cr enrichment was different. Higher protectiveness was due to Cr enrichment in the air-formed oxide on EP surface, which impeded further diffusion of metal cations in high temperature water. With increasing oxidation time at 300 $^{\circ}$C, the inner layer of the oxide formed on machined SS grew richer in Cr and its defect density decreased (i.e. oxide grew more protective with increasing time). It was proposed that the initial high NUG boundary area and high strain resulted in rapid oxidation of the machined surface forming an oxide with higher defect density that reduced with time due to enhanced mobility of ions in the thinner oxide and possible restructuring of the oxide.
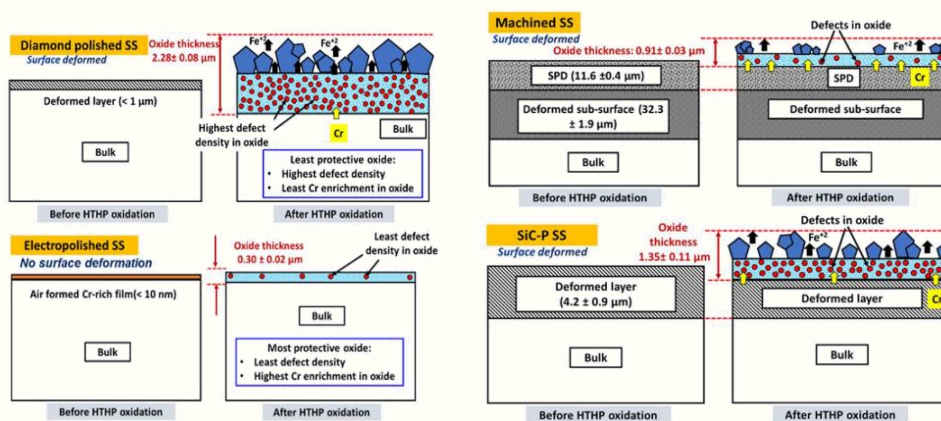
Schematic showing cross-sections of machined, SiC-P, diamond polished (DP) and electropolished (EP) SS before and after high temperature aqueous oxidation, indicating respective surface affected layer and oxide thickness.

3.1.6 A Multiscale Model for Simulation of Plastic Deformation Behavior of Ni-based Alloys with Explicit Consideration of the Effect of Grain Boundaries

For polycrystalline materials, the plastic deformation behavior is governed by pre-existing defects like dislocations and grain boundaries (GBs). During deformation, GBs are capable of acting as obstacles, sources and sinks to dislocations. In reality, all these traits often co-occur in conjunction with bulk plasticity within the grains. All these processes are inherently multiscale in nature, and are, thus, modeled discretely using a single length scale or time scale tool. The modeling efforts are then linked through some empirical coupling across the scales which may not be representative of the actual phenomena. It is, therefore, essential to explore new avenues to model polycrystal plasticity incorporating physically-justified GB modeling schemes. This is the prime focus of the current work. The multiscale approach adopted is presented in schematic.

Microstructural characterization provides the statistics on initial texture, grain size distribution and GB character distribution of the polycrystalline material. The statistical distribution of GBs determines the major CSL boundaries present in the alloy. Since thermally activated deformation mechanisms are prevalent under the investigated experimental conditions of uniaxial tension and compression at different temperatures, these GBs are modeled in the realm of atomistic simulations to quantify the activation parameters for partial dislocation nucleation from GBs. The extracted parameters are passed on to the flow rule of transition state theory based crystal plasticity model. At this level,

interfaces are explicitly modeled by assigning discreet thickness to the elements representing GB affected region and the associated parameters are directly taken from lower scale atomistic simulations. For bulk grains, dislocation dynamics simulations are utilized to calibrate the hardening parameters for single phase polycrystalline materials and different starting initial textures are utilized to achieve an optimum hardening parameter set for multiphase polycrystalline materials for use in crystal plasticity simulations. The approach is validated by comparison with the experimental stress-strain curves and deformed textures.
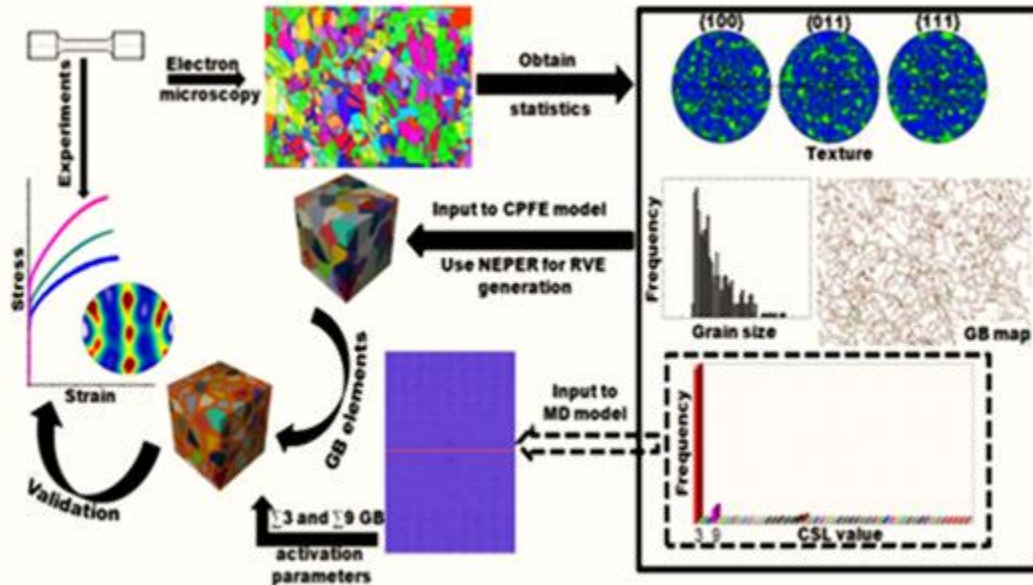
Schematic of multiscale methodology adopted in the present work
for appropriate inclusion of GB effects

3.1.7 Development of Hydrometallurgical Unit Operations for the Recovery of Cobalt, Rare Earths and Uranium from Secondary Resources

Any effort for resource (minerals/metals) security for a nation, necessarily involves augmentation of the exploitable resources be it primary or secondary. With depleting primary sources, utilization of any "secondary resource" for metal / mineral values assumed significance as this approach serves the objectives of "Wealth from Waste" and/or "Sustainability Development Goals". Amongst the various options available for utilization of secondary resources for recovery of mineral / metal values, the path of "Hydrometallurgy" stands ahead because this route is highly suitable for lean-tenor resources of complex and challenging. Compositions. The present work investigates the recovery of some clean energy metals like cobalt from lateritic origin Sukinda chromite overburden, rare earths from coal fly ash of Indian origin and uranium from crude sodium diuranate of phosphoric acid origin. The work pertaining to the thesis firstly demands selectivity in the extraction processes, like Co has to be selectively leached from COB, REE to be separately adsorbed from coal fly ash leach solution and uranium has to be separated primarily from lean content of REE. Thus, secondly, the challenge was to handle sources from lean content of the valuables or to separate lean values from major ones. Thirdly all the gap areas were targeted in the vexed topics which already consists huge volume of published literature. Fourthly, novelty of the work was established through four publications in standard

journals. Fifthly all the jobs were focussed on development of particular unit operations which will be scalable too. So finally, all the unit operations of hydrometallurgy were touched upon through developments in leaching, column separation, solvent extraction, precipitation etc. The experimental findings were supported by theoretical computation-based calculations adopting Taguchi/density functional theory (DFT) approach.
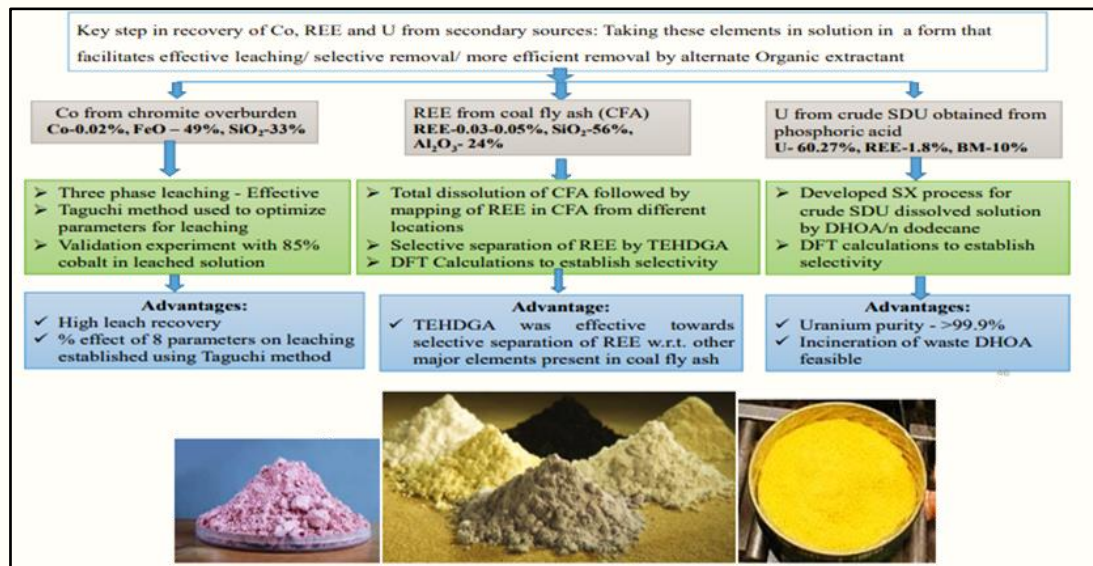
Schematic representing the output of present research work

3.1.8 Oxidation and Electrochemical Behaviour of an Alpha-phase Titanium Alloy in Different Environments

The properties of a material are greatly influenced by alloying element addition as well as temperature. This also holds good for titanium alloys which have a promising application in the nuclear/chemical industry due to their superior corrosion resistance. However, titanium alloys are typically not used in air at high temperature due to their poor resistance to oxidation. Given this, the study focuses on two aspects of an alpha-phase titanium alloy, Ti-Al-Zr. Firstly, the oxidation behaviour of the material was studied in (a) air at 760 °C, 0.1 MPa and (b) steam at 400 °C, 10 MPa. Secondly, the electrochemical behaviour of the material was studied in oxidizing nitric acid environments and the electrochemical properties are compared with SS 304L. It is shown that the oxidation mechanism of the alloy is entirely different in air and steam environments. Air oxidation also led to formation of an oxygen-enriched layer in the matrix (near to the surface).

The electrochemical behaviour of the oxygen-enriched layer was established in ammonia environment and it was shown that the presence of an oxygen-enriched layer resulted in a more protective anodic passive film. The electronic properties of the oxide, formed during steam oxidation, were studied and it was shown that growth kinetics of the oxide was dictated by both titanium interstitial and oxygen vacancies. On the other hand, growth kinetics of the anodic passive film formed in the ammonia environment was shown to be dominated by oxygen vacancies. The electrochemical behaviour of the was studied and compared with. SS 304L in oxidizing nitric acid environments (3 M nitric acid, V+5 ion

addition and at 75 °C). It is concluded that the alloy showed a superior corrosion resistance as compared to SS 304L in oxidizing nitric acid environments and can be a potential material for use in such applications. The cyclic voltammetry studies using Pt electrode established thermodynamics of different cathodic reactions and their kinetics in different oxidizing nitric acid environments. It was shown that the nitric acid reduction was influenced by acid concentrations, temperature and presence/absence of oxidizing ions.
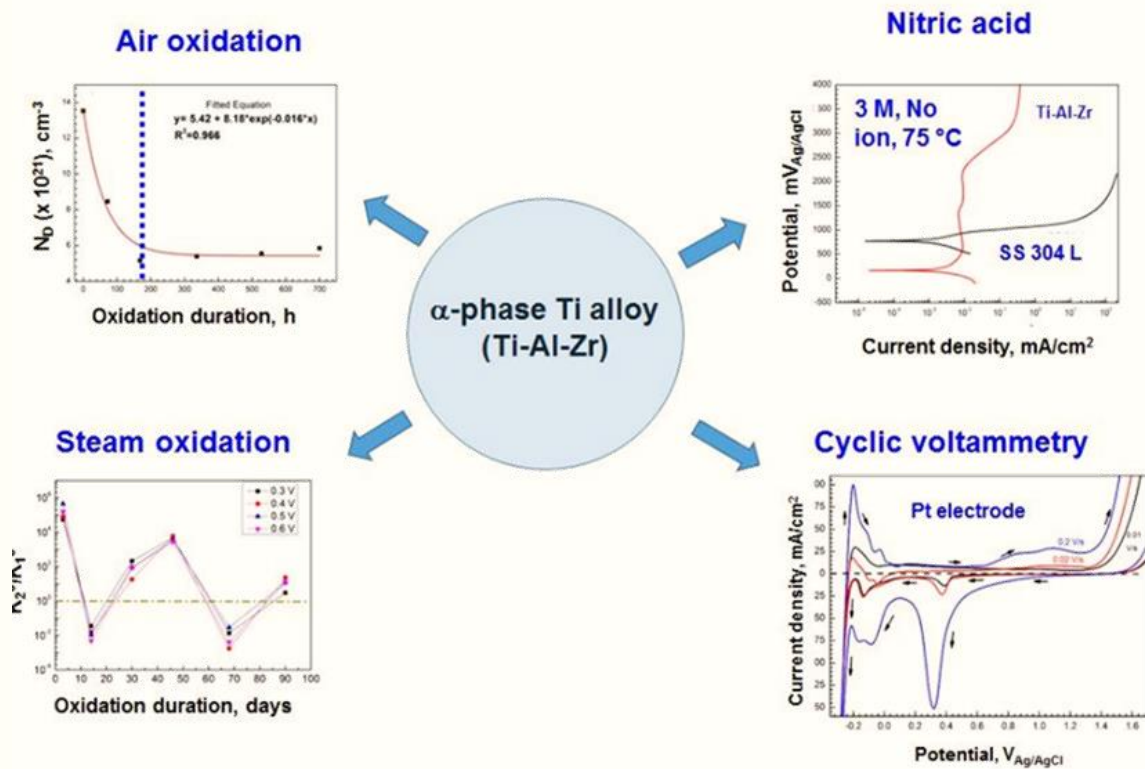
Study of different properties of an alpha-phasetitanium alloy, Ti-Al-Zr, in different environments

3.2 Indira Gandhi Centre for Atomic Research

3.2.1 Development of Fly Ash based High Performance Concrete Blended with Nanoparticles and Inhibitor for Marine Applications

The engineering community is becoming increasingly concerned about durability of concrete, since numerous incidents of premature deterioration have been recorded throughout the world. Because of its enormous economic impact, deterioration of concrete structures in aggressive marine environments require special attention. Further, as the global CO2 emissions from cement production account for ~ 8%, there is an urgent need to reduce the carbon footprints by using supplementary cementitious materials. To address this issue, this thesis was aimed at development of a novel high performance concrete composition (CFNI) with a combination of 56 wt. % OPC, 40 wt. % fly ash, 1 wt. % nano-CaCO3, 1 wt. % nano-TiO2 and 2 wt. % NaNO2 based anodic mixed inhibitor solution for marine applications. More than 500 specimens of four different compositions were tested to bring out the performance of CFNI concrete system. An improvement in the mechanical strength and durability was observed with the combined incorporation of additives. Moreover, the shortfalls associated with fly ash concrete with respect to early age strength was overcome due to the

synergistic properties. MIP results showed the presence of small gel pores at nanoscales (~10 nm) in CFNI specimens, indicating the refined and improved pore structure that prevents the permeation of ions, which is highly promising for applications in marine environments. A five times higher value of polarization resistance obtained in CFNI, as compared to the control concrete, indicate its better corrosion resistance. The probabilistic service life of the steel in concrete systems showed that the time to initiation of corrosion in CFNI specimens is six times higher than the control concrete. The CFNI specimens showed an enhanced resistance against bacterial and fungal attack as indicated by the reduced biofilm formation over the surface through CLSM analysis. Further, a four order reduction in the total viability count and ATP (Adenosine triphosphate) concentration and a three order reduction in the DNA intensity was observed in CFNI concrete as compared to control specimens. The residual strength reduction was low in CFNI concrete due to the densified microstructure and increased SiO_2 content under three chemical environments (seawater, acidic and sulfate) compared to control concrete specimens. Long term exposure studies in seawater showed that CFNI specimens had 87% reduction in the chloride penetration value than control specimens and the average depth of water penetration was significantly lower due to the pozzolanic reaction of the SCMs, filler effect of nanoparticles, low w/c ratio, and formation of favorable complex compounds. Schematic shown below summarizes the potential benefits of CFNI concrete as compared to conventional concrete.
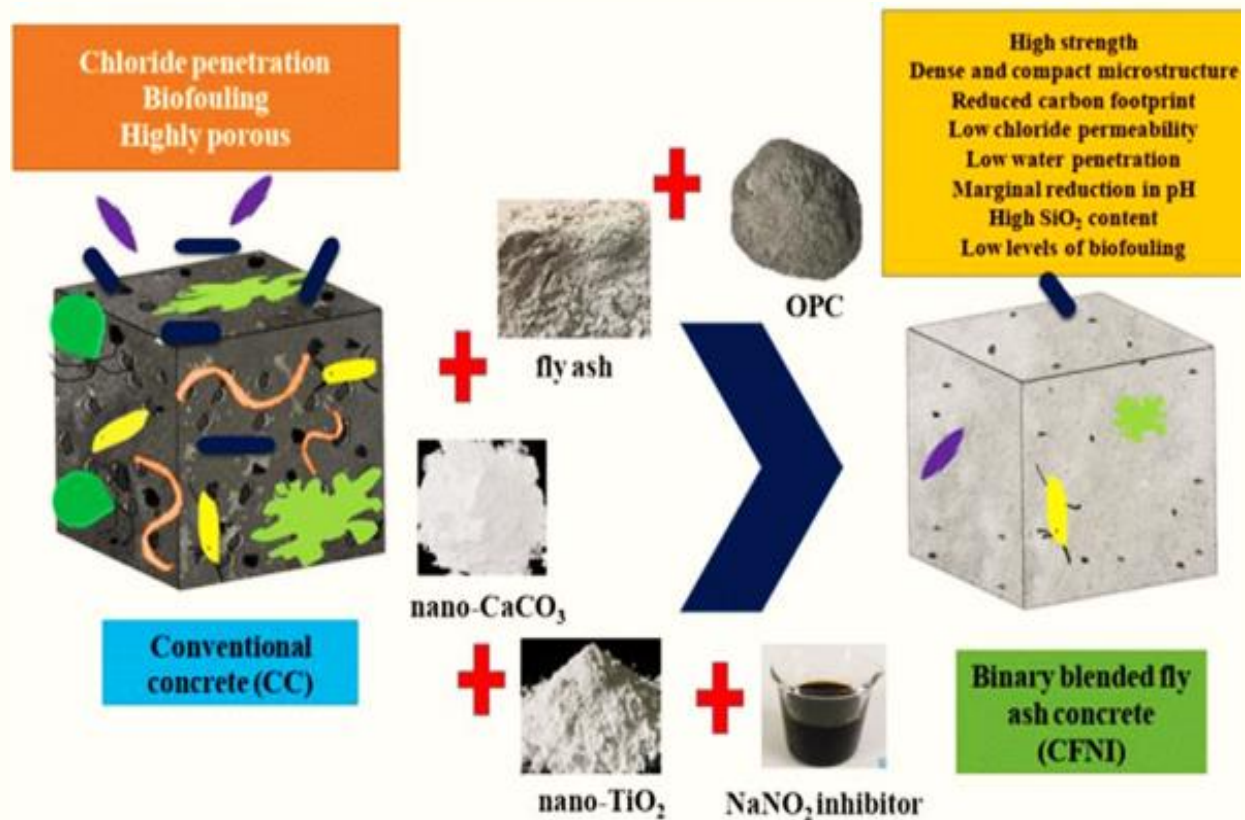
Potential benefits of CFNI concrete as compared to conventional concrete

3.2.2 Development of Interlayer Coatings on High-Density Graphite for Yttria Coating for Pyrochemical Reprocessing Application

High-density graphite (HDG) materials with excellent refractoriness and thermal shock resistance are widely used as induction melting crucible materials in cathode distillation and injection casting process (~1500 ˚C) employed in pyrochemical reprocessing application. However, the spontaneous oxidation of graphite materials beyond 500 ˚C in the presence of oxygen and the feasibility of forming metal carbides and intercalation compounds restrict the usage of bare HDG crucible in reprocessing applications. Therefore, a chemical barrier coating of thermodynamically stable yttria (Y_2O_3) on HDG is highly recommended for uranium melting applications. Further, to enhance the thermal cycle performance and durability of Y_2O_3 coating, the development of carbide/boride interlayers of intermediate coefficient of thermal expansion (CTE) value are in high demand. Thus, the present thesis focused on optimizing plasma spray parameters for top Y_2O_3 coating and comparative investigation of thermal cycle life with SiC and SiC-ZrB2 interlayers. As depicted in schematic, Y_2O_3 coating without any interlayer was found to delaminate due to thermal fatigue and sintering-induced densification at 10 thermal cycles (1550 ˚C). Partial oxygen ingress on prolonged exposure via vertical cracks found to commence HDG oxidation and complete spallation of Y2O3 coating. However, in the presence of SiC and SiC-ZrB2 interlayers, there was multi fold enhancement in Y_2O_3 coating thermal cycle life due to CTE mismatch minimization. Alongside, these interlayers act as an oxidation-resistant sealant at the Y2O3-HDG interface, protecting HDG from high temperature oxidation. Also it was confirmed that the respective oxides of interlayers (SiO_2, ZrO_2, and $ZrSiO_4$) completely cease HDG from further oxidation. Thus, during U-Zr melting applications, SiC or SiC-ZrB$_2$ composite interlayer enhances the melting cycles and impedes the carbon contamination in U-Zr ingot from HDG crucible by forming passive oxidation products as highlighted in schematic below.
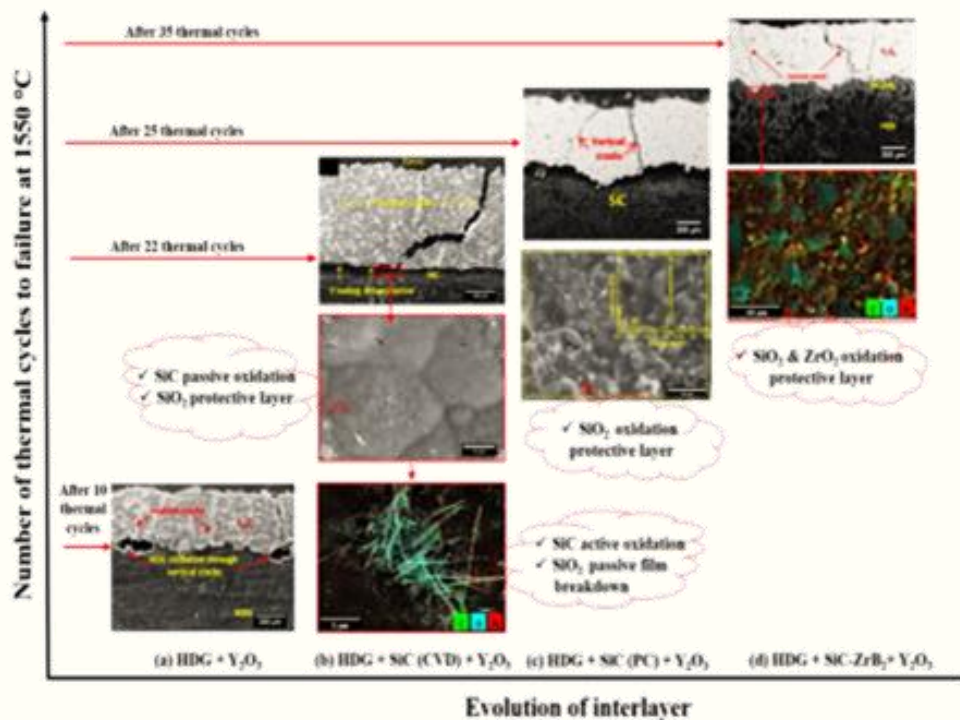
Evolution of interlayers (Sic-CVD, SiC-PC, SiC-ZrB2-PC) over HDG
with enhanced thermal cycle life of tio APS deposited Y_2O_3 *top coat*

3.2.3 Influence of Nitrogen on Tensile and Creep Deformation Behaviour of Type 316L Stainless Steel in the Framework of Internal-State-Variable Approach

In the present thesis, the influence of nitrogen content (0.07, 0.11, 0.14, 0.22 wt.%) on tensile and creep deformation behavior of type 316L austenitic stainless steel is systematically investigated in the framework of Internal-State-Variable (ISV) approach. The internal state variables considered for modelling include dislocation density and mean free path of dislocation for tensile behavior and internal stress and damage for creep. In the analysis of tensile strain-hardening behavior, a systematic increase in mobile and forest dislocation densities and a decrease in mean free path with an increase in nitrogen is observed. The results supported the observed high tensile strength properties and high work hardening with increasing nitrogen content. The transient and steady state creep deformation behaviour examined using sine hyperbolic creep rate law coupled with the evolution of internal stress indicated an increase in internal stress accompanied with lower dynamic recovery with increasing nitrogen.

The above results substantiated the experimentally observed beneficial role of nitrogen on extending the duration of transient and steady state creep regimes and the reduction in creep strain rate with increasing nitrogen levels. As damage evolution also plays an important role in creep behaviour, the steady state and tertiary creep behaviour of 316LN SS is examined in the framework of continuum damage mechanics approach using Kachanov-Rabotnov (KR) model. The superimposition of iso-damage contours on creep curves indicated higher creep damage development at lower strains with increasing nitrogen content. The introduction of the new parameter (ratio of strain rate to damage rate) indicated the predominance of damage rate over creep strain rate with increasing nitrogen content, complementing the observed propensity to intergranular damage at high nitrogen contents > 0.14%. The applicability of above ISV based constitutive models for structural design analysis is demonstrated by its implementation into the finite element code. The aforementioned observations in his investigations suggest the optimum nitrogen content (X in wt.%) in the range of 0.07% < X < 0.14%.

3.2.4 Total Focusing Method (Tfm) Based Phased Array Ultrasonic Techniques for Inspection of Thick and Attenuating Components

The study presents a systematic investigation on the development of total focusing method (TFM) based phased array ultrasonic techniques for inspection of thick and attenuating materials. A novel Angle Beam Virtual Source - Full Matrix Capture - Total Focusing Method (ABVSFMC-TFM) technique having the advantages of both FMC-TFM and plane wave imaging (PWI)-TFM is developed for inspection of thick and attenuating materials. The sensitivity, SNR and resolution of the developed technique are compared to the state-of-the-art phased array ultrasonic techniques.

Three different types of specimens have been used in the present study: (i) aluminum and austenitic stainless steel blocks with side drilled holes (SDHS), (ii) phased array Type B calibration block and (iii) alloy 617 forge block with planar defects to simulate lack of side wall defects in a narrow gap weld joint.

Effects of various experimental parameters on the resolution achieved in FMC-TFM phased array ultrasonic technique is systematically studied. It is observed from the study that the total effective aperture can be increased by increasing the number of phased array elements for an equipment with a large number of available channels. Alternately, it may also be increased by selecting nth element and thus increasing the effective aperture n times for a phased array equipment with a limited number of channels and a probe with a larger number of elements. A unified empirical relationship is reported for the effect of various experimental parameters on resolution (-6 dB spread) achieved using FMC-TFM. The best achievable resolution is found to be the function of the pitch size. To achieve high resolution at larger depth and/or in high attenuating materials, a new simple methodology based on a combination of FMC-TFM and SAFT (Synthetic Aperture Focusing Technique) is proposed that provided a resolution upto 1 mm at 150 mm depth in austenitic stainless steel block as shown in Schematic below.
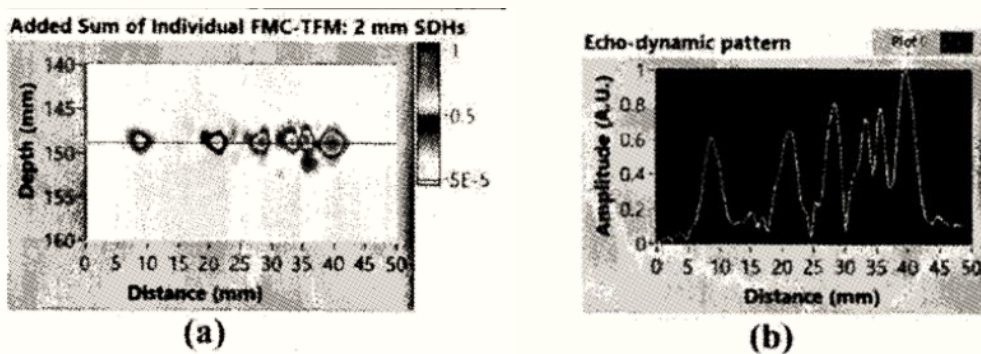
Schematic showing B-scan and corresponding echo-dynamic pattern for 2 mm diameter side drill holes at 150 mm depth in austenitic stainless steel using angle beam-FMC-TFM

ABVSFMC-TFM is demonstrated on thick 200 mm attenuating material Alloy 617 forged block as shown in schematic on right below. It led to improved sensitivity and higher signal to noise ratio (SNR) in inspection of planar defects (horizontal and vertical slots) as compared to that forFMC-TFM.The study indicated that the incident beam angle should be above 20° to obtain the bottom tip diffracted signal reliably as shown in schematic on left below.
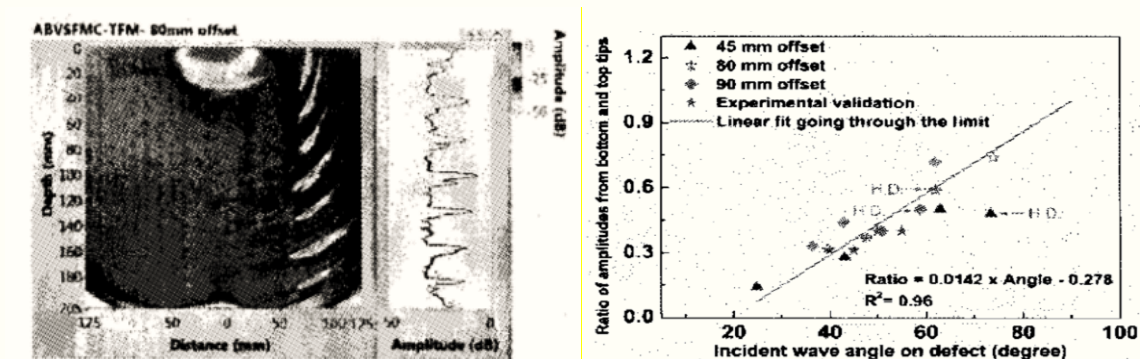
B-scan and corresponding echo-dynamic pattern obtained by ABVSFMC-TFM in alloy 617 forged block

Ratio of the bottom tip to top tip using ABVSFMC-TFM method

Further, sensitivity achieved in various advanced phased array ultrasonic techniques such as focused sector scan (FSS), FMC-TFM, ABVSFMC-TFM and PWI-TFM are studied for defects at different depths and specimens with different material attenuations. Resolutions achieved are found to be similar for all these advanced phased array beam forming techniques. However, transmission using multiple elements provides improved sensitivity in PWI and FSS (focused at the defect depth) as compared to FMC- TFM for defects at larger depths. The highest sensitivity has been observed in FSS followed by PWI-TFM, ABVSFMC-TFM and FMC-TFM, respectively. The ABVSFMC-TFM exhibited better SNR than PWI upto 175 mm depth in alloy 617 block. With 8 active elements and specific directivity, higher thickness/attenuating materials can be inspected with similar resolution and sensitivity in ABVSFMC-TFM as compared to FMC- TFM technique. This reduces the system cost and complexity.

3.2.5   Thermomechanical Fatigue Evaluation of Type 316 LN Austenitic Stainless Steel Weld Joint

Systematic investigations were performed on a type 316 LN austenitic stainless steel (SS) base metal (BM) and weld joint (WJ) under thermomechanical fatigue (TMF) employing in-phase (IP) and out-of-phase (OP) thermal-mechanical strain combinations using different temperature intervals (ΔT) in the range of 573-923 K and mechanical strain amplitudes $\Delta\varepsilon_{mech}/2$) varying from ±0.25% to ±0.6%. Concurrently, conventional isothermal low cycle fatigue (IF) tests were also carried out at for maximum temperatures (T_{max}) of the TMF cycles employing identical testing conditions. Important highlights of the work reported in the thesis are listed below.

1.   The phasing relationship employed for the TMF cycling has an important bearing on the stress response and cyclic life. A higher stress response coupled with reduced cyclic softening under TMF compared to isothermal cycling signified a marked effect of temperature cycling which imparts additional strengthening from the cold work effects in the former case. The weld joint displayed lower lives compared to the base metal under both IF and TMF cycling. Consistently lower lives were obtained under IP cycling compared to IF and OP, thus leading to a life variation sequence: IP TMF < IF < OP TMF.

2.   Dynamic strain ageing (DSA) was found to have a significant influence on the deformation behaviour and cyclic life under IF and TMF cycling. The serrated flow, an important manifestation of DSA, gets more pronounced with increasing $\Delta\varepsilon_{mech}/2$ for a given temperature range under IF and TMF cycling. The stress-strain hysteresis loops exhibited different types of serrations depending on the temperature regime of the TMF cycle and vary significantly with the temperature-mechanical strain phasing (IP and OP). However, the behaviour remained almost identical during the tensile and compressive parts under IF cycling. Repeated cold work effects arising from the lower temperature deformation under TMF cycling alter the metallurgical state of the material compared to IF cycling. This has important implications on the occurrence of DSA in terms of the nature and intensity of serrations. TMF yielded mostly mixed types of serrations. The variation in nature of hysteresis loops, the amount of hardening, softening and the position of cyclic stress-strain curves during the tensile and compressive ramps under TMF cycling indicate the dependence of deformation behaviour on the temperature regime of the cycle, phasing relationship and the $\Delta\varepsilon_{mech}/2$.

3. The influence of creep damage during steady-state operation was studied by performed creep-TMF and creep-IF tests by incorporating dwell periods of 60 s and 300 s at the peak tensile strain. The extent of reduction in cyclic life with temperature and hold duration is higher under creep-TMF compared to creep-IF cycling. Though the oxidation takes place to a greater extent under isothermal compared to the thermal cycling, the latter proved more damaging on account of a higher stress relaxation, reduced extent of substructural recovery and a greater propensity for DSA. Besides, TMF imparted greater creep damage as evidenced by more extensive intergranular cracking compared to IF cycling. The results obtained clearly highlighted the non- conservatism associated with the traditional design approach that relies on the isothermal database, strongly underlining the necessity of generating the fatigue data for the WJ under TMF cycling.

4. Thermal ageing resulted in a decrease in the stress response and the DSA effects compared to the as-welded condition. This had a strong bearing on the deformation behavior, fatigue life and development of damage in the weld joint. However, the beneficial effect of thermal ageing on life is found to decrease with increase in the T_{max} and $\Delta\varepsilon_{mech}/2$ due to the deleterious consequences of ageing-induced microstructural transformations in the weld region. The fatigue life of the aged joint was observed to be dictated by the opposing factors related to the beneficial effects associated with the deformation uniformity across the joint and the deleterious consequences of the precipitation of carbides and brittle intermetallic phases following for ageing treatment in the weld joint. Cracking due to localised deformation and strain incompatibility across the interfaces of austenite/δ-ferrite/σ-phase is established to be an important damage mechanism under IF and TMF cycling with and without hold times. The effect of microstructural embrittlement becomes more pronounced with an increase in the duration of hold, which together with the creep damage contributed to a decrease in the fatigue life.

5. The location of crack initiation in the weld joint under IF and TMF cycling is influenced by a combination of metallurgical notch effect and microstructural transformations, and seen to be sensitive to the imposed strain amplitude and type of fatigue cycle (IF and IP/OP TMF). The longer time of exposure to the identical average temperature during OP compared to IP TMF tests, coupled with the significantly higher tensile stresses (compared to IP and IF) led to cracking mostly in the weld zone in the OP TMF cycling. Coarse grain size with large scatter in strength in the HAZ region of the joint make it a preferred site for crack initiation during IP TMF and IF cycling due to high temperature tensile deformation.

3.3   Institute for Plasma Research

3.3.1   Superhydrophobic Surfaces Developed through Argon Plasma Processing for Self-cleaning and Water Harvesting Technologies

Due to the exellent water repellent property, superhydrophobic surfaces have been a trending research topic over the last one decade. Many researchers have employed various kinds of fabrication techniques to fabricate a variety of bioinspired smart materials with unique functional properties such as self-cleaning, anti-icing, anti-fogging, oil-water separation, water harvesting, omnibhobicity, oleophobicity, etc. Also, plasma-based methods to achieve superhydrophobicity have achieved great attention due to their ability for large-scale production, cost-effectiveness, and environmentally

friendly nature. Plasma-based processes such as ion beam irradiation, plasma etching, and physical vapor deposition (PVD) are widely used to produce hydrophobic and superhydrophobic surfaces.

The present thesis aims to develop superhydrophobic surfaces using argon plasma processing for self-cleaning and water harvesting technologies. Firstly, systematic static and dynamic wettability studies were carried out on the PTFE surface using low energy Ar ion beam. The effect of various ion beam parameters such as ion energy, ion dose, and angle of incidence was investigated in view of producing a superhydrophobic surface for self-cleaning applications. Radiofrequency (RF) Ar plasma etching process was used on the PTFE surface for producing an industrial-scale superhydrophobic surface. The influence of RF power, treatment duration, impurity, and surface temperature on Ar plasma-treated PTFE was studied. Further, the effect of plasma processing on the wettability of copper surfaces was investigated for the development of an efficient water harvesting device. The process was optimized in terms of type of condensation on the surface, water collection rate, and durability of the surface. After plasma processing, the water contact angle of the copper surface systematically increased to values ranging from 132° to 156°. Moist air condensation experiments were carried out on both pristine and plasma-treated copper surfaces using an in-house water harvesting device.
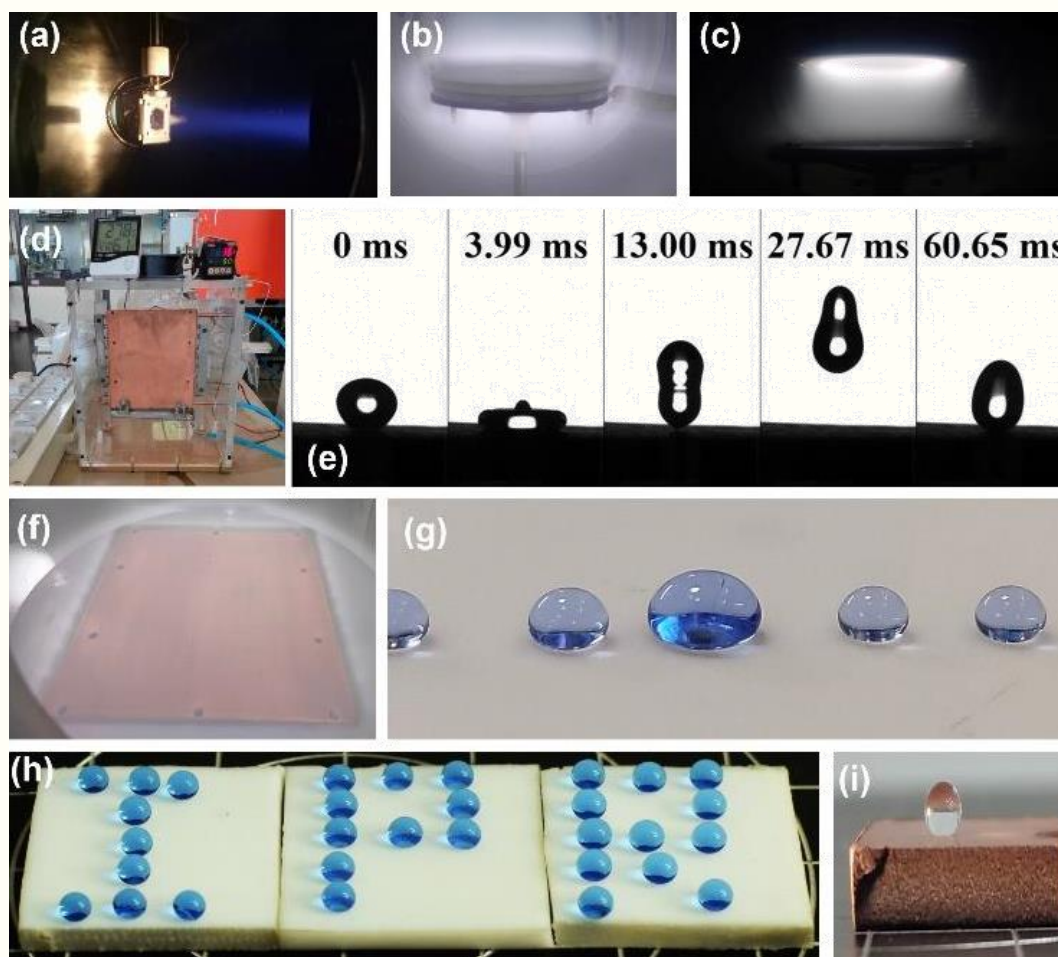
Schematic showing highlights of the argon plasma processing used to produce superhydrophobic PTFE and copper surfaces. (a) Ar ion beam, (b) RF plasma etching, (c) Thin-film deposition, (d) water harvesting setup, (e) bouncing water droplet, (f) Plasma etching of copper, (g) spherical water droplets on PTFE, (h) "IPR" written with water droplets, and (i) superhydrophobic copper surfac

3.3.2 Study of Plasma Activation of Water and its applications in Antimicrobial and Agricultural activities

Plasma activated water (PAW) has enormous potential to be used for numerous applications in the field of microbial inactivation, food preservation, enhancing seed germination and plant growth, and as a nitrogen source (as fertilizer) for agriculture and aquaculture, etc. Some of the major challenges in the current PAW technology are undissolved gases and reactive species that cause environmental pollution in the form of elevated concentrations of NOx and O3, high volume of PAW production, limited antimicrobial activity, and loss of PAW antimicrobial activity over time and its mechanism, and understanding the role of PAW in seed germination and plant growth.The present work discusses the design, development, and optimization of a plasma activated water setup that reduces the above-mentioned pollutants and optimization of process parameters such as plasma-water interaction time, plasma discharge power, gas flow rate, and gas type, etc. The plasma is characterized based on voltage-current waveform, and the species/radicals generated in the plasma are identified using optical emission spectroscopy. PAW is characterized by measuring the physicochemical changes (pH, oxidizing potential, and electrical conductivity) and the concentration of dissolved reactive oxygen-nitrogen species ($_{NO3}{}^-$ ions, $NO_2{}^-$ ions, dissolved O_3, and H_2O_2).

The present work successfully demonstrates the long-term antimicrobial activity of PAW with a significantly low exposure time for 6+ log10 CFU ml-1 reduction (< 10 s for bacteria and 15 minutes for fungi). Moreover, the reason for PAW exposure with seeds that enhances germination and plant growth was successfully determined. Some of these results are shown in the schematic below. The PAW treatment with bacteria and fungi damages the morphology of cells as shown in schematic (a1-a6), (b1) showed higher plant growth in PAW treated seeds compared to control. The PAW treatment removes the naturally occurring wax structure from its surface, making the seeds' surface hydrophilic and resulting in rapid water absorption, as shown by enhanced germination rate and better plant growth. Hence, the present work showed significant advancement in the current PAW technology.
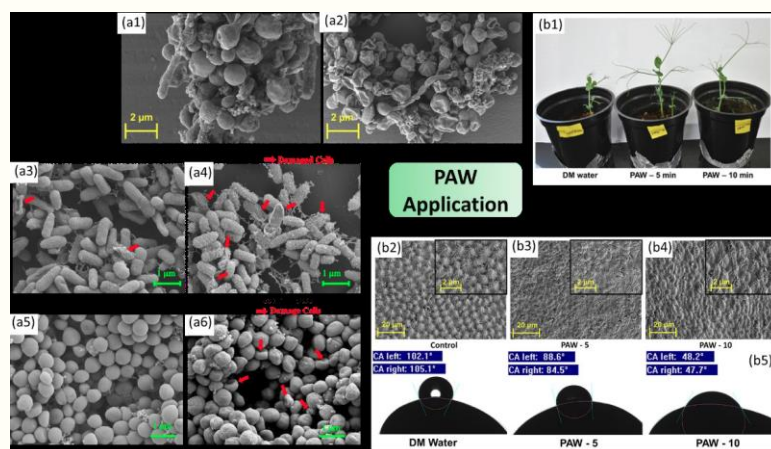
Schematic showing Antimicrobial (a1-a6) and agricultural applications (b1-b5) of plasma activated water

4. Life Sciences

During the period of the report, HBNI awarded 39 Ph.D. degrees in Life Sciences. Some of the theses are summarized below.

4.1 Bhabha Atomic Research Centre, Mumbai

4.1.1 A Comparative Study of Type I and Type II CRISPR-Cas Systems for their Applications in Modulation of Gene Expression using *rac*R as model

The CRISPR system is used for genetic manipulation in bacteria either through gene editing or silencing. There are two classes and many types of CRISPR systems, each with unique features. The under-utilized Type I (Cascade) system is compared to Type II (Cas9) and Type V (Cpf1) based on various parameters to determine their relative merits. The study provides a guide for selecting the appropriate Cas effector for a given application. Type I systems have been useful in studying essential genes, racR and components have been expressed in a eukaryotic model organism as a proof of concept towards genome interference platform. A standalone tool was developed to make the Type I-E CRISPR system easy to use and accessible, and it has been transferred to industry for commercialization.
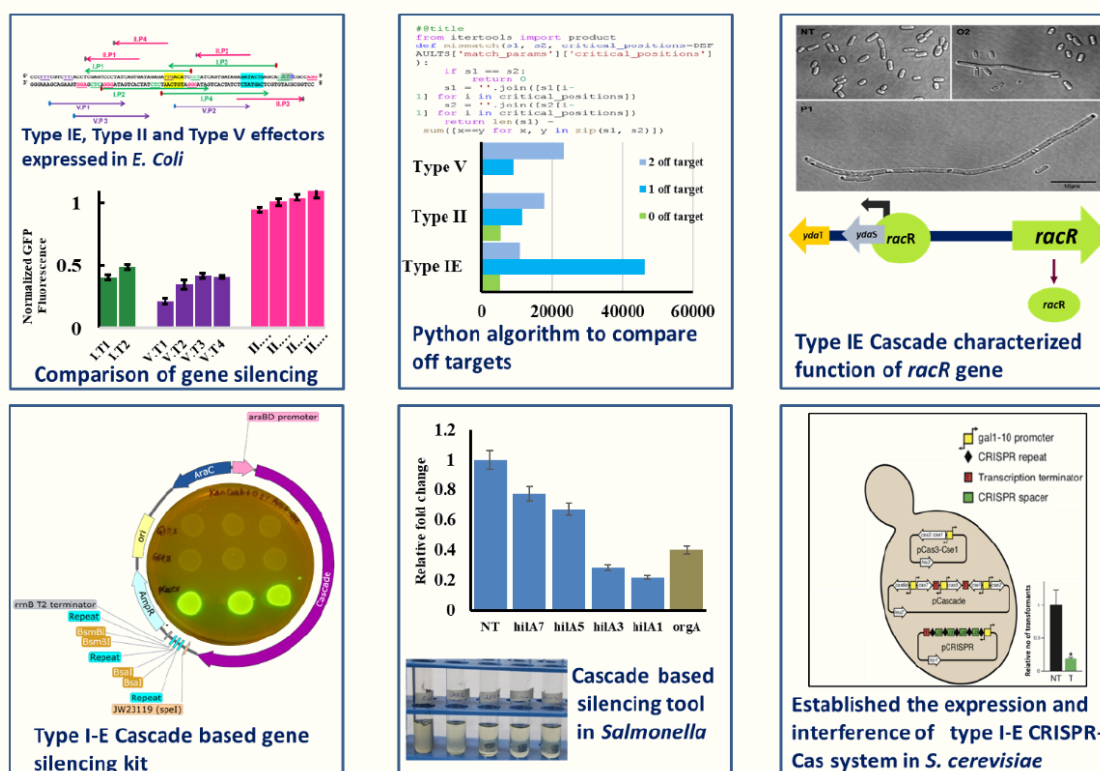
*Type I-E CRISPR System: Comparison with other types,
and novel applications*

4.1.2   Mechanistic Studies on Ubiquicidin-membrane Interaction & Development of Infection Imaging Probes

It was demonstrated that UBI selectively bind to the bacterial membrane and affect the bacterial membrane in variety of ways i.e. altered fluidity in bacterial membrane and permeabilization as well as depolarization of bacterial membrane. These changes at the membrane level resulted in loss of viability in bacteria. UBI derived fragments i.e. UBI (29-41) and UBI (31-38) also retained selective uptake in bacterial membrane, however, no effect on survival or growth of bacteria was observed. This work is the first report on antimicrobial action of Ubiquicidin or ribosomal protein S30. The mechanistic insights provided here can facilitate designing of improved antimicrobial agents and tracers for infection imaging. Intoduction of Lys-PG specific group, 2-APBA at the C-terminal of UBI (29-41) yielded an improved infection imaging probe by utilizing synergy between electrostatic and covalent interaction of peptide conjugate with the bacterial membrane. Through this work, introduction of 2-APBA is shown as an effective strategy of improving therapeutic potential of existing AMPs as well. Tracers labeled with ^{99m}Tc and ^{68}Ga were developed for SPECT and PET imaging. Limited clinical trials in patients with radiotracer ^{68}Ga-UBI (31-38) showed encouraging results.
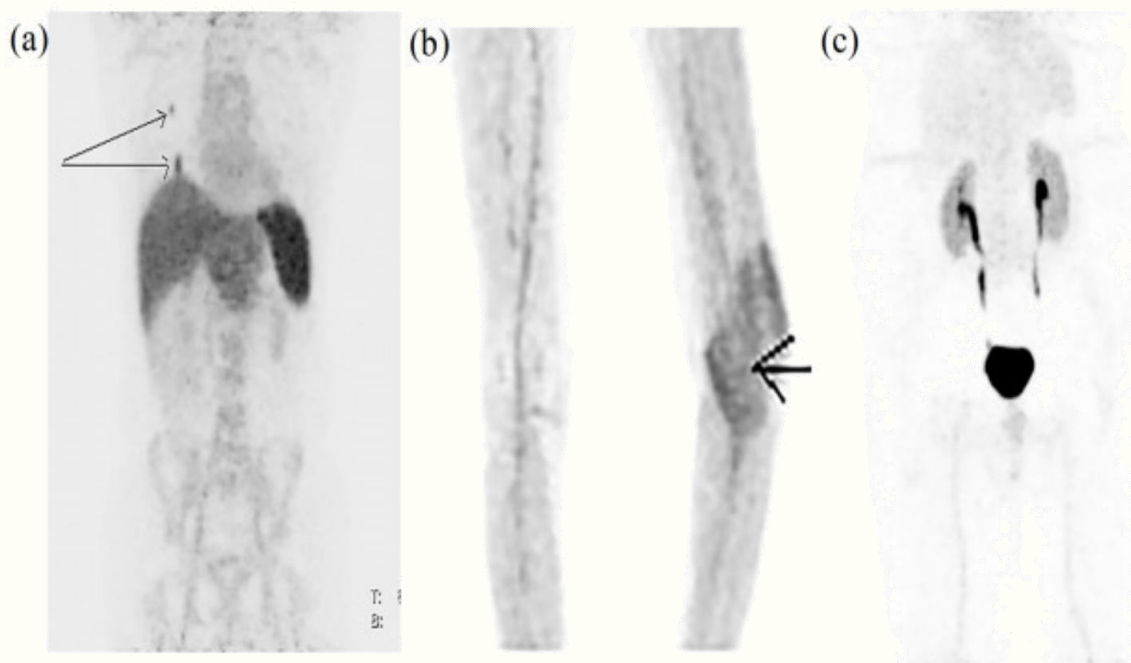
PET/CT images of patients injected with ^{68}Ga-UBI (31–38) at 1 h p.i. (a) Image showing lung infection (true positive scan). (b) Image showing for soft tissue infection in left knee (True positive scan) joint. (c) Image of a suspected left hip prosthesis infection (True negative scan).

4.1.3   Studies on Tumor Microenvironment Induced Changes in T cell Differentiation

The work explored in the thesis is based on effect of small molecules on tumor microenvironment induced changes in T cell differentiation. It has been established that tumor derived prostaglandin E2 induce the generation of a novel class of regulatory B cells (tBregs) which in turn suppress T cell responses through TGF-β mediated pathway and promote tumor progression in murine cancer model. The NS-398 and SB431542 were tested as potential immunotherapeutics in pre-clinical model. It has been observed that high H3K4me3, low H3K27me3 and high H3K27ac/ low 5-methyl cytosine are minimum epigenetic modification needed for FOXP3 expression. Finally, EPZ004777 and FG-2216 were established as epigenetic modifiers for potential immunotherapeutics.
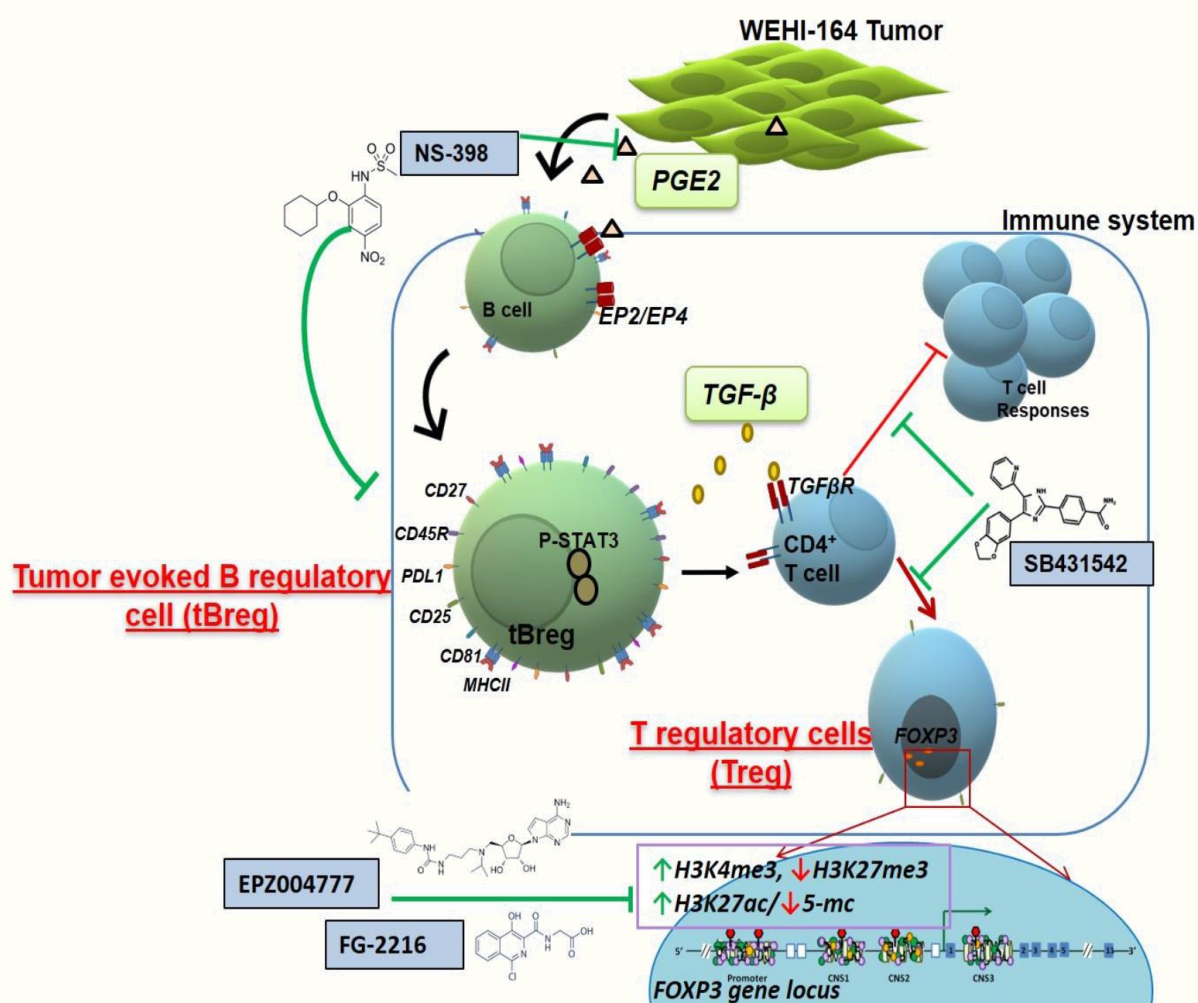
Effect of small molecules on tumor microenvironment induced changes in T cell differentiation

4.2 Institute of Mathematical Sciences, Chennai

4.2.1 Investigating How Chromatin Regulates Gene Expression and Cellular Processes

In eukaryotic species, DNA exists in the form of chromatin, which is a DNA-protein complex that aids in the packaging of DNA inside the nucleus of the cell. Along the hierarchy of the genome organization, the chromatin can form various 3D functional structures like topological domains, and loops between the cis-regulatory elements to name a few. These 3D structures can facilitate interactions or co-occurrences of transcription factors(TFs). TFs are a group of protein molecules that have preferential binding to a specific sequence of DNA. In eukaryotes, these TFs most often work in a combinatorial manner and can form complexes of multiple TFs. Although researchers in the field have explored such combinations of TFs in gene regulation, they are mostly limited to a few factors or mainly in linear genome context. The present work described a tool called ChromTogether that is open to others for use to capture pairs of TFs that co-occur or avoid each other in 3D spatial proximal regions of the chromatin.
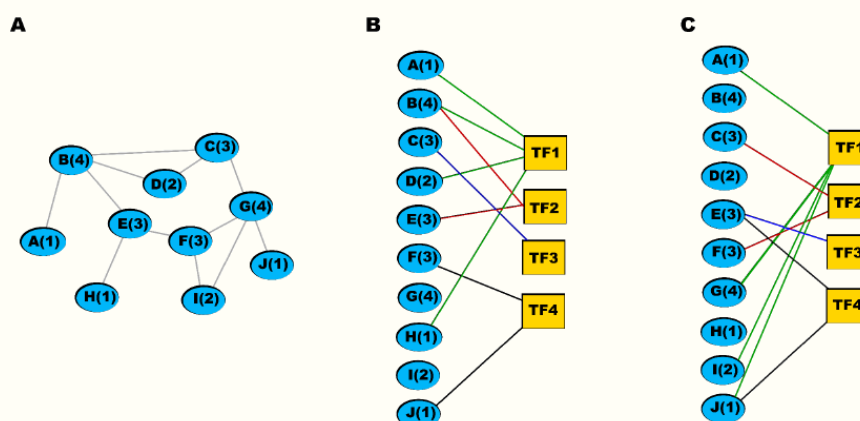
Schematic diagram of ChromTogether methodology. (A) shows the interaction network inferred from chromatin conformation capture techniques. (B) show the binding network between chromatin regions and TFs. (C) shows an example of one randomized network of the binding network. 1000 such randomized networks are constructed to identify co-occurring or avoiding TF pairs

Using above developed ChromTogether method on four human cell lines GM12878, K562, HeLa-S3, and MCF7, it was observed that TFs segregate into two main classes in their co-occurrence pattern. This segregation was observed in both 3D and 1D contexts as well as from both experimental evidence and in-silico predictions of TF binding sites on the genome. Further analyses suggest that one group of TFs are involved in regulating housekeeping genes, whereas the group is more involved in tissue-specific functions. In another part of the work in collaboration with the experimental group, it has been explored the properties of the centromere regions of the fungal species C. auris. It was found that the centromere regions of C. auris are unique and lack any sequence motifs, or repeat elements, and are GC-poor regions. Also, they occupy entire ORF-free regions and pericentric heterochromatin regions, unlike other fungal species of Ascomycota.

4.3   National Institute of Science Education and Research, Bhubaneswar

4.3.1   Role of GIGANTEA on the Developmental Regulation of *Arabidopsis thaliana*

The sessile plants have evolved a network of highly complicated signaling channels that enable them to adapt to changes in internal and external environmental inputs. The diurnal and circadian regulatory mechanisms, which are regulated by the biological clock, fine-tune the growth and development of a plant. GIGANTEA (GI) being a plant-specific nuclear protein, has been identified to have pleiotropic roles in overall growth and development in the plant including circadian rhythm, flowering time, and various abiotic stress tolerance. Despite its pivotal roles, it is surprising that GI null mutants are not lethal. It would be a great challenge to understand and connect the functional roles of GI at different developmental stages. Likewise, due to the absence of homology of GI with any protein of known function, its biochemical functions are poorly understood. The role of GI in flowering time regulation, circadian clock control, and light signaling is still being pursued. But less-known functions such as sucrose signaling, chlorophyll accumulation, oxidative stress resistance demand more attention. Recently, the emerging role of GI in biotic stress tolerance has been demonstrated, which indicates that still the understanding about the various functions of GI is incomplete. The present study has investigated the role of GI in plant defense mechanisms using a biotrophic pathogen. Although GI is a multifunctional protein, the role of its various functional domains is still in darkness. It has been tried to understand the role of putative domains of GIGANTEA by mutagenesis and functional analysis in transgenic plants. MicroRNAs (miRNAs) play important roles in regulating the flowering and reproduction of plants. Mature miRNAs are encoded by multiple MIRNA genes that can differ in their spatiotemporal activities and their contributions to gene regulatory networks, but the functions of individual MIRNA genes are poorly defined. Functional analyzation of the activity of all 5 Arabidopsis thaliana MIR172 genes, which encode miR172 and promote the floral transition by inhibiting the accumulation of APETALA2 (AP2) and APETALA2-LIKE (AP2-LIKE) factors (TFs). Taken together, the results indicate that the GI could be beneficial in generating transgenic crop plants, which possibly will be disease resistant or heavy metal stress-resistant, for sustainable agriculture.
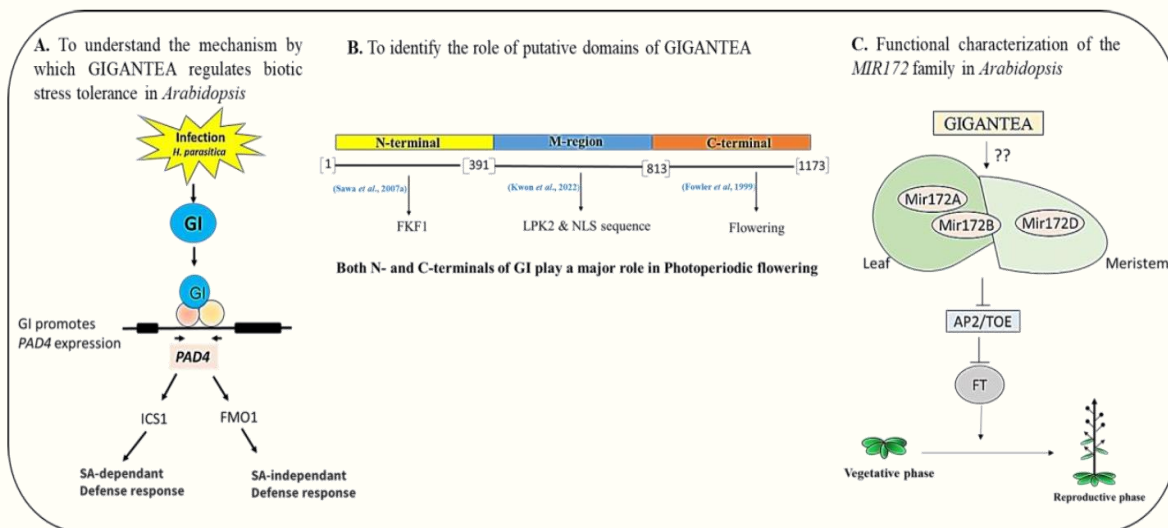
Role of GI in biotic stress tolerance

4.3.2 Molecular Characterization of Non-AUG Codon Recognition in the Translation Initiation Fidelity Mutant on the Regulation of Differential Protein Expression

The recognition of the AUG start codon and the selection of an open reading frame (ORF) is a fundamental process in protein biosynthesis. In *Saccharomyces cerevisiae*, over 13 translation initiation factors (eIFs) are responsible for accurately choosing the AUG start codon by scanning the mRNA from 5' to 3' directions. The eIF5^{G31R} mutation, a hyper-GTPase, causes a defect in translation initiation fidelity and uses the UUG codon to begin translation. This defect in translation initiation fidelity will change cellular proteome and have an adverse effect on cellular function. The eIF5^{G31R} mutation prefers the 'AAA' sequence in the -3 to -1 position for UUG codon selection. Bioinformatic analysis suggests that around 8% of yeast CDS contain UUG codons in good sequence context in their 5' untranslated region, potentially leading to short upstream ORFs, out-of-frame ORFs overlapping with the main ORF or N-terminal extensions from the main ORF. Using 2D-PAGE/MALDI-TOF and iTRAQ/MALDI-TOF proteomic techniques, altered protein expression in the eIF5G31R mutation has been identified. These changes affect cellular pathways such as nucleotide biosynthesis, carbohydrate metabolism, oxidation-reduction pathways, protein catabolism, autophagy, and lipid biosynthesis. The eIF5^{G31R} mutation causes the use of upstream UUG codons from the *URA6* mRNA, leading to a 0.55-fold decrease in uridylate kinase expression, impacting uracil mono-phosphate to uracil diphosphate conversion and nucleotide biosynthesis necessary for DNA and RNA synthesis. As a result, yeast cells are sensitive to hydroxyurea, DNA damage and have up-regulated marker proteins indicative of DNA replication stress. Additionally, catalase-T protein's up-regulation indicates underlying oxidative stress in eIF5^{G31R} mutant cells, which are sensitive to H_2O_2 and have higher cytosolic and mitochondrial ROS activity levels. The mutant cells also have lower glutathione levels and downregulation of the YAP1 protein, which regulates the redox pathway. The oxidative stress in the eIF5^{G31R} mutant cells also increases translation elongation transition time on polysomes and causes a 10% reduction in protein biosynthesis. In summary, the eIF5^{G31R} mutation alters the cellular proteome and reprograms cellular pathways that cause ROS generation and DNA damage.
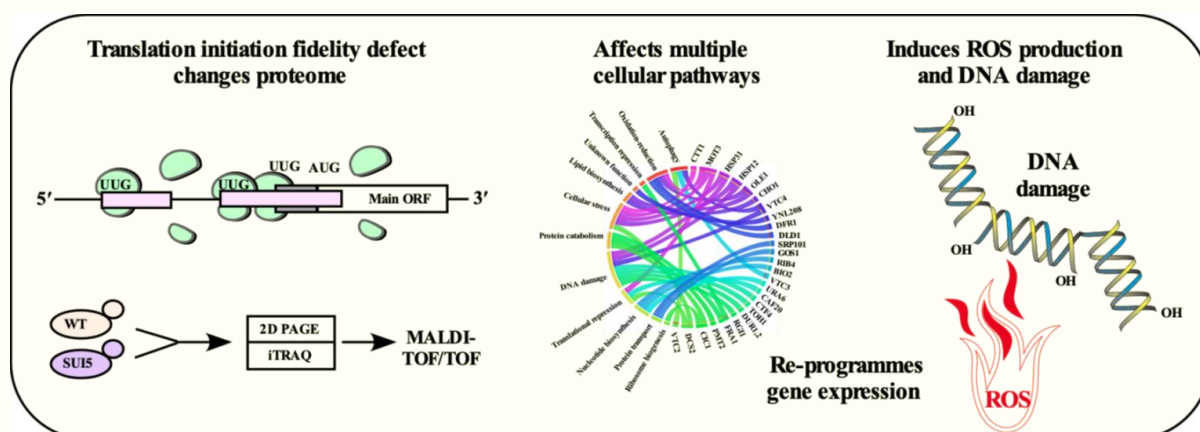

Translation initiation fidelity defective mutation changes cellular proteome that reprograms cellular pathways and induces ROS production and DNA damage

4.3.3 Light and Phytohormone Interaction in the Development of *Physcomitrella patens*

Light and hormone signals are known to interact the growth and development in flowering plants. However, it is not known how the light-hormone crosstalk influences the growth and development in non-flowering plants. In this study, *Physcomitrium patens* (formerly *Physcomitrella patens*), a moss has been utilized to investigate the influence of light-hormone interaction in a non-flowering plant. Mosses are among the pioneer group of plants that colonized land first. Different photoreceptors and

phytohormones have been identified in *P. patens*. In this study, the development pattern of different mutants such as *phy1*, *phy2*, *phy3*, *phy4* and *fhy1* of *P. patens*, defective in red or far-red (FR) light signaling, has been evaluated and correlated with the signaling pathway of phytohormones such as auxin and cytokinins. PpPHY1, PpPHY3 and potential FR light sensors in *P. patens* and PpFHY1 helps in the nuclear translocation of PpPHY1. In *P. patens* auxin enhances the chloronema to caulonema formation and rhizoid development. Cytokinins enhance the formation of gametophore buds. *phy1* and *phy3* mutants of P. patens show enhanced bud formation than the wild-type (WT) plants in white light indicating that PpPHY1 and PpPHY3 proteins inhibit the cytokinin response. These mutants also enhanced rhizoid production which indicates that auxin signaling is also inhibited by these mutants. phy3 plants show enhanced branching, which is a function of cytokinin, again indicating the inhibition of cytokinin response by PpPHY3. *fhy1* plant shows alternations in bud and gametophore formation from the WT plants indicating that PpFHY1 interacts with hormonal signaling pathways in *P. patens*. It is clearly not known how these proteins affect the auxin signaling in regulating the chloronema to caulonema formation. Future works will shed more light on this aspect. This study shows that the light signaling components such as PpPHY1, PpPHY3 and PpFHY1 interact with hormone signaling pathways and play independent roles in the development of *P. patens*.
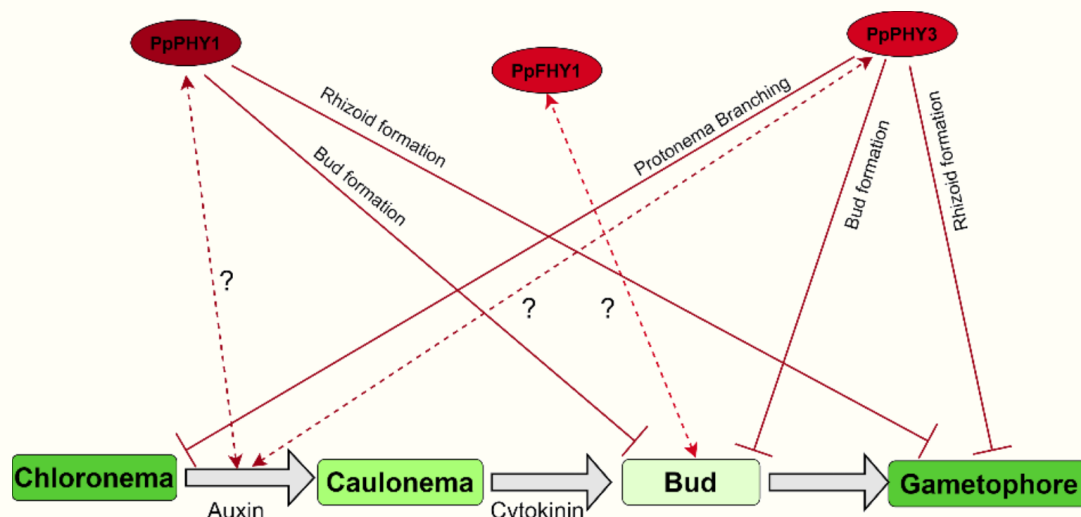

Role of PpPHY1, PpPHY3 and PpFHY1 in regulating hormonal response in P. patens

Solid arrows indicate the direct involvement in a process. Dashed arrows indicate the possible involvement. Question mark indicates that the interaction is presently unknown. Lines with blocked arrows indicate the negative regulation

4.4 Saha Institute of Nuclear Physics, Kolkata

4.4.1 Investigation of Nucleo-protein Interactions in Prokaryotic DNA Repair and Genome

Double-strand breaks (DSB) in DNA are the most common consequences of radiation damage and a plethora of proteins like RecombinaseA (RecA), RecombinaseB (RecB), RecombinaseC (RecC), RecombinaseD (RecD) etc. are responsible to repair the damaged DNA. In radiation-tolerant extremophiles like *Deinococcus radiodurans*, it is hypothesised that the damaged DNA is repaired by highly efficient DNA repair proteins like RecombinaseD2 (DrRecD2). In this study it was found that DrRecD2 prefers to bind the 5' terminal end of the single-stranded (ss) overhang through a controlled

and slow docking mechanism termed as 'drifting'. The translocation rate of DrRecD2 on single-stranded (ss) and double-stranded (ds) DNA was found to be 3.1 nucleotides per seconds and 1.4 nucleotides per seconds respectively. The dsDNA unwinding activity of DrRecD2 was observed even in absence of ATP, but a fast and iterative mode of unwinding was evident in presence of 5 mM ATP. DrRecD2 can displace the RecA monomers efficiently from the ssDNA in presence of 5 mM ATP. It was found that SSB can recruit DrRecD2 at the sites where the DNA is damaged. Apart from DNA repair pathways another important phenomenon that contributes to genome integrity and cell survival is the DNA folding and genome compaction. Here the DNA bending ability of E.coli IHF has been studied using smFRET. It was found that for both the wtIHF and scIHF the bend induced by these proteins on the dsDNA is not uniform but more constricted away from the 3' and 5' terminal ends, moreover, wtIHF induces more constriction near the A-tract region compared to scIHF. Overall, the broader distribution of the FRET efficiency histogram in case of wtIHF in contrast with scIHF suggests that wtIHF can bend the dsDNA at multiple angles whereas scIHF produces sharp and more restricted bends. The sharpest bend by wtIHF was found to be approximately 89 degrees when calculated from the terminal ends of the dsDNA, the was found to be approximately 91.5 degrees in case of scIHF. Similarly, when the flexure angles were calculated 5 nucleotides away from both the terminal ends of the dsDNA, the sharpest bends with wtIHF and scIHF were approximately 103 degrees and 110 degrees respectively.
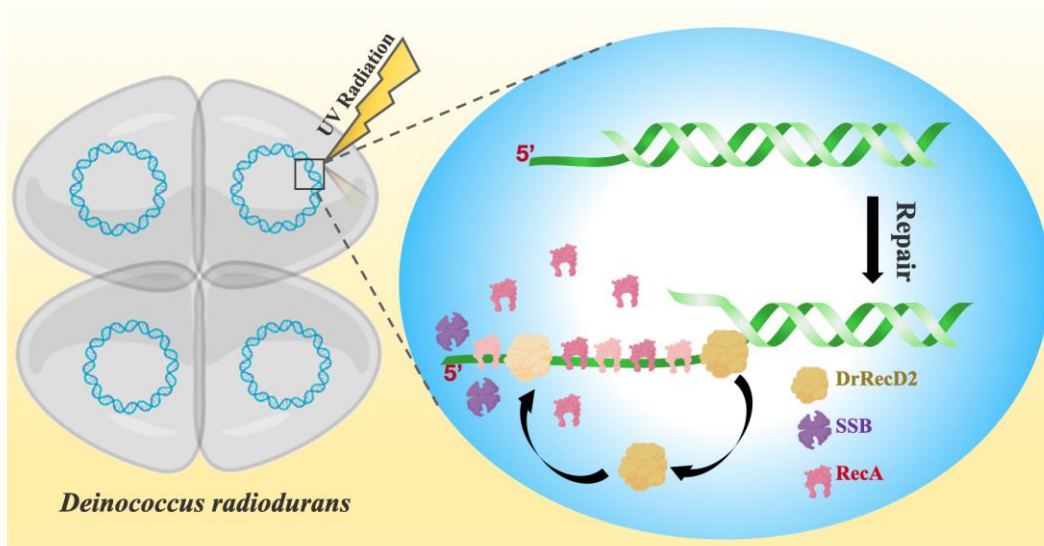
*Schematic diagram of DNA repair in Deinococcus radiodurans.*

4.4.2 Single Molecule Visualization of Rearrangement of Polypurine Reverse Hoogsteen Hairpin and Fork-DNA during their Modification for Gene Regulation

The DNA polymer structurally moulds itself based on the requirement of its participation in various cellular pathways. The structural modification of DNA promotes acquirement of secondary structures. The inherent dynamics of these secondary structures is found through breakage and re-joining of hydrogen bonds at a temp below its melting point. To make the way towards the functional aspects of the DNA, it is highly important to explore the properties from a mechanistic perspective where it is possible to witness the individual dynamic structural intermediates. It has been explored for the steps of formation of a non-canonical polypurine DNA hairpin, PPRH which is formed through Reverse-Hoogsteen bonding within the homo purine residues in the stem region primarily through smFRET (single-molecule Forster Resonance Energy Transfer. The intrinsic fluctuation of the hairpin causes it

to form DNA triplex, where the other end of the purine unit forms Watson Crick hydrogen bonding. It has been found being part of triplex, the Reverse-Hoogsteen bonds become much more rigid whereas the Watson Crick bonds are more flexible. The PPRH was found to go through a transient open looped state while promoting strand displacement of the complementary polypyrimidine strand. Further, the similar hairpin with Watson Crick bonds did not participate in DNA triplex formation due to lack of structural flexibility. The rearrangement of fork-DNA, that acts as an important intermediate for DNA replication, transcription and recombinational repair pathways has been explored. Specifically, it has been found that the structure specific dynamical changes in the fork DNA in presence of the protein RecG. RecG promotes fork reversal in a reversible manner in the partial fork structure where there is a 3'-overhang. The partial fork with a 3'-overhang mimics a structure where the progression of the lagging daughter strand is continued beyond the leading daughter strand. Additionally, the motility of RecG was found to be asymmetrical since it failed to display similar activity once the fork structure was altered to the one carrying a 5'-overhang. Next, RecG was exposed to a kind of fork where both the arms are blocked with complementary oligonucleotides mimicking a structure where both the leading and lagging strands have halted at the same time. It has been found that a functional switch of RecG from 'reiterative mode' to 'functional mode' where the unwinding of the daughter strand was carried out in an irreversible manner and that eventually promotes spontaneous formation of Holliday junction.

*Steps of formation of DNA triplex through PPRH*
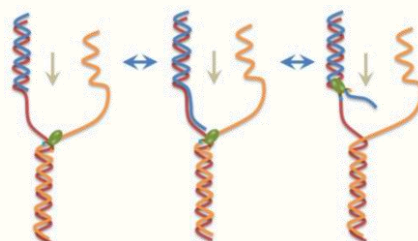
Fork Reversal by RecG

4.4.3   MFN2 Mediated Regulation of Mitochondrial Dynamics and MAM Junctions

Mitofusin 2 (MFN2) is one of the key regulators of mitochondrial dynamics. MFN2 promotes mitochondrial fusion of the outer mitochondrial membrane (OMM) in GTPase dependent manner. This protein is also enriched at the MAM (mitochondria associated membrane) junctions. This work focuses on the role of MFN2 in regulating mitochondrial fission-fusion balance and maintaining the MAM junctions. In this work, two-point mutations (R364W and T206I) associated with the neuropathy, Charcot-Marie-Tooth disease type 2A (CMT2A) were generated using site directed mutagenesis and integrated in stable cells. It was observed that both the mutations caused mitochondrial hyperfusion, a phenotype characterized by long filamentous mitochondrial morphology. The cells harbouring the mutation R364W-MFN2 showed decreased MFN2 ubiquitylation and increased ubiquitylation-mediated proteasomal degradation of the cytosolic fission protein DRP1 (Dynamin related protein 1); both the events catalyzed by the E3 ligase MITOL. This led to decreased mitochondrial fission;

potentiating the state of mitochondrial hyperfusion Additionally, R364W-MFN2 also promoted alterations at the MAM junctions (Figure1). The mutation T206I-MFN2 also promoted mitochondrial hyperfusion. This was however due to increased MFN2 stability. These cells were also susceptible to stress, showing increased ROS production and autophagic flux (under serum starvation) (Figure 1). This work shed light on the phenotype induced by the CMT2A linked MFN2 mutations, also providing a mechanistic insight for the debilitating neuropathy which can form a basis for future studies.
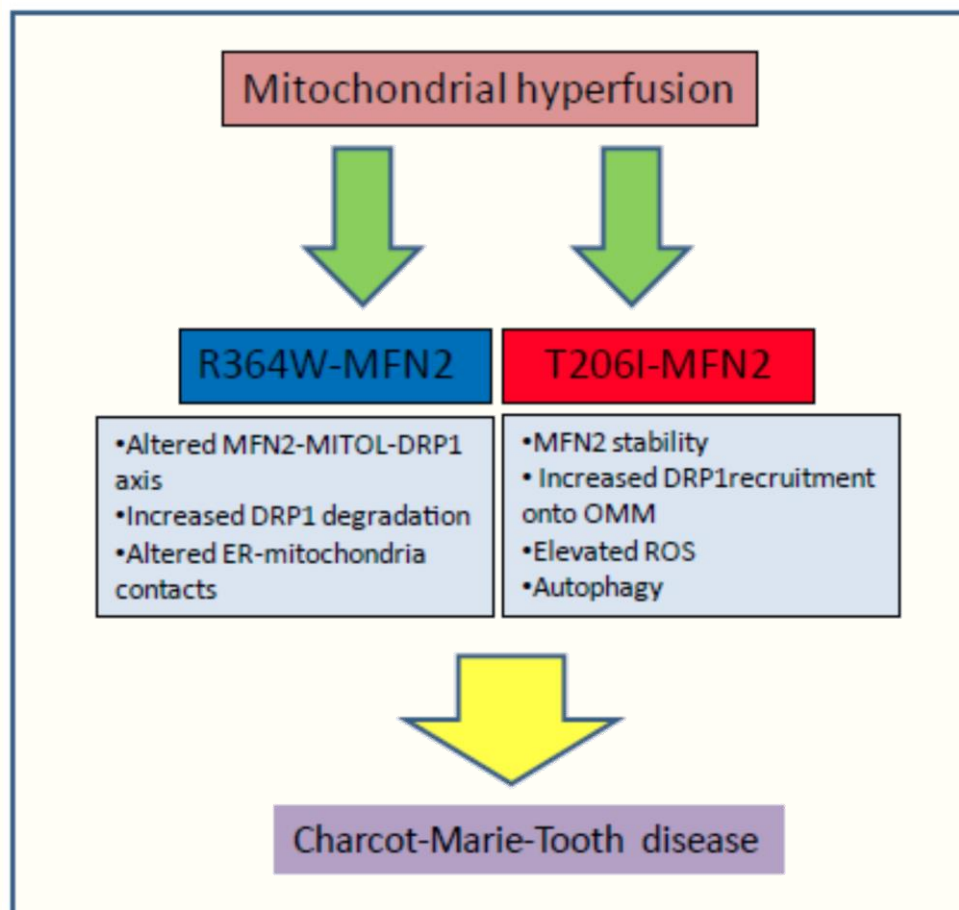
MFN2 mutations linked to CMT2A leads to mitochondrial hyperfusion and perturbs cellular homeostasis

4.4.4 Synthetic Genetic Reversible Logic gates in E. coli and its Application in Logical Information Transfer to Mammalian Cell

Reversible computing is the heart of quantum computing. Reversible logic gates (*Figure 1(A)*) are the key components of reversible computing that map inputs and outputs in a certain one-to-one pattern. Richard Feynman believed that, because of the high energy efficiency of biological reactions, living cells are attractive chassis for the implementation of reversible computation in living cells. Although synthetic genetic circuits have been used for conventional computation, reversible computation has never been implemented in living cells so far. This work gives the first implementation of reversible computation in living cells. Two types of approaches are described for implementing reversible logic. In the first approach, how the concept of artificial neural networks (ANNs) can be adopted to create a single-layer artificial network-type architecture with a population of engineered bacteria to realize reversible logic functions has been described. Using this approach, in the first part of the work, the

implementation of synthetic genetic reversible Feynman gate (2-bit) and Fredkin gates (3-bit) have been described. These functions are produced by a heterogeneous population of living *E. coli* cells that have been engineered to function as artificial neurons (*Figure 1(B)*). In the second part of this work, expand the device toolbox of reversible biocomputing by constructing a more complex 3-bit synthetic genetic double Feynman gate has been described. Practical implementation of reversible computing by creating an intercellular Feynman gate between bacteria and a cancer cell (*Figure 1(C)*) has also been studied. It has been shown that the intercellular device receives the input information from bacterial culture, computes, and transfers the information through shRNA wires to cancer cells, where output is generated. It has been shown that the engineered bacteria attach to, invade, and silence the two cancer-relevant AKT1 and CTNNB1 genes in a logical manner. Given the one-to-one input-output mapping, such reversible genetic logic gates may have applications in therapeutics, diagnostics, and sensing. This work may open new possibilities in energy-efficient reversible computing with cellular hardware.
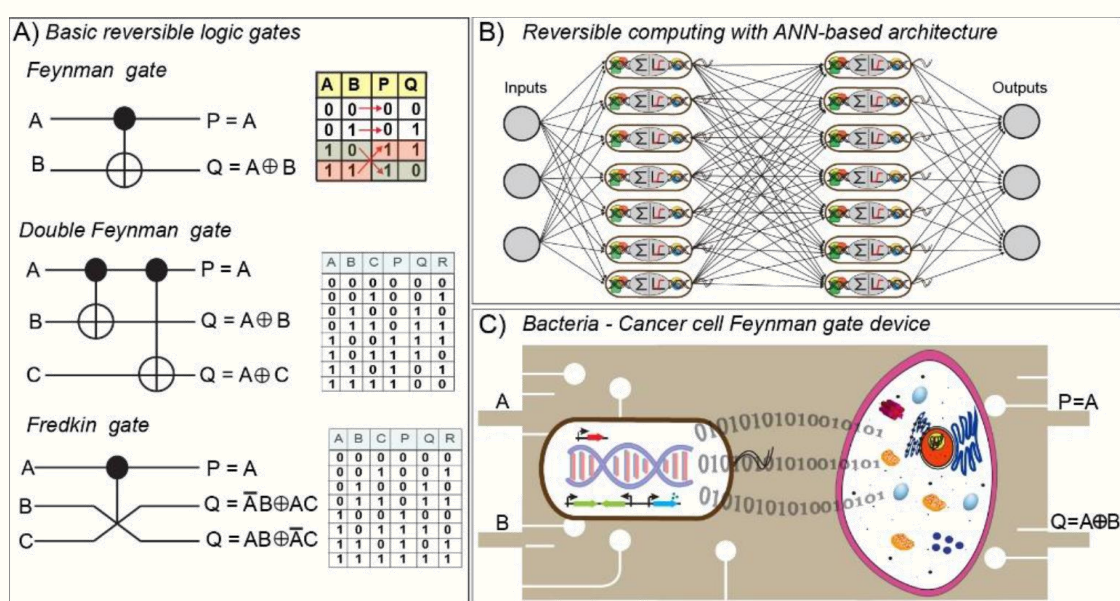

Reversible computing with engineered living cells. A) Basic 2-bit and 3-bit reversible logic gates. B) Implementation of reversible logic gates with ANN-type architecture of engineered E. coli cells. C) Application of reversible computing in silencing native genes in cancer cells

4.5   Tata Memorial Centre, Mumbai

4.5.1   Structural Evaluation of Germline Missense Mutations Causing Hereditary Breast Cancer

BRCA2 is well known for its crucial role in the DNA damage repair pathway via homologous recombination. Mutations in the BRCA2 gene are known to increase the lifetime of risk of hereditary breast and ovarian cancer by 40%. With the advancement in sequencing technologies and increasing awareness regarding breast cancer predisposition, many missense mutations have been identified in BRCA2. However, a significant fraction of these missense mutations remains uncharacterized due to the unavailability of family pedigree and lack of structural & functional studies. Therefore, predicting the risk associated with these missense mutations and pathogenic significance becomes difficult. Structural studies could provide important clues in understanding the functional effect of a missense mutation. Here, the structural impact of clinically identified missense mutations of BRCA2 was studied

using a multidisciplinary in-silico, in-vitro and biophysical approach. BRCA2 Arg2502Cys, identified from a case-control study, was characterized. Biophysical studies show that the Arg2502Cys mutation in hBRCA2 (residues 2350–2545) decreases the α-helical/β-sheet propensity of the wild-type protein and perturbs the tertiary structure conformation. Molecular dynamics simulations revealed alteration in the intramolecular H-bonds, and overall compactness and stability of the hydrophobic core were observed in the mutant protein. Therefore, the BRCA2 Arg2502Cys mutant perturbed the structural integrity and conformational dynamics of BRCA2 and could be potentially pathogenic. Another domain of BRCA2, the Tower domain (residues 2835-2964), was biophysically characterized, and it was found to exist as a dimer under native conditions. A scientifically rigorous workflow was also designed to evaluate the pathogenicity of BRCA2 variants of uncertain significance (VUS) using in-silico and molecular dynamics simulations. Results reported in this study will be helpful in the genetic counselling of patients having germline mutations in the BRCA2 gene and better assessment of risk associated with germline missense mutations.
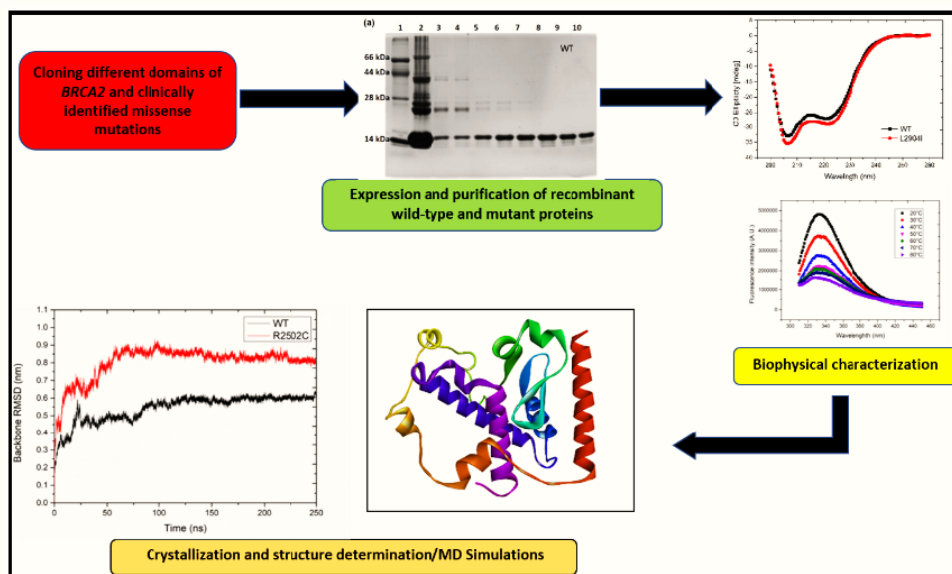

Flow-chart depicting the multi-modal characterization of clinically identified missense mutations of BRCA2.

4.5.2   Structure of Gankyrin interaction Network and their Role in Oncogenesis

PSMD10^{Gankyrin} is a component of the PA700 complex of the proteasome. It interacts directly with PSMC4, one of the 6 AAA ATPases in the base complex, and complex with PAAF1. PSMD10^{Gankyrin} coordinates the assembly of the base ATPase complex of the proteasome along with PSMD5 and PSMD9. A screen to identify differentially expressed genes in Hepatocellular carcinoma found PSMD10^{Gankyrin} overexpressed. It was established as an oncogene when PSMD10^{Gankyrin} over-expression in NIH3T3 cells transformed the cell line and induced tumor formation upon injection of PSMD10^{Gankyrin} over-expressing NIH3T3 cells in nude mice. Unlike other oncogenes like KRAS, which require an activating mutation, PSMD10Gankyrin promotes oncogenesis merely due to its higher expression in cancer cells. Several cancers, including pancreatic, colorectal, oral, and esophageal squamous cell carcinoma, exhibit overexpression of PSMD10^{Gankyrin}. PSMD10^{Gankyrin} over-expression in Breast Invasive Carcinoma and Hepatocellular Carcinoma correlates to poor survival in patients. In this work, a new role for PSMD10^{Gankyrin} in exosome secretion, trafficking CLIC1 into exosomes, and promoting cell migration has been discovered. PSMD10^{Gankyrin} has been crystallized in a new crystal form and devised

a method to screen for small molecules rapidly using these crystals. The biophysical evidence for using the shared interface peptide EEVD as a potential inhibitor of the protein interaction network in PSMD10^{Gankyrin}-driven malignancies have also been presented. Besides, a chemical framework that can be used to improve the design of new PSMD10^{Gankyrin} and CLIC1 inhibitors has been revealed. These findings will have an impact on disease biology and drug discovery.
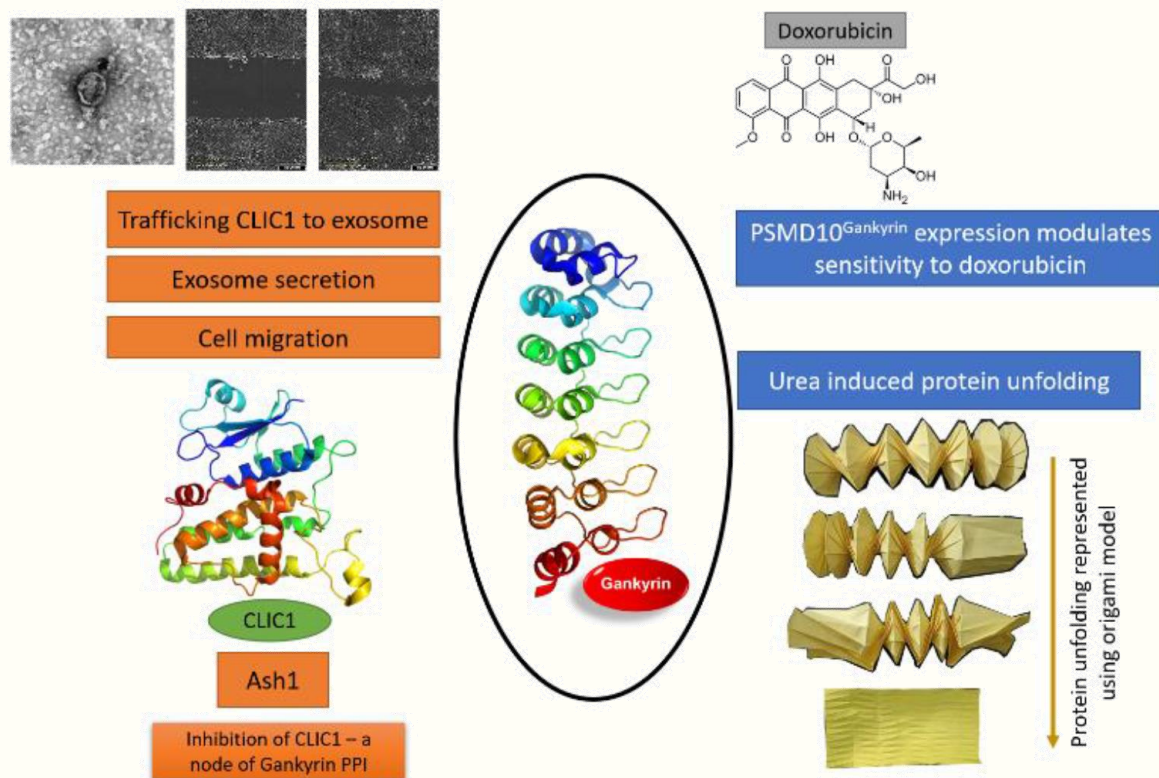

The role of PSMD10^{Gankyrin} – CLIC1 interaction in cell migration. Doxorubicin and Ash1 as a novel binder of PSMD10^{Gankyrin} and CLIC1 respectively. Urea induced unfolding of PSMD10^{Gankyrin} represented as origami model named "spring into action".

4.5.3 Genomic Approaches to Identify Novel Endogenous and Exogenous Genetic Elements associated with Human Cancer

As a part of the standard protocol of identification of the somatic mutations originating in cancer, the variants obtained from the tumor tissue are depleted against the germline variant database. However, the currently available germline databases are mainly representing the individuals from European ancestry (Caucasians). Several populations including Asian (especially Indian) have lower representation in the global databases. In order to address this, TMC-SNPdb 2.0, which represent variants from 1800 Indians (173 in-house, 598 from Genome Asia 100K, 1029 from IndiGenome project) has been developed. The study identified 305,132 novel ethnic specific germline variants. Utility of this resource was demonstrated in the tumor specific somatic analysis (224 in-house tumors), in which an average depletion of 3.44% and 4.21% variants were observed in paired and orphan tumors, respectively. This resource aims to reduce the false positive endogenous (somatic) mutations from the sequenced tumor sample. It was aimed to develop an algorithm to prioritize potential driver mutations using the domain conservation and structural information, occurring at low frequency within cancer genomics dataset. The analogous positions prioritized by the framework within proteins

were scored based on the biochemical/ functional context, mutation entropy across proteins, amino acid alteration frequency in COSMIC. Based on the cumulative score generated from the analysis, 3,579 and 81 potential driver mutations were identified from the TCGA and in-house tumor (n=224) somatic mutation analysis, demonstrating its utility.
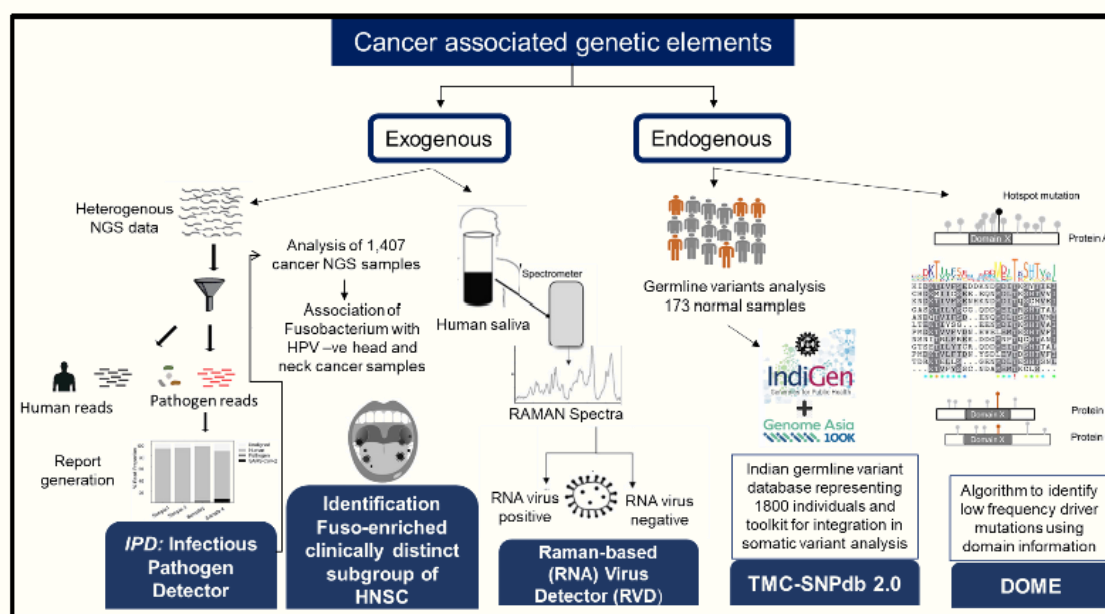

Schematic representation of findings from the study

A method for detection of cancer associated infectious pathogens from heterogenous NGS datasets has been developed. The method, named Infectious Pathogen Detector (IPD), was benchmarked against currently available pathogen analysis tools/pipelines for detection of SARS-CoV2 (RNA-virus), HPV (DNA-virus) and Fusobacterium (bacterium) validated samples. IPD was further applied to analyze the in-house and TCGA whole exome and transcriptome samples representing 7 tumor types. In this analysis, Fusobacterium nucleatum was found to be enriched in head and neck cancer samples and was exclusive to HPV presence. This enrichment and validation of the associated gene and miRNA expression candidates were performed in HNSC tumors, specifically in the tongue cancer patients. These Fusobacterium enriched tongue tumors showed a distinct molecular, immunological, and clinical feature, especially having poor survival and higher extracapsular spread. The genomic analysis of tumor samples identified a distinct sub-type of HPV negative HNSC patients.

4.5.4 Functional Relevance of Protein-protein Interactions – Case Study with Proteasomal Chaperones

Proteasome plays a critical role in maintaining the proteostasis/homeostasis of the cell. The process of protein degradation by proteasome is highly coordinated and strictly regulated. The strict regulation of proteasomal function owes to its complex structure. Dedicated chaperones mediate the assembly of the complex structure of the 20S core subunit and 19S regulatory subunit, which join and form functional proteasomes. Multiple chaperones like P28 (PSMD10), P27 (PSMD9), S5b (PSMD5), and Rpn14/PAAF1) are known to play a significant role in the assembly of the 19S regulatory subunit.

The functions of these chaperones, other than their role in the assembly, are not known. These proteins have specialized characteristics in their structure that are important for protein-protein interactions. Identifying such novel interactors of these proteins and their functional significance remains a matter of investigation. In the present study, it has been attempted to explore the PSMD9 interactome and investigated the functional significance of some interactions in mammalian cells. It has been reported that PSMD9 interacts with multiple ribosomal proteins both from smaller and larger subunits confirmed by western blotting and mass spectrometry.
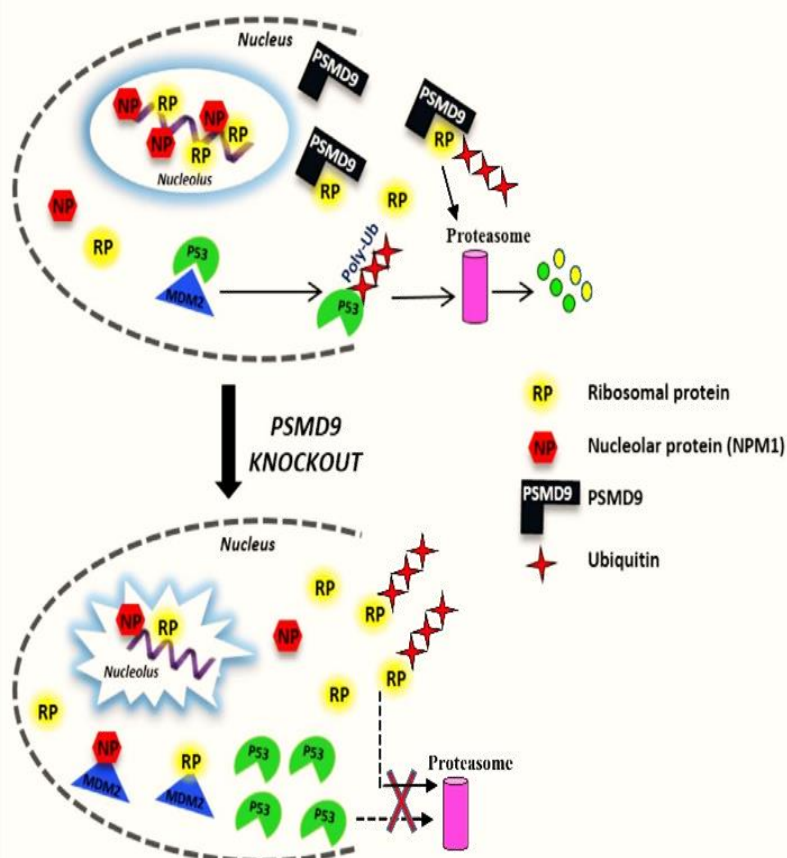
The model depicts the role of PSMD9-ribosomal protein interactions in maintaining nucleolar morphology and architecture

It has been observed that the interaction between ribosomal proteins and PSMD9 is physiologically relevant in maintaining nucleolar morphology and architecture. The PSMD9 seems to play an important role in homing ribosomal proteins into the nucleolus. Knockout out of PSMD9 results in loss of nucleolar structure and morphology; in turn, ribosomal protein and nuclear proteins redistribute into the nucleoplasm. This redistribution of proteins due to loss of PSMD9 indicates nucleolar stress. The important outcome of nucleolar stress is an accumulation of p53 due to ribosomal protein binding to the MDM2 and preventing its p53 ubiquitination potential—cells lacking PSMD9 protein show higher levels of P53 and slow degradation. The loss of nucleolar integrity and p53 accumulation in PSMD9 knockout cells results in their slow growth and less viability. It has also been demonstrated that PSMD9 knockout cells have more active S6 kinase and, therefore, more translation than control cells. The loss of PSMD9 also affects the localization of mTOR and LAMP1 in MCF7 cells.

5. Mathematical Sciences

During the period of report, HBNI awarded 11 Ph.D. degree in Mathematical Sciences in a variety of research areas such as Lie Algebra, Group Theory, Number theory, and Algebric Geometry. Some of the theses are summarized below.

5.1 The Harish-Chandra Research Institute, Prayagraj

5.1.1 Irreducible Modules for Loop of Lie Algebras

In the study of representation theory of Lie algebras, the classification of all the irreducible modules over an arbitrary Lie algebra is a considerably difficult problem. For any Lie algebra $\mathcal{L}$ and a commutative associative algebra $\mathcal{B}$ one can construct a Lie algebra $\mathcal{L} \otimes \mathcal{B}$, called loop algebra. Now it is interesting to find out relations between modules of $\mathcal{L}$ and $\mathcal{L} \otimes \mathcal{B}$. In the present doctoral work, thesis the representations of loop algebras for various Lie algebras have been studied. The problem of classifying irreducible modules over certain Lie algebras, namely loop-toroidal algebras, loop-Witt algebras and loop-Virasoro algebras has been solved.

The toroidal Lie algebra is the most general generalization of well-known affine Kac-Moody Lie algebra. For the loop-toroidal Lie algebras, all the irreducible modules with finite dimensional weight spaces when a part of the center acts non-trivially on the modules have been classified. The modules in this case turn out to be finite tensor products of irreducible highest weight modules for affine Lie algebras.

The Witt algebra W_n is the Lie algebra of the derivation algebra of Laurent ring polynomials, $\mathbb{C}[t_1^{+1}, t_1^{-1}, t_2^{+1}, t_2^{-1}, \ldots, t_n^{+1}, t_n^{-1}]$. In the loop-Witt algebra case, it was proved that under some natural conditions the modules of tensor fields exhaust all irreducible modules with finite dimensional weight spaces. It was found that all modules here are single-point evaluation modules.

The Virasoro algebra is the universal central extension of W_1. Irreducible modules for loop-Virasoro algebras with finite dimensional weight spaces are completely classified. Here, a a large class of irreducible modules with infinite-dimensional weight spaces has been constructed and the classes of those modules upto isomorphism have been identified.

5.1.2 Extension Theory for Non-degenerate Solutions of Yang-Baxter Equation

The purpose of the thesis was to provide a comprehensive analysis of skew left braces and their extensions. The first chapter provides a brief overview of the problems addressed in the thesis. In the second chapter, all abelian extensions of skew left braces ae classified by defining a suitable cohomology group and provide a Well's type short exact sequence connecting certain automorphism groups. The third chapter takes the analysis further by classifying all split extensions of skew left braces and establishing a connection between abelian and non-abelian extensions of skew left braces. With this connection, it is possible to generalise the Wells like exact sequence for trivial skew braces. Finally, in the fourth chapter, abelian extensions of Rota-Baxter groups are classified and a Well's type short exact sequence is defined for Rota-Baxter groups.

5.2   Institute of Mathematical Sciences, Chennai

5.2.1   Around Non-vanishing, Linear Independence, and Transcendence of L Values at Rational and Integer Points

The focal point of the thesis was to study the arithmetic nature of Dirichlet L values at positive integers. While non-vanishing of all these values was established in 1837, it took about 130 years to settle the nature of these numbers. Thanks to Dirichlet and Baker, Dirichlet L values corresponding to non-trivial Dirichlet characters at 1 are transcendental. It is an open question of Baker whether the Dirichlet L values at 1 corresponding to non-trivial Dirichlet characters with fixed modulus are linearly independent over the rational numbers. The best-known result is due to Baker, Birch and Wirsing, which affirms this when the modulus of the associated Dirichlet character is co-prime to its Euler's phi value. In the thesis, the extension of this result is discussed to any arbitrary family of moduli. The interplay between the resulting ambient number fields brings new technical issues and complications hitherto absent in the context of a fixed modulus. For k greater than 1, the study of linear independence of Dirichlet L values at k, corresponding to non-trivial Dirichlet characters depends critically on the parity of k and the Dirichlet characters. This has been investigated by a number of authors for Dirichlet characters of a fixed modulus and having the same parity as k. In the present work, this investigation is extended to families of Dirichlet characters modulo distinct pairwise co-prime natural numbers. The product of these Dirichlet L values gives the Dedekind zeta values associated with abelian number fields. The main results that make up the thesis are given below:

1.There are at most finitely many abelian number fields such that the derivative of their associated Dedekind zeta function at 1/2 is zero, whenever their associated Dedekind zeta function at 1/2 is nonzero. All such number fields (if exist) have degree less than 46369.

This result refines a result of Murty and Tanabe, both qualitatively and quantitatively. The research work has been extended to Galois as well as arbitrary number fields, borrowing tools from algebraic as well as transcendental number theory.

2. Let t and q be co-prime integers such that tq is co-prime to (t-1)(q-1). Then the set of all Dirichlet L values at 1 corresponding to non-trivial Dirichlet characters modulo t and q, is linearly independent over the rational numbers. In the process, a result of Okada about linear independence of the cotangent values over the rational numbers is also extended.

3. It is also proved that the set of all Dirichlet L values at 1 corresponding to non-trivial even Dirichlet characters is linearly independent over the algebraic numbers, conditional on co-primality of their moduli. This extends a result of Murty-Murty.

4. Let k be a positive integer greater than 1, and t and q be co-prime integers such that tq is co-prime to (t-1)(q-1). Then the set of all Dirichlet L values at k, corresponding to non-trivial Dirichlet characters modulo t and q and having the same parity as k, is linearly independent over the rational numbers. The spaces generated by such L values have been connected with the spaces generated by Hurwitz zeta values.

Here, the lower bounds of dimensions of finite sum of generalized Chowla-Milnor spaces over the linearly disjoint number fields are also computed. Moreover, it is possible to give precise formulae in case of generalized plus Chowla-Milnor spaces.

5.2.2   Packing and Covering: New Paradigms and Algorithms

In the thesis the packing and covering problems in the framework of Parameterized Complexity as well many classical problems in a special dynamic parameterized setting have been studied. The results obtained add to the list of results on these problems in the realm of parameterized algorithms.

Packing and Covering are some of the fundamental problems in graph theory. An H- Packing problem is, given a graph G, what is the maximum number of disjoint graphs in H one can find in G. Similarly in H-Covering problem it is desired to find the minimum number of disjoint graphs in H that together constitute the graph G. Both these problems are extremely well studied and proved to be NP-hard. The Covering problems that are studied in the present work encompass the very well-known Hamiltonicity problems.

The Packing and Covering problems where H is the class of cycles/paths have been studied with respect to the standard parameter (solution size) as well as some well-known structural parameters. For Arc-disjoint Cycle Packing, linear kernel on tournaments and polynomial kernel on α-bounded digraphs have been obtained. Next, the Vertex-Disjoint Cycle Packing problem is considered. For the Vertex-Disjoint Cycle Packing problem, Bodlaender et al. obtained polynomial kernels with respect to the size of vertex cover, the vertex-deletion distance to a cluster graph and the maximum leaf number. The research work carried out contributes some results to this line of work. Since the problem is still open on interval graphs, a natural subclass of interval graphs known as proper interval graphs is considered.

The problem parameterized by vertex deletion distance to proper interval graphs (t) has been studied. Just as chordal graphs have clique-tree decomposition structure, proper interval graphs have clique-path decomposition structure. The color coding, greedy strategy and multi layered dynamic programming have been to design an FPT algorithm running in time $2^{O(t \log t)}n^{O(1)}$. The bounded monotonicity properties of paths in proper interval graphs has been used to design FPT algorithms running in the same time for Cycle and Path Cover problems.

Some well-known parameterized problems in a dynamic framework where the input is a graph (an instance) along with a solution have also been studied. The graph gets updated by a series of edge insertions and deletions and our goal is to efficiently update a solution. In the context of parameterized algorithms, two relevant parameters are the edit distance k (number of updates) and the Hamming distance r (between the input solution and a solution to the updated instance). For a fixed collection of graphs π, given a graph G and an integer l, the π-Deletion problem is to determine if G has a set S $\subseteq$V(G) of vertices with |S| = l such that G-S belongs to π. π-Deletion is an abstraction of various classical problems in the graph theoretic framework. Examples include the classical Vertex Cover and Feedback Vertex Set. Due to a generic result by Lewis and Yannakakis, it is known that finding a minimum solution to π-Deletion is NP-hard in general for most choices of π. Hence, it has

been extensively studied in various algorithmic realms. The dynamic version of this problem referred to as Dynamic π-Deletion and show NP-hardness, fixed-parameter tractability and kernelization results are also defined. Then, for the specific cases of π-Deletion such as Dynamic Vertex Cover and Dynamic Feedback Vertex Set, improved FPT algorithms have been given with respect to k as the parameter and obtain linear kernels. Then, for the same parameterization, improved algorithms for Dynamic Connected Vertex Cover, Dynamic Dominating Set and Dynamic Connected Dominating Set have been described. For Dynamic Dominating Set and Dynamic Connected Dominating Set, it is shown that these running times are optimal (up to polynomial factors) assuming the Set Cover Conjecture.

5.3   National Institute of Science Education and Research, Bhubaneswar

5.3.1   Examples of Braided Quantum Groups In C*-Algebraic Framework

The thesis is concerned about the construction of q-deformations of the double cover of the group of motions of the Euclidean plane E(2) for non-zero complex deformation parameters $0<|q|<1$. These deformations yield braided locally compact quantum groups in the C*-algebraic framework, namely the braided quantum E(2) groups, over the circle group viewed as a quasitriangular quantum group. For real values of the deformation parameter q, these deformations coincide with Woronowicz's standard Eq(2) group. To accomplish this, at the beginning, the general theory of the construction of braided C*-

quantum groups over a quasitriangular quantum group is carefully developed using the notion of braided (twisted) tensor product induced by the braiding unitary in the representation category of the quasitriangular quantum group. Subsequently, in the same formalism, the dual of the braided quantum E(2) group is also constructed and it is shown that the bidual of the braided quantum E(2) group is isomorphic to the braided quantum E(2) group.
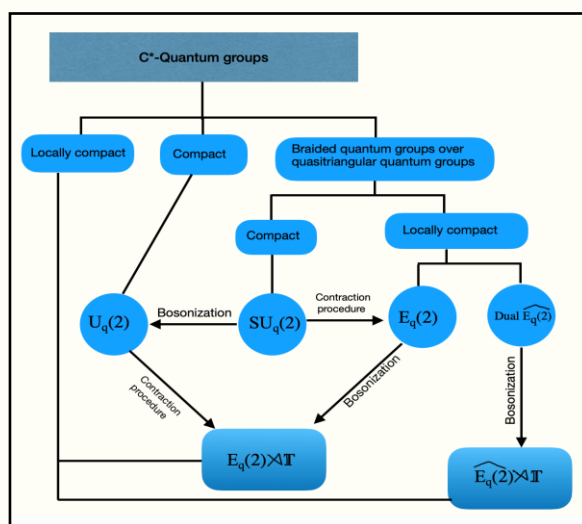
The present work also focuses on the construction of the bosonizations of the braided quantum E(2) groups and their duals, an analogous construction for the semidirect product of groups, which yields ordinary noncompact locally compact quantum groups with projection, along with the construction of the braided analogue of the contraction procedure between quantum E(2) and SU(2) groups in spirit of Woronowicz's quantum analogue of the classic Wigner-Inonu group contraction. The former objects, bosonizations, are constructed using the semidirect product multiplicative unitaries and the latter construction is carried out using a one-parameter group of automorphisms of braided quantum E(2) groups. As an application of the braided analogue of the contraction procedure, it is shown that the bosonization of braided quantum SU(2) group can be contracted to obtain the corresponding bosonization of braided quantum E(2) group.

6. Physical Sciences

During the period of report, HBNI awarded 97 Ph.D. degree in Physical Sciences in a variety of research areas such as Condensed matter physics, Nanoscience, Surface physics, Material science, Spintronics, X-ray Multilayer, Radiological Physics, Computational Spectroscopy, Density Functional Theory, Quantum information and computation, Nuclear physics, Neutrino Physics, Plasma Physics and Astroparticle Physics and Cosmology. Some of the theses are summarized below.

6.1 Bhabha Atomic Research Centre, Mumbai

6.1.1 First-Principles Studies on Fe-Zr Alloys and $BaZrO_3$ as Host Matrices for Nuclear Waste

The immobilization of metallic waste, generated from reactors, in a wasteform is important as it is categorized as high level waste (radioactivity > 3.7×10^{11} Bq/L). Stainless steel (SS) and Zirconium (Zr) alloys are found to be promising wasteform materials, under alloy melting route, for metallic waste. Fe-Zr intermetallics prominently appear in the microstructure of SS-Zr alloys and play an important role in accommodating the radionuclides present in the metallic wastes. Moreover, the oxide fission products present in the metallic waste will form a slag (due to higher melting point), which can be immobilized in ceramic matrices, e.g., $BaZrO_3$. In view of the above, the present work aims to evaluate the potential of Fe- Zr intermetallics and $BaZrO_3$ to serve as a wasteform for fission metals (FMs) and actinide (An's) oxides, respectively, by studying the energetics, structural and elastic properties of Fe-Zr intermetallics and $BaZrO_3$ in presence of of s−, p− and d−block FMs and An's using density functional theory (DFT) based simulations. Our calculated ground state stability suggests that only three intermetallics, $viz.$, cubic Fe_2Zr, tetragonal $FeZr_2$ and orthorhombic $FeZr_3$ intermetallics are energetically stable. Further, these phases are found to be mechanically and dynamically stable. Thermal properties of these intermetallics suggest that the higher volume fraction of $FeZr_3$ is preferable in the alloy microstructure. The energetics of incorporation of s−, p− and d−block FMs, $viz.$, Rb, Sr, Cs, Ba, In, Sn, Sb, Te, Y, Nb, Mo, Tc, Ru, Rh, Pd, Ag and Cd suggest that the incorporation of p− and d−block is easier than that of s−block FMs. The change in the elastic moduli on incorporation of FMs can be correlated to their solution energies. High pressure studies suggest that the Fe_2Zr phase undergoes a magnetic to non-magnetic phase transformation at around 30 GPa; while the $FeZr_2$ ($FeZr_3$) phase undergo structural phase transformation from I4/mcm (Cmcm) phase to P4/mmm phase at around 12 GPa (25 GPa). Finally, it can be concluded that Fe-Zr intermetallics can be used to incorporate the p- and d-block FMs.
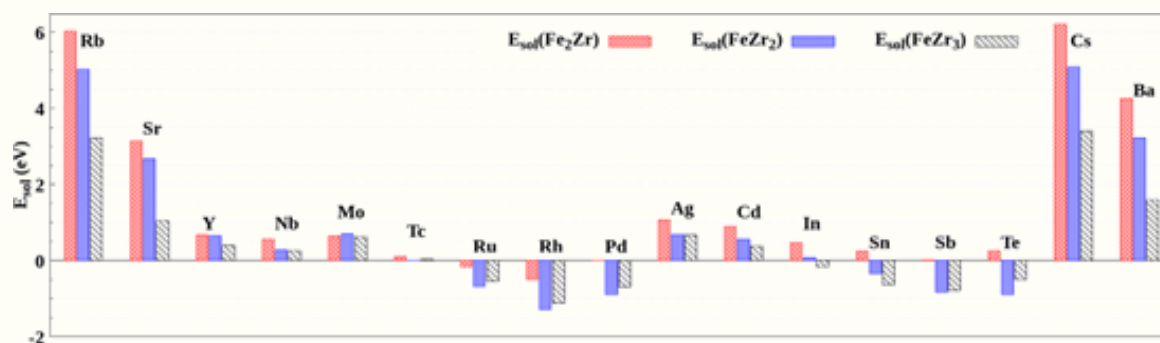
Lowest solution energies of s-, p- and d−block fission metals in Fe_2Zr, $FeZr_2$ and $FeZr_3$ phases.

The energetics of incorporation of actinides in the $BaZrO_3$ suggest that these prefer to occupy the Zr site of the compound. The incorporation of the actinides in the $BaZrO_3$ are endothermic. However, the actinides prefer to form solutionized $BaZrO_3$ phase rather than individual oxide segregated phases, viz., BaO, ZrO_2 and AnO_2 or $BaZrO_3$ and AnO_2 at the concentration close to 3.7 at%, which is a favorable condition for incorporation of the actinides. The actinide incorporated phases are found to be stable. The energetic and elastic properties suggest that $BaZrO_3$ can used to immobilize actinides.

6.1.2 Vibrational and Structural Investigations of Phase Transitions in Vanadium Based Framework Oxides

Investigation of structural phase transition induced by tuning external thermodynamic parameters can lead to discovery of new phases of same composition with exotic properties. Vanadium based framework oxides, mostly contain VO4 tetrahedra which can transform into compounds with higher coordination of vanadium under high pressure for better packing and can show structural phase transitions. Multiple oxidation states of vanadium make vanadium based framework oxides to exhibit a variety of phenomena under high pressure ranging from charge ordering, pressure-induced superconductivity, structural phase transitions, decomposition and amorphization etc. Vanadium oxides belonging to $A3(VO4)2$ family of compounds (A = Mn, Ni, Co Znand Mg) commonly crystallizes in orthorhombic *Cmca* structure with a wide variety of applications varying from as a catalyst to multiferroic to dielectric to electrodes in lithium-ion battery etc.

In the present work, Raman spectroscopic investigation of the members of $A3(VO4)2$ family of compounds ($Ni_3(VO_4)_2$, $Co_3(VO_4)_2$, $Mg_3(VO_4)_2$, $lt-Mn_3(VO_4)_2$, $Li_{0.2}Mn_{2.9}(VO_4)_2$ and $BaCu_2(VO_4)_2$) and the compound $Zn_4V_2O_9$ are carried out at different thermodynamical conditions. Later, the X- ray diffraction (XRD) investigations are carried out on $Mg_3(VO_4)_2$, $lt-Mn_3(VO_4)_2$, $Li_{0.2}Mn_{2.9}(VO_4)_2$ and $BaCu_2(VO_4)_2$) in which the anomalies observed in the Raman spectroscopic investigations were correlated to structural phase transitions in these compounds. Schematic below shows the brief summary of the research work carried out in the thesis which indicates the structural stability and phase transition observed in these compounds. Identifying structural phase transitions in this work have been carried out through both microscopic (Raman spectroscopy) and macroscopic (XRD) techniques. The four compounds $lt-Mn_3(VO_4)_2$, $Li_{0.2}Mn_{2.9}(VO_4)2$, $BaCu2(VO_4)_2$) and $Zn_4V_2O_9$ show structural phase transition while the remaining compounds show stable structure at high pressure. The new high-pressure phases of $lt-Mn_3(VO_4)_2$, $Li_{0.2}Mn_{2.9}(VO_4)_2$ and $Zn_4V_2O_9$ are recovered at ambient conditions.

The XRD data have also been used to get Equation of state parameters and the compound $Mg_3(VO_4)_2$, show the highest bulk modulus compared with other orthorhombic members. Observation of structural stability or only crystal to crystal transitions in some of the members of the family and investigating the mechanism involved in these structural transitions are important. In all the systems exhibiting structural transitions, the changes in the VO_4 distortion and/or increase in Vanadium coordination indirectly through Raman spectroscopy has been observed. The research work demonstrates the use of Raman spectroscopy to predict the increase/decrease of polyhedral distortion and/or coordination across structural phase transition.

Structural stability of A$_3$(VO$_4$)$_2$ family of compounds (Ni$_3$(VO$_4$)$_2$, Co$_3$(VO$_4$)$_2$, Mg$_3$(VO$_4$)$_2$, lt-Mn$_3$(VO$_4$)$_2$, Li$_{0.2}$Mn$_{2.9}$(VO$_4$)$_2$ and BaCu$_2$(VO$_4$)$_2$) *and the compound* Zn$_4$V$_2$O$_9$

6.1.3 Study of Influence of Environmental Parameters on Distribution of Thoron and Its Decay Products through Computational Fluid Dynamics (CFD) Modelling and Experiments

Thoron (^{220}Rn) is a source of significant radiological hazard in the environments of High Natural Background Areas (HNBRAs) and occupational facilities associated with thorium fuel cycle. In context of dosimetry, it is crucial to have in-depth knowledge of the behavior of ^{220}Rn and its decay products for accurate dose estimation. Their properties such as concentration profiles, decay product-aerosol attachment, depositions process etc. are greatly influenced by environmental parameters like air flow patterns, turbulence, aerosol properties, temperature profiles etc., which is difficult to study experimentally and analytically.

The present thesis addresses these limitations, by developing a CFD module to study the behavior of radioactive gases and their decay products in the indoor and occupational environments. For this, various algorithms and specific modules governing the relevant physical processes of radioactive gas and particulate behavior were coupled with the existing CFD structure. The developed CFD module was validated by comparing its simulated outcomes with solutions of test problems available in the literature. After due validation, CFD module was used to obtain insight into the behavior of radioactive gas and its decay products in confined volumes with respect to the variation of environmental parameters.
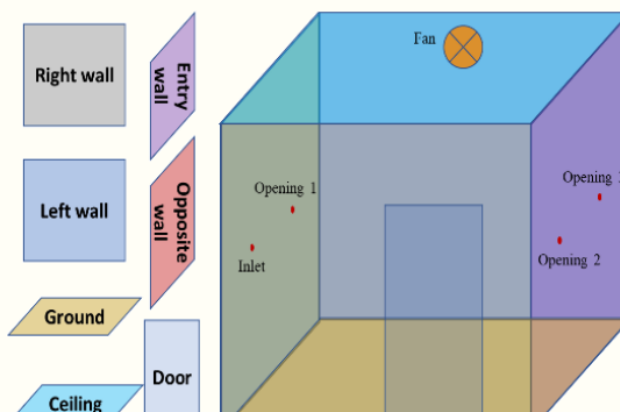
Model Calibration chamber

Two case studies demonstrating the effect of air flow patterns on ^{220}Rn and ^{222}Rn activity profiles in confined volumes were presented. In the first case, the effect of air flow patterns on ^{220}Rn concentration distribution in the HMGU Thoron Experimental Test House was studied. The study highlighted the complexity of concentration distribution with varying air flow patterns and its influence on inhalation dose. In the second case, effect of fan induced turbulent mixing on ^{222}Rn concentration profile was studied in a calibration chamber. The role of different parameters such as time, flow rates, Fan on/off conditions on ^{222}Rn gas concentration profile was analyzed.
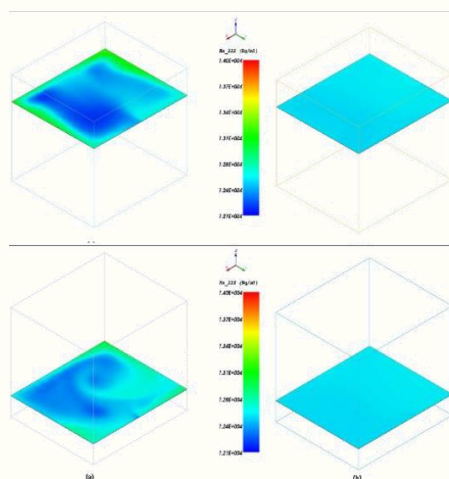
*Simulated profile of ^{220}Rn in calibration chamber*

Three different cases studies for the decay products dynamics were presented. In the first case, activity distribution and depositional behavior of ^{220}Rn and its decay products inside the flow-through Lucas Scintillation cell (LSC) was simulated for varying flow rate and inlet needle length. The outcomes were used to select the optimized operating parameters for ^{220}Rn measurements using LSC. In the second case, the CFD module was used to assess the effect of environmental factors on decay product-aerosols attachment. The effect of parameters like aerosols properties and temperature change on the attachment behavior was simulated. In the third case-study, effect of different air- flow patterns and aerosol sizes on ^{212}Pb concentration profile and deposition in a cubical calibration chamber was studied.

The developed CFD module will help in widening the scope of research related to ^{222}Rn-^{220}Rn, particularly with respect to their concentration profiling, decay products behavior and subsequently inhalation dosimetry in different types of indoor and occupational environments.

6.1.4 Fabrication and Characterization of Nano-structured Thin Films and Multilayers by Oblique Angle Deposition (OAD) Technique

Oblique angle deposition (OAD) has emerged as an extremely useful technique for the fabrication of new generation nanostructured thin film coatings. The excellent potential of OAD can be seen from the maturity of the technique in developing advanced thin film devices. Among the available techniques for nanofabrication, the various sophisticated nanostructures synthesized by OAD have demonstrated the simplicity and versatility of the technique in tailoring thin film nanostructures. Although, the field of oblique angle research has witnessed many impressive developments over the past 20-25 years, the field is still open with full of challenges in theoretical as well as experimental investigations.

The research work deals with a systematic investigation of optical, morphological and other related properties of nanoporous metallic (Ag), dielectric (TiO_x) and metal- dielectric (Ag/TiO_x) composite thin films fabricated using OAD methodology. The work also describes a novel angle constrained GLAD (collimated GLAD) arrangement to further improve the tunability/spatial selectivity of various thin film properties. The collimated GLAD technique applied for the deposition of TiO_x thin films revealed demonstration of an ultimate reduction (~50% from the bulk value) of refractive index to ~1.101 at 550 nm wavelength and single layer anti-reflection (SLAR) coating behaviour on glass substrate. The glancing angle deposition (GLAD) of Ag thin films at elevated substrate temperatures revealed the existence of a critical substrate temperature to observed prominent plasmonic absorption. The collimated GLAD technique utilized for Ag thin film depositions showed tunable coating morphology from continuous layer to discrete nanoislands across the substrate. The Ag/TiO_x nanocomposites fabricated using collimated GLAD arrangement showed spatially selective nanoplasmonic response along with plasmonic photocatalytic activity in the films.
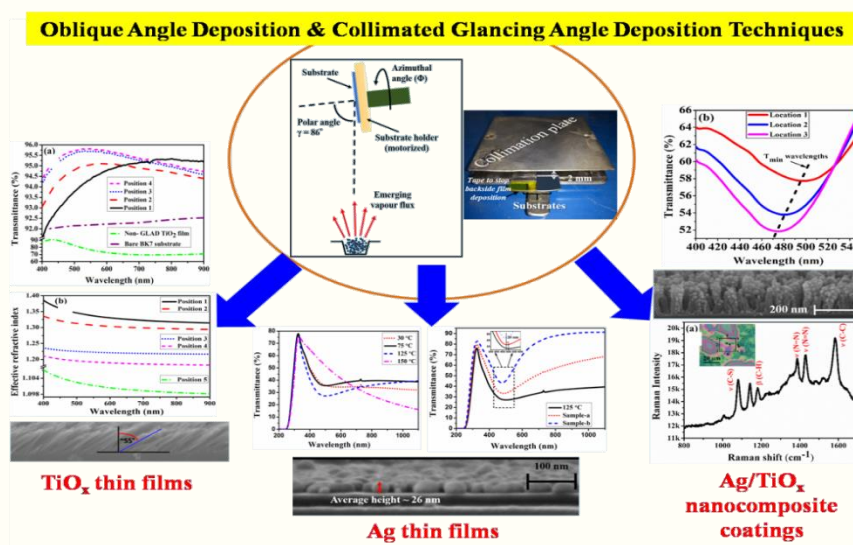
Some of the Important experimental results obtained with oblique angle deposition and collimated glancing angle deposition of dielectric (TiOx), metallic (Ag) and metal- dielectric (Ag/TiOx) nanocomposite thin films

6.1.5 Studies on Response Uniformity of RPC and Exploring Oscillation Dip and Valley, Non-Standard Interactions, and Earth's Core using Atmospheric Neutrinos at ICAL-INO detector

In the present work, experimental and physics simulation studies are performed in the context of the proposed 50 kt Iron Calorimeter (ICAL) detector at the India-based Neutrino Observatory (INO). ICAL would detect atmospheric muon neutrinos and antineutrinos separately in the multi-GeV range of energies over a wide range of baselines. A magnetic field of about 1.5 T enables ICAL to distinguish between muons and antimuons, and hence, neutrinos and antineutrinos. ICAL consists of iron layers as passive detector elements and resistive plate chambers (RPCs) sandwiched between them as active detector elements.

-

In the experimental part of the thesis, the effect of the non-uniformity of the graphite layer on the detector response of RPC is studied. A new code was written to simulate the charge transport in the two-dimension plane of the graphite layer. An experimental setup was developed to measure the

distributions of surface resistivity, potential, and time-constant. It was inferred using the simulations and experiments that the distribution of potential is independent of the non-uniformity in surface resistivity, whereas the time constant depends on this non-uniformity.
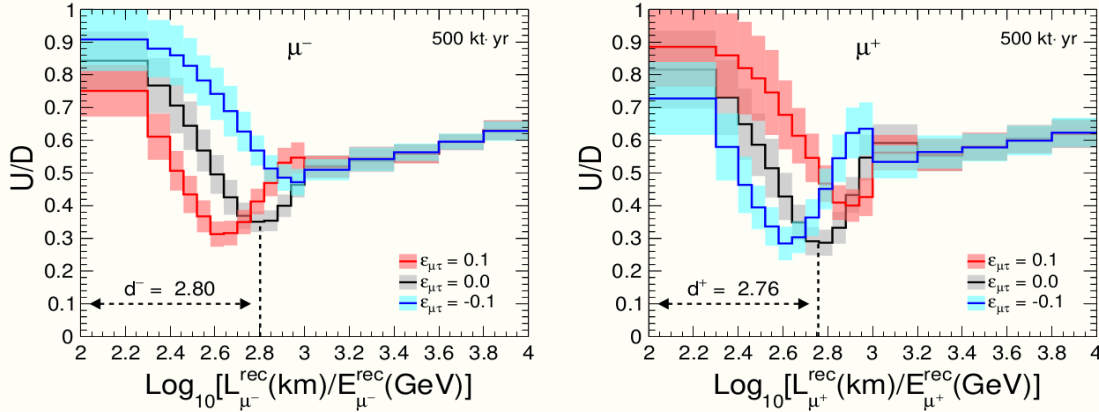

Oscillation dips move in opposite directions for reconstructed muons and antimuons.

In the physics simulation part, it was demonstrated for the first time that neutrino oscillation dip and valley can be observed at ICAL using the up/down ratio of reconstructed muons and antimuons separately. A method was formulated such that the location of the dip and the alignment of the valley can be used to measure an atmospheric oscillation parameter called the mass-squared difference. Further, a new approach was proposed to probe the neutral-current non-standard interactions (NSIs) using the oscillation dip and valley. The opposite shifts in the oscillation dips and the contrast in the curvatures of oscillation valleys for reconstructed muons and antimuons are used to constrain the NSI parameter in two separate ways. While passing through the Earth, the upward-going atmospheric neutrinos experience the matter effects, which modify the neutrino oscillation patterns. These matter effects depend upon the density of electrons inside Earth and can be used to perform the neutrino oscillation tomography of Earth complementary to gravitational measurements and seismic studies. It was demonstrated that the presence of Earth's core can be validated using the atmospheric neutrinos at ICAL.

6.2   Indira Gandhi Centre for Atomic Research, Chennai

6.2.1   Magnetic Nanoemulsion Based Sensors for Visual Detection of Defects in Ferromagnetic Materials: Effect of Stabilizing Moieties and Defect Geometries on the Detection Sensitivity

Magnetic flux leakage (MFL) is one of the most popular and cost- effective techniques for defect detection in ferromagnetic materials. When such materials are magnetized, MFL occurs in the vicinity of the defects due to magnetic permeability mismatch. Most of the conventional MFL sensors require time-consuming raster-scanning, and as an alternative, magnetic nanoemulsion (MNE)-based sensor has been developed for naked-eye wide area optical detection of defects.
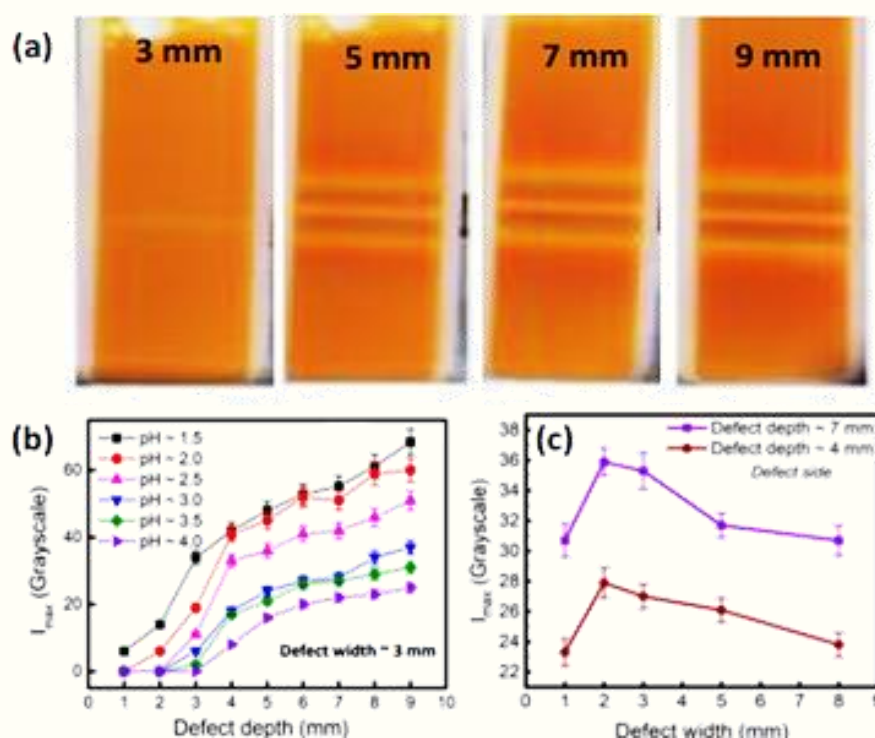
Schematic diagram showing (a) the optical patterns of the MNE sensor with increasing defect depth. (b) Monotonic increment of the intensity of the optical contrast with increasing defect depth. (c) Non-monotonic variation of the intensity with increasing defect width

Systematic investigations reveal that the defect detection sensitivity is the highest for the MNE with the lowest decay length of the inter-droplet force profiles. The lower decay length leads to field induced chain formation with more MNE droplets accommodated within the chains, which leads to a larger number difference of the MNE droplets between the defect edges (higher MFL) and the defect center (negligible MFL), thereby enhancing the optical contrast. Using the pH sensitive PAA stabilized MNEs, defect detection sensitivity is found to be the highest at pH 1.5, due to the lower decay length. However, considering the long- term colloidal stability and detection sensitivity, the PAA stabilized MNE at pH 3.5 is found to be the most suitable for the optical detection of defects (schematic (a) above). Further, the optical intensity is found to increase with the defect depth for a fixed defect width (schematic (b) above), whereas, for a fixed defect depth, non-monotonic variation in optical intensity is observed as a function of defect width (c) due to variations in the spatial coupling between the generated surface magnetic dipoles.

Inter-droplet force measurements on γ-Al$_2$O$_3$ stabilized Pickering MNEs reveal the importance of the electric dipolar interactions, in addition to the screened Coulombic interaction, due to the formation of an asymmetric image charge cloud near the polar/non-polar interface (schematic on the left (a) below). Incorporation of the comparatively long-range electric dipolar interaction to the inter-droplet force profiles yields good correlations between the experimental and theoretical results (left schematic b-c). The defect detection sensitivity of the γ-Al$_2$O$_3$ stabilized MNE-based sensor is found to be nearly invariant up to 70 days and 50 ^{0}C. Numerical modeling is performed for *a priori* generation of the optical patterns for a fixed defect geometry and type of MNE. The theoretically generated optical patterns are found to be in good agreement with the experimentally recorded optical patterns for defects of varied geometry, as shown in schematic on the right a-d.
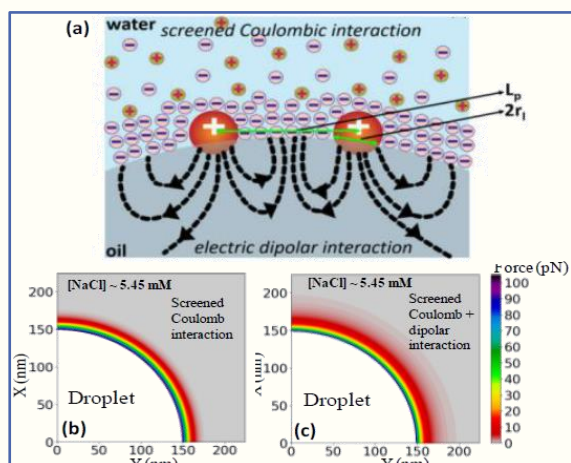
Schematic representation of (a) the electric Dipolar and screened Coulombic interactions. Surface plots showing the theoretically calculated repulsive force magnitudes (in the 1st quadrant) around a MNE droplet for the(b) screened Coulombic interaction alone and(c) Screened Coulombic along with electric dipolar interaction
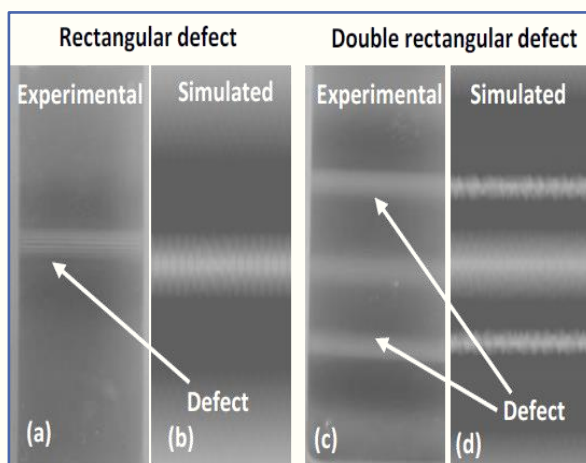
(a-b) Experimental and theoretical images of the rectangular defects. (c)-(d) Experimental and theoretical images of the double rectangular defects

The obtained results are beneficial for preparing MNE-based defect detection sensor with enhanced detection sensitivity and long-term colloidal stability.

6.2.2 Evolution of Superconducting Critical Properties of Bi-based High Temperature Superconductors under Extreme Conditions and in Proximity with Manganites

With the general formula given by $Bi_2Sr_2Ca_{n-1}Cu_nO_{2n+4+\delta}$ where n denotes the number of Cu-O planes, there are three members belonging to BSCCO family, namely, Bi-2201, Bi-2212, and Bi-2223. A superconducting transition temperature (T_C) of 20 K, 80 K, and 110 K is observed in this system for n = 1, 2, and 3, respectively. Pb substitution at the Bi site and the extreme conditions like external pressure and magnetic field can alter the superconducting properties.
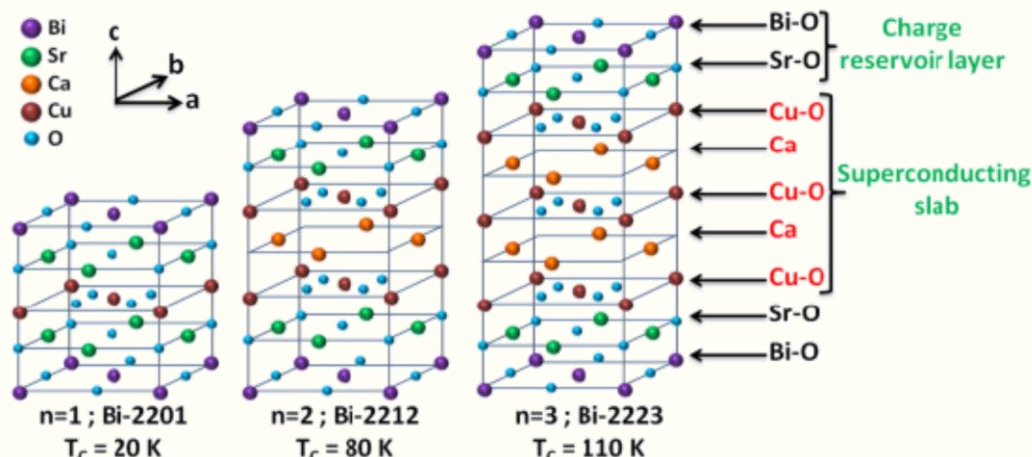
Schematic representation of the formula units of the three coexisting phases of the BSCCO

Evolution of superconductivity in multiphasic BSCCO system is qualitatively rationalized within the realm of proximity effect between the two coexisting phases and the establishment of a superconducting percolation path. The role of substituted Pb at the Bi site was found to enhance the superconducting properties of the BSCCO system by increasing the Bi-2223 phase content, acting as pinning centres, increasing the bulk moduli and the metallicity of the charge reservoir layers, and protecting the CuO plane from buckling. B(Pb)SCCO thin film grown on $SrTiO_3$ (STO) substrate exhibit superior superconducting $TC_{,OFF}$ of 107 K and $H_{C2}(0)$ of 184 T (H||c) due to Pb-assisted cation chemistry, enhanced Bi-2223 phase fraction (as high as 58 %) and the improved pinning mechanism. A microstructure and substrate-dependent enhanced JC as high as $\sim$105 Acm^{-2} was obtained in B(Pb)SCCO thin films.
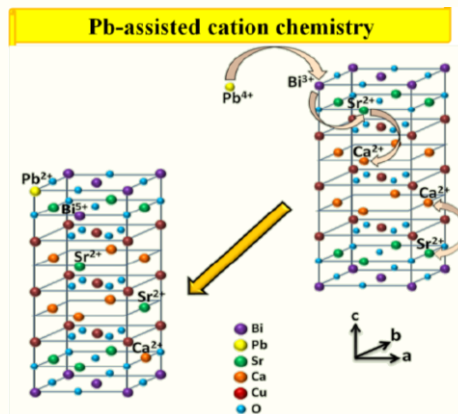
Schematic representation showing the series of events happening as a result of Pb^{2+} substitution at Bi^{3+} site in B(Pb)SCCO thin films

An enhanced CMR property as high as 31 % near room temperature is realized in the ultrathin heterostructure of PSMO and PCMO by the combined effects of strain, ex-situ annealing, and the magnetic proximity.
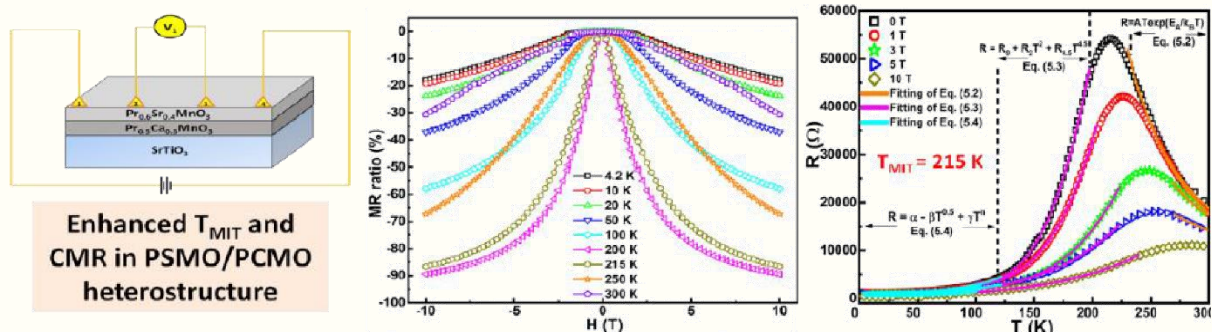
Enhancement in CMR and T_{MIT} of the annealed heterostructure of PSMO and PCMO

Superconductivity of B(Pb)SCCO was modified in proximity with manganite due to combined effect of magnetic exchange interaction arising from the manganite, the leakage of Cooper-pairs from the superconductor into the manganite, and the diffusion and transport of spin-polarized electrons from the manganite into B(Pb)SCCO. CMR ratio as high as $\sim$99 % observed in the B(Pb)SCCO/PSMO heterostructure, due to proximity effect, can be a potential candidate for prospective spintronics application.
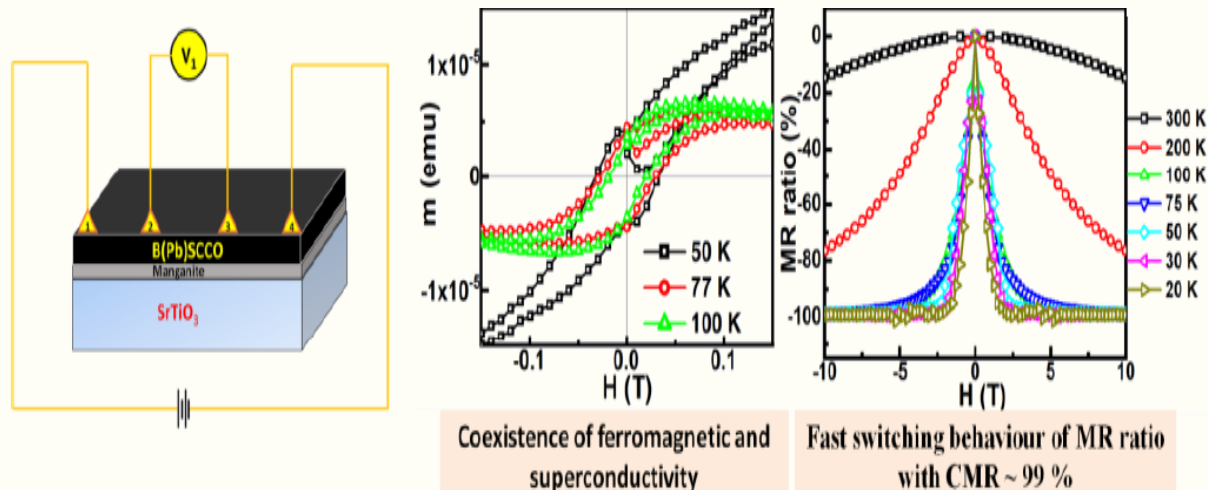
Coexistence of magnetism, superconductivity and large CMR in the heterostructure of B(Pb)SCCO and manganites (PSMO and PCMO)B(Pb)SCCO

6.2.3 Study of Phase Transformations in Some Secondary Explosives using Raman Spectroscopy, XRD and DFT Calculations

One of the prime objectives of the explosives research is to synthesize safer, greener, and more powerful explosives compared to the existing ones. The new materials must satisfy requirements such as high performance, insensitivity toward accidental stimuli, low solubility in water, hydrolytic stability, longevity, compatibility for storage and transport, and environmental safety. Phase transformation in solids is a fundamental subject that is directly related to material properties. In energetic materials, many properties such as chemical reactivity, thermal stability, crystal density, and sensitivity depend on the structure. Hence it is necessary to map the phase diagram of explosive materials at high pressures and temperatures to evaluate their performance and safety aspects. In the present work, thesis the pressure and temperature dependent changes in novel energetic materials 4,10-Dinitro-2,6,8,12-tetraoxa-4,10-diazaisowurtzitane (TEX), 2,4-dinitroanisole (DNAN) and Bis(3,5-dinitro-4-aminopyrazolyl) methane BDNAPM have been studied using Raman spectroscopy, X-ray diffraction (XRD) and density functional theory (DFT) calculations.
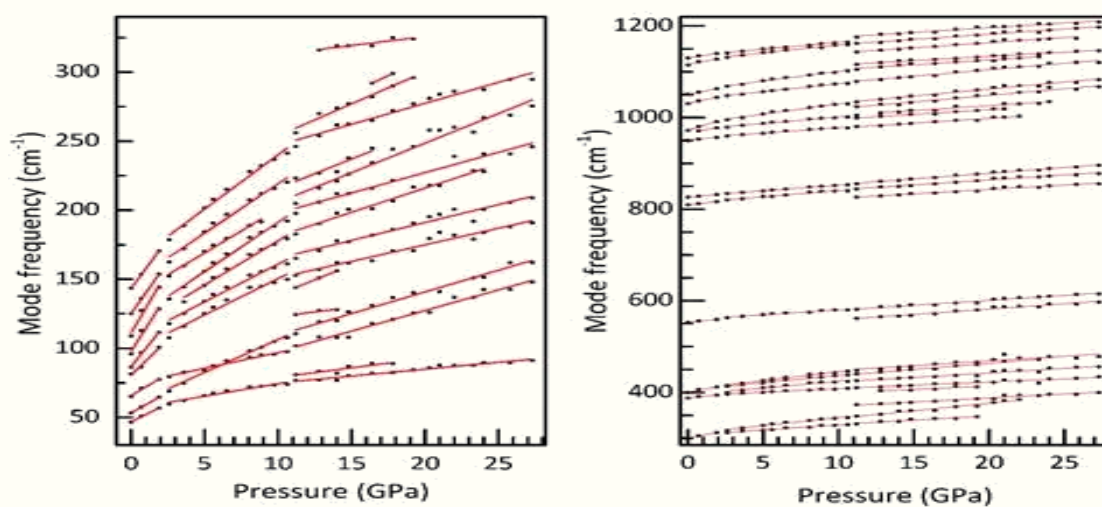
Change in mode frequencies of various Raman modes of TEX with pressure
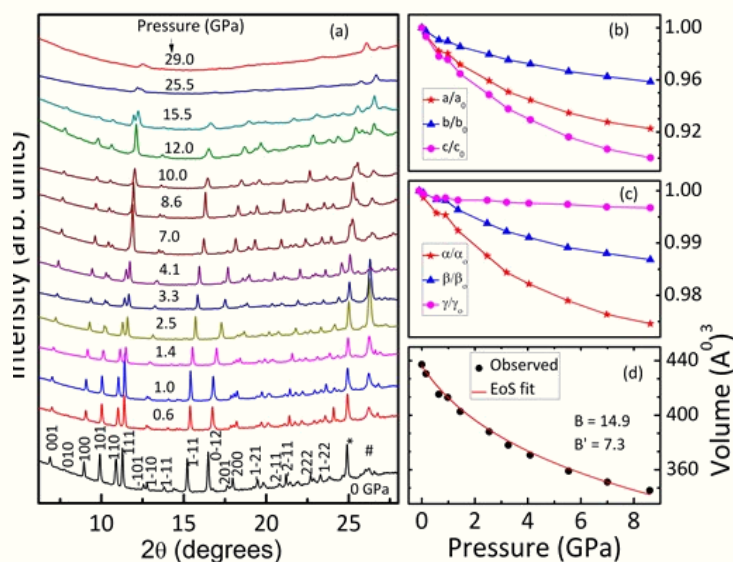
*Stacked XRD pattern with pressure. Gold peak is represented by * and tungsten peak is by #
(a), lattice parameters (b, c) and volume (d) at different pressures*

Vibrational frequencies of TEX molecule were calculated using Gaussian and the modes assigned sing potential energy distribution (PED) calculation. CASTEP codes were used to compute the properties such as electronic, optic, thermal, elastic and vibrational properties. Also pressure dependent changes in the crystal structure of TEX were studied up to 40 GPa using CASTEP codes. Two reversible phase transformations in TEX as a function of pressure have been observed: (i) a to a' transformation around 2 GPa that is a conformational change of the TEX molecule from exo-exo to exo-endo, and (ii) a' to b structural transformation above 11 GPa. These experimental result match with computation and XRD confirm this phase transformation. In the case of DNAN, pressure induced monoclinic to orthorhombic transition is observed with Raman spectroscopy and XRD around 3 GPa with a volume collapse of 10%. Bulk moduli for the monoclinic and orthorhombic phases are estimated as 11.9 GPa and 26.9 GPa respectively, pointing to a lower impact sensitivity of the orthorhombic phase. Temperature dependent Raman spectra in the range -194 to +130 °C show melting of the DNAN around 98 °C. In the case of BDNAPM, appearance of new external and internal modes indicates a structural phase transformation at 3.3 GPa. Also, many internal and external modes show discontinuity above 2.8 GPa. Ambient orthorhombic to monoclinic transformation at 3 GPa is observed with a 13% volume reduction.

6.2.4   Synthesis and Applications of Low Dimensional V_2O_5 Nanostructures

V_2O_5, the most stable oxide of the transition metal V, is a layered 2D van der Waals material. V_2O_5 can easily undergo surface reduction by creating oxygen vacancies, thereby increasing the surface activity, which is useful in applications such as gas sensing and catalysis. The role of such O-vacancies in determining the gas sensing properties and the gas sensing mechanism by V_2O_5 is not clearly understood. The layered structure of V2O5 facilitates its existence in two-dimensional (2D) form, which is still unexplored. In the present study, the V2O5 nanoparticles were synthesized via hydrothermal and solvothermal methods. An increase in defect density was manifested as a blue shift in the optical bandgap as a result of the Burstein-Moss effect. 2D V_2O_5 nanosheets were also successfully synthesized using chemical exfoliation technique. A 32-fold increase in the specific surface area was also observed for 2D V_2O_5 from the bulk.

The V_2O_5 nanoparticles showed an optimum temperature of 150 °C for gas sensing. A carrier saturation in the native oxygen defect states at 1.7 and 1.8 eV above 150°C observed from temperature dependent photoluminescence is found to be responsible for the maximum response at 150°C. Further, the mechanism of NH_3 sensing by V_2O_5 nanoparticles was investigated by employing in-situ Raman spectroscopy and optical absorption and photoluminescence emission study. It is observed that the vanadyl oxygen site is the energetically most favorable gas adsorption site at room temperature.
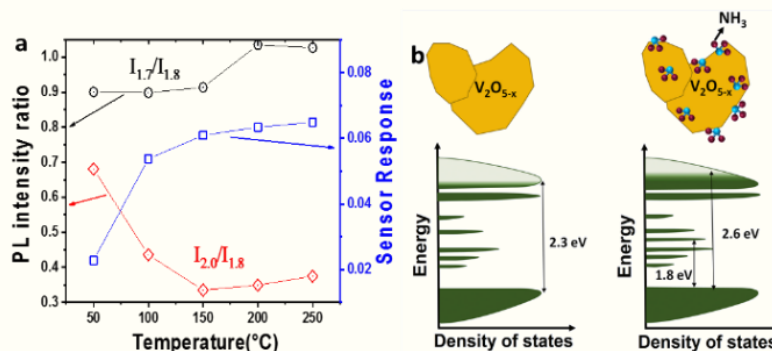
a) Photoluminescence intensity ratio of defect peaks with temperature. b) The schematic diagram of NH₃ sensing mechanism

Bilayer thin 2D V_2O_5 nanosheets with the lateral dimension of 100-300 nm were subjected for the study of its vibrational and electronic properties. Using UV-Vis spectroscopy, thickness dependent absorption edge blueshift from the bulk was manifested in bilayer V_2O_5, indicating electronic decoupling. The Raman spectroscopic studies on the exfoliated sample shows that the mode frequencies of bilayer 2D V_2O_5 were shifted from bulk values due to vibrational decoupling. The experimental observations were further confirmed by computing lattice vibrational modes using density functional perturbation theory. This novel observation can be used to fingerprint the formation of 2D V_2O_5 from their bulk counterpart.
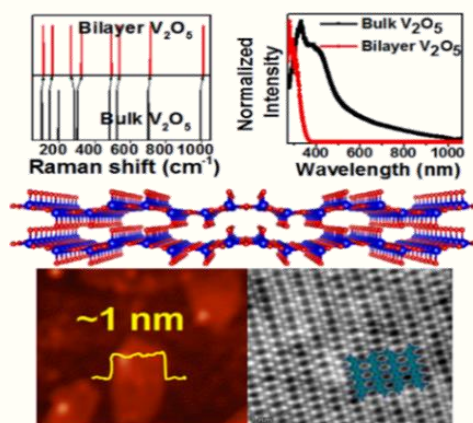
Schematic diagram showing the electronic and vibrational changes in 2D V2O5. The AFM and ARTEM images are also shown.

The 2D V_2O_5 nanosheets showed excellent performance as Zn-Li dual ion battery because of the easier diffusion pathway for the ion intercalation into the 2D V_2O_5 nanosheets and its high specific surface area. 2D V_2O_5 nanosheets were also used as a photocatalyst owing to its high specific surface area and enhanced separation of charges in the presence of light. 2D V_2O_5 nanosheets are also used as a highly selective chemiresistive sensor of NO_2 gas at room temperature attributed to the high surface activity and specific surface area of the material.
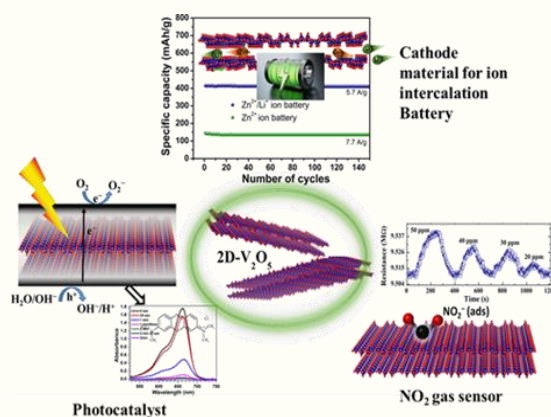
Schematic diagram showing the battery,photocatalytic, gas sensing applications of 2D-V$_2$O$_5$

6.2.5 Studies of Ion Beam Modification of Graphene and Carbon Nanomaterials with Novel Properties

In the present work, growth of multilayer graphene and various novel properties *e.g.,* bandgap engineering and impermeability nature were studied. Initially, a few layer graphene grown on various substrates (*e.g.,* MCD, BMCD and SiC) by depositing 4 nm Ni using a MBE system and annealing at 950 °C for one minute with RTA. Again, a 5 nm Ni layer deposited over graphene grown on SiC substrate to form Ni/graphene/Ni multilayer on SiC. The positive magneto-resistance (as shown in Fig. 1) shows the presence of antiferromagnetic exchange coupling between the nickel layers separated by graphene. This results in a bandgap opening of 0.045 eV in the 7-monolayer thick graphene. In order to verify the possibility of opening of bandgap in CVD grown monolayer graphene on copper substrate, single ion impacts of Ar- monomer and Ar-dimer ions are carried out with energy 35 keV/atom and a fluence of 1×10^{12} atoms/cm^2. Ar ion irradiated samples at this low fluence show craters of diameter 1.7±0.1 nm and depth 4.6±0.2 nm, while the surface of pristine graphene is smooth. The number density of craters per atom produced by Ar- monomers is higher than that of Ar-dimer ions. Semimetallic graphene is found to be metallic at the crater regions in both Ar- monomer and dimer irradiation. Fig. 2 shows the differential conductance versus bias voltage spectra from the ion impact and planar regions of Ar dimer irradiated sample. In the case of Ar dimer ion irradiated single layer graphene a bandgap opening is observed because of the combined effect of the compressive strain and breaking of the equivalence between A and B sublattices of graphene.
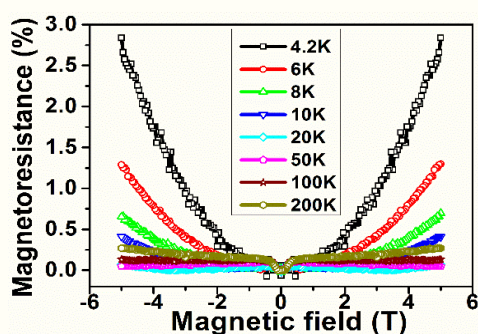
Variation of Magnetoresistance with magnetic field of Ni/graphene/Ni/SiC sample.
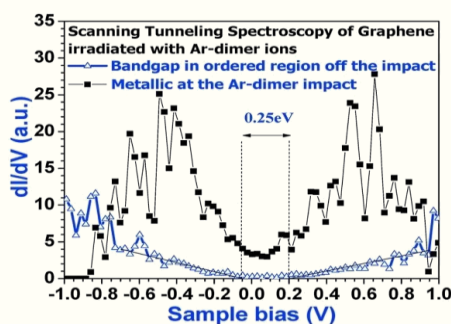
Differential Conductance versus bias voltage from ion impact and planar regions of Ar dimer irradiated sample.

Furthermore, the impermeability nature of graphene in the context of inter-diffusion processes in miscible Au/Cu and immiscible Ag/Cu systems is studied by depositing 30 nm of Au and Ag on Cu and monolayer graphene on Cu. One set of samples are annealed in high vacuum from 200-450 °C and RBS measurements with 2 MeV He$^+$ ions are carried out in-situ. Another set of samples are irradiated with 9 MeV Si^{6+} ions where electronic energy loss process is dominant. Compressive strain is induced during Au deposition (~30 nm) and thermal annealing (200-300 °C in a step of 20 °C), as evidenced by the blue shift of G and 2D peaks, as well as the splitting of G peak in Raman scattering results. For thermal annealing processes, graphene acts as a barrier layer in miscible system of Au/Cu upto 220 °C while it is not useful in immiscible Ag/Cu system which shows dewetting of Ag. Upon 9 MeV Si^{6+} ion irradiation, graphene acts as a barrier layer upto 1.07 dpa and 5.55 dpa for Au and Ag diffusion into Cu substrates respectively. Apart from that, the role of nanographite and Au in the formation of N-V centers in ultra-nano crystalline diamond (UNCD) films is also studied. Among UNCD/Si and UNCD/Au/Si samples, UNCD/Au/Si which has lesser nanographite content and presence of Au nanoparticles shows enhanced photoluminescence intensity. The quantum efficiency is found to be high for (N$^+$+Ne$^+$) ion implanted/annealed UNCD/Au/Si samples (~71%) due to the high lifetime and increased photoluminescence in comparison to bulk diamond (100%). The NV^0/NV$^-$ concentration ratio is high and the rate of conversion of NV$^-$ to NV^0 is also 1.2 times in (N$^+$+Ne$^+$) ion implanted/annealed UNCD/Si samples.

6.3   Institute of Physics, Bhubaneswar

6.3.1   Impacts of Dark Matter Interaction on Nuclear and Neutron Star Matter within the Relativistic Mean-field Model

A neutron star (NS) is a compact object that forms after a star with a mass greater than 8-20 times that of the sun collapses during a type-II supernova. It mainly comprises neutrons, with a small fraction of protons and leptons, to maintain charge neutrality. To explore various properties of NS, the equation of state (EOS) that calculates the interaction between nucleons and leptons is required. In the present work, the relativistic mean-field (RMF) and extended RMF (E-RMF) models were used to calculate the different properties of finite nuclei, nuclear matter (NM), and NS. In addition to the nucleons, an extra component known as dark matter (DM) inside the NS has also been studied. Since the NM parameters significantly affect the NS properties, it is imperative to analyze those quantities with the addition of DM. The DM model has been constructed assuming it interacts with nucleons by exchanging Higgs. Therefore, the system energy density and pressure are the addition of nucleons and DM. It was observed that the EOS becomes softer with increasing DM momentum. The energy density increases with the DM case without adding much to the pressure. It was found that the DM has marginal effects on the NM properties, except for the EOSs, and the binding energy per particle.

The properties of isolated, static, and rotating DM admixed NS were calculated, and it has been noticed that DM has significant effects on both static and rotating NS. The magnitude of maximum mass and its corresponding radius decrease by increasing the DM percentage. Also, the change in magnitude of curvature with and without DM was obtained as ~ 33% for the canonical star, and the value increases with mass. The binding energy for the DM admixed NS increased towards a positive value with the increase of DM momentum, which makes the NS unstable. From this study, It was concluded that a tiny amount of DM can accumulate inside the NS. If a star has more DM, it heats the

NS, accelerating the Urca process. With the DM admixed EOSs, I has also been also suggested that the secondary component might be a NS with DM content if the underlying nuclear EOS is sufficiently stiff. The f-mode frequencies of the DM admixed hyperon star for various EOSs were computed. The magnitude of f-mode frequencies decreases for softer EOSs because it predicts smaller mass compared to stiffer ones. One can constrain the f-mode frequency of the star using various observational data. The tidal Love numbers and deformabilities for gravitoelectric and gravitomagnetic cases for DM admixed NS were obtained. It has been observed that the magnitude of different Love numbers increases with DM percentage for a fixed value of DM momentum and vice-versa for tidal deformabilities. Also, with the addition of DM, the binary system sustains more time in its inspiral phases. Finally, it was suggested that one can include DM inside the compact objects while modeling the inspiral waveforms for the binary NS system.

6.3.2 Perusing Some Neutrino Mass Models at the LHC

Despite being a tale of theoretical and phenomenological success, the Standard Model (SM) fails to explain several issues. The discovery of neutrino oscillations − necessitating the neutrino to be massive − has provided arguably the most incontestable reason for going beyond the SM. Over the years, multifarious new physics models have been proposed to address this ill of the SM. This thesis peruses a few such scenarios in the context of the Large Hadron Collider (LHC) experiment. Particular attention is paid to the so-called see-saw models.

In the doctoral work, a comprehensive collider study of the type-II see-saw model has been performed. Considering all relevant production and decay modes, the most stringent limits on the triplet-like scalars are derived for a vast model parameter space by recasting several CMS and ATLAS searches. The derived limits are stronger by approximately 50–230 GeV than those obtained by CMS and ATLAS. The work also forecasts future limits by recasting an ATLAS search as well as designing a search strategy at the high-luminosity LHC (HL-LHC).

The phenomenology of the type-III see-saw model has been studied. First, a CMS multilepton search has been reinterpreted in the context of a realistic model accounting for the neutrino oscillation data. Then, the phenomenological implications of the information lost in decoupling the heavy fermions from high- to low-energy has been explored. After this, a genuine fermionic quituplet see-saw model has been introduced generating neutrino masses at tree-level via d = 9 effective operator. Heeding the lepton flavour violating decay constarints, the 95% CL limits on the new fermion masses are derived by recasting a recent CMS search, followed by an elaborate discussion on the possibility of some of these fermions being long-lived with signatures like disappearing charge track or displaced vertex at present and future colliders.

The thesis work then presents a search for heavy exotic leptons in final states with multiple leptons and fat-jets. The corresponding SM background being suppressed, the search strategy appears to carry through for a large class of models with exotic leptons within a large gauge multiplet, unlike many of the LHC searches that lose sensitivity when applied to more general models with similar final states. These considerations are then applied to realistic type-III seesaw models and by performing comprehensive analyses with several distinct final states, it is shown that the exotic leptons could be probed beyond the TeV scale.

6.4   Institute for Plasma Research, Gandhinagar, Gujarat

6.4.1   Collective Dynamics of Active or Self-propelled Particles

Natural world is abundant with fascinating collective behavior among biological entities over an extensive range of scales. Areal display of a flock of birds is a paradigmatic example. Likewise, cytoskeletal filaments inside cells are known to exhibit collective dynamics and patter formation in the micro scales. Various eukaryotic cells at various stages of life are known to exhibit collective dynamics to perform important biological tasks. Collective motion of a school of fish in large oceans is another well-known instance of biological collective behavior. Even at more larger scales, human crowd is known to performs collective dynamics. Above mentioned non-equilibrium biological systems are also known as living matter or living active matter, where the driving energy is injected at the smallest scales of the system, unlike energy injection at the largest scales in driven passive systems, such as steering a cup of tea. Motivated by living active matter, several synthetic particles have been synthesized in recent past that exhibit self-propulsion akeen to their biological counterparts. Due to several potential applications in some of the key areas, such as healthcare, environmental sustainability, climate changes, and more, a great amount of effort is being put world-wide to understand the properties of self-propelled particles or active systems.

In the present work, several problems in active matter physics have been addressed employing minimal models in two dimensions, using several particles based numerical simulation schemes. These problems are mainly categorized into four components. First, a small system of repulsive, point-like model of active or self-propelled particles of finite mass is investigated for their collective behavior. Essential differences between inertial and non-inertial collective behavior and effective thermodynamic properties are addressed. Self-propulsion or motility of the particles in the non-inertial limit is known to exhibit phase separation in to a high and a low-density phase, and consequent coexistence of these phases.

The phenomenon is known as motility induced phase separation or MIPS. Second component of the Thesis is the detailed investigation of softness and inertia of the finite size particles on MIPS and the investigation of the spatio-temporal properties of the particles in different MIPS phases. Alignment interaction between active entities of several classes of self-propelled particles is found to be responsible for various interesting collective dynamical properties. The third component of the Thesis deals with the investigation of collective dynamics of various non-reciprocal alignment interactions between the particles. Several interesting results due to the incorporation of the non-reciprocal alignment interaction are addressed in the Thesis. Final part of the Thesis investigates the effect of active particles in passive shear flows.

This preparatory work opens a new dimension of understanding shear flow and corresponding shear instabilities in presence of active or self-propelled particles. In addition to the problems from physical point of view, mentioned above, large scale CPU and GPU parallel numerical solvers, based on Brownian, Langevin, and Molecular Dynamics schemes, that have been used to address the problems of the present Thesis are developed. Several unsolved problems arising from this Thesis are highlighted that may bring further insights in our understanding this cross-disciplinary field of science.

6.5   National Institute of Science Education and Research, Bhubaneswar

6.5.1   Probing the QCD Phase Diagram via Net-proton Number Fluctuations at RHIC

The quantum-chromodynamics (QCD) phase diagram is the phase diagram of strongly interacting matter outlined by temperature, T, versus baryon chemical potential μ_B. It has at least two known phases: the hadronic phase, where quarks and gluons are confined, and the QGP phase, where they are de-confined. The QGP is believed to have existed in primordial universe. As the universe evolved and cooled, the quarks and gluons were confined within hardons. This quark-hadron phase transition is found to be a smooth crossover at vanishing μ_B from first-principle QCD calculations. At large μ_B, various QCD-based models predict this to be a first-order phase transition which terminates at a critical point, called the QCD critical point. Neither the presence of QCD critical point, nor the nature of quark-hadron phase transition have been experimentally verified yet.
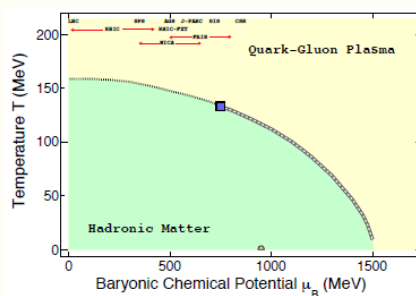
Schematic diagram showing a conjectured QCD phase diagram with hadronic phase and quark-gluon plasma (QGP) phase. The dashed line and solid ine indicate crossover and a first order phase transition respectively. The filled space represents the QCD critical point

By colliding heavy-ion nuclei at ultra-relativistic velocity, one tries to create the QGP at lab and understand the quark-hadron phase transition. Varying the collision energy of incoming nuclei, results in variation in T and μ_B of the system created, thus allowing for an experimental study of phase diagram. In this regard, the fluctuation of event-by-event net-proton number have been suggested as important observables as they are sensitive to critical point and nature of phase transition.The present work reports net-proton number fluctuations (which are measured via cumulants) up to sixth-order in Au+Au collisions at nine center-of-mass energies: $\sqrt{s_{NN}}$ = 7.7, 11.5, 14.5, 19.6, 27, 39, 54.4, 62.4, 200 GeV collected by STAR detector at RHIC facility, Brookhaven Lab, USA. These energies constitute the first phase of Beam Energy Scan (BES) program. The measurement of fourth order net-proton cumulant for top 5% central Au+Au collisions, exhibits a non-monotonic collision energy dependence with a significance of 3.1σ. The observed trend is consistent with QCD based model calculations that includes a QCD critical point. Various model calculations that do not include a critical point show monotonic variation with collision energy. The sixth-order net-proton cumulants (measured as proxy for net-baryon) for 0-40% central Au+Au collisions become progressively negative with decreasing collision energy – the negative sign and the observed trend are consistent with first-principle lattice QCD calculations (μ_B < 110 MeV, which corresponds to $\sqrt{s_{NN}} \geq$ 39 GeV) with a crossover quark-gluon phase transition. The overall significance of observing the negative sign is at a level of 1.7σ. While these are important observations, experimental confirmation of these would require more precision measurement from the upcoming second phase of BES program.

6.5.2   Nontrivial and Topological Magnetic States in Mn-rich In-based Ferrimagnetic Systems

Magnetic materials with competing magnetic interactions exhibit several non-trivial complex spin states beyond the conventional collinear ordering. For example, the geometrical frustration, exchange frustration, higher-order exchange interactions, and the spin-orbit coupling induced Dzyaloshinskii-Moriya interaction (DMI) may give rise to the stabilization of non-collinear and/or non-coplanar spin textures. Incorporating the notion of topology along with the non-trivial spin textures enables the finding of many exotic phenomena related to the magnetic, electrical, optical, and thermal properties. The unconventional response of these physical properties in quantum materials is vital to the development of future energy harvesting and information storage devices. The work presented in the thesis focuses on the finding of nontrivial and topological spin structures and related emergent phenomena in the Mn-rich In-based ferrimagnetic (FiM) materials. The first part of the thesis is dedicated to the control tuning of noncollinear ferrimagnetic state in $Mn_{2-x}PtIn$ system. The effective tuning of the degree of non-collinearity of the magnetic state enables control of the topological Hall effect (THE). The origin of the THE is attributed to the effective fictitious magnetic field as a result of finite scalar spin chirality given by $S_i \cdot (S_j \times S_k)$, where S_i, S_j, and S_k are the three nearest neighbour spins. In the second part, the effect of noncollinear magnetic ordering on the stabilization mechanism of antiskyrmion (askx) phase in the Mn-Pt(Pd)-Sn-In inverse tetragonal Heusler system is studied. Using Lorentz transmission electron microscopy (LTEM) and neutron diffraction study, it is revealed that the askx phase is stable only when the magnetic ground state is collinear in nature in the absence of DMI. Furthermore, a new topological phase of spontaneous (anti)meron chain within a natural 1-D like helical stripe is found. It is envisaged that the topological object within a helical background can be free from the ambiguous 'skyrmion Hall effect', which usually occurs during their current-driven motion. The third part of the thesis is dedicated to the role of non- coplanar spin structure of the uncompensated interfacial spins in the exchange coupled system. The THE measurement is utilized to exchange. This leads to the observation of a large exchange bias field in a special type of fully compensated ferrimagnet (FCF) Mn_3In.
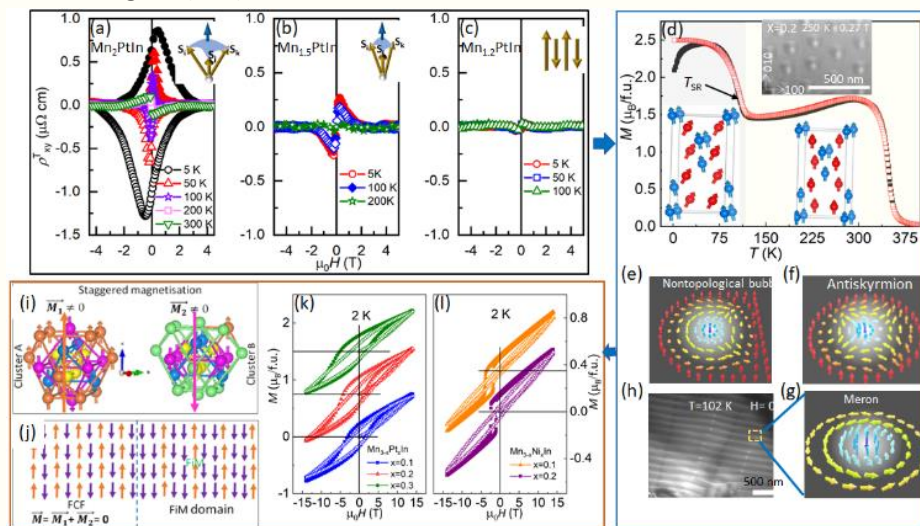
(a)-(c) Control tuning of topological Hall by manipulating the degree of non-coplanarity. (d) Lattice of antiskyrmion stabilize in the temperature T> TSR, where spins are collinear. Schematic of nontopological bubble (e), antiskyrmion (f), and meron (g). (h) Spontaneous (anti)merons in interstitial position. (I) Antiferromagnetic arrangement of the staggered cluster moment in Mn3In. (j) Formation of FiM domain within the FCF background. (k), (l) M-H loops indicating large exchange bias effect

6.5.3 Formulation of Relativistic Dissipative Hydrodynamics of Spin-1/2 Particles from Kinetic Theory

With the advent of heavy-ion collision experiments, the theory of relativistic hydrodynamics has become a highly active field of research that allows us to study the evolution of the strongly interacting medium of quark-gluon plasma (QGP). The non-central collision of heavy nuclei at ultra-relativistic speed deposits a very high angular momentum in the created hot and dense medium and may also produce a very large magnetic field. These effects can play important role in the dynamics of the medium. The experimental facility of RHIC at BNL found the first evidence of the medium being spin-polarized along the direction of this global angular momentum. Later, the medium was also found to be spin-polarized with a quadrupole structure in the plane transverse to the collision axis. While the former phenomenon (global spin-polarization) was explained aptly with a theoretical model that assumes the spin degrees of freedom are thermalized, the same model failed to explain the latter (longitudinal spin-polarization) both quantitatively and qualitatively. It was thus believed that dissipation of spin may play a role in the explanation of longitudinal spin-polarization.

In the present thesis, a theory of relativistic dissipative spin-hydrodynamics has been formulated both in the absence and presence of an external magnetic field. The theory of spin-hydrodynamics without any magnetic field showed for the first time, the dissipation mechanism of spin-current in a spin-polarizable relativistic fluid can depend on the gradients of multiple hydrodynamic variables. The evolution mechanism of the spin-polarization tensor, which acts as a chemical potential of spin, was also found for the first time. The framework of spin-hydrodynamics was further extended to include the effect of a magnetic field, where the fluid medium was assumed to be spin-polarizable as well as magnetizable. This led to the development of relativistic spin-magnetohydrodynamics. This work revealed that spin can affect the dynamics of particle diffusion as well as bulk and shear viscous pressures apart from the already established connection to spin diffusion. The framework of spin-magnetohydrodynamics also described the origin of magneto-mechanical effects such as Einstein-de Haas and Barnett's effects. To obtain a more realistic description of the dynamics of a complex system like QGP, the thesis also focused on the incorporation of different timescales associated with the relaxation of elastic and inelastic processes and the effect of the equation of state. These aspects were investigated for a fluid that is not spin-polarized. However, an extension to the spin-polarizable fluid is straightforward and should be attempted in near future. The theoretical frameworks developed in the thesis should be used as a basis to explore the phenomenological consequences that will help us gain insight to the mechanism of spin-polarization observed in heavy-ion collisions.

6.5.4 Studies on Linear and Nonlinear Optical Properties of Subwavelength Structures

Nonlinear Optics (NLO) is a rich subset of nonlinear science that deals with the study of interaction between intense light and matter. Interest in this field has grown continuously since its beginnings due to its wide range of applications in fields of medicine and information technology etc. This thesis is motivated by the necessity to characterize and explore the NLO properties (i.e. nonlinear refraction coefficient n_2 and nonlinear absorption coefficient β) of novel organic materials to access their capabilities towards various NLO applications.

A major fraction of the doctoral work is devoted to the investigation of the of pyrazole and imidazole based organic materials towards realizing species which can have high nonlinear response by working on design strategies. In design strategies, the basic principle adopted is to significantly modify the polarization in the excited state with respect to its ground state. To begin with in all these organic materials, a B←N coordination unit has been introduced to make the molecular geometry planar which could give rise to substantial change in the polarization upon optical excitation and consequently could potentially enhance the NLO response. Specifically, the NLO response of a molecule depends upon its molecular structure which is dictated by its conjugation length and dihedral angle. The work also explores the possibility of controlling as well as spectrally tuning their NLO response. In order to explore the NLO a highly sensitive single beam technique called Z-Scan has been adopted. The study showed that the NLO response of a molecule can be enhanced by increasing the conjugation length and decreasing dihedral angle.
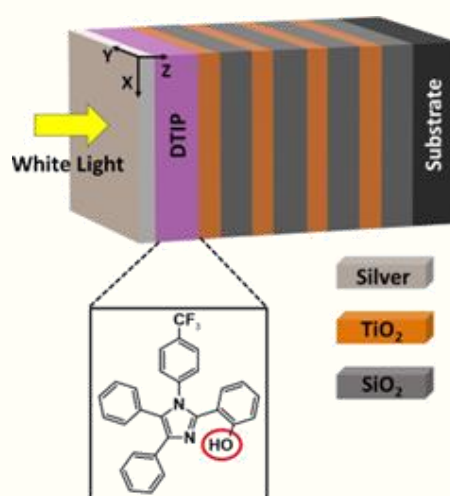
Schematic of the Ag-DTIP-DBR multilayer geometry. DTIP is the organic molecule that exhibits Excited State Intramolecular Proton Transfer process and is fluorescent in nature. This geometry displays three orders of enhancement in nonlinear coefficient values. Inset shows the molecular structure of DTIP molecule

The other part of the thesis explores the properties of optical Tamm Plasmon Polaritons (TPPs) at the interface of metal and Distributed Bragg-Reflector (DBR). In this investigation theorical as well as experimental findings showed that the efficient excitation of TPPs modes is greatly influenced by the thickness of the plasmon active metal film and the constituent and number of DBR layer. However, these TPP modes have a very narrow bandwidth ~ 10 nm, which limits its application in terms of frequency domain. With an intention to excite a broad TPP mode to make it applicable in broad frequency range, a layer of organic material (DTIP) as a buffer layer was introduced in between DBR and metal film. The DTIP molecule is fluorescent in nature which forms a backbone for designing various kind of organic-LEDs and proton transfer-based lasers. The experimental observation of this work revealed the excitation of broadband TPP mode with a spectral width of >50nm. The NLO properties of the geometry (DBR+DTIP+metal) were determined by using Z-scan which contrasted with what was observed for DTIP solution and film. The magnitudes of NLO coefficients in this geometry was at least an order higher. The plausible reason for this enhancement is the local field confinement at the interface of DTIP-DBR geometry.

6.5.5 Spin to Charge Conversion in Heterostructures Comprising Metallic Ferromagnets, Heusler Alloy along with Heavy Metal and Antiferromagnets

Spintronics based devices allow to minimize the size of the device and faster response. The study of spin current efficiency in different materials is one of the emergent research topics in modern days. Spin pumping and inverse spin Hall effect (ISHE) are popular tools to study the spin current efficiency in the materials. Here in this work, spin pumping and ISHE study have been carried out in different ferromagnet (FM)/HS heterostructures where the HS materials are chosen to be a heavy metal (HM) like Pt or antiferromagnetic (AFM) materials like IrMn, NiMn, Co_3O_4 and Mn_3Ga. In the first part of this thesis, spin to charge conversion efficiency was investigated in Heusler alloy/Pt bilayer systems. The ISHE study in such Heusler alloy $Co_2F_{0.4}M_{0.6}Si$/Pt bilayers reveals that it exhibits high spin mixing conductance and spin transparency. Afterwards spin to charge conversion is investigated in CoFeB/ IrMn, NiFe/ Mn_3Ga, Co/ Co_3O_4 and CoFeB/NiMn/Pt systems via angle dependent ISHE and spin pumping.
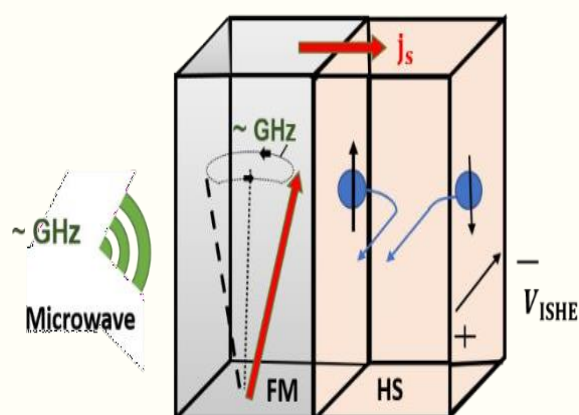
Schematics representation of ISHE mechanism. Under the influenced of microwave field, pumped spin current gets into the adjacent HS and its converted into charge current via SOC of HS.

Prominent spin pumping voltage is observed in all the systems which indicates efficient spin current propagation in the samples. The spin diffusion length of semiconducting AFM Co_3O_4 is found to be ~2.5 nm which is much higher than the spin diffusion length of other AFMs. The manipulation of spin current propagation in Pt/NiMn/CoFeB heterostructures was demonstrated by varying the thickness of low SOC AFM NiMn.

The present study shows that antiferromagnets are a very potential class of materials for spin-to-charge conversion physics and spintronic applications. It is important to choose the right combination of the HS and the FM materials for this kind of applications. The work also shows that Heusler alloys are very promising because they exhibit low damping, and the spin pumping can be efficiently achieved. The future work carried in these directions may hold potential for efficient spintronic applications.

6.5.6 Holomorphic and Numerical Bootstrap Studies of Conformal Field Theory

Conformal field theory is ubiquitous and its applicability is multifarious. In the present work, two techniques have been studied to understand conformal field theories and their applications to physics as well as mathematics. Conformal field theory (CFT) is composed of a quantum field theory with

conformal symmetry (angle preserving symmetry), and it is characterized by "CFT data." The first technique is devoted to classifying conformal field theoriesin two dimensions, in particular, rational conformal field theories (RCFT), using the analysis of the modular invariant linear differential equation (MLDE) satisfied by their characters. In this method, an RCFT is classified by two non negative integers. These two non negative integers have been computed for the well known three classes of RCFTs and anticipated the solutions of the MLDE. Later, third-order MLDEs have been solved explicitly for fully classifying three-character RCFTs and a few potential new three-character RCFTs have been found. The second technique is the numerical conformal bootstrap, by which one can compute CFT data and classify the space of CFTsin various dimensions. Using this method the tricritical Ising model in two dimensions and beyond has been studied and one of the critical exponents to high precision has been computed.

6.5.7   Defect Engineering in ZnO Nanostructures for Optoelectronic Applications

ZnO nanorods are chemically doped with Co to study the influence of point defects on their nonlinear optical properties. The open aperture z-scan traces show that the undoped samples show two-photon absorption (TPA), whereas the Co-doped samples exhibit saturable absorption (SA) characteristics. The DFT calculations confirm that defect bands are created within the bandgap of ZnO by Co doping, and we correlate that such impurity bands can facilitate electronic transitions and enhance the nonlinear optical parameters of the sample.
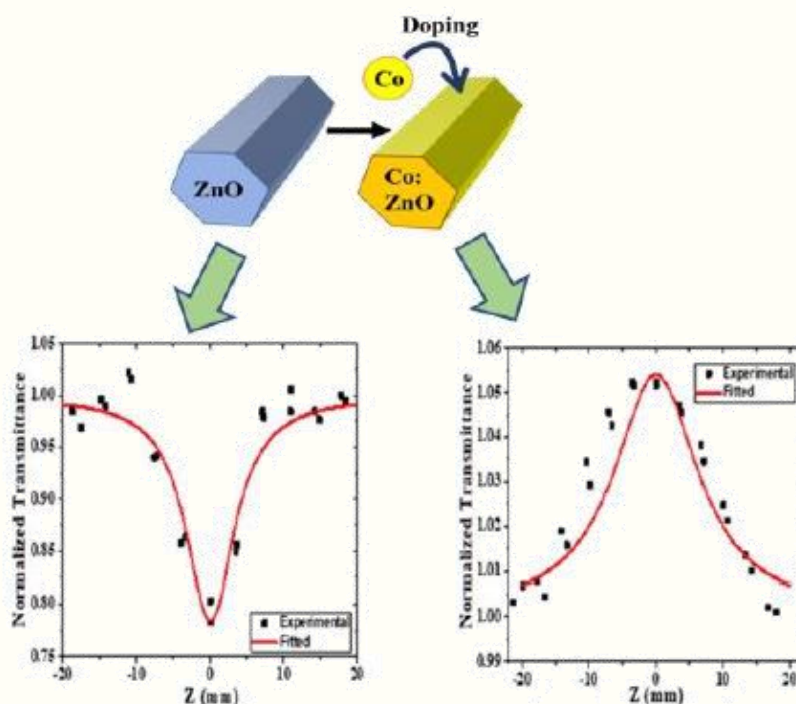
Undoped ZnO showing TPA and Co-doped ZnO showing SA

In ZnO nanorods doped with Eu, we have studied its effect of doping on optical and electrical properties. Eu-doped single ZnO nanorod devices are fabricated to investigate the electrical conductivity of the individual nanorods. The optical bandgap is found to increase initially for low doping concentrations due to the Burstein-Moss effect, and then the bandgap decreases suddenly for higher doping due to bandgap renormalization phenomena. The transport mechanism in the nanorods is found to be thermally activated at high temperatures, and the NNH conduction process becomes dominant at low temperatures.
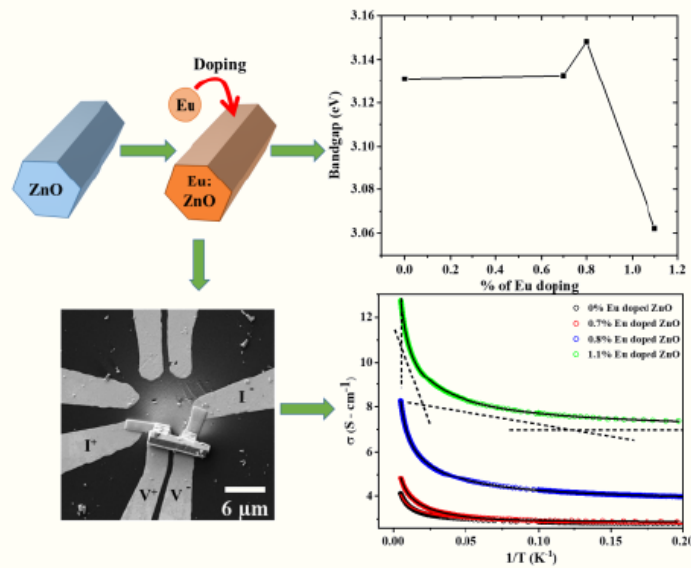
Bandgap and conductivity of undoped and Eu-doped ZnO

Vertically grown ZnO nanorods are irradiated with low-energy inert gas (Xe) ions to introduce point defects in the crystal. Here, we studied the microstructural evolution and optical properties of the nanorods. Bandgap narrowing effect and increase of Urbach energy are observed in the implanted samples because of the creation of a large number of Zn_i and V_O, and our DFT calculations also corroborate well with the experimental results. We show that low energy inert gas ion implantation can modulate the intrinsic defects in ZnO and tune its optoelectronic properties.

On the other hand, extended defects are created in terms of morphological modifications during the growth process of the nanostructures.
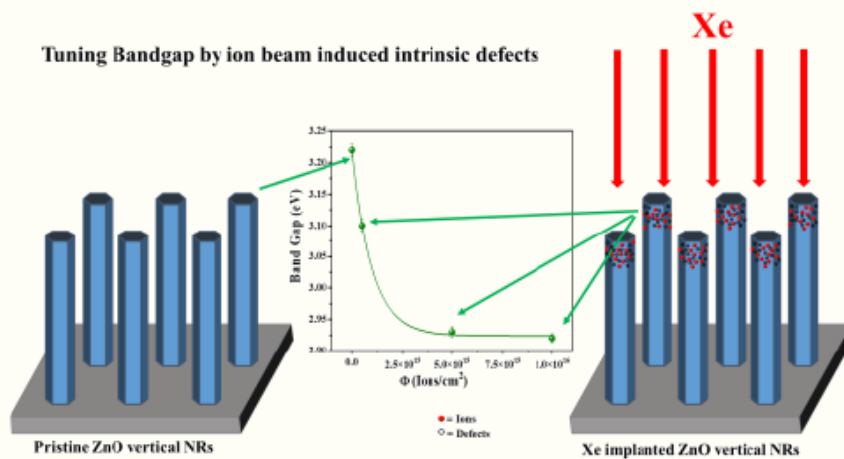
Bandgap tuning by Xe ion irradiation in ZnO nanorods

Layer-by-layer stacked ZnO hexagonal microdisks having various morphological defects are synthesized using a CVD method. The optical emission spectra studied using the temperature-dependent PL technique show the presence of an excitonic surface peak at low temperature, and the PL peaks fit well using the modified Varshini and Bose-Einstein type model. The hexagonal cross-section of the microdisks can support whispering gallery modes (WGM), and we show that they can be modified significantly by various morphological deformations.
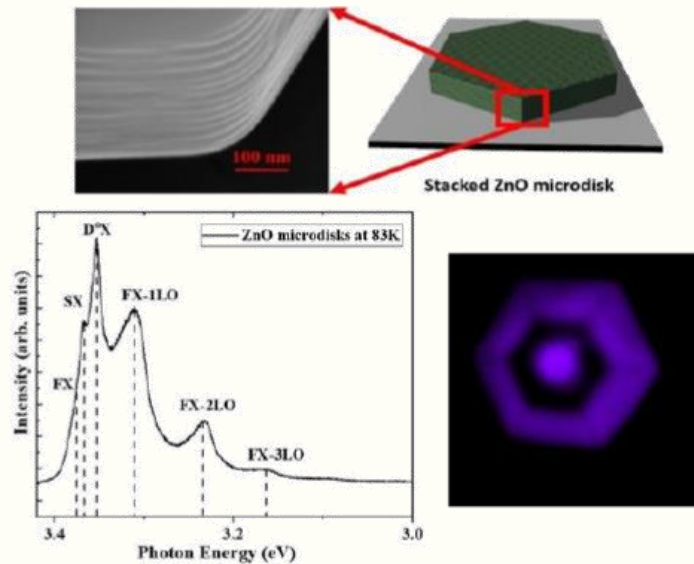
Excitonic peaks and WGM from Zno hexagonal microdisks

6.6   Raja Ramanna Centre for Advanced Technology, Indore

6.6.1   Studies on Ni/AlN and Ru/C Systems for Planar X-ray Waveguide Applications

In the present thesis work, the effect of film composition, interface quality and structural parameters on confinement properties of two different x-ray waveguide (XWG) Ni/AlN and Ru/C systems is investigated. The design parameters of both XWGs are optimized from rigorous electric field intensity (EFI) calculations using recursive formalism at 8.05 keV and 20 keV photon energies, respectively, for resonant beam coupling geometry (schematic (a) shown below). The optimized Ni(9nm)/AlN(11nm)/Ni(20nm) and Ru(7nm)/C(18nm)/Ru(20nm) structures are found to provide EFI enhancement of TE_0 mode by ~30-times at 8.05 keV and ~128 times at 20 keV, respectively (schematic (c) and (d) shown below).
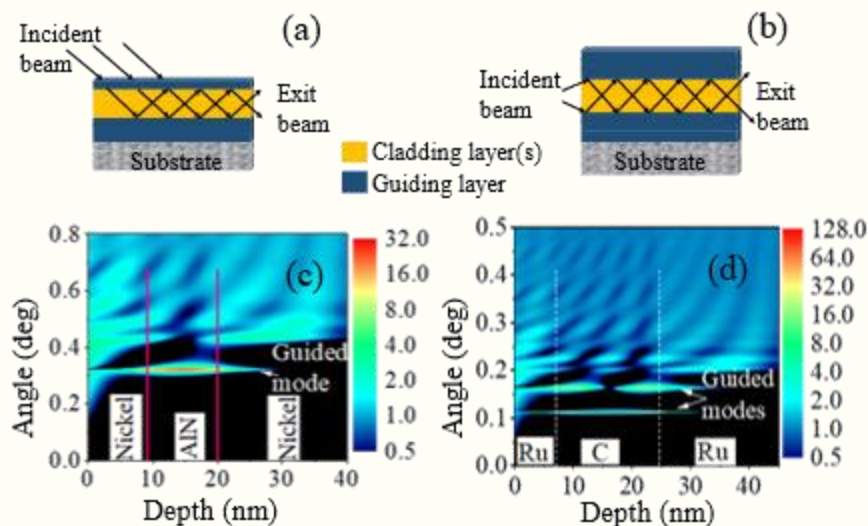
Schematics of a) resonant beam coupling and b) Front coupling geometries to couple incident X-rays with the guiding layers. Contour plots of EFI for optimized c) Ni(9 nm)/AlN(11nm)/ Ni(20nm) XWG at 8.05 keV and, d) Ru(7nm)/C(18nm)/Ru (20 nm) XWG at 20 keV photon energy. The field confinement inside the guiding layer is visible at ~0.32° for Ni/AlN/Ni and at ~ 0.111° and ~0.162° for Ru/C/Ru XWG

For experimental investigations, various thin films (Ni, AlN, Ru & C), bilayers (AlN/Ni & Ni/AlN) and waveguides are deposited using ion beam sputtering technique.

X-ray reflectivity (XRR) characterization of AlN-on-Ni interfaces suggest that an interfacial layer is formed in this case. To investigate the low contrast interfaces in Ni/AlN/Si system, resonant soft x-ray reflectivity (SXR) technique is used. Soft x-ray optical constants of Ni are worked out for SXR analyses where various features corresponding to Ni 2p-3d and satellite transitions are observed. In this case, no interfacial layer is formed, suggesting the interfaces formed by Ni and AlN are asymmetric. Resultantly, EFI inside XWG reduces to ~26 at 8.05 keV from the optimized case (~30). The confinement properties of Ni/AlN/Ni waveguide system are found from the XRR and grazing incidence X-ray fluorescence (GIXRF) tests for as deposited as well as after 15 months of deposition. The structure is found to provide same intensity enhancement (~26) for as deposited and aged sample. From similar investigations on Ru/C/Ru system, it is found that its intensity enhancement for TE_0 mode reduces to ~42 from optimized value of 128 due to experimental variation in design parameters (thickness, roughness, and density) from the optimized ones.

Thus, the present work underlines the importance of investigations of surface/interface properties of potential waveguide system before utilizing them for XWG applications and emphasizes the importance of controlled deposition for fabrication of XWG, especially at higher photon energies.

6.7   Saha Institute of Nuclear Physics, Kolkata

6.7.1   A Study on Some Aspects of Hot and Dense QCD Matter

In the work presented in the thesis, the anisotropic QED and QCD plasma have been studied. The QED plasma can be found in the interior of the neutron stars, magnetars, whereas, the quark-gluon plasma is believed to be produced in the early universe after few micro seconds of big bang. This extreme matter is also produced in the laboratory where two nuclei are collided. Initially after the nuclear impact, very large pressure anisotropy is expected. A highly momentum space anisotropy is expected in this situation which is incorporated by deforming the distribution function. A general structure of gluon self-energy in the presence of two anisotropies has been constructed. An additional unstable mode compared to the single anisotropy case has been found which can have important influences on the isotropization of QGP.

Various aspects of the magnetized plasma produced in the non-central heavy ion collisions have also been explored. The presence of the magnetic field generated in heavy ion collisions introduces an extra scale in the system. One can work in different regimes for theoretical calculations. Immediately after the collisions, the magnetic field strength is very high and one works within the strong field limit (LLL approximation). The field strength decays rapidly with time and in this situation one can use weak field expansion. In the weak magnetic field approximation, a completely analytic expression for the chiral susceptibility is obtained which is an important quantity to study the chiral phase transition. It is found that the chiral susceptibility increases in presence of chemical potential as well as magnetic field. The soft contribution to the damping rate of hard photon has been calculated. In weak field approximation the thermal and thermomagnetic contributions to damping rate get separated out for each transverse dispersive mode. The total damping rate for each dispersive mode in presence of magnetic field is found to be reduced than that of the thermal one. It was shown that the mean free

path of photon is larger than the size of fireball and the photon can be treated as direct probe. The shear viscous coefficients of hadronic matter in presence of temperature and magnetic field within relaxation time approximation have been investigated. It was observed that the transport coefficients are anisotropic. It was also found that the value of viscosity over entropy density is lower in presence of magnetic field than the value of it in thermal medium. An imaginary part of the heavy quark-antiquark potential at finite temperature and magnetic field has been evaluated. All the Landau level summations which can be applicable in the entire magnetic field have been considered. The anisotropic structure of complex heavy quark potential is obtained which explicitly depends on the longitudinal and transverse directions. The dissociation probability has been calculated and the results compared for LLL approximations and all Landau level contributions.

6.7.2   Black Holes, Holography, and Quantum Information

Black holes are one the most mysterious objects in the universe. Classically, they trapped space-time so much that nothing can go out from them. However, quantum considerations near the black hole horizon revealed that a black hole radiates like a black body at a given temperature. This radiation is known as Hawking radiation and seriously obstructs our understanding of fundamental laws in nature. It is called a paradox as the same theory that predicts the radiation is being violated therefore. One way to quantify the paradox is with a measure like the entanglement entropy. The entanglement entropy curve for an evaporating black hole should follow the Page curve: which describes the entanglement entropy of the Hawking radiation over time; an initial rise characterizes the Page curve for evaporation, then a maximum at the so-called Page time, and finally, a fall to zero by the evaporation time. In the present doctoral work, the behaviour of two quantum information-theoretic quantities: entanglement entropy and complexity has been studied within the context of gauge/ gravity duality. Entanglement entropy (EE) is a thoroughly studied quantity that quantifies the entanglement between two sub-systems.

On the other hand, complexity tries to estimate the number of minimal gates required for an initial state to go into a final state by using a set of universal gates. Studying entanglement entropy and complexity has led to many novel insights into quantum gravity within the framework of AdS/CFT correspondence. The thesis primarily focuses on three aspects of these quantities. First, the time dependence of entanglement entropy when a black hole is attached to a non-local & non-unitary bath is studied. Second, the growth of sub-region complexity is explored, or mixes stated complexity associated with an eternal black hole or radiation region within the doubly holographic setup. Finally, the implication of bath deformation on entanglement entropy & mixed state complexity is studied. While coupling a black hole with a non-unitary & non-local bath, it was found that the Page curve knows this non-unitarity and that islands are always present. On the other hand, while studying the mixed state complexity in the doubly holographic framework, an interesting discontinuity of the mixed state complexity associated with the black hole or radiation region at the Page time was discovered. Finally, the deformation of the bath has a significant effect on the Page time, Page curve and mixed state complexity. The Page time displays a monotonic growth with the deformation, which measures the amount of deformation one introduces to the bath. Conversely, mixed state complexity associated with the black hole decreases with the same parameter. In summary, incorporating island regions changes the behaviour of entanglement entropy and mixed state complexity significantly.
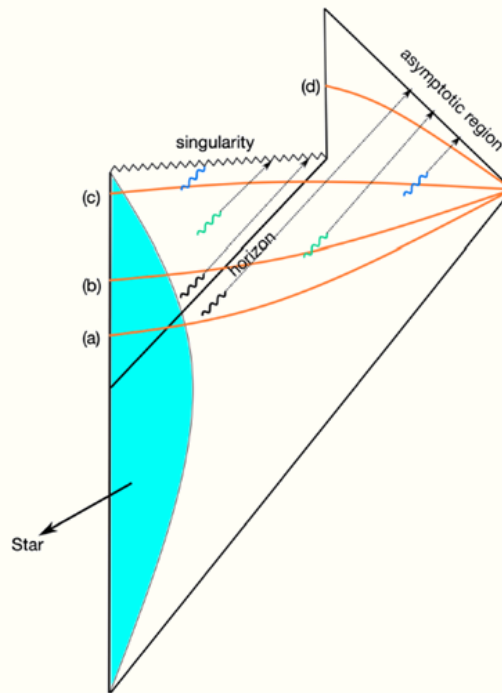
The Penrose diagram for an evaporating black hole in asymptotically flat space-time. All the uni-colour modes are entangled with each other. The interior partner of the entangled couple goes straight into the black hole singularity, whereas the exterior partner escapes to the asymptotic region as Hawking radiation

6.7.3   Explorations in Entanglement and Holography

Entanglement entropy is a quantitative measure of quantum entanglement between two parts of a bipartite quantum state. It happens to be a useful order parameter for the purpose of identifying certain topological phase transitions in many body systems. Unfortunately, though, an exact analytical calculation of entanglement entropy for quantum systems in more than 2 spacetime dimensions is elusive. The AdS/CFT correspondence proves helpful in this regard as it provides a geometrical interpretation on entanglement entropy for quantum field theories with a holographic dual- in terms a minimal area hypersurface in the bulk gravitational spacetime.

  In the present thesis, calculations of entanglement entropy and its cousins in different holographic configurations have been performed. The calculations are done in the limit of very small subregion size where it is possible to extract analytical results in a perturbative way. The spacetime dual to some excited state of the boundary QFT with non-trivial conserved charges has been chosen, and the effect of excitations on the change in entanglement has been studied. One of the principal achievements of the work has been to successfully formulate a 'first law of entanglement thermodynamics' even beyond the leading order correction to entanglement entropy over the ground state of the relevant QFT- by allowing appropriate corrections in the entanglement temperature and chemical potential. The validity of such proposal in both relativistic CFT, and non-relativistic Lifshitz theories has been checked. The nature of some mixed state entanglement measures in an excited state of a Lifshitz quantum field theory has also been observed, and their behaviour compared with relativistic CFTs. It is found that the entanglement wedge cross-section grows differently with increasing excitations compared to the mutual and tripartite information. The holographic entanglement entropy proposal

is also applied to emergent open-string geometries with a horizon induced by an electric field in 3, 4, and 5 spacetime dimensions. Despite such spacetimes not being regular solutions of the gravitational equations of motions, A good qualitative agreement in three and four dimensions with earlier results in usual anti de-Sitter spacetime is found. By taking a high temperature limit in the open string metric, it is found that the holographic entanglement entropy matches with one quarter of the area of the induced horizon; this renders a physical meaning to the area of the induced horizon as well.
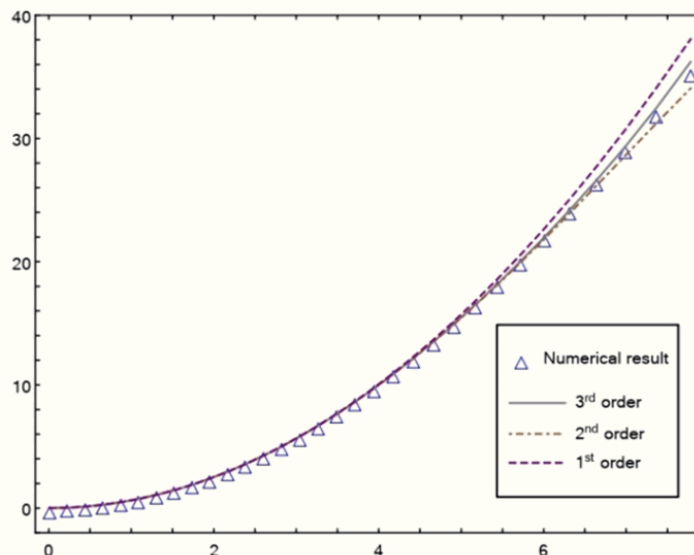
Change of holographic entanglement entropy over empty AdS at different orders in the perturbation series, and comparison with numerical result

6.7.4 Addressing Late Time Cosmic Acceleration and Dark Energy from Theoretical Considerations Along with Observational Predictions and The Impact of Primordial Black Hole Evaporation in Cosmological Observables

The aim of the work carried out in the thesis is to study two phenomena of the evolution of Universe namely, late time acceleration of the Universe or Dark Energy (DE) and impacts of Primordial Black Holes (PBHs) evaporations on cosmic processes relevant in the late time cosmology. Different models of DE from theoretical aspects have been explored along with predictions from current and future experimental data to understand the nature and origin of the late cosmic acceleration and DE. Effects of PBHs evaporations (via Hawking radiations) on cosmological observables are also studied to understand PBH mass distributions as well as their abundances.

The phenomenology of the late time cosmic acceleration is investigated with dynamical DE models like the quintessence model and Slotheon field model (a model inspired from extra-dimensional theory gravity) of DE. Cosmological perturbations are calculated in the framework of these models. The evolutions of the matter density perturbations are obtained and the impacts of inhomogeneities of such DE field on matter power spectrum has been studied. The computed matter power spectrum is then compared with the same obtained for the ΛCDM model and it appears that the results for Slotheon DE model are more akin to that for the ΛCDM than same obtained when the quintessence model is used. Since the ΛCDM does not deal with fluctuations and inhomogeneities in DE, any future experimental detection of such inhomogeneities may create tensions for the ΛCDM model but the Slotheon model could still be a viable model for DE. Moreover, it is explored whether these two

models of DE are consistent with the swampland criteria of string theory. It is found that the Slotheon field model of DE is more in agreement with the swampland criteria than the general quintessence scenario.

In the thesis, the possibility of a coupling between the two dark sector components namely, DE and Dark Matter (DM) is also explored. Interacting Dark Energy (IDE) scenario is considered to address two phenomenological problems, namely, high-f problem of pseudo-Nambu-Goldstone-boson (pNGB) Dark Energy model and excess trough of 21cm signal observed by EDGES experiment. It is found that the presence of non zero coupling between DE and DM can better address the problem for both the DE models (quintessence and Slotheon) and the Slotheon model with such interaction can obviate the high-f problem most efficiently. In addition, the influence of DE-DM interactions on the 21cm signal originated from the neutral hydrogen atom is explored and the excess absorption feature of the signal reported from the EDGES experiment is addressed. It is found that such excess absorption profile can be obtained when DE-DM interactions are considered. Moreover, larger cross section of DM-baryon interaction and larger coupling strength of DE-DM interaction are appeared to be more favourable for achieving the excess absorption feature. In addition, it is found that presence of such interaction raises the possibility of probing larger mass ranges of DM in the context of the EDGES result.

The effects of PBH evaportions on late cosmic processes has also been studied, especially through its influence on cosmological observable like 21cm spectrum. Synchrotron radiation flux is also computed and Inverse Compton (IC) radiation flux originated due to the interaction of electron/positron, produced from the evaporation of PBHs situated at the Galactic Centre (GC) region, with the surrounding medium has been computed. By considering these cosmological probes three mass distributions of PBHs namely, monochromatic mass distribution, power law mass distribution and lognormal mass distribution, which appear in the literature in the context of different formation mechanisms and formation times of PBHs have been examined and constrained.

6.8 The Harish-Chandra Research Institute, Prayagraj

6.8.1 Searching for New Physics via Approaches Beyond the Standard Model

In the present thesis, various new physics contributions have been addressed by going beyond our SM with extended EW sectors. The work also aims to find out their effects in the high luminosity run of the LHC. The major findings of the thesis can be highlited via some points discussed below.

The available data on the 125 GeV scalar h is analyzed to explore the room for new physics in the electroweak symmetry breaking sector. The first part of the study is model-independent, with h couplings to standard model particles scaled by quantities that are taken to be free parameters. At the same time, the additional loop contributions to h → γγ and h →Zγ, mediated by charged scalar contributions in the extended scalar sector, are treated in terms of gauge-invariant effective operators. Having justified this approach for cases where the concerned scalar masses are a little above the Z-boson mass, the existing data is fitted to obtain marginalized 1σ and 2σ regions in the space of the coefficients of such effective operators, where the limit on the h → Zγ branching ratio is used as a constraint. The correlation between, say, the gluon fusion and vector-boson fusion channels, as reflected in a non-diagonal covariance matrix, is considered. After thus obtaining model-independent fits, the allowed values of the coefficients are translated into permissible regions of the parameter spaces of several specific models. In this spirit four different types of two

Higgs doublet models are constrained, and models with one or two Y = 2 scalar triplets, considering the correlatedness of the scale factors in h-interactions and the various couplings of charged Higgs states in each extended scenario.

Though the 125-GeV scalar, as the Higgs boson of the standard model, is disfavoured as a dark matter portal by direct searches and the observations on relic density, a heavier scalar in an extended electroweak sector can fit into that role. This possibility is explored in the context of two Higgs doublet models (2HDM). Taking Type-I and Type-II 2HDM as illustrations, and assuming a scalar gauge singlet dark matter particle, It is shown that the heavy neutral CP-even scalar (H) can (a) serve as a dark matter portal consistently with all data, and (b) have a substantial invisible branching ratio, over a wide region of the parameter space. Using this fact, the rates of LHC signals where H is produced via (i) gluon fusion, in association with a hard jet, and (ii) vector boson fusion have been estimated. Invisible decays of the H can then lead to monojet + missing energy in (i), and two forward jets with large rapidity gap + missing energy in (ii). The second kind of signal usually yields better significance for the high-luminosity run. The cut-based analyses are supplemented with those based on gradient boosted decision trees (XGboost) and artificial neural network (ANN) techniques, where the statistical significance distinctly improves.

Similar kind of study has been done again where a scenario where an SU(2) triplet scalar acts as the portal for a scalar dark matter particle has been considered. The regions of the parameter space have been identified, where such a triplet coexists with the usual Higgs doublet consistently with all theoretical as well as neutrino, accelerator, and dark matter constraints, and the triplet-dominated neutral state has a substantial invisible branching fraction. LHC signals are investigated for such regions, in the signal state same – sign dilepton + ≥ 2 jets + missing energy. While straightforward detectability at the high-luminosity run is predicted for some benchmark points in a cut-based analysis, there are other benchmarks where one has to resort to gradient boosting/neural network techniques to achieve appreciable signal significance.

Further, the high-scale validity of a Type-X two Higgs doublet scenario has been studied which explains the observed value of muon (g − 2). This region allows a pseudoscalar physical state, which is well below the observed 125-GeV scalar in mass. A second neutral scalar particle can be both above and below 125 GeV in such a scenario. Admissible regions in the parameter space are obtained by using the most recent data on muon (g−2), theoretical constraints such as low-scale perturbativity and vacuum stability, and also all experimental constraints, including the available LHC results. Among other things, both the aforesaid orders of CP-even neutral scalar masses are included in our benchmark studies.

Two-loop renormalization group equations are used to predict the values of various couplings at high scales, and the regions in the space spanned by low-scale parameters, which retain perturbative unitarity as well as vacuum stability up to various scales is identified. It is thus concluded that such a scenario, while successfully explaining the observed muon (g − 2), can be valid up to energy scales ranging from 10^4 GeV to the Planck scale, thus opening directions of thought on its ultraviolet completion.

6.9   The Institute of Mathematical Sciences, Chennai

6.9.1   Scattering Amplitudes from Generalized Recursion

Quantum field theory is one of the cornerstones of modern theoretical physics whose most of the physics contents are encoded in Scattering amplitudes. The conventional approach to obtain amplitudes is to write down Lagrangian and derive all the Feynman rules therein. But this field theoretic description for massless particles with spin very quickly leads to huge off-shell redundancies from gauge symmetries and various field redefinitions, appearing in intermediate processes but are absent in observables. However, the modern S-matrix program directly deals with the particles involved in scattering, without any reference to quantum fields and their attendant redundancies. In recent years, the S-matrix program of quantum field theory has witnessed a number of remarkable developments: for example, on-shell techniques like the Britto-Cachazo-Feng-Witten (BCFW)} recursion relations and generalised unitarity have enormously reduced the complexity of seemingly impossible computations which guided the NLO revolution in QCD and have even been used to calculate classical observables such as potential in the Binary black-holes up to high order in Post Newtonian and Post Minkowskian expansion.
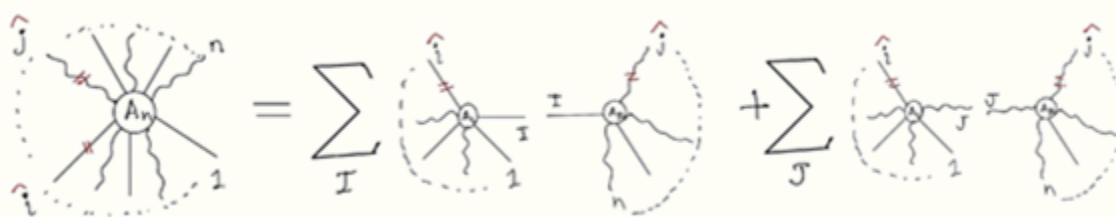
Schematic showing recursion relation for n-particle amplitude with massive (I) and massless (J) shift. The solid and wavy lines denote massive and massless external particles. The sum over I, J denotes all possible channels

In the present work, the spinor-helicity formalism for massive particles developed by Arkani-Hamed et al. is used to study a new class of recursion relations for tree-level amplitudes in gauge theories. Since these recursion relations are based on a combined complex deformation of massless as well as massive external momenta, these are referred as ''Generalized Recursion''. These new recursion relations have been used to study tree-level amplitudes in massive scalar QCD as well as amplitudes involving massive vector bosons in Higgsed Yang-Mills theory. The validity of the recursion relations is proved by showing that in the limit of infinite momenta of two of the external particles, the amplitude is controlled by an enhanced Spin-Lorentz symmetry paralleling the proof of BCFW shift for massless gauge theories.

One of the possibly many advantages of the generalized recursion has also been explored by studying tree-level scattering amplitudes involving a pair of massive vector bosons and an arbitrary number of gluons in the massive spinor-helicity formalism. It is shown that for a specific colour-ordering of the massive particles with respect to the gluons, the generalized recursion relations are more efficient as compared to the BCFW recursion relations. It is also shown that the high energy limit of this particular class of amplitudes reproduces the well-known MHV and NMHV amplitudes in the pure Yang-Mills theory. In this process, a novel representation of the NMHV amplitude has been obtained.

6.9.2 Higher Order Corrections and Resummation in Perturbative QCD

The Quantum Chromodynamics (QCD) radiative corrections to observables at high energy colliders are essential to understand the underlying quantum dynamics of the scattering events. There are many accurate measurements already available from these colliders and they provide ample opportunity to investigate various theories that attempt to describe the physics. Theoretical predictions with unprecedented accuracy have already set stringent constraints on the parameters of the Standard Model (SM), also for many beyond the SM (BSM) scenarios. The foreseen high luminosity and high energy in the future phase of colliders calls for more theoretical efforts to achieve the predictions beyond the present level of accuracy. Through this thesis, an attempt has been made to provide some useful frameworks and results which would pave the way for uplifting the theoretical accuracy of the results associated with observables of some of the important processes at the colliders. In the first of the thesis, the two-loop four-point amplitudes have been presented for the productions of two scalar and two pseudo-scalar Higgs bosons through quark annihilation in Higgs effective field theory. It was found that no contact renormalisation was needed that could arise from short distance behaviour for the quark-initiated channel. Using these results it is possible to make the prediction of an observable for the production of di-Higgs or di-pseudo-Higgs arising from a subdominant channel which is important at this time of very high precision physics. In the second part of the thesis, the problem of threshold enhanced logarithms and the resulting corrections in the context of resummation at soft-virtual plus next-to soft-virtual (SV+NSV) limit has been discussed. The numerical impact of SV+NSV resummed corrections to the Higgs production in the gluon fusion channel as well as to the rapidity distribution of di-lepton pair in the Drell-Yan process for the 13 TeV LHC has been reported. For both the processes, the numerical predictions used on the K factors considering the resummed contributions from NSV terms beyond leading logarithmic approximation imply better perturbative convergence compared to fixed order or SV resummed contributions. In addition, the dependence on the renormalisation scale gets reduced upon the inclusion of NSV resummed making the prediction more reliable. Howeverit was found that the sensitivity to factorisation scale increases in the presence of resummed NSV terms implying the importance of beyond NSV terms (NSV terms form off-diagonal channles) for the case of Higgs production (for the case of the Drell-Yan process) within the resummed framework.
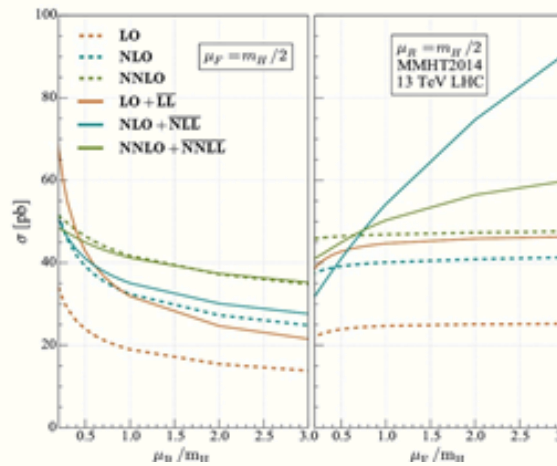
Schematic showing scale variation of the resumed results against the fixed order w.r.t. the renormalization and factorization scales for the Higgs production

6.9.3 Aspects of Compatibility of quantum Devices and Quantum Communication using Quantum Switch

Incompatibility of quantum devices is one of the fundamental features of quantum mechanics that makes it distinct from classical physics. A set of quantum devices is said to be compatible if those devices can be implemented simultaneously on a quantum system. Otherwise, the set is incompatible. These quantum devices can be measurements, channels, instruments, etc. Incompatibility of quantum devices is not only important from the foundational perspective, but also important for its applications in different information-theoretic tasks. In the major part of the present work, several aspects of incompatibility of quantum devices have been studied. More specifically, (1) the conceptual problems in an existing definition of compatibility of quantum instruments (called as traditional compatibility) has been discussed and it has been shown that another definition of compatibility of quantum instruments (called as parallel compatibility) does not have such drawbacks, (2) the compatibility of quantum instruments has been further characterized and quantified, (3) the properties of layers of classicality in the compatibility of measurements has been studied, (4) the information loss due to quantum measurements has been studied and this study is based on the notion of measurement-channel compatibility.
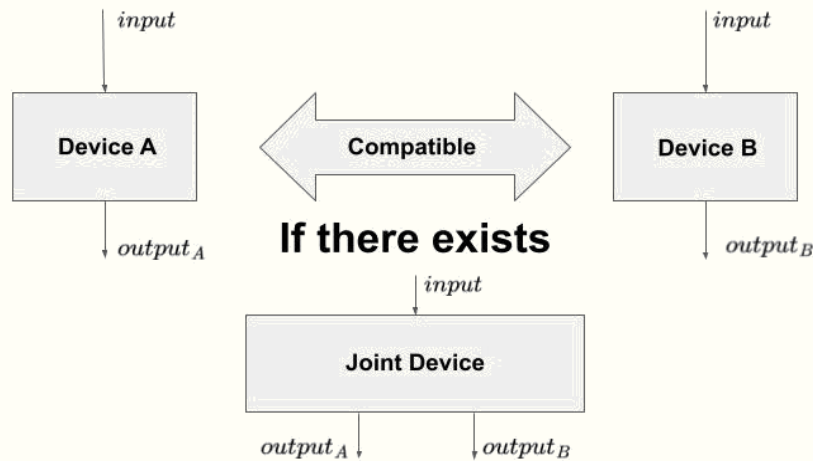
Schematic diagram of incompatibility of quantum devices

Quantum switch, in the simplest scenario, is a circuit that implements indefinite causal order between two quantum channels with the help of a qubit ancilla (that is known as the control qubit) prepared in a superposed state. Quantum switch has several applications in different information-theoretic, thermodynamic tasks. In a part of this thesis, the improvement in quantum communication using quantum switch has been studied. For example, it has been shown that that some useless (for communication) channels may provide useful communication under the action of quantum switch for several information-theoretic tasks: quantum random access codes, quantum steering, etc. It has been demonstrated that the quantum switch can also be useful in preventing the loss of coherence in a system when only coherence-breaking channels are the available for communication. It has been shown that if a useless quantum channel does not provide useful communication even with the help of a quantum switch, concatenating the channel with another suitable quantum channel, and subsequently using the switch, one may achieve useful communication. It is hoped that the results obtained will be useful for future quantum communication technology.
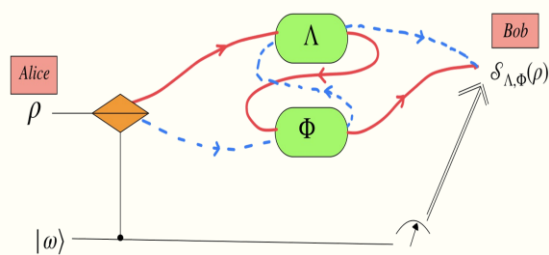
Schematic diagram of quantum switch. Here, the state of the control qubit is |ω⟩,
Λ and Φ are the quantum channels and ρ is the state of the system.

6.9.4   Thermo-mechanical Response of Glassy Systems

Glassy materials are everywhere in our day-to-day life in the form of various applications, especially in the form of different speciality glasses. To develop various new applications and to improve the existing ones, a detailed theoretical understanding of thermal and mechanical properties of these materials in diverse conditions is needed, and this has been an active area of research for several decades. In particular, the focus has been on developing the microscopic perspective of different macroscopic properties, where computer simulations have been an important technique.
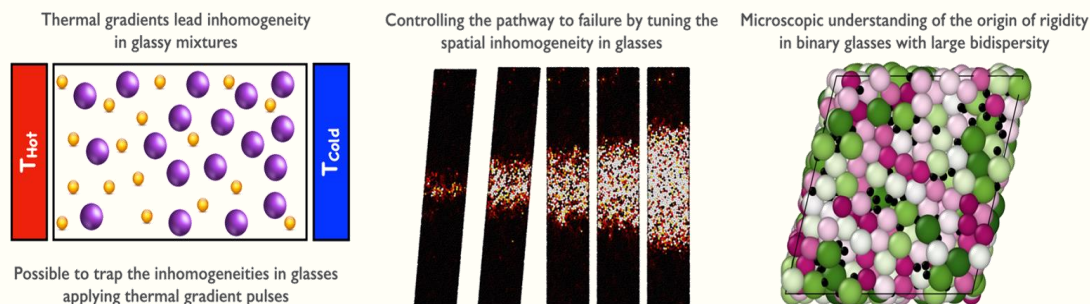
Microscopic understanding of the response of glossy systems to thermal
gradient and mechanical deformation

In the present thesis, a very extensive numerical study is presented to understand the thermal and mechanical response of model glassy systems to external perturbations in the form of a temperature gradient and shear respectively. First, it is characterized in detail how a thermal gradient generates spatial concentration inhomogeneity in glassy liquids by studying the coupling of heat and mass transport. Further, a thought experiment is explored using thermal gradient pulses to illustrate formation of long-lived inhomogeneous glassy states at temperatures below the glass transition temperature. The microscopic failure mechanism of these inhomogeneous samples is subsequently determined from the detailed analysis of shear band formation, which reveals a controlled pathway to failure via the designed inhomogeneity. Next, the focus of the study is on Poiseuille flow of a confined soft glass, under two different thermalization protocols, resulting in the presence or absence of thermal gradient across the channel, which affects the local rheology of the confined glass differently, indicating the possibility of tuning the flow. Finally, for a binary mixture with large size bidispersity among the particles, which display large separation in structural relaxation timescale of large and small species, the interdiffusive properties are shown to result in finite-size effects in single particle dynamical quantities. Further, the shear response of the same binary reveals that rigidity sets in even when the small particles are mobile; but these particles affect the hardness of the material. The present study focused on different thermal and mechanical responses contributes significantly to improved understanding of glassy systems.

6.10   Variable Energy Cyclotron Centre, Kolkata

6.10.1 Hydrodynamic Modeling of QCD Fluid with Critical Point in the Equation of State

Quark-Gluon plasma (QGP), a deconfined (or weakly interacting) state of quarks and gluons, is one of the phases of the strongly interacting matter that exists under extreme conditions of temperature and/or density. A locally equilibrated QGP is formed in ultra-relativistic heavy-ion collisions, the space-time evolution of which is governed by the equations of relativistic hydrodynamics. The highly nonlinear nature of the equations renders it difficult to solve them analytically. In the absence of any first principle calculations, a model for initial condition is required to solve the equations. The equations also need a model for the equation of state (EoS) at arbitrary baryon chemical potential (μ_B), as first principle lattice quantum chromodyn   amics (QCD) can only provide reliable results for the EoS at μ_B close to zero. This thesis is devoted to developing a state-of-the-art numerical simulation code for heavy-ion collisions that includes developing a (3+1)-dimensional causal relativistic viscous hydrodynamics in addition to making improvements to the already existing models in the literature.

A model for the EoS with critical point (CP) as incorporated into the hydrodynamic code along with the scaling behavior of transport coefficients (shear and bulk viscosity) which are expected to diverge as powers of correlation length near a CP. If we are not too close to the CP then the back reaction of critical fluctuations on bulk hydrodynamic variables can be neglected, and the formalism developed in this study can be used to study signatures in order to pinpoint the location of CP in the QCD phase diagram. Along this direction, the effect of CP on the thermal vorticity using the developed framework has been studied. It was found that the absolute value of thermal vorticity gets suppressed as the critical point is approached. As thermal vorticity can be related to the polarization of spin-1/2 particles, It is argued that polarization of Λ- hyperons can be used as an indicator for the QCD critical point. In the dissertation, the movements in the Glauber model are also made by proposing a modified mechanism for energy deposition. the chemical relaxation time of a meson gas has been computed and it is argued that the hadronic phase obtained as a result of phase transition from the expanding QGP must freeze out chemically at the chiral crossover temperature. This is an entirely different viewpoint towards looking at the chemical freeze out.
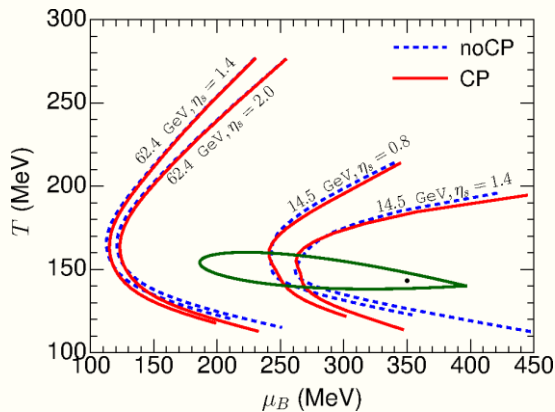
Trajectories traced by fluid cells at x=y=0 and with different space-time rapidities are shown for two colliding energies with and without the critical point. The collision is between Au+Au at an impact parameter, b=5 fm. The critical point is shown by the black dot and the green line marks the boundary of the critical region

6.10.2 Clustering in Light Nuclei

A nucleus is composed of nucleons. However, the spatial rearrangement due to correlation among nucleons gives rise to different clusters. The most prevalent cluster in nuclei is in the form of ^{4}He (α particle) due to its high stability and excessive inertness. The α-clustering phenomenon has been a topic of contemporary research since the emergence of heavy ions.

Here, the α-clustering property in nuclei have been studied in the light mass region (A < 50) at beam energies $\approx$ 15 MeV/A. The effect of clustering in nuclei has been explored through indirect (Dissipative nuclear reactions) and direct (Resonance particle decay spectroscopy) ways.

The indirect way includes two experiments on complex fragment emission from energy equilibrated composites and measurement of the cross sections of the emitted fragments. The deviation of cross sections from the standard statistical model calculations reveals the influence of the cluster structure of nuclei on the reaction mechanism. In the 1st experiment, cluster correlation has been observed in the dissipative binary decay of ^{24,25}Mg at excitation energy of $\approx$54 MeV. In the 2nd experiment, suppression of complete fusion has been observed when weakly bound clustered nucleus ^{9}Be is present in the entrance channel.

The direct probing of resonant cluster states includes experiments on two self-conjugate nuclei ^{12}C and ^{16}O. The decay particles (α's) from the excited nuclei have been detected and reconstructed kinematically to decipher the cluster states of these nuclei. In the 3rd experiment, the decay mechanism of the Hoyle state of ^{12}C (3α clustered state) has been investigated and upper limit of decay components have been quantified with high precision. In the 4th experiment, the 4α clustered state in ^{16}O (Hoyle analogue state) has been investigated. The experimental findings neither support nor reject the theoretically predicted 15.1 MeV state as the Hoyle analogue state in ^{16}O. However, this study being 1st complete kinematical experiment, points to the further improvements required to efficiently probe this state in future.
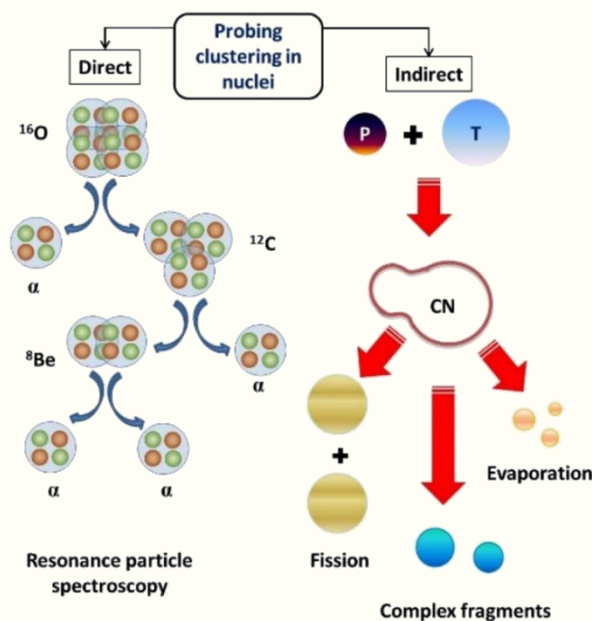
Schematic diagram showing mechanisms adopted for probing clustering in nuclei

Section III
List of students who have completed
Ph.D. during the period August 1, 2022-July 31, 2023

Discipline: Applied Systems Analysis

S. No	Name of the Student	CI	Enrollment No	Title of the Thesis
1	Mehboobun Nahar Milky	NISER	APSA11201704003	Disrupted Lives: A Qualitative Study of Experiences of Living with Cancer Patients and their Family Caregivers

Discipline: Chemical Sciences

S. No	Name of the Student	CI	Enrollment No	Title of the Thesis
1	Aswani Kumar	BARC	CHEM01201304006	Probing the Effect of Radiation on local Structure in Waste Immobilization Matrices.
2	Rashmi Joshi	BARC	CHEM01201604007	Synthesis, Characterization and Cancer Therapy Evaluation of Fe_3O_4 and Upconversion Based Nanostructured Materials
3	Meghnath Sen	BARC	CHEM01201704004	Synthesis and Characterization of Inorganic Materials for Potential Applications in Neutron Dosimetry
4	Nishith Ghosh	BARC	CHEM01201704007	Interface-Selective Vibrational Spectroscopic Study of Aqueous Interfaces: Application to Atmospheric and Biological Systems
5	Pranav Utpalla	BARC	CHEM01201704012	Investigation of the Molecular Packing in Polymer Nanocomposites and its Role on the Bulk Physical Properties
6	Saikrishna D.	BARC	CHEM01201804007	Development of Analytical Methods for the Determination of Beryllium for Application in Environmental Monitoring
7	Bommadeni Arun	IGCAR	CHEM02201504002	Optimization of Sampling and Measurement Techniques for Tritium and Carbon-14 in the Atmosphere
8	Shirley Auxilia L.	IGCAR	CHEM02201504011	Synthesis, Characterization and Leaching Studies of $Ca_{10}(PO_4)6X_2$, (X= OH, F) and Its Simulated Radionuclide (Re, Cs, Nd, Sr) Substituted Analogues for the Immobilization of Radioactive Waste.
9	Vijayalakshmi T	IGCAR	CHEM02201504012	Synthesis, Characterisation and Evaluation of Crosslinked Poly(ionic liquid)s as Sorbents for Antimony, Chromium and Iodine
10	Murukutti Mahima Kumar	IGCAR	CHEM02201604001	Synthesis and Characterization of Nano-Crystalline Zeolites using Kaolin and Fly Ash for Nuclear Waste Immobilization

11	Rasitha T P	IGCAR	CHEM02201604002	Fabrication of Superhydrophobic Coatings on Cr-Mo Steel, Titanium and Aluminum: Corrosion, Biofouling and Durability Studies
12	Litun Swain	IGCAR	CHEM02201604010	Chemical and Electrochemical Characterization of LiCl-KCl Eutectic and LiCl-UCl$_3$ Melts Containing Moisture as ImputityIn LiCl-KCl Eutectic With Applications To Processioning
13	Jegan G	IGCAR	CHEM02201604011	Synthesis and Evaluation of Hexaalkyl Phosphoramides as Extractants for Actinide Extraction and Applications
14	Ujjwal Kumar Maity	IGCAR	CHEM02201704005	Development of Novel Analytical Methods for Determination of Atom Percent Fission, Spatial Profiling and Plenum Gases
15	Manish Chand	IGCAR	CHEM02201804016	Studies on Nuclear Activation Techniques for the Elemental Characterization of Environmental and Nuclear Materials
16	Arpita Chatterjee	NISER	CHEM11201604001	Studies of N-Arylation, Ring-opening and Dearomatization of 5-Aminopyrazoles
17	Nabin Sarkar	NISER	CHEM11201604005	Conjugated Bis-Guanidinate (CBG) Stabilized Aluminum Complexes: Synthesis and their Catalytic Applications
18	Somnath Banerjee	NISER	CHEM11201604012	Photophysical Studies on Some Organic Aggregates and Inorganic-Organic Hybrid Nanomaterials
19	Bedadyuti Vedvyas Pati	NISER	CHEM11201604015	Synthesis of Isocoumarins, 1,6-Diketones, and 1,3-Enynes via Rhodium and Palladium-Catalyzed C–H/C–C Bond Activation
20	Gopal Krushna Das Adhikari	NISER	CHEM11201604017	Synthesis of Hexahydrobenzo-[c]phenanthridine and β-Carboline-1-one Derivatives via Transition Metal Catalyzed C-H Bond Activation
21	Kasturi Sahu	NISER	CHEM11201604018	Synthesis, Characterization, and Applications of Free-base and Metal Complexes of β-Thiocyanatocorroles
22	Priyabrata Biswal	NISER	CHEM11201604022	Activation of Methanol as a C1 Source Using Pd, Ru and Co-compounds to Make New C-C Bonds
23	Rajat Kumar Tripathy	NISER	CHEM11201604023	Metal-Organic Frameworks (MOFs) and their Derived Materials as Electrocatalyst for Energy Conversion and Storage Application
24	Shalini Pandey	NISER	CHEM11201604027	Enhancement of diaCEST MRI Contrast Efficiency: Hydrogen Bonding and Carbon Dots

25	Smruti Rajan Mohanty	NISER	CHEM11201604028	Transition Metal Catalyzed Alkenylation and Alkylation of Inert C-H Bonds
26	Sruti Mondal	NISER	CHEM11201604029	Synthesis and Spectroscopic Characterization of Metallocorroles and Porphyrins and their Applications
27	Subrakant Jena	NISER	CHEM11201604030	Ground and Excited-state Dynamics of Sulfur and Selenium Containing Molecules of Biological Significance
28	Biplab K. Pandia	NISER	CHEM11201604032	Manganese Pincer Catalyzed Organic Transformations
29	Juhi Dutta	NISER	CHEM11201704001	Noncovalent Interactions with Carbon in Small Molecules and Proteins: Theoretical Predictions and Experimental Challenges
30	Krishna Mishra	NISER	CHEM11201704002	Studies of Photophysical Processes in Semiconductor Materials and their Applications
31	Prakash Nayak	NISER	CHEM11201704004	Tetra-coordinated Boron Functionalized Phenanthroimidazole and Pyrazole based Fluorophores: Synthesis, Characterization, Photocatalytic and Sensing Applications
32	Shubhranshu Shekhar Choudhury	NISER	CHEM11201704007	On/In Water Catalysis with Cholinium Hydroxide: The Combined Experimental and Computational Studies
33	Manjari Chakraborty	NISER	CHEM11201704008	Assessing the Behaviour of Some Monocationic, Dicationic and Binary Mixtures of Monocationic Ionic Liquids through Spectroscopic Investigations
34	Deepak Kumar Panda	NISER	CHEM11201704012	Computational Studies of Deep Eutectic Solvents
35	Malaya Kumar Sahoo	NISER	CHEM11201704018	Inorganic-Organic Hybrid Frameworks & their Derived Materials towards Clean Energy Applications
36	Ranjit Mishra	NISER	CHEM11201704024	Design of Inorganic-Carbon Composites, Porous Carbons for Sustainable Environmental and Electrochemical Energy Storage/Conversion Applications
37	Shyamal Kanti Bera	NISER	CHEM11201704025	Metal-free Approaches towards the Construction of Heterocycles
38	Sudip Sau	NISER	CHEM11201704027	Sustainable Approaches towards C-X (-N, -C, -O) Bond Formation Reactions in Organic Synthesis
39	Komal Yadav	NISER	CHEM11201704028	Computational Studies of the Mechanisms and Dynamics of Chemical Reactions
40	Naupada Preeyanka	NISER	CHEM11201704029	Synthesis, Characterization, and Photophysical Studies on Some Inorganic,

S. No	Name of the Student	CI	Enrollment No	Title of the Thesis
				Organic, and Inorganic-Organic Hybrid Nanomaterials
41	Tanmayee Nanda	NISER	CHEM11201704031	Transition-Metal Catalyzed C-C Bond Activation of Cyclopropenones and C-H Bond Activation of Phenoxyacetamides
42	Shyam Kumar Banjare	NISER	CHEM11201804007	Weak Chelation Assisted C-H Bond Activation via Cobaltacycles: A Sustainable Approach towards the Synthesis and Functionalization of *N*-Heterocycles

Discipline: Engineering Sciences

S. No	Name of the Student	CI	Enrollment No	Title of the Thesis
1	Arvind Kumar Bind	BARC	ENGG01201304020	Mechanistic Approach to Understand the Hydride embrittlement of Zr-2.5Nb Alloy
2	Shyam Rao Ghodke	BARC	ENGG01201304026	Assessment of Change in Mechanical Properties of OFE Copper and Titanium Grade-2 Materials used in Linear Accelerator and Fusion Reactor using SPT Specimens
3	Mousumi Singha	BARC	ENGG01201304033	Studies on Recovery of Metal Ions from Low Level Effluent using Complexation-Filtration-Extraction Hybrid Technique
4	M. K. Pradhan	BARC	ENGG01201304042	Study on Response of Group of Piles in Cohesionless Soil under Dynamic Loads
5	Soumya Prakash Nayak	BARC	ENGG01201304045	Investigation on Electrically Exploded Conductor Based Inductive Energy Storage System for Pulse Sharpening Applications
6	Bathe Bhagwan Narayan	BARC	ENGG01201304048	Analysis of State of the Art Stream Ciphers
7	Ravindra Kumar Sharma	BARC	ENGG01201404008	Design and Parametric Studies of Plasma Focus Device & its Pulsed Power Components
8	Suman Paik	BARC	ENGG01201404025	Deformation and Fracture Behaviour of FCC-based Single Crystals: Experimental and Numerical Studies
9	Srijit Bandyopadhyay	BARC	ENGG01201504019	Reliability based Approach for Evaluating the Response of Structures Considering Soil Structure Interaction
10	Amit Kumar Mishra	BARC	ENGG01201504032	Adaptive Filtering for State Estimation of Nuclear Reactor Systems
11	Soumyadip Uday Sankar Mondal	BARC	ENGG01201518001	Development of Hydrometallurgical Unit Operations for the Recovery of Cobalt, Rare Earths and Uranium from Secondary Resources

12	Sourav Mukhopadhyay	BARC	ENGG01201604008	Design and Characterization of Silicon Pixel Detector and its Readout Electronics for High Energy Physics Experiments
13	Neelima Khare	BARC	ENGG01201604010	Tribocorrosion Studies on Heat Treated 13Cr Martensitic Stainless Steel Sliding under Dry, Noncorrosive and Corrosive Mediums
14	Anupreethi B	BARC	ENGG01201604016	Optimization of In-core Detector Locations for Neutron Flux Mapping in Advanced Heavy Water Reactor
15	Annesha Das	BARC	ENGG01201604017	A Study on the Effect of Surface Finishing Operations on the Electrochemical Nature of Oxide Film Formed on 304L SS in Aqueous Environments
16	Menka Sukhwani	BARC	ENGG01201618003	Study and Design of ASIC Based Frontend Readout Electronics Topologies for High Energy Physics Experiments
17	Sai Karthik Nouduru	BARC	ENGG01201804016	Nodular Corrosion of Zr-2.5Nb Alloy in Gas Phase - Role of Contaminants and Initial oxide
18	Prafful Kumar Sinha	BARC	ENGG01201804018	Oxidation and Electrochemical Behaviour of an Alpha-phase Titanium Alloy in Different Environments
19	Ragavendran M	IGCAR	ENGG02201405015	Effects of Arc, Laser, and Hybrid Laser-Arc Welding Processes on the Weld Attributes of Type 316LN Stainless Steel Weld Joints
20	A Saikumaran	IGCAR	ENGG02201405017	Study of Microstructural Evolution in Multi-component $CrFeMoVNb_x$ (x=0,1) Alloys and Correlation with Mechanical Properties
21	Suresh Kumar Telagathoti	IGCAR	ENGG02201405018	Thermomechanical Fatigue Evaluation of Type 316LN Austenitic Stainless Steel Weld Joints
22	Pathan Fayaz Khan	IGCAR	ENGG02201504001	Design and Development of Heart Rate Variability Biofeedback System for Magnetoencephalography and Electroencephalography Studies
23	Mahesh Kumar Patankar	IGCAR	ENGG02201504005	Design and Development of High Temperature Radiation Tolerant SiC MEMS Pressure Sensor for Fast Reactor Applications
24	Praveen C	IGCAR	ENGG02201505003	Influence of Nitrogen on Tensile and Creep Deformation Behaviour of Type 316L Stainless Steel in the Framework of Internal-State-Variable Approach

25	Pavan A R	IGCAR	ENGG02201505011	Study of the Effect of Advanced Welding Processes on the Microstructure, Mechanical Properties and Residual Stresses of Thick type 316L(N) Stainless Steel Weld Joints
26	Madhura B	IGCAR	ENGG02201505013	Development of Interlayer Coatings on High Density Graphite for Yttria Coating for Pyrochemical Reprocessing Application
27	Sumana	IGCAR	ENGG02201505014	Total Focusing Method (TFM) Based Phased Array Ultrasonic Techniques for Inspection of Thick and Attenuating Components
28	Prashant Sharma	IGCAR	ENGG02201604009	Design, Modeling and Performance Evaluation of Annular Linear Induction Pumps under Variable Voltage Variable Frequency Supply Conditions
29	Y V Harinath	IGCAR	ENGG02201604011	Degradation Studies on Incoloy-800HT and Nickel Coated SS 316L in Static Molten FLiNaK Salt
30	Manu Harilal	IGCAR	ENGG02201604018	Development of Fly Ash Based High Performance Concrete Blended with Nanoparticles and Inhibitor for Marine Applications
31	Rajesh Patel	IGCAR	ENGG02201704009	Advanced Signal Processing Techniques to Analyze the Human Brain and Heart Activities Recorded during Cognitive Workload Task
32	Chinmoy Mallick	IPR	ENGG06201504003	Studies of Cavity Modes on Plasma and its Influence on Ion Beam in a Microwave Ion Source
33	Vivek Mahendrakumar Pachchigar	IPR	ENGG06201704002	Superhydrophobic Surfaces Developed through Argon Plasma Processing for Self-cleaning and Water Harvesting Technologies
34	Vikas Rathore	IPR	ENGG06201804005	Study of Plasma Activation of Water and its Applications in Anti-microbial and Agricultural Activities
35	Vikas Singhal	VECC	ENGG04201404002	Development and Implementation of First Level Event Selection Process on Heterogeneous Systems for High Energy Heavy Ion Collision Experiments

Discipline: Life Sciences

S. No	Name of the Student	CI	Enrollment No	Title of the Thesis
1	Rajesh K. Chaurasia	BARC	LIFE01201504008	Retrospective, Cumulative and Rapid Biodosimetry - An Approach by Molecular Cytogenetics
2	Pooja Patheja	BARC	LIFE01201504016	Studies on Macrophage Conditioned Medium Induced Tunneling Nanotubes and Microplasts Formation in Human Breast Cancer Cells
3	Prakash Kalwani	BARC	LIFE01201604002	Establishment of CRISPR-based Gene Modulation in Anabaena and Characterization of the Putative CRISPR-associated Protein, Alr1562
4	Kavitha Premkumar	BARC	LIFE01201604004	Studies on Tumor Microenvironment Induced Changes in T Cell Differentiation
5	Devavrat Tripathi	BARC	LIFE01201604012	To Study the Effect of Polyphenols on the Invasion and Differentiation of Thyroid Cancer Cell Line
6	Reema Devi Rajan Singh	BARC	LIFE01201604013	Radiation as a Stressor for Lipid Accumulation in *Chlorella sorokiniana* (KMN3) and its Mechanism of Action
7	Gargi Bindal	BARC	LIFE01201604014	A Comparative Study of Type I and Type II CRISPR-Cas Systems for their Applications in Modulation of Gene Expression using RacR as Model
8	Jyotsna Bhatt	BARC	LIFE01201604015	Mechanistic Studies on Ubiquicidin-Membrane Interaction & Development of Infection Imaging Probes
9	Vinayaki Seikilar Pillai	BARC	LIFE01201604016	Exploring the Relevance of Clinical Variants of Human Translin and Identification of Inhibitors of Translin-DNA Interaction
10	Jasraj Vaishnav	BARC	LIFE01201704002	Radiation Processing for Development of Minimally Processed Ready-to-Cook (RTC) Cauliflower and its Impact on Flavor Quality
11	Hiral Uday Mistry	BARC	LIFE01201704007	Structure-Function Studies of Component Proteins of Transcription-Coupled Nucleotide Excision Repair (TC-NER) Complex
12	Ria Ghosh	IMSc	LIFE10201404001	Emergent Patterns of Activity in Disordered Biological Systems: Role of Heterogeneities in Organizing the Collective Dynamics of Excitable Cell-Assemblies and Tissues

13	Vivek Ananth R P	IMSc	LIFE10201604001	Compilation, Curation and Exploration of Natural Product Spaces to Enable Traditional Knowledge Based Drug Discovery
14	Vadnala Rakesh Netha	IMSc	LIFE10201604002	Investigating how Chromatin Regulates Gene Expression and Cellular Processes
15	Durga Prasad Biswal	NISER	LIFE11201404003	Light and Phytohormone Interaction in the Development of *Physcomitrella patens*
16	Shashank Patole	NISER	LIFE11201404009	Study on Persister Cell Formation in a Clinical Isolate of *Klebsiella pneumoniae*
17	Anamika Singh	NISER	LIFE11201504001	Role of GIGANTEA on the Developmental Regulation of *Arabidopsis thaliana*
18	Anup Kumar Ram	NISER	LIFE11201504002	Molecular Characterization of Non-AUG Codon Recognition in the Translation Initiation Fidelity Defective Mutant on the Regulation of Differential Protein Expression
19	Maynak Chakraborty	NISER	LIFE11201504007	Genetic Variants of *LAMC1*, *ATP1B1* as Risk Factors and Transcriptional Regulation of *CASP8AP2* in the Pathophysiology of Fuchs Endothelial Corneal Dystrophy
20	Tusar Kanta Acharya	NISER	LIFE11201704006	Elucidating the Involvement of Thermosensitive Ion Channels (TRPV4 and TRPM8) in Mitochondrial Structure-Function Relationship: Significance in Physiology and Diseases
21	Rajdeep Das	SINP	LIFE05201504011	MFN2 Mediated Regulation of Mitochondrial Dynamics and MAM Junctions
22	Rajkamal Srivastava	SINP	LIFE05201604008	Synthetic Genetic Reversible Logic Gates in *E. Coli* and its Application in Logical Information Transfer to Mammalian Cell
23	Subhoja Chakraborty	SINP	LIFE05201604009	To Design and Generate Specific Protein Inhibitors against Falcipain 2 from *Plasmodium falciparum*, a Drug Target for the Malarial Parasite
24	Debolina Bandyopadhyay	SINP	LIFE05201704003	Single Molecule Visualization of Rearrangement of Polypurine Reverse-Hoogsteen Hairpin and Fork-DNA during their Modification for Gene Regulation
25	Debayan Purkait	SINP	LIFE05201704007	Investigation of Nucleo-Protein Interactions in Prokaryotic DNA Repair and Genome Architecture using Single-Molecule Spectroscopy

26	Sheikh Burhan Ud Din Farooqee	TMC	LIFE09201304011	Functional Relevance of Protein-Protein Interactions- Case Study with Proteasomal Chaperones
27	Mukund Sudharsan M G	TMC	LIFE09201404003	Structure of Gankyrin Interaction Network and their Role in Oncogenesis
28	Desai Sanket Shashikant	TMC	LIFE09201504001	Genomic Approaches to Identify Novel Endogenous and Exogenous Genetic Elements Associated with Human Cancer
29	Naini Shibojyoti Chakraborty	TMC	LIFE09201504004	Study of Organelle Dynamics, Relative Organelle Positioning, and Inter-organelle Contact Sites
30	Parui Aasna Lakhikant	TMC	LIFE09201504005	Allosteric Regulation of Serine Protease HtrA2
31	Joshi Asim Sandeep	TMC	LIFE09201504015	Understanding the Complexities of Human Lung Cancer Genome
32	Mudassar Ali Khan	TMC	LIFE09201604012	Structural Evaluation of Germline Missense Mutations Causing Hereditary Breast Cancer

Discipline: Mathematical Sciences

S. No	Name of the Student	CI	Enrollment No	Title of the Thesis
1	Debasish Karmakar	HRI	MATH08201504002	Some Problems in Number Theory
2	Nishant	HRI	MATH08201704003	Extension Theory for Non-degenerate Solutions of Yang-Baxter Equation
3	Priyanshu Chakraborty	HRI	MATH08201704004	Irreducible Modules for Loop of Lie Algebras
4	Krishnarjun K	HRI	MATH08201804001	On the Analytic Properties of Certain Dirichlet Series
5	Abhishek Sahu	IMSc	MATH10201504011	Packing and Covering: New Paradigms and Algorithms
6	Ashwin Jacob	IMSc	MATH10201604003	New Directions in Parameterized Deletion Problems
7	Gaurav Sood	IMSc	MATH10201604006	A Study of QBF Merge Resolution and MaxSAT Resolution
8	Neelam	IMSc	MATH10201804001	Around Non-vanishing, Linear Independence and Transcendence of L Values at Rational and Integer Points
9	Sunil L Naik	IMSc	MATH10201804005	Prime Divisors of Non-zero Fourier Coefficients of Hecke Eigenforms
10	Atibur Rahaman	NISER	MATH11201604002	Examples of Braided Quantum Groups in C*-Algebraic Framework
11	Rajeeb Ranjan Mohanta	NISER	MATH11201704003	Contractivity of Ornstein-Uhlenbeck Semigroup and Approximation Property of Mixed q-Deformed Araki-Woods Von Neumann Algebra

Discipline: Physical Sciences

S. No	Name of the Student	CI	Enrollment No	Title of the Thesis
1	Sudip Kumar Sarkar	BARC	PHYS01201604003	Investigation of Nano-scale Phase Separation in Fe-Cr Alloys using Complementary Techniques
2	Raman Sehgal	BARC	PHYS01201604007	Simulations and Measurements of Cosmic Muons with Position Sensitive Detectors for Muon Tomography
3	Atula Charan Sahoo	BARC	PHYS01201604011	Isotope Selective Photoionization Spectroscopy of Atomic Samarium using Pulsed Dye Laser
4	Kawsar Ali	BARC	PHYS01201604012	First-Principles Studies on Fe-Zr Alloys and $BaZrO_3$ as Host Matrices for Nuclear Waste
5	Romesh Chandra	BARC	PHYS01201604015	Design and Characterization of High Power Backward Wave Oscillator
6	Tarun Kumar Agarwal	BARC	PHYS01201604016	Study of Influence of Environmental Parameters on Distribution of Thoron and its Decay Products through Computational Fluid Dynamics (CFD) Modelling and Experiments
7	Anil Kumar	BARC	PHYS01201604017	Studies on Response Uniformity of RPC and Exploring Oscillation Dip and Valley, Non-Standard Interactions, and Earth's Core using Atmospheric Neutrinos at ICAL-INO Detector
8	Swayam Kesari	BARC	PHYS01201704007	Vibrational and Structural Investigations of Phase Transitions in Vanadium Based Framework Oxides
9	Rajnarayan De	BARC	PHYS01201704014	Fabrication and Characterization of Nano-structured Thin Films and Multilayers by Oblique Angle Deposition (OAD) Technique
10	Deepak	BARC	PHYS01201704023	Structural, Electronic and Magnetic Correlations, and Exchange Bias effect in Negative Magnetization Materials
11	Khorsed Alam	HRI	PHYS08201405006	Theoretical Studies of Materials for Electrocatalysis in Metal-Air Batteries and Hydrogen Generation
12	Chirag Srivastava	HRI	PHYS08201505002	Sequential Detection of Bipartite and Genuine Multipartite Entanglement
13	Atri Dey	HRI	PHYS08201604001	Searching for New Physics via Approaches Beyond the Standard Mode
14	Brij Mohan	HRI	PHYS08201604002	Quantum Speed Limit and Reverse Quantum Speed Limit

15	Arun Kumar Panda	IGCAR	PHYS02201504002	Texture Evolution and Atomistic Simulation of Nano-hardness of Thin Films
16	Arun Aravind	IGCAR	PHYS02201504003	Observational and Numerical Modelling Studies of Atmospheric Flow Field and Dispersion of Air-borne Releases over Kaiga
17	Dhilipan P	IGCAR	PHYS02201504022	Quantum State Determination and Entanglement Distillation using Single Photon Interferometry
18	Rajitha R	IGCAR	PHYS02201504024	Study of Phase Transformations in Some Insensitive Secondary Explosives Using Raman Spectroscopy, XRD and DFT Calculations
19	Chandrasekaran S	IGCAR	PHYS02201504029	Statistical Analysis and Uncertainty Evaluation in Dose Assessment Due to Spatial Distribution of Naturally Occurring Radioactive Materials (Norm) in Beach Sand of South East Coast of India Using Probabilistic Approach
20	Abhirami S	IGCAR	PHYS02201604005	Quantum Coherence Modulation in Bismuth Selenide Topological Insulator Thin Films and Studies on Superconductor-topological Insulator Heterostructures
21	Manali Nandy	IGCAR	PHYS02201604007	Magnetic Nanoemulsion Based Sensors for Visual Detection of Defects in Ferromagnetic Materials: Effect of Stabilizing Moieties and Defect Geometries on the Detection Sensitivity
22	Jagnaseni Pradhan	IGCAR	PHYS02201604009	Studies of Ion Beam Modification of Graphene and Carbon Nanomaterials with Novel Properties
23	Reshma P R	IGCAR	PHYS02201604013	Synthesis and Applications of Low Dimensional V_2O_5 Nanostructures
24	Gayathri V	IGCAR	PHYS02201704001	Evolution of Superconducting Critical Properties of Bi-based High Temperature Superconductors under Extreme Conditions and in Proximity with Manganites
25	Pew Basu	IGCAR	PHYS02201704010	Studies on Shielding Effectiveness of Composite Materials and Build-up Factors for Stratified Configurations
26	P Anand Kumar	IGCAR	PHYS02201718001	Structural Properties of Transition Metal Borides under Pressure and Irradiation
27	Mohammad Shabbir	IMSc	PHYS10201504002	Lie Algebraic Decomposition of Black Hole Partition Functions
28	Vinay Vaibhav	IMSc	PHYS10201505002	Thermo-mechanical Response of Glassy Systems
29	Soumya Sajal Sur	IMSc	PHYS10201505003	Investigations into Quantum Compass Models in Two Dimensions

30	Arindam Mitra	IMSc	PHYS10201505005	Aspects of Compatibility of quantum Devices and quantum Communication using Quantum Switch
31	Sabiar Shaikh	IMSc	PHYS10201604001	Study of Z_N Symmetry in $SU(N)$ Gauge Theories in the Presence of Matter Fields
32	Semanti Dutta	IMSc	PHYS10201604006	Exact Renormalization Group and the O(N) Model
33	Arkajyoti Manna	IMSc	PHYS10201704006	Scattering Amplitudes from Generalized Recursion
34	Aparna Sankar	IMSc	PHYS10201704007	Higher Order Corrections and Resummation in Perturbative QCD
35	Biswajit Das	IoP	PHYS07201404011	Probing Anomalous Higgs Boson Couplings at Colliders
36	Debjyoti Majumdar	IoP	PHYS07201604007	Rigidity and collapse of melting DNA
37	Pranjal Pandey	IoP	PHYS07201704005	Aspects of Flat Space Holography
38	Saiyad Ashanujjaman	IoP	PHYS07201704009	Perusing Some Neutrino Mass Models at the LHC
39	Harish Chandra Das	IoP	PHYS07201804002	Impacts of Dark Matter Interaction on Nuclear and Neutron star Matter within the Relativistic Mean-field Model
40	Shivam Kumar Mishra	IPR	PHYS06201404005	Radiation Reaction Effects on Laser Driven Acceleration of Charged Particles
41	Soumen De Karmakar	IPR	PHYS06201604002	Collective Dynamics of Active or Self-propelled Particles
42	Pawandeep Kaur	IPR	PHYS06201604003	Molecular Dynamics Study of Convection Cells in 2D Yukawa Liquids
43	Swapnali Khamaru	IPR	PHYS06201604004	Exploring Electron Plasmas Confined in Toroidal Magnetic Field: A 3D Particle-in-Cell Simulation Study
44	Satadal Das	IPR	PHYS06201604009	Studies on External Electrode Influence on Magnetized Plasma Properties in Linear Device
45	Devshree Mandal	IPR	PHYS06201604010	Some Studies on Interaction of Laser with Overdense Plasma
46	Ayushi Vashistha	IPR	PHYS06201604011	Study of Laser Interacting with Magnetized Plasma
47	Nidhi Rathee	IPR	PHYS06201604012	Breaking of Large Amplitude Electrostatic Waves in Inhomogeneous Plasma
48	Mahammad Mustakim	NISER	PHYS11201404005	Structure and Dynamics of Binary Colloids in an External Potential: Role of Depletion Interaction
49	Palash Dubey	NISER	PHYS11201504004	Fermion Zero Modes of Supergravity
50	Chandiprasad Kar	NISER	PHYS11201504013	Studies of $B^0_{(s)} \to \mu^+ \mu^-$ Decays with CMS Experiment at LHC
51	Anupa Kumari	NISER	PHYS11201604001	Studies on Linear and Nonlinear Optical Properties of Subwavelength Structures

52	Debasish Mallick	NISER	PHYS11201604003	Probing Thermalization and Deuteron Production Mechanism via Fluctuations in Heavy-ion Collisions in STAR at RHIC
53	Jagannath Santara	NISER	PHYS11201604005	Holomorphic and Numerical Bootstrap Studies of Conformal Field Theory
54	Rashmi Rekha Sahoo	NISER	PHYS11201604006	Studies on Nonlinear Frequency Conversion Techniques using $\chi^{(2)}$ Processes
55	Tanim Firdoshi	NISER	PHYS11201604008	Microwave Electrometry with Rydberg Atoms in Thermal Atomic Vapor
56	Charanpreet Singh	NISER	PHYS11201604010	Manipulation of Non-trivial Magnetic States in Electron Doped Noncollinear Antiferromagnetic Mn_3Sn
57	Dukhishyam Mallick	NISER	PHYS11201604011	Studying Multiplicity and Rapidity Dependence of K* Production and Probing Initial Conditions of High Energy Collisions with ALICE at the LHC Energies
58	Ashish Pandav	NISER	PHYS11201605002	Probing the QCD Phase Diagram via Net-Proton Number Fluctuations at RHIC
59	Bimalesh Giri	NISER	PHYS11201704001	Nontrivial and Topological Magnetic States in Mn-rich In-based Ferrimagnetic Systems
60	Abhishek Mondal	NISER	PHYS11201704005	Role of Pump Beam Topology in Nonlinear Frequency- Conversion Processes
61	Aloke Kumar Das	NISER	PHYS11201704006	Top Quark Analysis and Trigger Studies with CMS Run 2 Dataset & Outer Tracker Upgrade for HL-LHC
62	Anirban Dinda	NISER	PHYS11201704007	Black-hole Thermodynamics of Higher Derivative Theories of Gravity
63	Koustuv Roy	NISER	PHYS11201704017	Spin to Charge Conversion in Heterostructures Comprising Metallic Ferromagnets, Heusler Alloy along with Heavy Metal and Antiferromagnets
64	Mrinal Kanti Sikdar	NISER	PHYS11201704018	Defect Engineering in ZnO Nanostructures for Optoelectronic Applications
65	Samapan Bhadury	NISER	PHYS11201704022	Formulation of Relativistic Dissipative Hydrodynamics of Spin-1/2 Particles from Kinetic Theory
66	Shailja Sharma	NISER	PHYS11201704023	Topological Aspects of Electromagnetic Wave Propagation in One-dimensional Photonic Crystal
67	Soheli Mukherjee	NISER	PHYS11201704024	Phase Transitions in Disordered Spin-1 Ferromagnets
68	Surbhi	NISER	PHYS11201704028	Third Order Nonlinear Properties in WSe_2 Thin Films
69	Tirtha Mandal	RRCAT	PHYS03201504010	Investigation on Intense, Ultra-short Laser Foil Interaction through Fast Electron Generation, Characterization and X-ray Studies

70	Rahul Gaur	RRCAT	PHYS03201504013	Electromagnetic and Nonlinear Beam Dynamics Studies of 3 MeV, 325 MHz RFQ for 1 GeV, 1 MW H- Linear Accelerator
71	Chiranjit Debnath	RRCAT	PHYS03201504015	Synthesis and Characterization of Lithium Niobate Nanoparticles and Nanocomposites for Optical Applications
72	Madhusmita Baral	RRCAT	PHYS03201604005	Crystal Structure and Physical Properties of Co and Ni based Half Heusler Alloys: A Combined Theoretical and Experimental Study
73	Durga Prasad Khatua	RRCAT	PHYS03201704013	Ultrafast Photoexcited Carrier Dynamics in Two-Dimensional Molybdenum Disulfide
74	Kiranjot	RRCAT	PHYS03201704014	Studies on Ni/AlN and Ru/C Systems for Planar X-ray Waveguide Applications
75	Arnab Purohit	SINP	PHYS05201304016	Search for a Low Mass Standard Model-like Higgs Boson and Measurement of Properties of the Observed 125 GeV Higgs Boson in gg Final State with the CMS Detector at the LHC
76	Debabrata Bhowmik	SINP	PHYS05201504009	Searching for Dark Matter with the CMS Detector in Proton-Proton Collisions Containing Large Transverse Momentum Imbalance in Association with a Higgs boson Decaying to Two Photons
77	Sourav Chakraborty	SINP	PHYS05201504022	Carrier Induced Ferromagnetism in Diluted Spin Systems
78	Md Samsul Islam	SINP	PHYS05201604010	Study of Heavy Flavour Decay Muons at Forward Rapidity in Proton-Proton and Heavy-Ion Collisions at LHC Energies
79	Vishal Kumar	SINP	PHYS05201604011	Comparative Study of Gas Detectors and their Suitability for Imaging
80	Gourab Saha	SINP	PHYS05201604016	Search for Non-Resonant Higgs Boson Pair Production in the HH W+W- Decay Channel in p - p Collisions using CMS Data at Ö =13 TeV at the LHC
81	Ayan Kumar Patra	SINP	PHYS05201704001	Black Holes, Holography, and Quantum Information
82	Arunava Kar	SINP	PHYS05201704005	Geometric and Electronic Structures of Ultra-Thin Films on Metal/Semiconductor Surfaces: A Combined Experimental and Theoretical Study
83	Upala Mukhopadhyay	SINP	PHYS05201704006	Addressing Late Time Cosmic Acceleration and Dark Energy from Theoretical Considerations along with Observational Predictions and the Impact of Primordial Black Hole Evaporation in Cosmological Observables
84	Arunima Bhattacharya	SINP	PHYS05201704009	Radiative Corrections and Threshold Resummed Predictions to Pseudoscalar Higgs Boson Production in QCD

85	Promita Roy	SINP	PHYS05201704012	Studies of Optimization of Gaseous Ionization Detectors for Muon Imaging
86	Saikat Bhattacharjee	SINP	PHYS05201704014	Systematic Study of Reaction Mechanisms with Strongly and Weakly Bound Projectiles on Rare-Earth Target Nuclei
87	Rezwana Sultana	SINP	PHYS05201704018	Characterization of Sputter Deposited Zr-Doped Hafnium Oxide Thin-Films
88	Karimul Islam	SINP	PHYS05201704020	Deposition and Characterization of Niobium Oxide Thin-Films
89	Md Saifuddin	SINP	PHYS05201704021	Nanostructuring, Ordering and Surface-interface Tuning of Organic and Metal-organic Thin Films
90	Ritesh Ghosh	SINP	PHYS05201704023	A Study on Some Aspects of Hot and Dense QCD Matter
91	Sabyasachi Maulik	SINP	PHYS05201804002	Explorations in Entanglement and Holography
92	Chiranjib Das	SINP	PHYS04201504004	Beam Dynamics and RF Design of 80 MHz RFQ Injector for ANURIB
93	Mitali Mondal	VECC	PHYS04201504013	Development of Resistive Plate Chambers for Muon Detection System of the CBM Experiment at FAIR
94	Santu Manna	VECC	PHYS04201604002	Clustering in Light Nuclei
95	Sushant Kumar Singh	VECC	PHYS04201604003	Hydrodynamic Modeling of QCD Fluid with Critical Point in the Equation of State
96	Joy Mukherjee	VECC	PHYS04201704007	Study of the Growth and Physico-Chemical Properties of Ion Induced Nano-layered Structure

Section IV
List of students who have completed M.Tech. and M.Sc. (Engg.) during August 1, 2022-July 31, 2023

M.Tech.

S. No	Name of the Student	CI	Discipline	Enrollment No	Title of the Thesis
1	Arun	BARC	Civil Engineering	ENGG01201801011	Condition Assessment of in-situ Concrete and Evaluation of Seismic Margin for Aging Reinforced Concrete Residential Buildings in Mumbai
2	Adarsh Patel	BARC	Electrical Engineering	ENGG01201801017	Design, Modeling, Simulation, Implementation and Testing of DC-DC Converter with High Frequency Link
3	Ashutosh Kumar Jha	BARC	Electrical Engineering	ENGG01201801018	Study & Analysis of Plasma Torch Characteristics along with Design Validation of Suitable DC Power Source used in Plasma Incinerator for Radioactive Solid Waste Management
4	Kanhaiya Mishra	BARC	Electrical Engineering	ENGG01201801025	Calibration of Room Temperature Vibrating Sample Magnetometer for Magnetic Qualification of Soft Magnetic Material and Its Optimization for Magnetic Susceptibility Measurements
5	M. S. Kiran	BARC	Electrical Engineering	ENGG01201801026	Study of Magnetostrictive Properties of Terfenol–D and Demonstration of its Application for Magnetic Field Measurements
6	Abhinav Dubey	BARC	Mechanical Engineering	ENGG01201801037	Development of a Methodology for Evaluation of Stress-Strain Curves of Materials through Ball Indentation at The Bi-Metallic Interface and Experimental Validation
7	Neha Sharma	BARC	Mechanical Engineering	ENGG01201801046	Study on Pressure Drop & Heat Transfer Characteristics of Pins with Special Geometrical Features

8	Nikhil Pandey	BARC	Mechanical Engineering	ENGG01201801047	Development of Natural Circulation Valve for Nuclear Research Reactor
9	Nitin Kumar	BARC	Mechanical Engineering	ENGG01201801048	Investigation of Effect of Grain Boundary Voids on Mechanism of Material Deformation Process using Multiscale Material Modelling
10	Vivek Singla	BARC	Mechanical Engineering	ENGG01201801055	Development and Validation of The Reflood Model for Deformed LWR Core
11	Ram Sharma	BARC	Radiological Safety Engineering	ENGG01201801066	Numerical Simulation of HPGe System for Health Physics Samples of Non-Standard Geometries
12	Dharmendra Singh	BARC	Electronics Engineering	ENGG01201901001	Modeling and Analysis of Total Power Control Loop of 1000 Mwe Light Water Reactor
13	Gopal Agarwal	BARC	Electronics Engineering	ENGG01201901002	Development of Narrow band Data Test Waveform for SDR Application using Various Baseband Processing Blocks
14	Satyam Rawat	BARC	Electronics Engineering	ENGG01201901005	Local Oscillator Signal Generation Scheme for Wideband (Complete VHF) Super-Heterodyne Transceiver
15	Bharat Jain	BARC	Instrumentation Engineering	ENGG01201901009	Study, Simulation and Design of Seismic Detection and Trigger Systems for Nuclear Power Plants
16	Siddharth V. Pratihast	BARC	Instrumentation Engineering	ENGG01201901010	Study, Design and Simulation of Temp-erature Compensated Voltage Reference Interfaced with EPICS Based Controller for Precision Magnet Power Supply
17	Vishnumolakala Sriharsha	BARC	Instrumentation Engineering	ENGG01201901012	Design and Development of Low Current Measurement System for Inverted Magnetron Gauge for Particle Accelerator

18	Pardeep Kumar	BARC	Instrumentation Engineering	ENGG01201901013	Development and Performance Analysis of Multi-Axes Motion Control System for Double Crystal Monochromator
19	Smit Mamgain	BARC	Electrical Engineering	ENGG01201901021	Study and Measurement of Magnetic Susceptibility of Magnetic Liquids by Quincke's Method
20	Purva Bhoj	BARC	Electrical Engineering	ENGG01201901024	Developing Algorithms and Hardware Implementation of Protection Relay for Safety Related Electrical Power Supply System for NPP
21	Jayesh Balpande	BARC	Electrical Engineering	ENGG01201901025	Design, Modelling and Simulation of Multi-Loop Feedback Regulation Scheme for Precision True- Bipolar DC Current Power Supply
22	Rishabh Gupta	BARC	Computer Engineering	ENGG01201901027	Comparative Study of Self Supervised Learning Algorithms for Scene Classification
23	Shlagha Singh Chouhan	BARC	Computer Engineering	ENGG01201901028	Comparative Study of Algorithms for Query-By-Example in Speech Data Retrieval
24	Gopikrishnan S	BARC	Mechanical Engineering	ENGG01201901030	Development of Three Position Four Port Hydraulic Distributor Block
25	Sanket Dilip Kalokhe	BARC	Mechanical Engineering	ENGG01201901033	Minimization of Axial Thrust on the Impeller of Mixed Flow Canned Motor Pump
26	Sudhanshu Kumar	BARC	Mechanical Engineering	ENGG01201901036	Determination of the Hot Processing Conditions of Cast Zircaloy-4
27	Abhishek Kumar	BARC	Mechanical Engineering	ENGG01201901038	A Simplified Modelling Approach for Evaluation of Seismic Response of Large No. of Coupled Systems
28	Abhimanyu Bhardwaj	BARC	Mechanical Engineering	ENGG01201901040	Active Control of Dynamic Response of Structure using Piezoelectric Actuators

29	Ajay Yadav	BARC	Chemical Engineering	ENGG01201901043	Studies on Separation of Mo from Tummalapalle SDU Sourced Uranyl Nitrate Solution
30	Kachchhi Tanuj Chandubhai	BARC	Chemical Engineering	ENGG01201901045	Studies on Modeling and Analysis of Electrochemical Reactor for Hydrogen Transport
31	Priti Suresh Shinde	BARC	Civil Engineering	ENGG01201901051	Numerical Simulation of Shake Table Tests Performed on Corroded and Un-Corroded RC Frames
32	Mayank Vikhona	BARC	Civil Engineering	ENGG01201901052	Finite Element Analysis of RCC Structural Slab & Grade Slab System Subjected to Low Velocity Impact Load
33	Yogesh Naik	BARC	Civil Engineering	ENGG01201901053	Effects of Rock/Soil Properties on Blasting Vibrations
34	Anil Narayan Kulkarni	BARC	Civil Engineering	ENGG01201901055	Study of Incoherency Effect of Design Basis Ground Motion on The Seismic Response of a Large Safety-Related Nuclear Structure
35	Aviral Chauhan	BARC	Mechanical Engineering	ENGG01201901066	Computational Model Development for Reactor Pressure Vessel Lower Head Heat Transfer
36	Divya Purohit	BARC	Mechanical Engineering	ENGG01201901067	Investigation of Optimized Water Cooled Apertures for 9.5 Mev, 10 kW Industrial LINAC
37	Pranshu Pareek	BARC	Chemical Engineering	ENGG01201901071	Studies on Purification of Strontium from Simulated High Level Radioactive Liquid Waste using Liquid Membrane in Hollow Fibre Contactor
38	T Sraddha	BARC	Radiological Safety Engineering	ENGG01201901076	Effect of Chemical Composition on the Measurement of Aerosol Mass Concentration using Beta Attenuation Technique
39	Ashish Gadhvi	BARC	Electrical Engineering	ENGG01202101002	Analysis, Optimization and Demonstration of Magnetostriction based Electromagnetic Actuator

40	Abhishek Dutta	BARC	Electrical Engineering	ENGG01202101011	Design of a Prototype Building Management System for a Cyclotron
41	Gangani Milan Kantilal	BARC	Instrumentation Engineering	ENGG01202101015	Modelling and Simulations for the Design of Acoustic Emission Sensor in Leak Detection System
42	Shubam Gupta	BARC	Electronics Engineering	ENGG01202101017	Study of Effectiveness of Assertion based Design and Verification for HDL Designs in Safety Critical Applications
43	Shubham Tripathi	BARC	Electronics Engineering	ENGG01202101018	Design and Development of Low Level RF System for Medical Cyclotron
44	Akanksha Agrawal	BARC	Computer Engineering	ENGG01202101026	Handwritten Character Recognition for Data Entry Automation
45	Nadiminti Sai Sirisha Kamala	BARC	Computer Engineering	ENGG01202101028	Development of Model-Based Dose Calculation Algorithm for Bhabhatron - II Telecobalt Machine
46	Kewal Bhatt	BARC	Mechanical Engineering	ENGG01202101029	Evaluation of Stress-Strain Curves of Thin Sheets Considering Substrate Stiffness in Ball Indentation Test
47	Nitish Kumar	BARC	Mechanical Engineering	ENGG01202101030	Increasing Carbon Dioxide Removal Efficiency in Enclosed Environment Using Suitable Absorbent
48	Bijender Singh	BARC	Mechanical Engineering	ENGG01202101032	Flow Physics Study in the Inlet Plenum of Reactor Pressure Vessel (RPV) of a Typical Pressurised Water Reactor (PWR)
49	Solanke Pawankumar Karbhari	BARC	Mechanical Engineering	ENGG01202101036	Natural Circulation Flow and Heat Transfer Studies to Optimize the Geometry of Tray Rod Assembly
50	Ravinder Singh	BARC	Mechanical Engineering	ENGG01202101043	Development of an Analytical/Mathematical Model for the Prediction of Physical Set Parameters of The Vertical Drop Bed Type Impact Test Machine
51	Mayank Soni	BARC	Chemical Engineering	ENGG01202101048	Experimental and Modelling Studies on Freeze Desalination Process

52	Gaurav Kumar	BARC	Chemical Engineering	ENGG01202101049	Studies on Concentrating HCl-H_2O Mixture for Integration of Hydrolysis and Electrolysis Steps of Cu-Cl Cycle
53	Jagtap Saee Mahendra	BARC	Metallurgical Engineering	ENGG01202101053	Investigation of Metallurgical Properties of Zircaloy-4 Cladding Subjected to Out-of-Pile LOCA Integral Test
54	Sarode Prafulla Subhash	BARC	Metallurgical Engineering	ENGG01202101054	Calciothermic Reduction (CTR) Process for the Production of NdPr Metal Required for NdFeB Permanent Magnet
55	Ankit Yadav	BARC	Metallurgical Engineering	ENGG01202101055	Effect of Hydride Rim and Hydride Orientation on Mechanical Behavior of PHWR Fuel Clad
56	Bodke Sushil Uttamrao	BARC	Radiological Safety Engineering	ENGG01202101059	Modelling of Hydro dynamics and Radio-nuclide Transport in the Bay Area of Visakhapatnam Harbour
57	Sitesh Sil	IGCAR,	Mechanical Engineering	ENGG02201401012	Simulation and Validation of Effectiveness of Water Injection in Early State of Degraded Core
58	Kapil Motwani	RRCAT	Electrical Engineering	ENGG03201901001	Design and Development of Switched Mode Pulsed Power Supply of 400V/50A for Hydrogen Arcing Discharge
59	Abhishek Srivastava	RRCAT	Electrical Engineering	ENGG03201901002	Analysis, Design and Development of Fast–Ramped, Switch-Mode Power Converter for Inductive Load
60	Swarnim Sharma	RRCAT	Electrical Engineering	ENGG03201901003	Development of Prototype SCADA System for Electrical Substation At RRCAT
61	G Vivek	RRCAT	Electronics Engineering	ENGG03201901004	Study, Development and Performance Analysis of Fiber Bragg Grating (FBG) based Temperature Measurement System using Ratio-Metric Interrogation Technique

62	Balkrishna Arora	RRCAT	Electronics Engineering	ENGG03201901005	Design and Simulation of 8-Way RF Power Combiner at 75.6 MHz
63	Gaurav Kanyal	RRCAT	Electronics Engineering	ENGG03201901006	Design and Study of a Wideband Solid-State RF Amplifier
64	Ankita Kumari	RRCAT	Electronics Engineering	ENGG03201901007	Design and Development of RF Down Conversion Module for Digital Beam Position Monitor of LINAC-3
65	Vikash Sahoo	RRCAT	Engineering Physics	ENGG03202101012	Study of the RF Cavity for Compact Superconduct-ing Medical Cyclotron
66	Nitin Mishra	BARCTS(AMD), Hyderabad	Exploration Geosciences	ENGG1G201901001	Identification of Tectonic Framework and its Implication on the Genesis of Uranium Mineralisation through Remote Sensing, Geological Mapping and Detailed Petrographic Techniques in Hulkul-Doranahalli Sector of Kurlagere-Gogi (Kg Fault), Yadgir District, Karnataka
67	Manish Patel	BARCTS(AMD), Hyderabad	Exploration Geosciences	ENGG1G201901002	Application of Remote Sensing and Geological Mapping to Identify Shear Zones Sympathetic to Main Central Thrust and Dirang Thrust as Favourable Locales for Uranium Mineralisation Around Dirang, West Kameng, Arunachal Pradesh
68	Jyotiskar Hazarika	BARCTS(AMD), Hyderabad	Exploration Geosciences	ENGG1G201901003	Petrogenetic Studies of the Metamorphic Zonation and Sequencing of Mineralizing Events through EPMA Technique of the Uranium-Mineralised Migmatites as an Aid for Uranium Exploration Around Kurludih Area, Balrampur District, Chhattisgarh
69	Rajat Kumar Das	BARCTS(AMD), Hyderabad	Exploration Geosciences	ENGG1G201901004	Use of Sedimentary Facies and Structural Analytical Techniques to Decipher Controls of Polymetallic

					Mineralization in and Around Jhal- Juba-Banjhapali-Chiwarakuta Area Along Eastern Margin of Singhora Proto-Basin, Mahasamund Dist., Chhattisgarh
70	Debayan Sengupta	BARCTS(AMD), Hyderabad	Exploration Geosciences	ENGG1G201901005	Characterisation of Great Boundary Fault (GBF) Involving Metamorphosed Volcano-Sedimentary Hindoli Group and Sediments of Vindhyan Supergroup using Geological, Geophysical Techniques and Structural Mapping to Identify Guides for Locating Uranium Haloes Along Barliyas-Motipur-Malikhera Area, Bhilwara and Chittaurgarh Districts, Rajasthan
71	K Pushkala	BARCTS(AMD), Hyderabad	Exploration Geosciences	ENGG1G201901006	Application of Petromineralogical, Geo-chemical And Radiometric Techniques to Explore Potential Kudada Type Uranium Mineralisation Hosted in Dhanjori Mafic-Ultramafic Sequence From Kudada to Rakha, Singhbhum Shear Zone, Eastern India
72	Swagat Pradhan	BARCTS(AMD), Hyderabad	Exploration Geosciences	ENGG1G201901007	Characterization of Quartz Pebble Conglo-merate (QPC) and its Palaeo-Environment of Deposition by using Provenance-Specific Heavy Mineralogical Analysis: Implications on Uranium Mineralisation in Sarara Inlier, Udaipur Distric, Rajasthan
73	Shivam Soni	BARCTS(AMD), Hyderabad	Exploration Geosciences	ENGG1G201901008	Use of Granulometric Analysis Techniques and Mineralogical Studies of Quaternary Unconsolida-ted Sediments for Provenance and Depositional Environment

					in Parts of Brahmagiri Mineral Sand Deposit, Puri District, Odisha
74	Harshit Varshanay	BARCTS(AMD), Hyderabad	Exploration Geosciences	ENGG1G201901009	Use of Sedimentary Facies Analysis Techniques to Decipher the Depositional Environment and its Role in Uranium Mineralization in the Badami Group of Sediments, Gujanal–Yaranhatti Tract in Western Part of Kaladgi Basin, Belgaum District, Karnataka
75	Vijay Yadav	BARCTS(AMD), Hyderabad	Exploration Geosciences	ENGG1G201901010	Use of Facies Analysis Technique to Establish the Control of Uranium Mineralisation Within Middle - Upper Siwalik Transition Zone, Ambtilla-Duhl Bhatwalan Area, Distt. Una, H.P.
76	Shivam Pandey	BARCTS(AMD), Hyderabad	Exploration Geosciences	ENGG1G201901011	Modelling of Magnetic and IP/Resistivity Data for Delineation of Metamorphite Type Uranium Mineralization Near Pathargora, East Singhbhum District, Jharkhand
77	Ramsevak Singh	BARCTS(AMD), Hyderabad	Exploration Geosciences	ENGG1G201901012	Imaging of Subsurface By 2D And 3D Modeling and Inversion of Ground Geophysical Data to Delineate Target Zones for Uranium Exploration Along Hulkal-Halbhavi-Madnal Tract, Bhima Basin, Karnataka
78	Srijon Guha	BARCTS (NFC), Hyderabad	Chemical Engineering	ENGG1A201801005	Computational Model Development for Fuel Dispersion from Corium Jet and Associated Heat Transfer
79	Avijit Chakraborty	BARCTS (NFC), Hyderabad	Electrical Engineering	ENGG1A201801013	Prediction, Comparison and Validation of Performance of A 5 M3/H Alip using Different Computational Models and Evaluation of the Effects of Annular Gap

					Buttons on the Performance of the Alip
80	Ausali Meher Manoj	BARCTS (NFC), Hyderabad	Electrical Engineering	ENGG1A201801016	Design of Hot Zone of Bright Annealing Furnace at SSTP
81	Vaishnav Hutton	BARCTS (NFC), Hyderabad	Mechanical Engineering	ENGG1A201901004	Study of Effect of Material Anisotropy on Crack Initiation Toughness and Fracture Resistance of Zr2.5Nb Pressure Tube Material
82	Phani Srikanth Kannepalli	BARCTS (NFC), Hyderabad	Chemical Engineering	ENGG1A201901008	Studies on Chlorination of Zirconium Scrap in Water Cooled Scrap Reactor
83	Mohammed Muzammil Ahmed	BARCTS (NFC), Hyderabad	Metallurgical Engineering	ENGG1A201901009	Effect of Pre-existing Manufacturing Flaws on Mechanical and Corrosion Properties of Alloy 800 Steam Generator Tubes
84	Sukanta Bhattacharyya	BARCTS (NFC), Hyderabad	Mechanical Engineering	ENGG1A202101009	Establishing Effects of Long-Term Service in H_2S Environment in Steel And its Laboratory Simulation

M.Sc. (Engg.)

S. No	Name of the Student	CI	Discipline	Enrollment No	Title of the Thesis
1	Sanjay Kumar Pandey	IGCAR	Engineering Sciences	ENGG02201905003	Experimental and Numerical Investigation of Ductile Crack Initiation and Growth in Austenitic Stainless Steel Grade 316LN for Nuclear Application

Section V
List of students who completed D.M., M.Ch. and M.D. degrees during August 1, 2022-July 31, 2023

D.M. Degree

S. No	Name of the Student	CI	Academic Programme	Enrollment No
1	Dr. Naveen K	TMC	D.M.-Medical Oncology	HLTH09201910054

M.Ch Degree

S. No	Name of the Student	CI	Academic Programme	Enrollment No
1	Dr. Sneha Raj	TMC	M.Ch.-Gynaecological Oncology	HLTH09201910006
2	Dr. Mor Akash Gopal	TMC	M.Ch.-Surgical Oncology	HLTH09201910011
3	Dr. Tanvi M Shah	TMC	M.Ch.-Surgical Oncology	HLTH09201910014
4	Dr. Nishant	TMC	M.Ch.-Surgical Oncology	HLTH09201910018
5	Dr. Mundhada Rohit Omprakash	TMC	M.Ch.-Surgical Oncology	HLTH09201910020
6	Dr. T G Vasanthraja	TMC	M.Ch.-Surgical Oncology	HLTH09201910022
7	Dr. Amita Sekhar Padhy	TMC	M.Ch.-Surgical Oncology	HLTH09201910024
8	Dr. Swarnim Kumar	TMC	M.Ch.-Surgical Oncology	HLTH09201910028

M.D. Degree

S. No	Name of the Student	CI	Academic Programme	Enrollment No
1	Dr. Abhiram Y	TMC	M.D. Anaesthesiology	HLTH09202009011
2	Dr. Akshat Dnyanesh Shah	TMC	M.D.-Anaesthesiology	HLTH09201909013
3	Dr. Ashwini V. Wanjari	TMC	M.D.-Anaesthesiology	HLTH09201909017
4	Dr. Vikas Atmaram Sonwane	TMC	M.D.-Anaesthesiology	HLTH09201909019
5	Dr. Ankita Medhi	TMC	M.D.-Anaesthesiology	HLTH09202009007
6	Dr. Awchar Padurang Limbaji	TMC	M.D.-Anaesthesiology	HLTH09202009028
7	Dr. Badrinath Pandhrinath Katre	TMC	M.D.-Anaesthesiology	HLTH09202009009
8	Dr. Chandni Jitesh Rana	TMC	M.D.-Anaesthesiology	HLTH09202009019
9	Dr. Chawathey Shreyas Arun Vandana	TMC	M.D.-Anaesthesiology	HLTH09202009002
10	Dr. Dilip Sagar Apte	TMC	M.D.-Anaesthesiology	HLTH09202009020
11	Dr. Mehak Kinra	TMC	M.D.-Anaesthesiology	HLTH09202009026
12	Dr. Minal Vinod Bichewar	TMC	M.D.-Anaesthesiology	HLTH09202009015
13	Dr. Momin Mariya Aqueel Ahmad	TMC	M.D.-Anaesthesiology	HLTH09202009027
14	Dr. Mulchandani Yoshita Jaiprakash	TMC	M.D.-Anaesthesiology	HLTH09202009004
15	Dr. Nara Himaja	TMC	M.D.-Anaesthesiology	HLTH09202009005
16	Dr. Nisha Lilly Ninan	TMC	M.D.-Anaesthesiology	HLTH09202009013
17	Dr. Pankaj Ishwar Dadmal	TMC	M.D.-Anaesthesiology	HLTH09201809020
18	Dr. Pavithra P S	TMC	M.D.-Anaesthesiology	HLTH09202009008
19	Dr. Rinto P O	TMC	M.D.-Anaesthesiology	HLTH09202009012
20	Dr. Sailee Jambhulkar	TMC	M.D.-Anaesthesiology	HLTH09202009006
21	Dr. Sargam Kant	TMC	M.D.-Anaesthesiology	HLTH09202009021

22	Dr. Shruti Anand Shahare	TMC	M.D.-Anaesthesiology	HLTH09202009022
23	Dr. Snehal Ravindra Mahatme	TMC	M.D.-Anaesthesiology	HLTH09202009016
24	Dr. Surya V	TMC	M.D.-Anaesthesiology	HLTH09202009003
25	Dr. Tandale Kiran Ambadas	TMC	M.D.-Anaesthesiology	HLTH09202009017
26	Dr. Tarhane Sonal Rameshwar	TMC	M.D.-Anaesthesiology	HLTH09202009018
27	Dr. Thanawala Insiya Zuzar	TMC	M.D.-Anaesthesiology	HLTH09202009025
28	Dr. Vidya Nair	TMC	M.D.-Anaesthesiology	HLTH09202009010
29	Dr. Vidya Gulab Hole	TMC	M.D.-Anaesthesiology	HLTH09202009024
30	Dr. Aswathi S	TMC	M.D.- Immuno-Hematology & Blood Transfusion	HLTH09202009060
31	Dr. Itkare Tejasvini Bharat	TMC	M.D.-Immuno-Hematology & Blood Transfusion	HLTH09202009061
32	Dr. Shruthi Meenaxi Henriques	TMC	M.D.-Immuno-Hematology & Blood Transfusion	HLTH09202009059
33	Dr. Surve Bhagyashri Avinash	TMC	M.D.-Immuno-Hematology & Blood Transfusion	HLTH09202009062
34	Dr. Harkal Santosh Kumar Kerbarao	TMC	M.D.-Microbiology	HLTH09202009001
35	Dr. Abhishek Palsapure	TMC	M.D.-Nuclear Medicine	HLTH09202009054
36	Dr. Abhishek Uppal	TMC	M.D.-Nuclear Medicine	HLTH09202009055
37	Dr. Edamadaka Yeshwanth	TMC	M.D.- Nuclear Medicine	HLTH01202009002
38	Dr. Gondhane Abhay Indrasingh	TMC	M.D.- Nuclear Medicine	HLTH01202009005
39	Dr. Lakhule Bhaskar Parasram	TMC	M.D.- Nuclear Medicine	HLTH01202009006
40	Dr. Mangle Prathamesh Surendra	TMC	M.D.-Nuclear Medicine	HLTH09202009056
41	Dr. Marotkat Mandar Sudhir	TMC	M.D.-Nuclear Medicine	HLTH09202009057
42	Dr. Narwadkar Yoga Sandeep	TMC	M.D.- Nuclear Medicine	HLTH01202009004
43	Dr. Parth Baberwal	TMC	M.D.- Nuclear Medicine	HLTH01202009003
44	Dr. Rajkotia Saloni Yashvantrai	TMC	M.D.-Nuclear Medicine	HLTH09202009053
45	Dr. Yogendra Yadav	TMC	M.D.-Nuclear Medicine	HLTH09202009058
46	Dr. Aamir K Nazar	TMC	M.D.- Palliative Medicine	HLTH01202009001
47	Dr. Anshita Sharma	TMC	M.D.- Palliative Medicine	HLTH09202009033
48	Dr. Kashish Vats	TMC	M.D.- Palliative Medicine	HLTH09202009034
49	Dr. Kudal Dhanashri Hari	TMC	M.D.- Palliative Medicine	HLTH09202009032
50	Dr. Adhav Kshitija Jagdish	TMC	M.D. Pathology	HLTH09202009089
51	Dr. Aditi Sanjay Arora	TMC	M.D.-Pathology	HLTH09202009083
52	Dr. Ankan Ghosh	TMC	M.D.-Pathology	HLTH09202009085
53	Dr. Archita Juneja	TMC	M.D.-Pathology	HLTH09202009084
54	Dr. Jain Medha Bharat	TMC	M.D.-Pathology	HLTH09202009090
55	Dr. Johari Megha Anand	TMC	M.D.-Pathology	HLTH09202009091
56	Dr. Mayur Nana Indave	TMC	M.D.-Pathology	HLTH09201909035
57	Dr. Nikhil Singh	TMC	M.D.-Pathology	HLTH09201909025
58	Dr. Padwale Pooja Balsing	TMC	M.D.-Pathology	HLTH09202009092
59	Dr. Purvi Bansal	TMC	M.D.-Pathology	HLTH09202009086
60	Dr. Shiromani Bansal	TMC	M.D.-Pathology	HLTH09202009081
61	Dr. Thakur Puja Rajendrababu	TMC	M.D.-Pathology	HLTH09202009088

62	Dr. Vishal Omrahul Tayade	TMC	M.D.-Pathology	HLTH09201809037
63	Dr. Aarushi Singla	TMC	M.D.-Radiation Oncology	HLTH09202009042
64	Dr. Ajay Thomas Alex	TMC	M.D.-Radiation Oncology	HLTH09202009046
65	Dr. Akshay Dinesan	TMC	M.D.-Radiation Oncology	HLTH09202009036
66	Dr. Bharath Kumar	TMC	M.D.-Radiation Oncology	HLTH09202009035
67	Dr. Ikhe Mangesh Nanasaheb	TMC	M.D.-Radiation Oncology	HLTH09202009048
68	Dr. Joyita Sarkar	TMC	M.D.-Radiation Oncology	HLTH09202009039
69	Dr. Kanoja Ankita Suresh	TMC	M.D.-Radiation Oncology	HLTH09202009045
70	Dr. Kavita Dilip Jadhav	TMC	M.D.-Radiation Oncology	HLTH09201909067
71	Dr. Krishnan Anuradha Gopal	TMC	M.D.-Radiation Oncology	HLTH09202009050
72	Dr. Madhavi Megha Chandrakant	TMC	M.D.-Radiation Oncology	HLTH09201809055
73	Dr. Namrata Vilas Pansande	TMC	M.D.-Radiation Oncology	HLTH09201909061
74	Dr. Neha Vilas Rahul	TMC	M.D.-Radiation Oncology	HLTH09201909066
75	Dr. Peddi Manideep	TMC	M.D.-Radiation Oncology	HLTH09202009049
76	Dr. Priyanshu Tripathi	TMC	M.D.-Radiation Oncology	HLTH09202009051
77	Dr. Rahat Malhotra	TMC	M.D.-Radiation Oncology	HLTH09202009037
78	Dr. Ranjan S	TMC	M.D.-Radiation Oncology	HLTH09202009040
79	Dr. Sam David	TMC	M.D.-Radiation Oncology	HLTH09202009043
80	Dr. Sangle Rasika Keshavrao	TMC	M.D.-Radiation Oncology	HLTH09202009044
81	Dr. Shivani Pradeep Sable	TMC	M.D.-Radiation Oncology	HLTH09202009041
82	Dr. Shubham Shamrao Bagde	TMC	M.D.-Radiation Oncology	HLTH09202009047
83	Dr. Yogesh Shaligram Rathod	TMC	M.D.-Radiation Oncology	HLTH09201909064
84	Dr. Aayush Mathur	TMC	M.D.-Radiodiagnosis	HLTH09202009072
85	Dr. Amar Sopanrao Jakure	TMC	M.D.-Radiodiagnosis	HLTH09202009074
86	Dr. Atif Ahmed Gul Mohammed Shaikh	TMC	M.D.-Radiodiagnosis	HLTH09202009067
87	Dr. Aughad Pallavi Prafulla	TMC	M.D.-Radiodiagnosis	HLTH09202009079
88	Dr. Bornak Gauri Bhimrao	TMC	M.D.-Radiodiagnosis	HLTH09202009068
89	Dr. Chirag Nooh Kurane	TMC	M.D.-Radiodiagnosis	HLTH09202009064
90	Dr. Deokar Shonal Sanjay	TMC	M.D.-Radiodiagnosis	HLTH09202009078
91	Dr. Dipali Punwatkar	TMC	M.D.-Radiodiagnosis	HLTH09202009077
92	Dr. Joshi Akansha Rajesh	TMC	M.D.-Radiodiagnosis	HLTH09202009070
93	Dr. Mahommed Etemaduddin Mubbaashiruddin	TMC	M.D.-Radiodiagnosis	HLTH09202009073
94	Dr. Nishita Vishukumar Patel	TMC	M.D.-Radiodiagnosis	HLTH09202009065
95	Dr. Pratik Nilkanth Jirge	TMC	M.D.-Radiodiagnosis	HLTH09202009080
96	Dr. Pritesh Upendrabhai Shah	TMC	M.D.-Radiodiagnosis	HLTH09202009069
97	Dr. Renuka Mahender Ashtekar	TMC	M.D.-Radiodiagnosis	HLTH09202009075
98	Dr. Shivam Kumar Rastogi	TMC	M.D.-Radiodiagnosis	HLTH09202009071
99	Dr. Shubham	TMC	M.D.-Radiodiagnosis	HLTH09202009066
100	Dr. Swapnil Ankush Lamkane	TMC	M.D.-Radiodiagnosis	HLTH09202009076

HBNI Ranked 15 in
Research Institutions Category
(Among Top 50 Research Institutions)

HBNI ranked 17 in University Category
(Among Top 100 Universities)

HBNI ranked 30 in Overall Category
(Among Top 100 Overall Category)

Core value of HBNI

Contact Details

VICE CHANCELLOR

Prof. U. Kamachi Mudali   022-25597638   vicechancellor@hbni.ac.in

VICE CHANCELLOR's OFFICE

PA to VC   022-25597621   vcoff@hbni.ac.in

DEAN

Prof. P.D. Naik   022-25595398   deanhbni@hbni.ac.in

REGISTRAR

Prof. P. C. Selvin   022-25597625   registrar@hbni.ac.in

ASSOCIATE DEANS

Prof. D. K. Maity   022-25597623   asso_dean@hbni.ac.in

Prof. Naveen kumar   022-25597629   nkumar@hbni.ac.in

Prof. Dipanwita Dutta   022-25592041   ddutta08@hbni.ac.in

Prof. Haridas Pal   022-25597674   hpal59@hbni.ac.in

Prof. B. K. Nayak   022-25597675   bknayak@hbni.ac.in

Prof. S. K. Ghosh   022-25597624   sunilg@hbni.ac.in

ASSISTANT DEAN

Dr.(Mrs.) Anshu Singhal   022-25597616   asinghal@hbni.ac.in

DEPUTY REGISTRAR

Shri Suresh P. Nair   022-25597637   dy.registrar@hbni.ac.in

ADMINISTRATIVE OFFICER(III)

Smt. Bharati Suvarna   022-25597611   ao3hbni@hbni.ac. in